Understanding Steel Corrosion in Oilfield Brines

By
Yannick Garsany

A thesis submitted for the degree of

DOCTOR OF PHILOSOPHY

October 2002

Department of Chemistry
University of Southampton

UNIVERSITY OF SOUTHAMPTON

ABSTRACT

FACULTY OF SCIENCE

CHEMISTRY

Doctor of Philosophy

UNDERSTANDING STEEL CORROSION IN OILFIED BRINES

By Yannick Garsany

During the recovery of oil and gas, an aqueous brine saturated with carbon dioxide is one component of a multiphase flow through carbon steel pipes. In many oilfields, including Wytch Farm in Southern England and Trinidad, enhanced rates of steel corrosion are thought to result from the presence in the brine of the anions of weak acids, particularly acetate ions. This thesis examines the premise that the enhanced rate of corrosion results from the presence in the brine of acetic acid and this proton donor reduces alongside the free proton in the cathodic reaction leading to corrosion.

Experiments have used both simulated brines (3 % NaCl + sodium acetate (NaOAc), saturated with CO_2) and brine samples from the oilfields. The programme requires a detailed understanding of the speciation within the brines. This has been examined using a computer package (PHREEQC 2.2) available on the World Wide Web and physical constants from the literature. It is shown that deviations from ideal solution behaviour must be taken into account. The influence of other species in the brine, particularly bicarbonate has also been considered. The conclusions of the speciation calculation have been tested by examining the voltammetry of the solutions at a Pt rotating disc electrode (RDE) and a good fit between the predicted and experimental limiting current densities has been demonstrated. The voltammetry shows that NaCl/NaOAc/CO_2 solutions behave identically to NaCl/NaOAc/HOAc solutions of the same pH. It is also confirmed that the thermodynamics of hydrogen evolution depend only on the solution pH but the rate of hydrogen evolution depends on the concentrations of both free proton (pH) and undissociated acetic acid because of the rapid dissociation of the acetic acid. Moreover, in the conditions of interest, the concentration of acetic acid is far higher than that of free proton and acetic acid reduction is the major cathodic process.

The voltammetry of carbon steel (X65) RDE in the acetate containing brines, both simulated and oilfield, has been defined over the temperature range 298 – 333 K. It has been demonstrated that the reduction of acetic acid at a steel cathode leads to one or two reduction waves (depending on the conditions) close to the corrosion potential and the combined limiting currents correspond to those expected for mass transport

controlled reduction of acetic acid. The corrosion potential shifts positive in conditions where there is acetic acid in the solution. Tafel and linear polarization techniques have been used to measure the corrosion current densities as a measure of the corrosion rate. Using simulated brines it has been demonstrated the rate of corrosion is directly related to the concentration of acetic acid in the brine.

Overall, the rate of corrosion of the carbon steel in the oilfield brines can be understood by calculating the acetic acid concentration taking into account all components of the brine and a model emphasising the role of acetic acid as the cathodic reaction in corrosion.

Contents

Acknowledgements

There are no words in which I could express my gratitude to Pr. Derek Pletcher not only for his patient supervision throughout the duration of this work, for his constant support and enthusiasm as progress was made but also for the friendship developed during the course of my Ph. D studies. I would like to thank him for giving me the opportunity to learn new skills, and for his help and encouragement during the writing of this thesis.

My acknowledgements also go to Dr. Bill Hedges (BP Amoco Ltd.) for his support and enthusiasm throughout the duration of this work. I also gratefully acknowledge the assistance of Dr. Richard Chapman (BP Amoco Ltd) in setting up PHREEQC 2.2 for the calculations. I would also like to thank Mr. Alistair Clark for his help and assistance during the use of the SEM.

I would like to take this opportunity to thank BP Amoco Ltd. for financial support.

On a more personal note, I would also express my thanks to all those past and present members of Derek 's group: Mat, Martin, Dzimitri, Ahmed, Richard and Raquel. Special thanks are due to Yvonne, John and Martin, for being really good friends (from the very first day!) and putting up with my grumpy character during the last three years.

Also thanks to Toby, Richard, Matt, Doug, Tim, Raquel and Steve for the laughs during lunch and tea breaks. Thank you to all of you for the Friday nights in the Staff Club and the memorable nights out!!!!! A big thanks to Toby and Matt for helping me with my numerous computer problems, merci beaucoup lads!!!!!! Special thanks also to Raquel, Nicolas and Sam for proof reading my Thesis.

I also gratefully thank my housemates, Becky and Renes for all their tremendous help and support during the last two years. Merci beaucoup you two, you have been terrific. Thank you to Vincent for his support and friendship during all these years.

Also big thanks to all the lads from the Handball team. Thank you to the French connection: Mathieu, Julien, Sam, Shella (I know, you are from Mauritius!), Stephane, Nicolas, Mitch (not really sure of the spelling!), Rene, Isabelle, Fabrice. I also thank Lucy for supporting and encouraging me during the last few months, and finally I apologise to all those I forgot to mentioned.

I want now to gratefully acknowledge my parents, Max and Erise, because they are deeply responsible for what I have become. Thank you very much for your help and support. There are no words in which I could express my gratitude to the both of you, your love and loyalty means more to me now than ever. Thanks to the rest of my family; my sisters Nadine and Laetitia, my grandparents: Meme Pothin and Pepe Pothin, Meme Minie, my uncles, my aunts and cousins. A special thank to Dodo and Sylvie for being there for me whenever I needed it.

To all and everyone I am grateful.

Yannick.

This thesis is gratefully dedicated to my family:
Erise Garsany, Max Garsany, Nadine and Laetitia Garsany.

Chapter One

1 Introduction

1.1 What is oil and where does it come from?

According to the most widely accepted theory, "oil" in nature is composed of compressed hydrocarbons, and was formed millions of years ago in a process that began when aquatic plant and animal remains were covered by layers of sediment -- particles of rock and mineral. Over millions of years of extreme pressure and high temperatures, these particles became the mix of liquid hydrocarbons that we know as oil. Different mixes of plant and animal remains, as well as pressure, heat, and time, have caused hydrocarbons to appear today in a variety of forms: crude oil, natural gas, and coal.

The word "petroleum" comes from the Latin words *petra*, or rock, and *oleum*, oil. Oil is found in reservoirs in sedimentary rocks. Tiny pores in the rock allowed the petroleum to seep in. These "reservoir rocks" hold the oil like a sponge, confined by other non-porous layers that form a "trap" as illustrated in figure 1.1.

The world consists of many regions with different geological features formed as the Earth's crust shifted. Some of these regions have more and larger petroleum traps. In some reservoir rocks, the oil is more concentrated in pools, making it easier to extract, while in other reservoirs it is diffused throughout the rock. Oil is the major fuel used by people today. In 1995, the entire global oil consumption was determined to be 69 million barrels a day [1], compared to 59.7 million barrels per day in 1985 [2]. Because oil is liquid, it can be mined by drilling and pumping rather than excavation and it can be transported in tankers and pipelines.

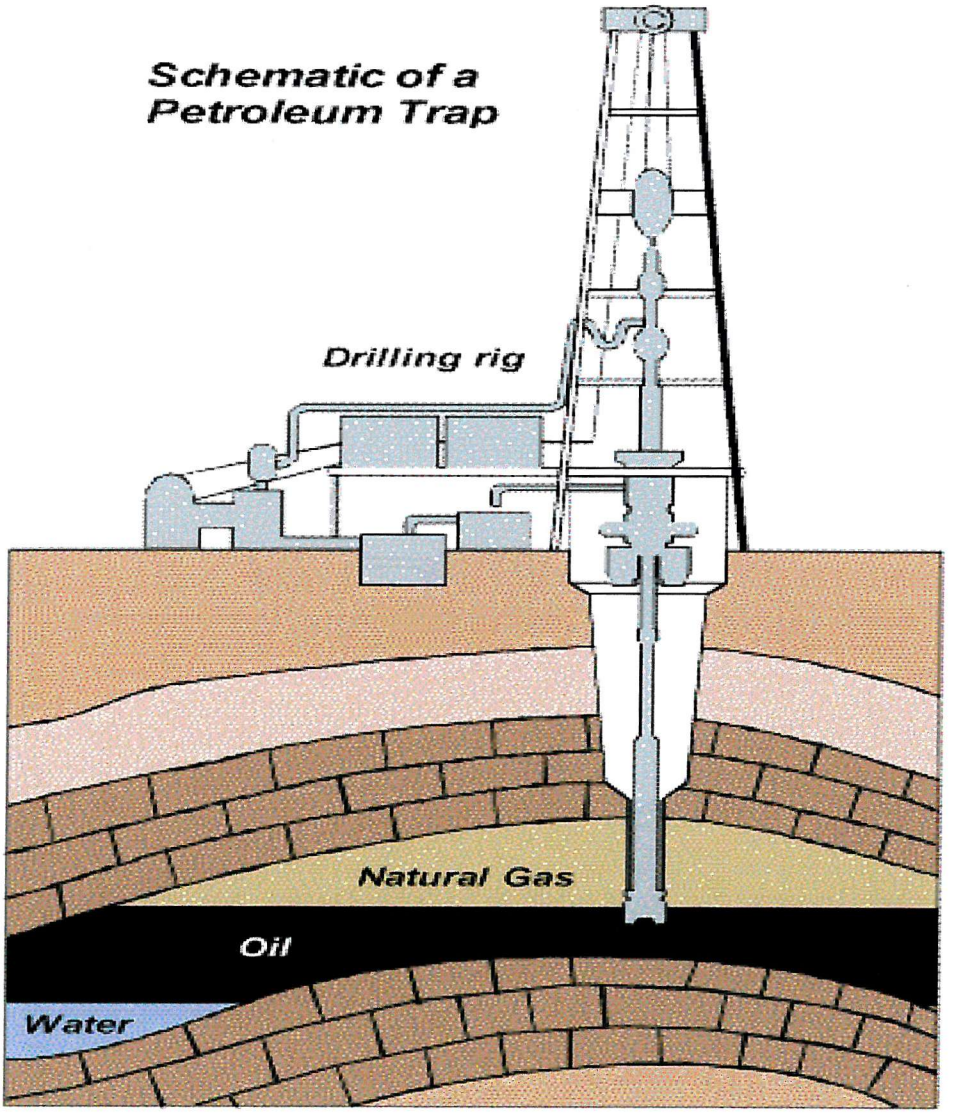

Figure 1. 1 *Schematic of a petroleum trap.*

1.2 How is oil extracted?

Most oil, initially, is produced by "natural lift" production methods; the pressure underground is high enough to force the oil to the surface. The underground pressure in older reservoirs, however, eventually dissipates, and oils no longer flow to the surface naturally. It must be pumped out by means of an "artificial lift"; a pump powered by gas or electricity.

Over time, these "primary" production methods become ineffective, and continued production requires the use of additional "secondary" production methods. One common method uses water to displace oil, using a method called "waterflooding," which provides the means of additional recovery by injecting water into the reservoir to help maintain the high pressure in the reservoir, thereby providing the energy to continue producing the oil.

Finally, producers may need to turn to "tertiary" or "enhanced" oil recovery methods. These techniques are often centered on increasing the oil's flow characteristics through the use of steam, carbon dioxide and other gases or chemicals [3]. For example, in the North Sea these new oil-extraction methods could extend the oil production past the point where half the reserve is removed [2].

1.3 Corrosion in the oilfield environments

Oilfield production environments can range from practically zero corrosion to very high rates of corrosion. Crude oil at normal production temperatures (less than 120°C) without dissolved gases is not, by itself, corrosive. The controls of corrosion in many oilfields are dependent on efficient separation of the crude oil from other species. While the rates may vary, the species causing the most problems are nearly universal. CO_2 and H_2S gases, in combination with water, define the most corrosive environments in oil and gas production.

A consequence of the advanced technologies that enables higher total production from a reservoir has been an increase in the corrosivity of oil production environments. Secondary and tertiary recovery techniques applied to old oilfields enable them to produce economically for many years after their predicted decline. The drilling of wells in deep water with higher temperature and pressure and in otherwise inaccessible areas offshore [4] adds to the complexity of production. Corrosivity increases for the following reasons:

- Oil, water and gas are produced in every oilfield. Water is reinjected downhole to maintain reservoir pressure and stability, and often waterflooding (using sea water or fresh water sources) is used to drive oil out of the formation. As the oil matures and the number of old fields relative to new fields increases, the number of aqueous environments increases and the corrosion becomes a more widespread problem.

- Water injection from seawater or fresh water sources contributes to "souring" of oilfields with H_2S, usually resulting in an increase in the corrosion rate.

- Tertiary recovery techniques are often based on miscible and immiscible gas floods. These gas floods invariably contain a high percentage of CO_2, which dramatically increases the corrosivity of the fluids produced. Consequently, over the last twenty-five years, CO_2 corrosion has become an intrinsic part of the petroleum industry.

1.4 Costs and controls of corrosion

The approximate annual economic cost of corrosion in the United States was first estimated in 1949 by Uhlig to be $5 billion, 2.1 % of GNP [5]. In 1971, a major study of the cost of corrosion in the United Kingdom carried out by the Government Committee on Corrosion and Protection found that in the oil and gas industry the estimated cost of corrosion was £180 million per year [6]. By 1976, the estimated cost of corrosion in the United States had risen to $70 billion, 4.2 % of GNP [6]. A recent survey [7] of BP Exploration's corrosion in the North Sea estimated that corrosion accounts for over 10 % of the lifting costs per barrel of oil.

The cost of corrosion in the oil and gas industry is extremely difficult to assess accurately. The corrosion cost issues range from added cost for the new construction, to maintenance cost on aging/corroding equipments, the costs of inspections and structural integrity evaluations, to the costs associated with corrosion related failures

and outages. Low cost materials are the natural choice for oil and gas production and transportation facilities. Unfortunately these materials (carbon steel, low alloy steel) have a low resistance to corrosion. Therefore, the corrosion risks of these materials have to be managed periodically. Corrosion monitoring is important because it allows plant engineering and management to be aware of the extent of damage caused by corrosion and also to be aware of the rate at which this damage is occurring. Although zero corrosion assumed as the baseline is unattainable, it is possible to keep corrosion under control using methods falling into the following four categories [8]:

- Design
- Using cathodic protection
- Coatings
- Conditioning the environment e.g. use of additives

Design in relation to corrosion is always a matter of economics. The designer's job is to achieve the desired life for minimum cost, whether capital, maintenance or replacement. The selection of a material which optimizes the corrosion resistance for a given component lifetime greatly reduces the need for a costly maintenance during that lifetime. Design against corrosion in steel pipe systems for undersea and underground pipelines is of particular importance as there is a danger of not only of loss and damage to the pipe structure but also of loss of the contents. A further consequence can be severe environmental damage.

Cathodic protection is extremely successful in reducing the rate of external corrosion of steel pipelines [9, 10]. Further, polyvinylchloride (PVC) pipe wraps, with and without epoxy resin, or bitumen paints are also used for external protection, but whatever the protective coating chosen, provision should be made for cathodic

protection [8]. For example, in the 1970s the installation of 4000 km of undersea steel pipelines in the North Sea [6] was achieved with zinc alloy sacrificial anodes combined with insulating coating to provide external corrosion protection. Although less popular, interior coating is also used to prevent corrosion. Dip-coating with PVC is found satisfactory for mild steel pipes where high pressures and relatively low temperatures are met [8].

Finally, conditioning the environment can help controlling the corrosion rate. In the oil and gas industries, this is usually done through the use of corrosion inhibitors. In general, inhibitors slow down the corrosion rate by affecting either the anodic and/or cathodic processes. The large majority of these inhibitors are organic compounds [11] (i.e. imidazolines and imidazoline salts, long chain quaternary amines, quaternary pyridine compounds, and phosphate esters) and function by adsorbing on the steel surface and inhibiting the anodic and/or cathodic reactions. Corrosion inhibitors must be economical and compatible with the environment to accomplish the adequate protection [12]. In practice, corrosion inhibitors are often used at concentrations varying from a few parts per million to thousands parts per million (ppm) [12], and are either applied batchwise or continuously depending on the facilities available for application and the severity of corrosion. Commercial inhibitors usually consist of one or two of the above inhibitor compounds in a solvent or solvent surfactant mixture, film enhancer and demulsifier [13].

However, inhibitors do not always perform as intended in the field [14, 15], the reasons for such problems are complex and not yet well understood. In laboratory tests inhibition is often studied on freshly polished surfaces. Many researchers [16-19] have shown that inhibitors perform differently on freshly prepared surfaces and corroded surfaces. In the field, inhibitors encounter steel surfaces that are covered with different kinds of corrosion products, such as mill scale from pipe production and rust from storage and pipeline testing. Furthermore, a pipeline may have been in operation for several years before increasing water cut necessitates the use of corrosion inhibitors. In this case, the metal surface might be covered with iron

carbonate precipitates and different types of scale. These products may significantly affect the performance of the corrosion inhibitors. In practice, the selection and application of corrosion inhibitors are complicated because the corrosion environments in the oil field are so variable.

1.5 CO_2 corrosion in the petroleum industry

1.5.1 The early days

Carbon dioxide corrosion is a relatively recent problem associated with the Petroleum Industry. In the 1920's, the very first studies into oil and gas corrosion began in the United States with an investigation by the Bureau of Mines followed by a comprehensive survey led by the American Petroleum Industry [20]. Both of these studies, however, only reported on general corrosion. The problems associated with CO_2 corrosion were only recognized by the oil and gas industry in the 1940s [21]. After ten years of intensive research the American Petroleum Industry published a set of recommendations but research slowly declined. However, in the early seventies as North Sea extraction began after BP discovered the huge Forties Field, the problems related with CO_2 corrosion re-appeared in Europe. Hence, there is an enormous surge in research into readdressing the problems of CO_2 corrosion in the oil and gas industry.

1.5.2 More recent times

The enhanced corrosion rate of pipeline carbon steels in oxygen – free, CO_2 – containing aqueous solutions has been a serious problem in the oil and gas industry for many years. In recent years, the interest in CO_2 corrosion has greatly intensified due to the development of new processes for the in – situ thermal recovery of heavy oil and secondary/tertiary recovery of conventional oil [22, 23]. Severe corrosion of well tubing, well casing and surface production facilities has been reported,

particularly when a low pH and high ratio water/oil are present [24, 25]. Carbon dioxide is found to cause enhanced rate of general corrosion and localized corrosion, sometimes as pitting corrosion [26]. Dissolution of CO_2 lowers the solution's pH, but the enhanced corrosion of carbon steels caused by CO_2 is greater than can be attributed to solution acidification [27]. Rosenfeld [28] reported that the corrosion rate in water is enhanced by a factor of 16 by the presence of CO_2.

The type of corrosion caused by dissolved CO_2 varies considerably according to the precise environmental conditions [26]. The severity of corrosion depends particularly on temperature, CO_2 partial pressure, pH and material characteristics [29-31]. Ikeda et al. [30] reported that the temperature where carbon steel shows the highest susceptibility to severe corrosion is around 100°C. The corrosion rate of carbon steel increases with the partial pressure of CO_2. De Waard et al. have published a monograph and estimate the corrosion rate from carbon dioxide partial pressure and temperature [32]. The presence of chromium (Cr) in the carbon steel (about 2 % by mass) allows the steel to be more corrosion resistant to general and localized corrosions below about 60°C. Ikeda et al. have shown the influence of Cr on the corrosion rate for CO_2 aqueous environments at 60°C: the higher the Cr content in the steel, the lower the corrosion rate [30]. However, for Videm et al. [33], the corrosion resistance of the carbon steel is not related to the Cr content alone. Other aspects, especially the carbon content and structure, have notably large effects. Further, for many researchers the effect of the steel microstructure also plays an important role in CO_2 corrosion [34-38]. It has been reported that normalized carbon steel with ferritic-pearlitic microstructure showed less localized corrosion at temperature below 80°C than the hardened and tempered alloy steel with martensitic microstructure [37, 38].

Recent studies on the corrosion of steel by CO_2 in the petroleum industry have clearly demonstrated that the nature of production waters plays a determining role in the mechanisms of this type of corrosion. In many oilfields, enhanced rates of carbon steel corrosion are thought to result from the presence in the brine of the

anions of weak acids, particularly acetate ion, typically at concentrations in the range of 1 – 2 mM. The effect of acetic acid and formic acid with condensed water, which was taken from a gas well, was investigated by Legezin et al. [39], and they reported the increase of the corrosion rate due to the addition of these organic acids. Possible mechanisms for the enhancement in the rate of corrosion of carbon steels in this situation have been discussed in several papers [40-47]. Hedges and McVeigh [42] investigated the role of acetate ions on the rate of CO_2 corrosion of carbon steel specimens. The linear polarization technique was used to determine the corrosion rate, and the results obtained showed that the presence of these acetate ions in the "water formation" of oilfield brines could significantly increase the rate of corrosion of carbon steel. The authors reported that even at low concentration (on a ppm scale), the presence of these acetate ions increases the corrosion rate more markedly than the presence of bicarbonate ions decreases it. They suggested that acetate ions could attack and reduce the iron carbonate films on the carbon steel.

1.5.3 The role of acetate in CO_2 corrosion of carbon steel

The question of the role of acetic acid is as old as CO_2 corrosion itself [20]. In the waters produced by oil and gas wells, the presence of anions of weak organic acids, mainly acetate ions, has been reported since the years 1940-1950 [48-50]. During that period, the question of the role of these organic species on the CO_2 corrosion of steels was raised, and very rapidly a certain correlation between the corrosivity of oil and gas and the presence of organic acids was found [48]. However, because the concept of in situ pH was not fully understood, it was not possible to distinguish between the acids and their dissociated forms (e.g. carboxylic acids and carboxylate ions). Similarly, the different species could not be identified separately. They were therefore simply described as "organic acids" [20] or, sometimes "propionic acid".

However, the concentration of these carboxylic species would still be too low to make the brine lastingly corrosive, even if they were in the acid form, Moreover, works published by Stock et al., involving short exposures of polished specimens, revealed no difference between CO_2 corrosion with and without acetic acid [51]. Finally, certain oilfields whose "formation water" contains considerable quantities of propionic acid/acetate were indeed not corrosive at all, constituting repeated exceptions to the correlation envisaged at the time. In 1950s, based on this field experience, together with few simple laboratory tests [51], it was concluded that CO_2 [50, 52] was principally responsible for the corrosion of the steels. The presence of organic acids was forgotten for about 30 years, and research was only focused on correlations [52] between corrosivity and the CO_2 partial pressure.

In the 1980s, better understanding of in situ pH showed fundamental errors in the previous approach [53]. Crolet et al. showed [40] that at the pH levels of produced waters, the propionic acid/acetate is, in fact, present in the form of both free acid and carboxylate anions, a classical buffer system. The authors also [40] suggested that the contribution of these organic buffers becomes rapidly minor compared to carbonic buffers. Nevertheless, in the 1950s CO_2 was thought to be the only source of acidity, and this explained why simple laboratory tests did not show any corrosion in the complete absence of CO_2 [51]. Further, in the "water formation", the two forms are present, acetate ions and free acetic acid, and their sum is generally referred to as the total acetates (i.e. acetic acid in the 1950s).

However, in the 1950s, certain fields containing high concentrations of propionic acid/acetate were found to be not corrosive at all, this simply implies that these acetates had been falsely assigned as acetic acid. Bonis et al. [54] showed that only acetate ions were present, and it is difficult to see how these could be a source of corrosivity. Further, Bonis et al. [54], have also shown that fields containing high concentrations of CO_2 were always corrosive, whatever the organic acids present. The one containing low concentrations of CO_2 are corrosive only in the presence of small amount of organic acids (free acetic acid). The correlation between the CO_2

partial pressure and corrosivity exits only when the free acetic acid concentration is taken into account, even at very low concentration.

1.6 Why does corrosion occur in crude oil?

Crude oil consists of a highly complex mixture of hydrocarbons [55], which often contains significant quantities of dissolved and free gases, notably CO_2 and H_2S. During the recovery of oil and gas, an aqueous brine saturated with carbon dioxide is one component of a multiphase flow through carbon steel pipes. The principal cause of corrosion in crude oil is due to the presence of "formation water" that accompanies the oil. If the carbon steel is in contact with the hydrocarbon rather than the "formation water" then corrosion does not occur.

In practice, the steel is in contact with an emulsion of oil and brine varying in concentration from 1 to 10% NaCl [56] and contains various amounts of inorganic ions [53] such as Ca^{2+}, Mg^{2+}, K^{+}, $SO_4^{2-}$and Cl^{-} saturated with carbon dioxide and sometimes containing a weak organic acid such as acetic acid [40, 42, 57]. Metals in aqueous environments corrode by an electrochemical mechanism. The theoretical basis for electrochemical corrosion testing is derived from the mixed potential theory, the formulation of which is usually attributed to Wagner and Traud [58]. This theory separates the oxidation and the reduction reactions and postulates that the total rates of all oxidation reactions are equal to the total rates of all reduction reactions on a corroding surface. That is, the sum of the anodic oxidation current must equal the sum of the cathodic reduction currents. This must be true to avoid accumulating charge on the metal. Oxidation reactions occur at the anodic sites on a corroding metal or at the anode in an electrochemical cell and in the case of steel can be represented by the reaction:

$$Fe \rightleftharpoons Fe^{2+} + 2e^{-} \qquad (1)$$

This is the generalized corrosion reaction that removes the metal atom by oxidizing it to its ion. In this reaction, the number of electrons produced equals the valence of the metal ion produced. The mixed potential theory proposed that all the electrons generated by the anodic reactions are consumed by corresponding reduction reactions. Reduction reactions occur at the cathodic sites of a corroding metal or the cathode of an electrochemical cell. Possible cathodic reactions (electron-consuming) include:

1. Evolution of hydrogen from aqueous solutions,

$$2H^+ + 2e^- \rightleftharpoons H_2 \text{ (acidic solutions)} \quad (2)$$

$$2H_2O + 2e^- \rightleftharpoons H_2 + 2OH^- \text{ (neutral or alkaline solutions)} \quad (3)$$

2. Reduction of dissolved oxygen in acid or neutral solutions,

$$O_2 + 4H^+ + 4e^- \rightleftharpoons 2H_2O \text{ (acidic solutions)} \quad (4)$$

$$O_2 + 2H_2O + 4e^- \rightleftharpoons 4OH^- \text{ (neutral or alkaline solutions)} \quad (5)$$

3. Reduction of a dissolved oxidizer in a redox reaction such as,

$$Fe^{3+} + e^- \rightleftharpoons Fe^{2+} \quad (6)$$

Other cathode reactions are possible, the only criteria are that the reaction must consume the electrons produced by the anode process and that the overall energy change associated with the corrosion chemistry must be favourable. Consequently, crude oil corrosion increases with the ratio of "formation water" to oil.

1.7 Kinetics of an electrode reaction [59, 60]

In this thesis, voltammetry is used extensively for the study of corrosion. The conclusions result from analysis (a) close to the corrosion potential and (b) at potentials away from the corrosion potential. The kinetic of a simple electron transfer reaction:

$$O + ne^- \rightleftharpoons R \qquad (7)$$

is given by the Butler – Volmer equation:

$$j = j_o\left[\exp\left(\frac{\alpha_a nF}{RT}\eta\right) - \exp\left(-\frac{\alpha_c nF}{RT}\eta\right)\right] \qquad (1\text{-}1)$$

α_a and α_c are constants (between 0 and 1 and generally approximately 0.5) known as the transfer coefficients for anodic and cathodic reactions respectively, and η, the overpotential is defined as the deviation of the potential from the equilibrium potential for the couple O/R, i.e.

$$\eta = E - E_e \qquad (1\text{-}2)$$

E_e, the equilibrium (or reversible) potential, is given by the Nernst equation:

$$E_e = E_e^0 + \frac{RT}{nF}\ln\frac{c_O^\sigma}{c_R^\sigma} \qquad (1\text{-}3)$$

E_e is related to the standard potential of the couple O/R, E_e^0, and the surface concentrations of O and R, c_O^σ and c_R^σ. j_o, the exchange current density, is a measure of electron transfer activity at equilibrium potential (i.e. $\eta = 0$). The Butler – Volmer equation must be regarded as the fundamental equation of electrode kinetics, and it

shows the way in which current density varies with exchange current density, overpotential, and the transfer coefficients.

Above a critical value of the overpotential, one of the exponential terms of equation (1-1) may be omitted. Thus for sufficiently positive values of the overpotential, equation (1-1) has a limiting form:

$$j = j_o \exp\left(\frac{\alpha_a nF\eta}{RT}\right) \tag{1-4}$$

Taking base 10 logarithms and rearranging equation (1-4), the anodic current density is given by:

$$\log j = \log j_o + \frac{\alpha_a nF}{2.3RT}\eta \tag{1-5}$$

Conversely at high negative overpotentials, the cathodic current density is given by:

$$\log(-j) = \log j_o - \frac{\alpha_c nF}{2.3RT}\eta \tag{1-6}$$

Equations (1-5) and (1-6) are known as the Tafel equations (named after Tafel [61]) and are the basis of a simple method of determining the exchange current density and a transfer coefficient.

1.8 Kinetics of corrosion [8, 62, 63]

When a metal is in contact with either a solution or even a film of aqueous solution, it will corrode and in the case of steel, this can be represented by the reaction:

$$Fe \rightleftharpoons Fe^{2+} + 2e^- \quad (1)$$

On open circuit, reduction reactions occur at the surface of the corroding steel so that no net current flows. To simplify the discussion, it will be assumed that the cathodic reaction is hydrogen evolution

$$2H_2O + 2e^- \rightleftharpoons H_2 + 2OH^- \quad (2)$$

Since both these reactions are occurring at potentials well displaced from the equilibrium potential for the reaction, the rate of these reactions can be written in terms of Tafel equations:

$$j_a = j_{a,0} \exp\left(\frac{\alpha_a nF}{RT}\left[E - E_e^a\right]\right) \quad (1\text{-}7)$$

$$j_c = j_{c,0} \exp\left(-\frac{\alpha_c nF}{RT}\left[E - E_e^c\right]\right) \quad (1\text{-}8)$$

where $j_{a,0}$ is the exchange current density for the Fe/Fe^{2+} couple,

$j_{c,0}$ is the exchange current density for hydrogen evolution,

E_e^a is the equilibrium potential for the Fe/Fe^{2+} couple

E_e^c is the reversible potential for H_2/H^+ couple,

E is the applied potential.

Simplifying equation (1-7) and (1-8) gives:

$$j_a = j_{a,0} \exp\left(\frac{E - E_e^a}{b_a}\right) \quad (1\text{-}9)$$

$$j_c = j_{c,0} \exp\left(\frac{E_e^c - E}{b_c}\right) \quad (1\text{-}10)$$

where b_a and b_c are constants given by:

$$b_a = \frac{RT}{\alpha_a nF} \quad (1\text{-}11) \qquad b_c = \frac{RT}{\alpha_c nF} \quad (1\text{-}12)$$

When corroding, the surface of the metal will take up a potential, commonly referred to as "the corrosion potential," denoted by the symbol E_{corr}, where no net current flows. At the corrosion potential, the total rate of the anodic reaction (i.e. oxidation of Fe) is equal to the total rate of the cathodic reaction (i.e. hydrogen evolution). In other words, the current for the oxidation of the metal must be balanced by the current for the reduction of water:

$$-j_c = j_a \quad (1\text{-}13)$$

where j_c and j_a are the cathodic and the anodic current density respectively.

Figure 1.2 shows a typical current-potential curve for metal in such solution; the dashed curves show the individual contributions of the anode and the cathode reactions to the measured current. The corrosion potential, E_{corr}, is an example of a mixed potential. It can be seen that its value depends on current-potential curve response and, therefore on the thermodynamics and kinetics of two independent electrode reactions, the oxidation of the metal and hydrogen evolution. The corrosion potential for a metal in a particular environment can be determined from a current–potential curve as shown in figure 1.2 or it may be measured versus a reference electrode directly using a digital voltmeter.

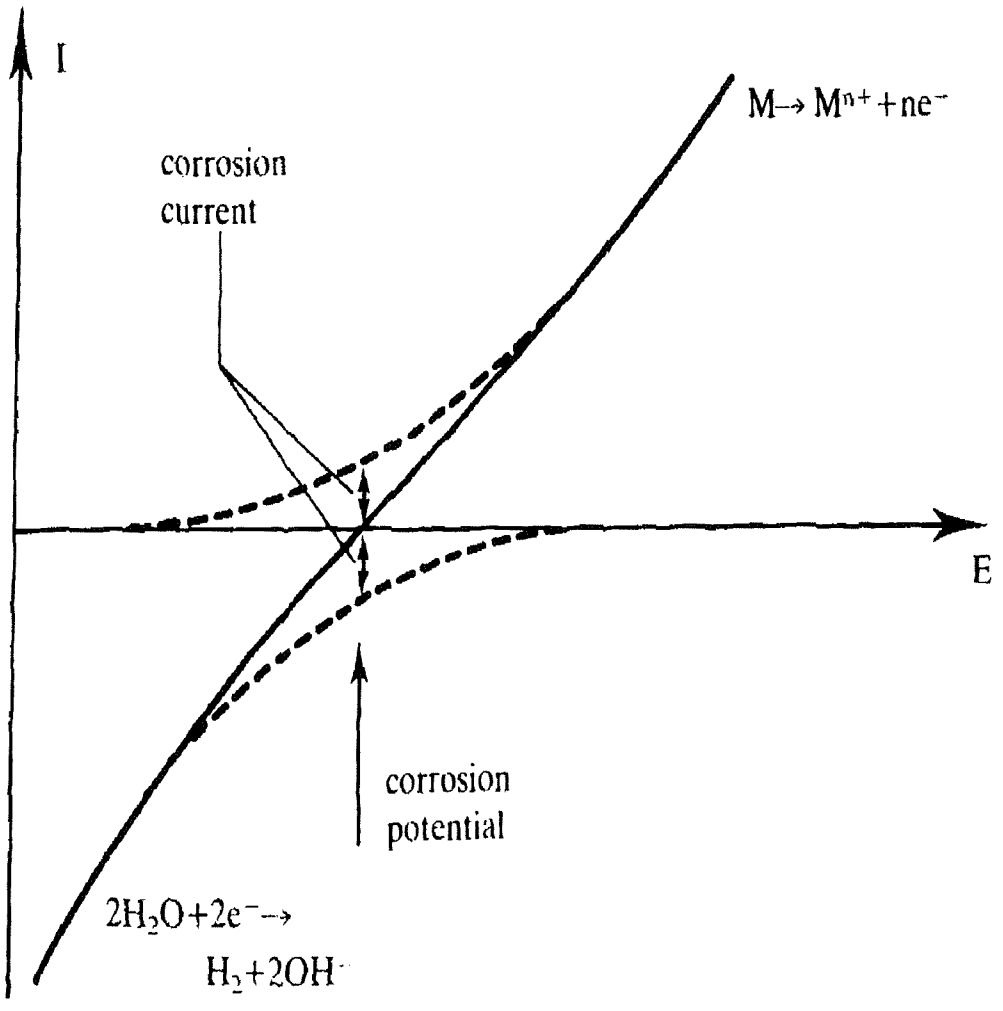

Figure 1. 2 *Current-potential curves for a metal in a deoxygenated aqueous solution. The dashed curves show the partial current for the oxidation of the metal and hydrogen evolution [60].*

At any potential away from E_{corr}, according to the mixed potential theory, the net measured current density is given by:

$$j = j_a + j_c \qquad (1\text{-}14)$$

By substituting equations (1-9) and (1-10) into equation (1-14) we obtain an expression for the current density as a function of potential:

$$j = j_{a,0} \exp\left(\frac{E - E_e^a}{b_a}\right) - j_{c,0} \exp\left(\frac{E_e^c - E}{b_c}\right) \quad (1\text{-}15)$$

At the corrosion potential, E_{corr}, although no net current is observed, both iron oxidation and hydrogen evolution are taking place but at equal rate. The current density at the corrosion potential for each of these reactions is called the "corrosion current density", j_{corr}, and is related to metal loss by Faraday's law [60]:

$$\Delta w = \frac{j_{corr} M}{nF} \quad (1\text{-}16)$$

where Δw is the rate of corrosion (in kg m^{-2} s^{-1}), j_{corr} is the corrosion current density (in A m^{-2}), M is the atomic weight of the metal (kg mol^{-1}) and F is the Faraday constant (in C mol^{-1}).

Further, at the E_{corr}, the total current density is zero, therefore

$$-j_c = j_a = j_{corr} \quad (1\text{-}17)$$

Hence, we obtain:

$$j_{corr} = j_{a,0} \exp\left(\frac{E_{corr} - E_e^a}{b_a}\right) = -j_{c,0} \exp\left(\frac{E_e^c - E_{corr}}{b_c}\right) \quad (1\text{-}18)$$

By combining equations (1-15) and (1-18), the relationship between the net current density, j, the corrosion current density, j_{corr}, and the corrosion potential, E_{corr}, is obtained:

$$j = j_a + j_c = j_{corr}\left[\exp\left(\frac{E - E_{corr}}{b_a}\right) - \exp\left(\frac{-(E - E_{corr})}{b_c}\right)\right] \quad (1\text{-}19)$$

This equation resembles the Butler – Volmer equation for a single reaction. However it should be stressed out that the derivation of this equation mattes several assumptions [64, 65]:

- There are no competing secondary reactions.
- Mass transfer plays no part in controlling the rates of iron oxidation or hydrogen evolution.
- Both reactions are charge transfer controlled.
- The entire surface behaves as cathode and anode rather than the reactions occurring at particular sites.
- Ohmic drops in the solution and at the surface of the electrode are negligible.

If we consider the anodic part of equation (1-19) i.e. at a potential significantly positive to the corrosion potential:

$$j_{a,0} = j_{corr} \exp\left(\frac{E - E_{corr}}{b_a}\right) \qquad (1\text{-}20)$$

Taking base 10 logarithms and rearranging equation (1-20), the anodic current density is given by:

$$\log j_{a,0} = \log j_{corr} + \frac{E - E_{corr}}{2.3 b_a} \qquad (1\text{-}21)$$

Conversely, at potentials significantly negative to the corrosion potential, for the cathodic process, the cathodic current density is given by:

$$\log(-j_{c,0}) = \log j_{corr} - \frac{(E - E_{corr})}{2.3b_c} \quad (1\text{-}22)$$

Equations (1-21) and (1-22) are similar to equations (1-5) and (1-6). They are the basis of a simple method of determining the corrosion current density, j_{corr}, and the Tafel slopes for the two reactions. These relationships are best represented graphically on a plot of the logarithm of the current against potential as illustrated in figure 1.3.

1.8.1 Measurement of corrosion rate by extrapolation

The corrosion current cannot be determined directly from the current-potential curve (i.e. the experimental current is zero at the corrosion potential). The corrosion current can, however, be determined by measurement of steady state current density for both hydrogen evolution and Fe oxidation as a function of potential and extrapolation of the currents to the corrosion potential (of course, they should be the same and equal to the corrosion current). The extrapolation is carried out by plotting $\log j$ vs. E when the data for each electrode reaction should give a linear plot (or Tafel plot), as illustrated in figure 1.3.

The principles behind the extrapolation technique can be understood from the following procedure. The specimen is initially made to act as a cathode in the electrochemical cell. The cathodic $\log j$ vs. E curve is measured over the potential range defined by E_{corr} and some potential negative to E_{corr} as shown schematically by the continuous line in figure 1.3. Increasing the applied potential in the positive direction away from E_{corr} now makes the specimen act as an anode. The anodic current increases with increasing positive potential, giving rise to measured anodic process shown in figure1.3.

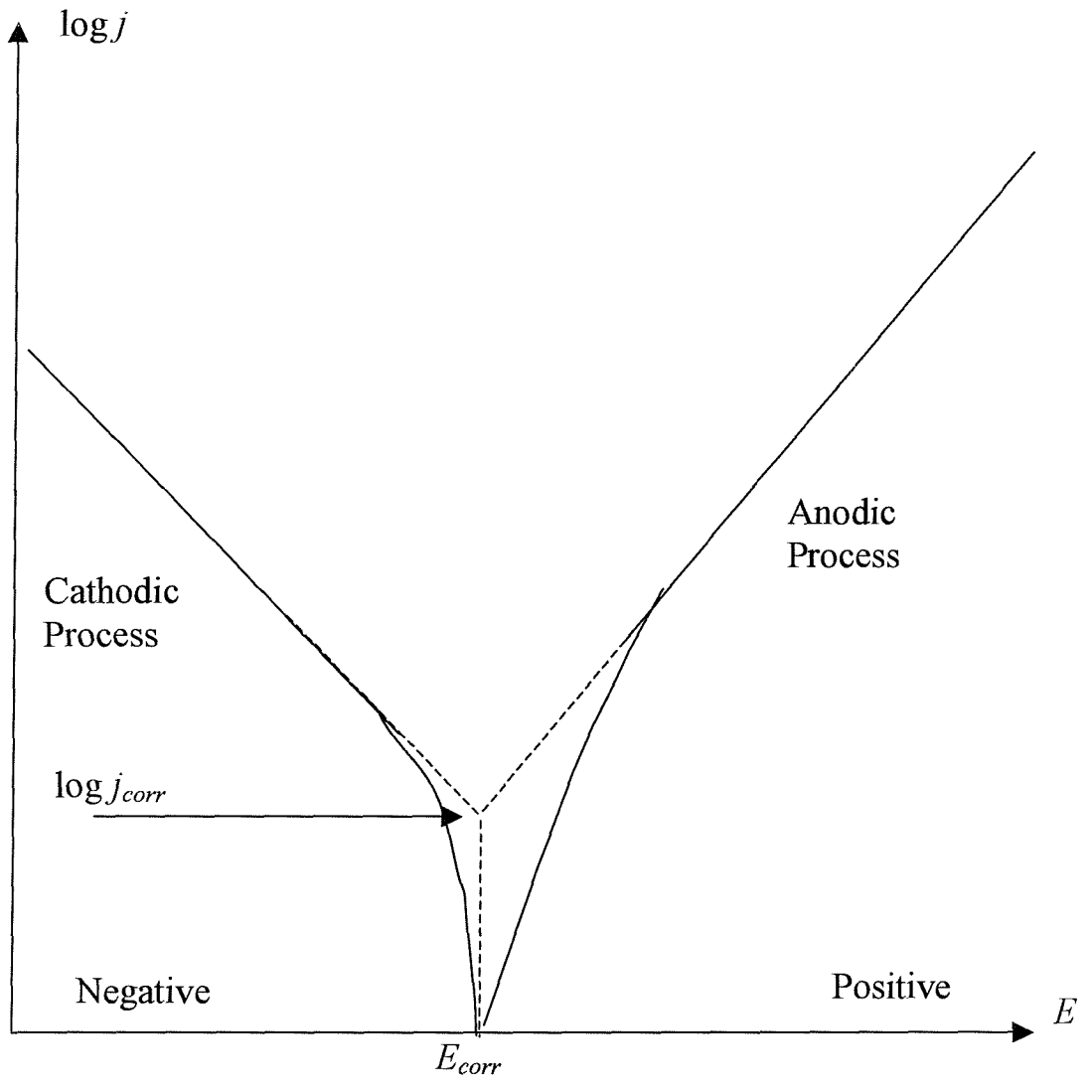

Figure 1. 3. *A schematic illustration of a Tafel plot.*

The extrapolation technique for measuring j_{corr} depends on the ability to identify a linear Tafel region. Corrodents in which more than one reduction reaction is operative or in which the rate of arrival of the reductive species (e.g. hydrogen ions) at the cathode surface begins to determine the reduction rate (i.e. mass transfer [66]) exhibit less distinct linear regions, making extrapolation less certain. It is essential to obtain a polarization curve in which the linear Tafel region spans over a range of at least two orders of magnitude of the current density [66]. However, these disadvantages can largely be overcome using the linear (resistance) polarization technique.

1.8.2 Measurement of corrosion rate by linear (resistance) polarization

The value of j_{corr} can also be measured by another technique known as "linear polarization" and is due to Stern, Geary and Weisert [66, 67]. This technique is based on the theoretical and practical demonstration that at potentials very close to E_{corr} ± 10 mV, the plot of the potential – current curve is approximately linear, as illustrated in figure 1.4. Its greatest attraction is that the measurement does not interfere significantly with the corroding system due to the relatively small perturbations used (i.e. E_{corr} ± 10 mV).

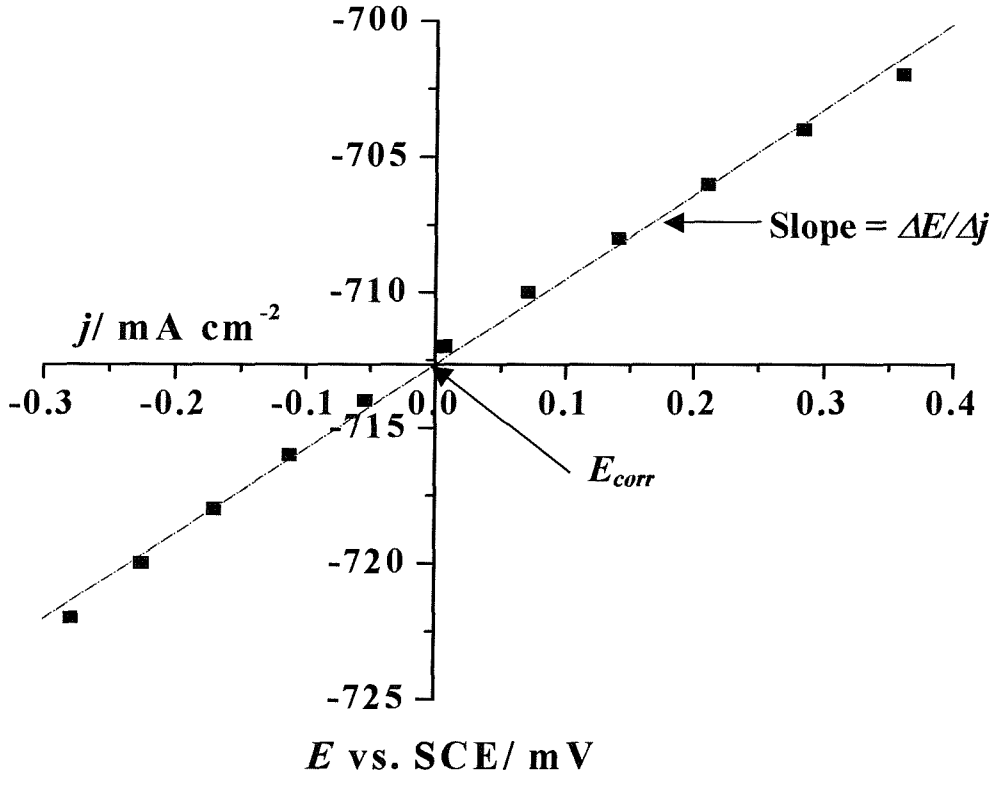

Figure 1. 4 *Measurement of the corrosion rate by linear polarization.*

This slope, $\Delta E/\Delta j$, has the units of resistance; hence, the technique is sometimes called the "polarization resistance technique". Accepting the constancy of the slope $\Delta E/\Delta j$, it has been shown [66, 67], that j_{corr} is related to the inverse of this slope by the equation referred to as the Stern – Geary equation:

$$j_{corr} = \left[\frac{b_a b_c}{(b_a + b_c)}\right]\frac{\Delta j}{\Delta E} \qquad (1\text{-}23)$$

where b_a and b_c are taken from the experimental Tafel plots. Equation (1-23) is commonly written as:

$$j_{corr} = \left[\frac{\beta_a \beta_c}{2.3(\beta_a + \beta_c)}\right]\frac{\Delta j}{\Delta E} \qquad (1\text{-}24)$$

where β_a and β_c are the anodic and cathodic Tafel slopes, respectively. It should be noted that β_a is referred to as the inverse of the slope of the Tafel plot. Hence,

$$\beta_a = \frac{1}{anodic\ slope} \qquad anodic\ slope = \frac{1}{2.3b_a}$$

therefore $\beta_a = 2.3b_a$ and similarly $\beta_c = 2.3b_c$

According to Stern, the quotient $\Delta E/\Delta j$ is called polarization resistance by analogy to $R = E/I$ from conventional Ohms law. Clerbois [68] has suggested that the inverse, $\Delta j/\Delta E$, be called the corrodance by obvious analogy to the inverse of electrical resistance, which is the "conductance". It is generally accepted that the quantity $\beta_a\beta_c/2.3(\beta_a + \beta_c)$ is a constant C. Hence; j_{corr} is given by the relationship:

$$j_{corr} = C\left(\frac{\Delta j}{\Delta E}\right) \qquad (1\text{-}25)$$

However, to ultimately evaluate the corrosion rate it is essential to determine the value of C. This may be determined either experimentally or estimated [8]. As in the paper by Hedges and co-workers [42] and generally in corrosion laboratories in the oil industry, the Tafel slopes for hydrogen evolution and iron dissolution were taken

as 120 mV and 60 mV respectively. Equation (1-24) provides a unique basis for rapidly measuring relative corrosion rates or changes in corrosion rate. The advantages of electrochemical corrosion rate measurements, particularly linear polarization techniques are:

- ❖ They permit rapid corrosion rate measurements and can be used to monitor corrosion rate in various process streams.

- ❖ These techniques may be used to accurately measure very low corrosion rates, which are both difficult and tedious to perform with conventional weight loss or chemical analytical techniques. The measurement of low corrosion rates is especially important in nuclear, pharmaceutical and food processing industries, where trace impurities and contamination are problems.

- ❖ Electrochemical corrosion rate measurements may be used to measure the corrosion rates of structures, which cannot be visually inspected or subjected to weight loss tests. Underground pipes and tanks and large chemical plant components are examples.

In the early 1950s, using an assumption based on weight loss experiments; works done by Bonhoeffer and Jena [69], Simmons [70], and Skold et al. [71] showed an empirical correlation between the value of the slope $\Delta E/\Delta j$ and the corrosion rate in the proximity of E_{corr}. The term "polarization resistance" was suggested by Bonhoeffer and Jena [69]. It was in fact Stern and Geary [66] who proved the linear relationship based on the mixed potential theory and the electron transfer kinetics. In 1958, Stern [72] showed how linear polarization could be used to evaluate corrosion rates. Stern and Weisert [67] showed that it could apply to systems with activation or diffusion controlled $(\beta_c = \infty)$ reduction reactions and yields corrosion rates differing by no more than a factor of three from the actual rates. However, it should be noted that in earlier work [67], it was shown that corrosion rates determined by linear

polarization are in good agreement with corrosion rates obtained by weight loss methods.

In 1961, a study by Evans and Koehler [73] involving monitoring the corrosion rate of two Al alloys in the food industry highlighted the potential of the linear polarization technique to measure the corrosion rate in food processing industries, when other techniques such as weight loss and gas evolution proved invalid. Kilpatrick [74] was the first to describe an electrode system involving all three electrodes made from mild steel, for use in oilfields. The technique was modified by Wilde [75] to measure in situ corrosion rates within water-cooled nuclear reactors. An evaluation employing mathematical and graphic methods has led to the conclusion that the various assumptions of linearity are sufficient for the technique to be valid in many practical corrosion systems [76]. Since those early days linear polarization techniques have gained worldwide acceptance and have been used successfully in a wide variety of environments. Accordingly, it must be accepted that linear polarization is a useful, if approximate, electrochemical technique for measuring the corrosion rates.

1.8.3 Measurement of corrosion rate using other techniques

Traditionally, corrosion coupons are often used for corrosion monitoring both in laboratory and field. The corrosion coupons are carefully measured and weighed before exposure to the environment of interest. After exposure, they are cleaned and dried, and re-weighed and then the corrosion rates are calculated in millimeter per year. One should also record special observations concerning localized corrosion, such as pitting, crevice corrosion etc...

Based on the electrochemical nature of a corrosion process, electrochemical techniques have been developed for corrosion monitoring. Technology for corrosion is advancing rapidly, and laboratory development of sophisticated electrochemical

techniques is noteworthy, including impedance spectroscopy and electrochemical noise measurements.

Electrochemical impedance is usually measured by applying an AC potential to an electrochemical cell and measuring the current response through the cell as a function of frequency (frequency range from millihertz to around 100 kHz). Normally this AC potential is a small excitation signal. Suppose that a sinusoidal potential is applied, the response to this potential is an AC current containing the excitation frequency and its harmonics. This current signal can be analysed as a sum of sinusoidal functions (Fourier series). Measurements are made over a wide range of frequencies, producing the electrochemical spectrum. A number of display formats may be used in helping the investigator to understand and analyse impedance data to determine the individual element of the equivalent circuit. The familiar Nyquist and Bode plots are model independent representations of electrochemical impedance spectroscopy and therefore are the first choice of analysis methods [77-79]. Application of this method to corrosion problems has become widespread and many authors have described this technique [80-84].

Because AC methods use measurement of impedance over a broad range of frequencies, they are capable of giving more detailed information than LPR. It has been used for identifying corrosion reaction mechanisms, and methods are now being developed to extract kinetics parameters (rate constant, transfer coefficients) for multistep reaction schemes [85]. However, unlike polarization resistance, the instrumentation available for the field is the same as used in the laboratory, using computers and running on mains electrical power. Sub-millihertz frequency signal measurements normally are required to obtain more complete corrosion impedance spectra. Each such measurement can last for several hours. This would be a time consuming experiment without the aid of computer-controlled instruments. The higher skill required to interpret results, the instrumentation, and power requirements are some of the limitations of electrochemical impedance spectroscopy for routine pipeline corrosion monitoring.

A technique, which is attracting much attention at present, is the measurement and analysis of electrochemical noise, apparently random behavior emanating from corroding systems. Electrochemical measurements are represented by data records in which current or potential variations are plotted as a function of time. This method is particularly valuable since it allows the measurement of corrosion rates and study of corrosion phenomena without the need of any disturbance of the corroding specimen. The use of this technique for the study of corrosion problems has been investigated by various authors [86-89]. Gabrielli et al. [90] have shown that the noise signal may be generated by rupture events in passive oxides, hydrogen gas evolution, or other causes. In practice, shifts of potential ("potential noise") can be measured, or currents passing when the potential is maintained constant ("current noise"). Essentially there are two methods of measuring potential noise:

- The potential of one working electrode is measured relative to a low noise reference electrode.

- The potential between two equivalent working electrodes is measured.

As with potential noise, there are two ways of measuring current noise:

- The current flowing to a potentiostatically-controlled electrode can be recorded.

- The current flowing between two working electrodes can be measured. This has the advantage that the potential of the electrodes will find its own level. This also means that the potential noise of the couple pair may be measured at the same time as the current noise.

The easiest way to quantify noise is by the standard deviation of the signal about its mean value. This method was suggested by Hladky and Dawson as a measure of corrosion rate [87]. Several other workers have used this method to evaluate

corrosion rates [89, 91]. Roberge et al. [92] suggested that the simplest way to measure noise was by measuring current noise between two identical electrodes through a low value resistor. This reduces the risk of extraneous noise from instruments. Electrochemical noise technique has the same type of field instrumentation limitations as electrochemical spectroscopy.

However, linear polarization resistance (LPR) is perhaps the singly most important technique and has already been used in industrial practice for many years. Its working principle has been described in the previous section. Polarisation resistance methods, and the instrumentation for LPR are available commercially.

1.9 Mechanisms of Carbon dioxide corrosion

A range of possible mechanisms for carbon dioxide induced corrosion in oxygen free environments has been put forward. The presence of CO_2 can influence both iron oxidation and hydrogen evolution. When CO_2 is added to an aqueous solution it first hydrates to give a weak acid, carbonic acid (H_2CO_3) [93]:

$$CO_2 + H_2O \rightleftharpoons H_2CO_3 \qquad (8)$$

and then the carbonic acid dissociates in two steps to give bicarbonate and carbonate anions [93],

$$H_2CO_3 \rightleftharpoons H^+ + HCO_3^- \qquad (9)$$

$$HCO_3^- \rightleftharpoons \tfrac{1}{2} H_2 + CO_3^- \qquad (10)$$

Leading to an acidic solution (pH 3.90). In acidic solutions (pH < 4) only a small fraction of dissolved CO_2 exists as H_2CO_3 [94]. Dissolution of CO_2 lowers the solution's pH, but the enhanced corrosion of carbon steels cause by CO_2 is greater than can be attributed by the solution acidification [95]. The hydration of CO_2 is,

however, a slow reaction, $K_1 = 3.42 \times 10^{-2}$ [96]. Also present in solution is carbonic acid, $pK_A = 3.75$ [97] and carbon dioxide, $pK_A = 6.35$ [97]. The equilibrium concentrations of carbonic acid and carbon dioxide at 1 atm are 0.074 mM and 29 mM respectively.

CO_2 has a clear accelerating effect on the reduction rate in deoxygenated solutions. There appears to be complete agreement among researchers that high corrosion rates in CO_2 solutions can be explained, at least in part, by CO_2 increasing the electrochemical reduction [98]. In CO_2 saturated solutions, the most important cathodic reaction is hydrogen evolution [99]:

$$2H^+ + 2e^- \rightleftharpoons H_2 \qquad (2)$$

and it has been shown that the rate determining step in the hydrogen ion reduction can be the diffusion rate of H^+ ions from the bulk solution. Unfortunately in CO_2 corrosion of carbon steels, it still remains ambiguous, which is the determining step. Several people have proposed that the cathodic reaction controls the rate of corrosion in CO_2 solutions [100, 101] at temperatures below 60°C, with the corrosion rate increasing with the partial pressure of the gas. This is consistent with the observation by many researchers [95, 102-107] that the cathodic evolution of hydrogen is accelerated by dissolved CO_2.

In CO_2 system at low pH (pH < 4) the hydrogen ion reduction is still the dominant cathodic reaction due to the high concentration of H^+ ions. At intermediate pH (4<pH<6), in addition to the hydrogen ion reduction, a new cathodic reaction becomes important, the direct reduction of carbonic acid:

$$H_2CO_3 + e^- \rightleftharpoons \tfrac{1}{2} H_2 + HCO_3^- \qquad (11)$$

This additional cathodic reaction is often listed as the cause for the carbonic acid to be more corrosive than a completely dissociated acid at the same pH [108]. Several

authors have proposed very detailed mechanisms involving both hydration of CO_2 in the solution (a reaction known to be slow) [95, 104, 108], or on the steel surface [98, 102]. In general, the evidence for these multistep sequences is very weak. Gray et al. [109] presented a detailed analysis for the reduction of aqueous carbon dioxide on a rotating carbon steel electrode. The results obtained showed that the addition of carbon dioxide to the brine increases the reduction current by introducing an additional reduction reaction in which carbon dioxide is hydrated to carbonic acid which is then reduced to hydrogen as illustrated below:

$$CO_{2(aq)} + H_2O \longrightarrow H_2CO_{3(aq)} \qquad (12)$$

$$2H_2CO_{3(aq)} + 2e^- \longrightarrow H_{2(g)} + 2HCO_3^-{}_{(aq)} \qquad (13)$$

This mechanism was confirmed, when the authors showed that the limiting current density was identical to that estimated assuming a preceding chemical reaction with the known rate constant for carbon dioxide hydration.

The effects of temperature and pressure have also been considered, with the rate of reduction of CO_2 species to hydrogen increasing with increasing temperature [101, 110]. The reaction rate increases as the CO_2 solubility increases with increasing the CO_2 partial pressure [32]. The concern is not only any interference CO_2 may have, but also the role of pH and of buffering capacity. Hurlen at al. [105, 111] have shown that the rate of cathodic reaction in the absence of CO_2 is affected not only by the pH but also by the buffer capacity, as expressed by its concentration. Huerlen et al. [105, 111] have found that in sufficient concentration of acetate buffer no effect of CO_2 can be seen at low overpotentials with respect to the corrosion potential.

The role of CO_2 on the anodic reaction of ferrous materials has been reported in some detail. Several mechanisms [112-116] have been reported by which H_2CO_3 and HCO_3^- accelerate the rate of the anodic reaction. Rogers and Rowe [112]

proposed that the carbonic acid reacts with iron to form iron carbonate, via iron bicarbonate, as shown below:

$$Fe + 2H_2CO_3 \longrightarrow Fe(HCO_3)_2 + H_2 \quad (14)$$

$$Fe(HCO_3)_2 \longrightarrow Fe^{2+} + 2HCO_3^- \quad (15)$$

$$HCO_3^- \longrightarrow H^+ + CO_3^{2-} \quad (16)$$

$$Fe^{2+} + CO_3^{2-} \longrightarrow FeCO_3 \quad (17)$$

Davies and Burstein [117] suggested that the accelerated reaction in a mildly alkaline bicarbonate solution was due to the formation of the complex ion, $Fe(CO_3)_2^{2-}$ from carbonate and iron via iron carbonate, and that the reaction rate is controlled by the diffusion of this complex species away from the metal surface as illustrated by the following reactions sequence:

$$Fe + 2H_2O \longrightarrow Fe(OH)_2 + 2H^+ + 2e^- \quad (18)$$

$$Fe + HCO_3^- \longrightarrow FeCO_3 + H^+ + 2e^- \quad (19)$$

$$Fe(OH)_2 + HCO_3^- \longrightarrow FeCO_3 + H_2O + OH^- \quad (20)$$

$$FeCO_3 + HCO_3^- \longrightarrow Fe(CO_3)_2^{2-} + H^+ \quad (21)$$

The mechanism proposed by Castro et al. [114, 115] involves the formation of another complex ion, this time proposed as $Fe(HCO_3)^+$. However, in these water/CO_2 corroding systems it has most often been assumed that the sequence of anodic dissolution of iron is the same as in other acids, the pH dependent mechanism proposed by Bockris et al. [118]:

$$Fe + OH^- \longrightarrow FeOH + e^- \quad (22)$$

$$FeOH \longrightarrow FeOH^+ + e^- \quad (23)$$

$$FeOH^+ \longrightarrow Fe^{2+} + OH^- \quad (24)$$

The formation of solid corrosion product layers and their specific identities affect the rate and the mechanism of carbon steel corrosion in aqueous CO_2 solutions [98, 119, 120]. Works at higher temperatures [26, 101, 116] have suggested that a solid film of $FeCO_3$ can form on the surface of the carbon steel and form an effective shield against corrosion. It was found [26, 116] that this could occur at temperatures as low as 40°C, and that its stability is strongly dependent on the flow characteristics of the system. In general, ferrous carbonate films significantly reduce the rate of uniform corrosion and figure prominently in the behavior of carbon steels serving in CO_2 environments [119, 120]. It can be seen from the above summary that the roles attributed to CO_2 in the corrosion of carbon steel are numerous and varied. All the main possible reactions that could occur in CO_2 corrosion are summarized in figure 1.5.

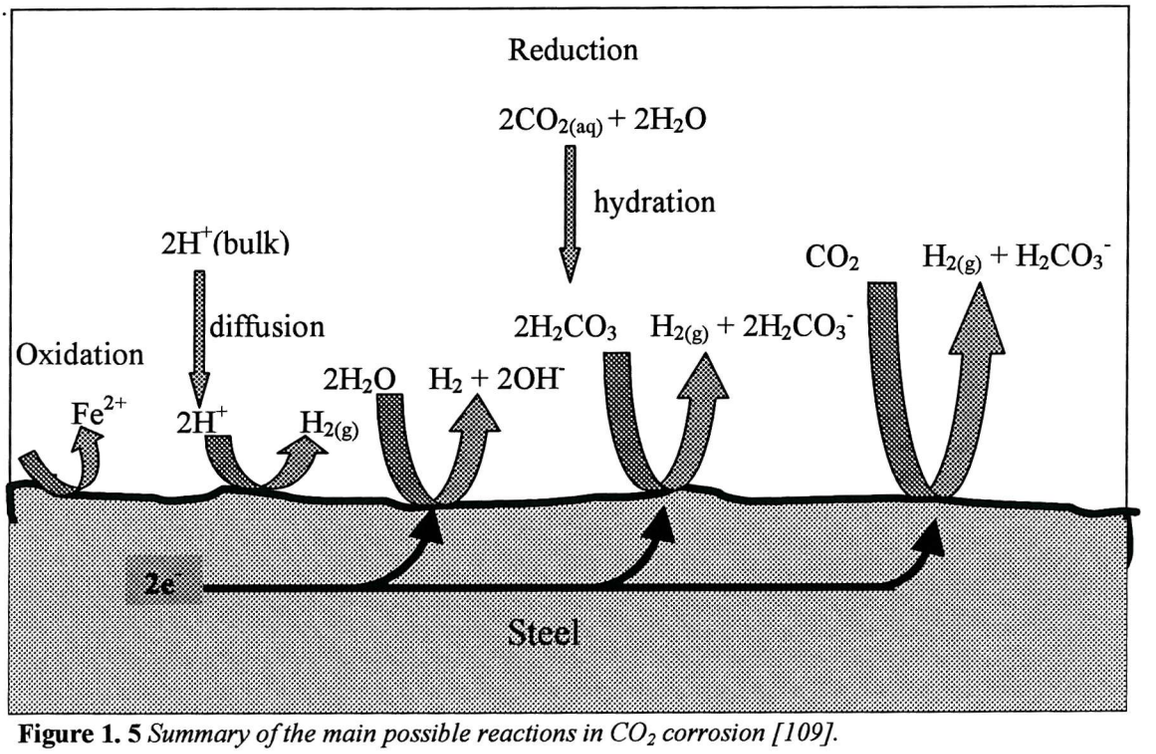

Figure 1. 5 *Summary of the main possible reactions in CO_2 corrosion [109].*

The overall reaction of CO_2 corrosion can be written as follows [93]:

$$Fe + H_2CO_3 \longrightarrow FeCO_3 + H_2 \qquad (25)$$

and is dependent on the pH, CO_2 partial pressure and temperature [29, 32, 110].

1.10 Electrochemistry of Acetic/Acetate and other Weak Acid Buffers at Pt Electrode

The electrochemistry of weak acids in aqueous solutions is not a new topic and the early work is summarized in two books [121, 122]. In the period 1960-1963, two papers used voltammetry at Pt rotating disc electrodes [123, 124] to define the mechanism and kinetics of the reduction of acetic acid in acetate buffers. More recently, with the development of Pt microelectrodes, the reduction of protons from solutions containing strong and weak acids has been the object of several investigations [125-134]. Measurements have been carried in solution with and without supporting electrolyte, and the effects of ionic strength on mass transport properties have been examined [126-129]. Other workers [125, 130, 131, 133] have focused their interests on verifying the kinetics of the electrode process involved in the reduction of these weak monoprotic acids.

Pt microelectrodes have been used intensively because they offer several unique properties [135-137] (steady state currents at short time, high rates of mass transfer to the electrode surface, electrochemical measurements results in little ohmic contribution, minimize the formation of H_2 bubbles due to much more efficient transport in the spherical bubbles) and the advantage of a reduced requirement of conductance of the supporting electrolyte. Therefore, the study of acidic species in media of low conductance has been feasible. It is generally accepted that hydrogen evolution in acetate buffers occurs via the diffusion of both free proton and acetic acid to the electrode surface and their reduction via the dissociation of the acetic acid

$$HOAc \rightleftharpoons H^+ + OAc^- \qquad (26)$$

Followed by the reduction of the free proton

$$H^+ + e^- \rightleftharpoons \tfrac{1}{2} H_2 \qquad (27)$$

This reaction mechanism scheme is refered to as a preceding chemical reaction scheme (CE). The dissociation reaction is fast (with a rate constant of ~ 10^{-6} s^{-1} [138]), so that the cathode reaction may, in most conditions, be considered to be

$$HOAc + e^- \longrightarrow \tfrac{1}{2} H_2 + OAc^- \qquad (28)$$

In consequence, it is not possible to distinguish the reduction of acetic acid and free proton. Hence, the voltammograms for acetate buffers at Pt electrodes show reduction waves at a potential close to that predicted by thermodynamics for the reduction of proton at the experimental pH while the current is determined by the concentration of both the free proton and the acetic acid. At sufficiently negative potential, the evolution of hydrogen becomes mass transport controlled with respect to both acetic acid and free proton. Daniele et al. [130, 133] have shown that the chemical reaction preceding the electron transfer is fast for those acids whose dissociation constants, K_a, is larger than ~ 1×10^{-6}. It has been demonstrated using Pt microelectrodes that the steady state limiting current, I_L, for weak acids whose dissociation reaction is fast can be predicted by [126, 130, 133, 139]

$$I_L = 4Fr\left[D_{H^+}[H^+]^b + D_{HA}[HA]^b\right] \qquad (1\text{-}26)$$

where D_{HA} and $[HA]^b$ are the diffusion coefficient and the bulk equilibrium concentration of the undissociated acid, and D_{H^+} and $[H^+]^b$ are the diffusion coefficient and bulk concentration of free proton, F is the Faraday constant, and r is the electrode radius. Daniele and co-worker [130, 133] have shown that the wave position of weak acids depends on both the equilibrium dissociation constant and the

analytical concentration of the acid present in solution. The results obtained showed that at a given concentration, the reduction wave becomes more negative with decrease in the dissociation constant. On increasing the acid concentration, weak acids showed a cathodic shift, whereas strong acids display a positive shift. Furthermore, it has been demonstrated that the reduction wave heights of strong and weak acids at Pt microelectrodes depend linearly on the total concentration of the acid over a wide range of concentration [126, 127, 134].

1.11 Electrode processes

An electrode reaction is a class of chemical reaction involving the transfer of electrons across the interface between a solid surface (such as inert metal, semiconductor or even an insulator electrode) and an adjacent solution phase [60].

A simple electron transfer reaction can be represented by the general reaction

$$O + ne^- \rightleftharpoons R \qquad (7)$$

where n is the number of electrons involved in the electrode reaction, and the oxidized form in solution, O, will be converted to R, the reduced form, according to the pathways shown in figure 1.6 [140].

In general the rate of the electrode reaction is governed by the rates of the following processes [140]:

- Mass transfer of O from bulk solution to the electrode surface and R from the surface to bulk solution.

- Electron transfer at the electrode surface.

- Chemical reactions (homogeneous or heterogeneous) following or preceding the electron transfer.

- Other surface reactions (e.g. adsorption, desorption, electrodeposition).

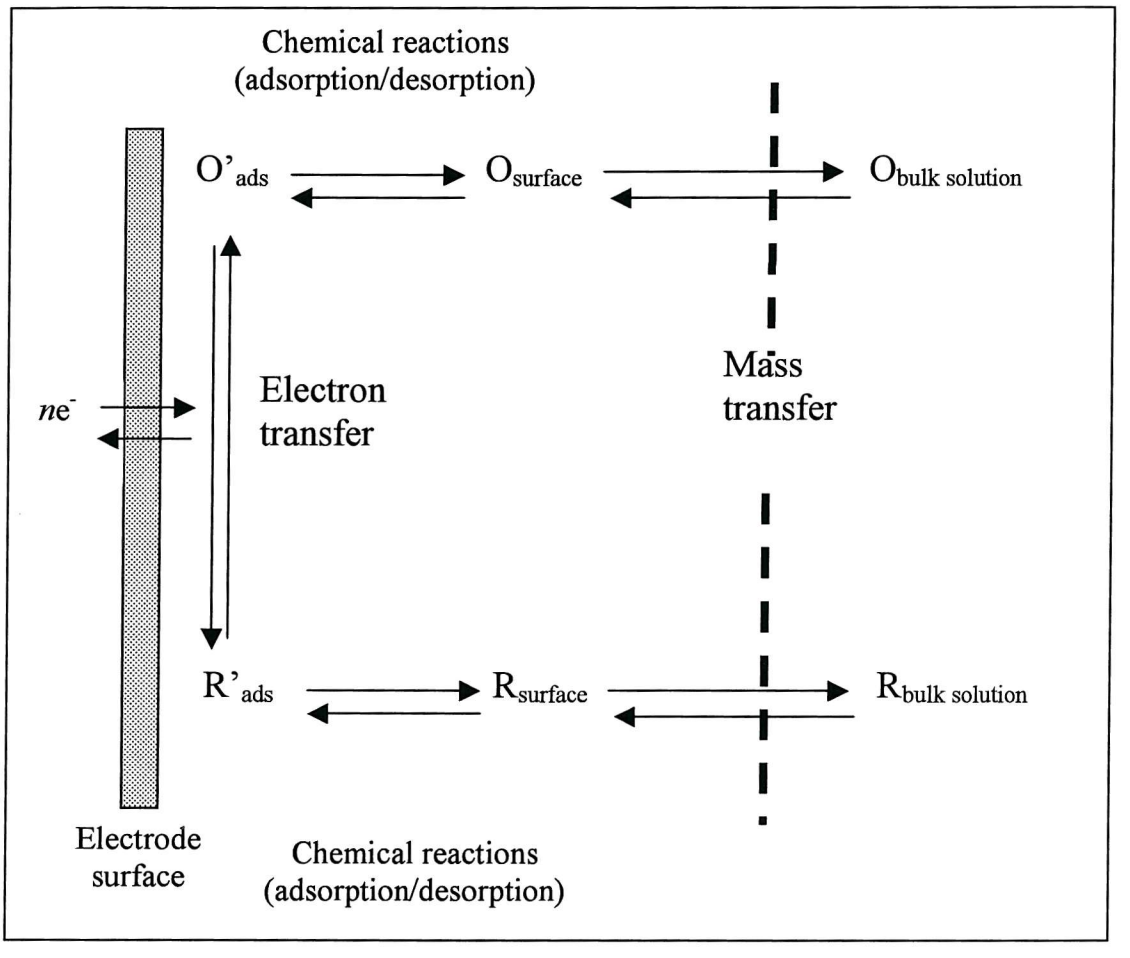

Figure 1. 6 *Pathway of a general electrode reaction [140].*

The simple electrode reaction, conversion of O to R, must occur in three steps according to the following scheme [60]

$$O_{bulk} \xrightarrow{\text{mass transport}} O_{electrode}$$

$$O_{electrode} \xrightarrow{\text{electron transfer}} R_{electrode}$$

$$R_{electrode} \xrightarrow{\text{mass transport}} R_{bulk}$$

The rate of the overall electrode process will always be limited by the slowest of these three steps. As shown above, the supply of reactant and the removal of product from the electrode surface are essential to a continuing chemical change. Mass transport can be regarded as the physical movement in solution from one place to another. In general, there are three modes of mass transport: diffusion, convection and migration [60].

Diffusion is the movement of species due to a concentration gradient, i.e. movement of species from a concentrated region of the solution to a more dilute region, until the concentrations become equal. The net movement of substance is proportional to the concentration gradient and the two are linked by a diffusion coefficient [63]. Convection is the movement of species in the whole solution due to external mechanical forces i.e. flowing the electrolyte solution at a known rate past the electrode surface, rotating the electrode surface with respect to the electrolyte, stirring the solution, motion of bubble or natural convection. Migration is the movement of ions due to an electrical potential gradient, but can be excluded by adding a large concentration of supporting electrolyte to the electroactive species (to ensure that migration does not contribute significantly to the transport of electroactive species), and hence will be ignored from this point.

Mass transfer can be monitored using electroanalytical techniques. In the work presented here, rotating disc electrodes (Pt or X65 carbon steel) were employed as working electrodes to study the electrochemistry of acetate/acetic acid buffers (with CO_2 saturation in some cases). Rotating disc electrodes have become one of the most popular system for kinetic and mechanistic studies, because it combines an ease of construction and the ability to control and vary the rate of mass transport over a very wide range. These are fabricated with a polished disc of the chosen electrode material surrounded by a sheath of an insulating material with a diameter significantly larger than that of the electrode. The structure is rotated about an axis perpendicular to the surface of the disc electrode. The rotated structure acts as a pump; it pulls the solution vertically upwards and then throws it outwards because

the solution cannot get through the solid material. Therefore, close to surface the convection becomes radial.

To help our understanding of experiments with rotating disc electrode, the use of a model where the continuously varying flow conditions are replaced by an equivalent system in which the zones for diffusion and convection have been separated is frequent. This model is widely referred to as the Nernst diffusion layer model [60] and is illustrated in figure 1.7:

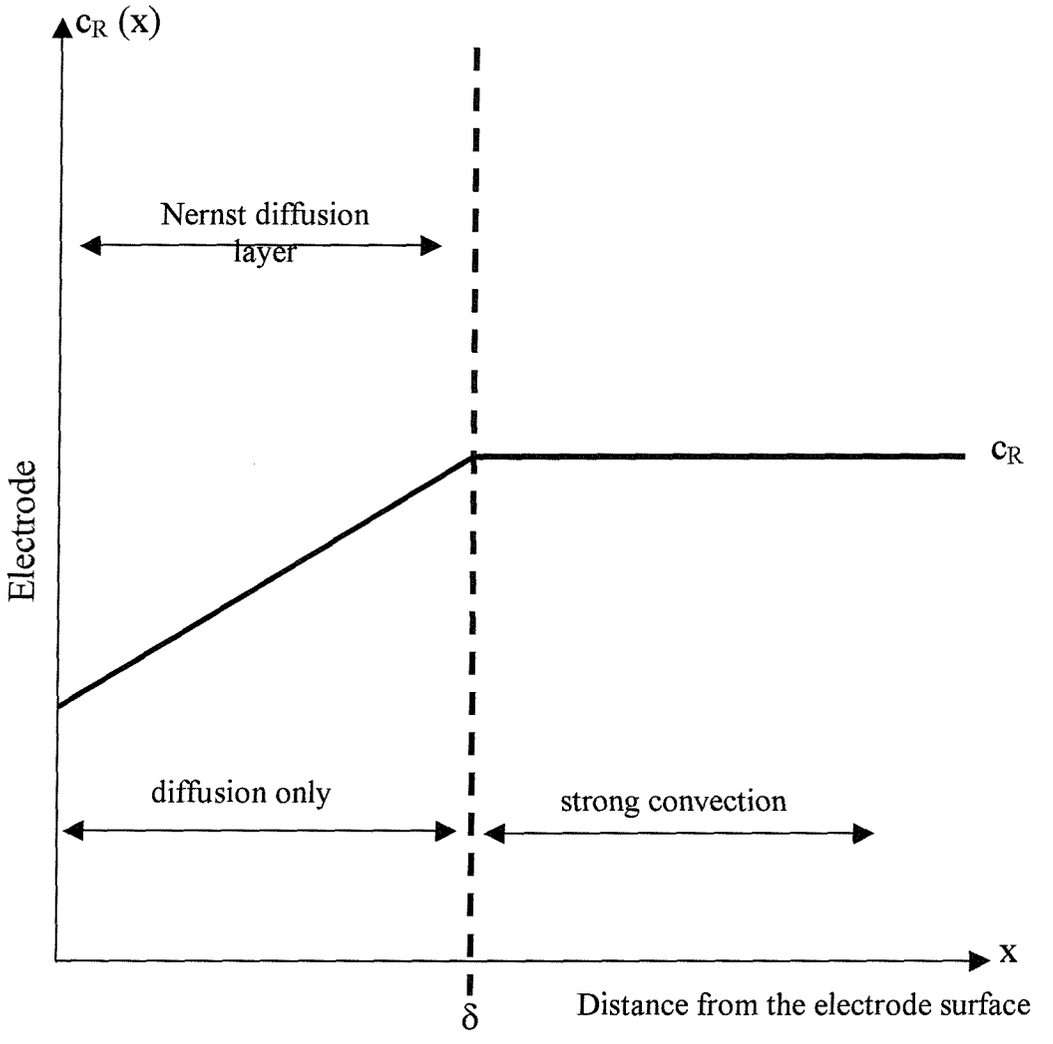

Figure 1. 7 *Nernst diffusion layer model for an oxidation of R to O at a rotating disc electrode. The solution initially contains only R [60].*

It can be seen from figure 1.7, that the electrolyte is divided into two zones. Close to the electrode surface, one assumes a boundary layer, thickness δ, where the solution is totally stagnant and mass transport is only by diffusion. On the other hand, outside of this layer, strong convection occurs for the concentration of all species to be held at their bulk value. Clearly, the rate of convective diffusion to the disc electrode depends strongly on the rotation rate of the disc. This is taken into account in the Nernst diffusion layer [60] model as shown in equation (1-27)

$$\delta = \frac{1.61\,\nu^{1/6} D^{1/3}}{\omega^{1/2}} \qquad (1\text{-}27)$$

where ν is the kinematic viscosity (i.e. viscosity/density), D is the diffusion coefficient of the electroactive specie (R), and ω is the rotation rate of the disc electrode. It can be noted that the stagnant layer thickness will become thinner as the rotation rate of the disc electrode increases. Hence, there is a maximum and a minimum limit to the rotation rate, which may usefully be employed. The upper limit to the rotation rate, ω, depends on experimental factors such as any eccentricity of the rotation of the RDE support. A minimum rotation rate is obligatory for the theory to hold because it is necessary that the forced convection dominate diffusion as well as natural convection [60].

The Nernst diffusion layer concept allows a trivial derivation of the current density at a rotating disc electrode for potentials where the electrode is mass transport controlled. The concentration of the electroactive species, R, at the surface is determined by the potential, while the rate of diffusion depends also on the thickness of the diffusion layer, and hence, on the rotation rate of the disc electrode. The diffusional flux through the Nernst diffusion layer can be expressed as

$$J = \frac{nFD\left(c_R - (c_R)_{x=0}\right)}{\delta} \qquad (1\text{-}28)$$

At high enough overpotential, $(c_R)_{x=0} = 0$ and the current density must become independent of potential. The limiting current density, j_{lim}, is given by:

$$j_{\lim} = \frac{nFDc_R}{\delta} \tag{1-29}$$

$$j_{\lim} = nFk_m c_R \tag{1-30}$$

where k_m is known as the mass transfer coefficient. For potential where the surface concentration of the electroactive specie is zero, the equation relating the limiting current density and the rotation rate is found by combining equations (1-27) and (1-30):

$$j_{\lim} = 0.62nFD^{2/3}\nu^{-1/6}c\omega^{1/2} \tag{1-31}$$

where j_{lim} is the limiting current density (in A m^{-2}), D is the diffusion coefficient of the electroactive specie (in m^2 s^{-1}), n is the number of electrons transferred, F is the Faraday constant (in C mol^{-1}), ν is the kinematic viscosity (in m^2 s^{-1}) and $\omega^{1/2}$ is the square root of the rotation rate of the disc electrode (in rad s^{-1}). Equation (1-31) is known as the Levich equation, and it provides an excellent test that shows whether the current is entirely mass transport controlled; a plot of j_{lim} versus $\omega^{1/2}$ should be linear and pass through the origin, and the slope of such a plot may be used to estimate the diffusion coefficient for the electroactive species.

1.12 Overall aim of this Project

The overall objective of this project was to understand the way in which the chemistry of aqueous acetate/ acetic acid containing brines influences the mechanism and increases the corrosion of carbon steel. It was felt that the environment determines the rate of corrosion of the carbon steel in a number of ways:

- ❖ Solution speciation
- ❖ Electron transfer kinetics
- ❖ Nature of surface film

and that these factors are strongly interactive.

In this thesis the emphasis has been

- ❖ To determine a knowledge of the speciation within these complex aqueous solutions.
- ❖ To understand the electrochemistry of such media at both platinum and carbon steel (X65) rotating disc electrode in order to demonstrate that the solution composition as well as surface films determine the rate of corrosion.
- ❖ To compare the electrochemistry of these acetate/acetic acid buffers with real "formation water" samples.
- ❖ To examine changes in the surface morphology of the corrosion film due to acetic acid and carbon dioxide using SEM.

Chapter Two

2 *Experimental Work*

2.1 Chemicals

The following table contains the chemicals, which have been used in this project. The chemicals were used as received.

Chemical	Supplier	Purity
Sodium acetate Tri-hydrate	BDH	99 %
Sodium Chloride	BDH	99.9 %
Sodium propionate	Aldrich	99 %
Sodium lactate	Aldrich	99 %
Sodium formate	Aldrich	99.9 %
Acetic acid	BDH	100 %
Propionic acid	Aldrich	99 %
Lactic acid	Aldrich	90 %
Formic acid	Aldrich	95 %
Sulphuric acid	Fishers chemicals	98 %

Table 2. 1 *Chemicals used during this project.*

Unless otherwise stated, the solutions were prepared with deonised water from a Whatman Analyst System. Except when otherwise stated, the electrolyte used throughout the project was 3% (0.5M) NaCl (BDH) and different concentrations of sodium salt of weak acids, a simple representative of water that accompanies oil production. In reality, this water usually contains NaCl, $MgCl_2$, $CaCl_2$, HCO_3^- and trace quantities of several elements and organic compounds. The brine sample also contains dissolved gases including carbon dioxide but not oxygen.

2.2 Gases

Table 2.2 shows the specification for N_2 (BOC Ltd, England):

N_2	Impurities (volume per million, vpm)			
	O_2	Ar	H_2O	HC
> 99.99 %	≤ 2	≤ 5	≤ 3	≤ 0.1

Table 2. 2 *A summary of the specification for N_2.*

Table 2.3 shows the specification for CO_2 (BOC Ltd, England):

CO_2	Impurities (volume per million, vpm)			
	O_2	Ar	H_2O	HC
> 99.8 %	≤ 2	≤ 5	≤ 3	≤ 0.1

Table 2. 3 *A summary of the specification for CO_2.*

All solutions were degassed with a fast stream of N_2 or saturated with CO_2 prior to any measurements; for experiments with CO_2 saturated solutions, it was essential to work with a CO_2 atmosphere above the solution. Oilfield brines used for this study were supplied by BP Amoco Ltd. Four samples taken at two different oilfield sites, The Wytch Farm facility (South of England) and Trinidad oilfields were used in this work. The brines did not appear to contain suspended solids and were usually colourless (one of the samples, A2, was yellow/orange). No chemical pretreatment was therefore carried out with these brines. They were just saturated with the appropriate gas prior to the introduction of the electrode (Pt or X65 carbon steel).

2.3 Electrodes, cells, procedures

2.3.1 Voltammetry recorded at a Pt rotating disc electrode

A Pt rotating disc electrode was used as a working electrode for the electroanalytical studies (area, 0.16 cm^2). The Pt RDE (Pine Instruments) was initially cleaned by polishing with alumina powder (1 μm, then 0.3 μm and 0.05 μm) on a moist polishing cloth (Beuhler Ltd. mounted on a Petri dish). The electrode was rinsed between the various polishing stages with deionised water. The electrode was then polished on an alumina-free polishing cloth moistened with distilled water. Finally, immediately before each set of experiements, the Pt rotating disc electrode was further cleaned electrochemically in a degassed 1 M sulphuric acid solution. All voltammograms in the acetate/acetic acid buffers (with or without CO_2 saturation) were recorded at a potential scan rate of 20 mV s^{-1}.

2.3.2 Voltammetry recorded at X65 carbon steel rotating disc electrode

The carbon steel specimens selected for study were supplied by BP Amoco Ltd. The composition of the X65 carbon steel used is given in table 2.4.

Steel Type	**Weight % (Fe balance)**						
	C	Mn	Si	P	S	Cr	Cu
X65 carbon steel	0.18	0.77	0.10	0.026	0.04	0.14	0.25

Table 2. 4 *A summary of the X65 carbon steel composition.*

The X65 carbon steel were cylinders 30 mm in height and 4.7 mm diameter. The sides were protected with shrinkable Teflon tubing so that only a disc, area 0.17 cm^2, was exposed to the solution under study. Before each experiment, the disc was rubbed with fine Emery paper (600) to ensure complete removal of any corrosion film and then polishing with alumina powder (1 μm, then 0.3 μm and

0.05 μm) on a moist polishing cloth (Beuhler Ltd. mounted on a Petri dish), rinsing with deionised water after each polish. Voltammograms for the steel samples were always recorded by scanning the potential from the negative limit in order to minimize the influence of any corrosion film. In addition, the voltammograms were recorded as soon as possible after immersion of the steel sample in the solution. These precautions made the responses reproducible (if potential scans started at corrosion potential, the response depends on the thickness of the corrosion film that is allowed to form). This experimental procedure should, however, always be noted when discussing the relevance of the data to the corrosion field. Unless otherwise stated, all voltammograms were recorded employing a potential scan rate of 5 mV s^{-1} (to minimize extensive changes to the steel surface during an experiment).

A three-compartment glass electrochemical cell fabricated in the Department's Glass Workshop with a volume of 50 cm^3 was used for all the experiments as shown in figure 2.1.

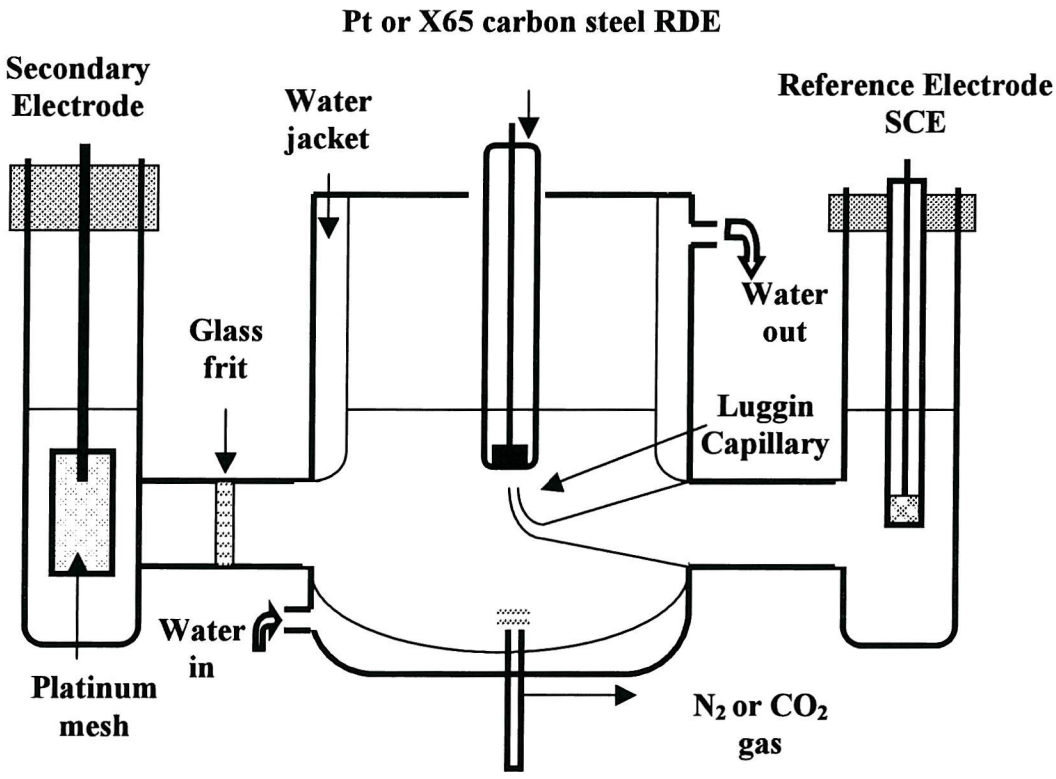

Figure 2. 1 *Conventional Three Compartments voltammetric cell.*

A platinum mesh was used as a secondary electrode. The potential at the working electrode was measured versus a saturated calomel electrode (SCE), which was housed within the Luggin capillary compartment. The tip of the Luggin capillary was placed approximately at 1 mm from the surface of the electrode in order to minimize the IR drop. The working electrode was separated from the Pt mesh secondary electrode by a glass frit. The cell is surrounded by a jacket filled with water so that the temperature of the solution under study was adjusted to within $\pm 2°C$ of the required value using a thermostatically controlled water bath (Julabo F20).

2.4 Instrumentation

The voltammetry was carried out with an EG&G Model 173, a potentiostat controlled by a PC operating the Headstart^{TM} Software (EG&G, Princeton Applied Research) through a Computer Graphics Interface. The same software allows output data to be handled and presented as required. The rotation of the RDE electrodes was controlled with a Pine Instruments Unit for the Pt electrode and with an EG & G Model 616 RDE Unit for the X65 carbon steel electrodes. A Julabo F20 water bath was used to maintain the constant temperature of the solution circulating through the jacketed cell.

2.5 pH

In the early stage of this work, it became clear that the pH either of the simulated solutions or oilfield brines plays an important role in determining the concentration of acetic acid. Also the solutions were found to behave non-ideally (see Chapter Three) and hence the measured pH and the value calculated from simple equations was frequently different. As a result the pH measurement was carefully calibrated. Several pH-meters were tested, and after careful consideration,

all pHs were measured with a Hanna Instrument HI 9321 Microprocessor pH meter that had been carefully calibrated with two buffers (pH 4.00 and pH 7.01).

2.6 Tafel extrapolation and Linear resistance polarization procedures

The experimental set-up consists of the conventional three compartments voltammetric cell and a computer –controlled potentiostat. Before all experiments, the glassware was thoroughly washed with nitric acid, then rinsed with distilled water and left to dry. The solutions were continuously saturated with N_2 or CO_2 throughout the experiments. To prevent air from entering the cell, the lid of the cell was smeared with silicone grease. The reference electrode was a saturated calomel electrode (SCE), while the counter electrode was always a Pt mesh. A desktop computer, running the Headstart^{TM} Software (EG & G, Princeton Applied Research) was used to control the EG & G Model 173A potentiostat via the computer graphics interface. Scans were made from a potential of – 300 mV versus E_{corr} to a potential of + 300 mV versus E_{corr} using a scan rate of 5 mV s^{-1}. Similar to Tafel polarization measurements, linear polarizations were made using the experimental set-up.

2.7 SEM Studies

2.7.1 Instrumentation

Electron microscopy experiments were carried out on a Philips XL30 ESEM, based at Southampton University in The Electrochemistry Group. This microscope combines high vacuum, "low vacuum" and ESEM into one instrument. It offers a wide range for user selections of kV, magnification, gas type, gas pressure and detector type. It also combines a scanning electron microscope and EDAX/EDX analyzer. The specimen stage of the SEM can accommodate samples as large as 50 mm length and 50 mm breadth. The specimen stage can be rotated through 360°

and tilted within -10° to +70° of the plane parallel to the detector. The available magnification range is between 22-400,000 and the working distance is fully variable from 5 to 50 mm. The accelerating voltage ranges from 0.1 kV to 30 kV. The display output is controlled by a modern Windows NT based interface and the pictures are taken digitally.

2.7.2 Surface preparation

In order to compare the results and ensure that all steel specimens were identical, a standard pre-treatment surface preparation was necessary. Before testing, the flat ends of the steel cylindrical specimens were polished with a range of 320-600-1200 grit metallurgical silicon carbide wet/dry paper (Emery Paper). In order to provide a flat surface, a smooth glass plate was placed beneath each sheet and the sheet was then moistened with deionised water. Ensuring that the specimens were always held perpendicular to the Emery Paper, a rotation rate of 4900 rpm was adopted for all the polishing to achieve an evenly polished surface. Following the finest grade paper, a smoother polishing was achieved with 1.0 μm, 0.3 μm and 0.05 μm alumina (Al_2O_3) powder (Buehler Ltd.).

A small amount of Al_2O_3 was placed on a moist polishing cloth (mounted on a Petri dish) and slurry of alumina was formed on the addition of a few drops of deionised water. The specimens were polished in the same manner as with the Emery Paper. Separate Petri dishes were used for the different sizes of alumina powders. Between each grade, the specimens were rinsed with deionised water. Finally, to ensure that all the alumina powder was removed, the steel specimens were polished on moist polishing cloth (Buehler Ltd.) free of alumina powder. Immediately before immersing the steel specimens into the appropriate environments, the discs were degreased by washing with acetone then rinsed with copious amounts of deionised water.

2.7.3 Corrosion procedure

The experiments were carried out in the glass cell filled with 1 L of brine purged with the appropriate gas (N_2 or CO_2) for at least 1 hour prior to immersion of the X65 carbon steel into the vessel (see figure 2.2).

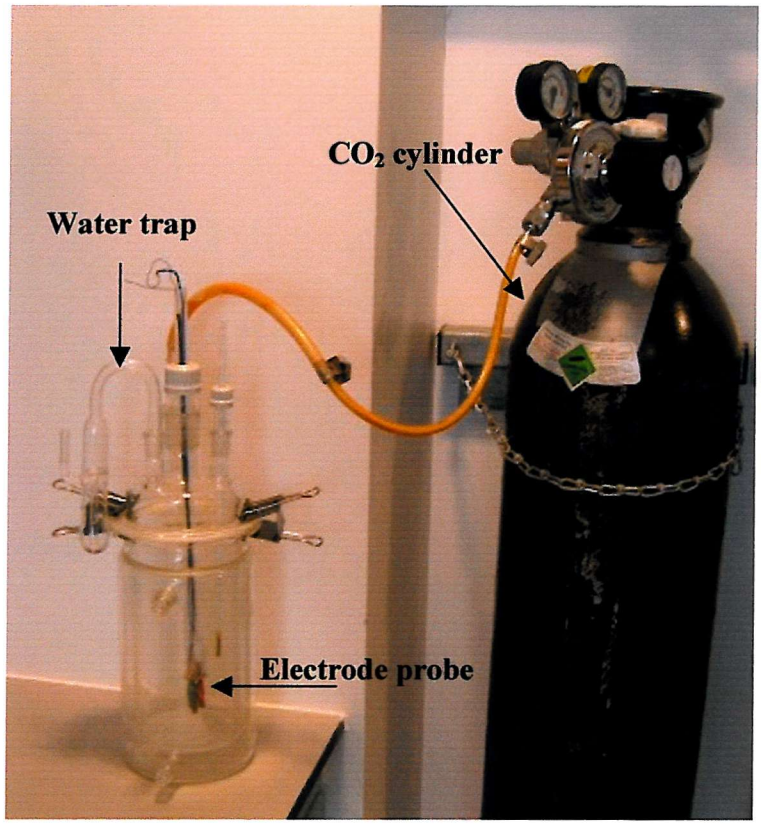

Figure 2. 2 *The glass cell used for the Corrosion film studies.*

The solution was continuously purged with the appropriate gas throughout the experiment. The cell is surrounded by a jacket filled with water so that the temperature of the solution under study was adjusted to within ± 2°C of the required value using a thermostatically controlled water bath. To prevent air ingression, all the components of the cell were smeared with silicone grease on surfaces not in contact with solution. A minimum of three X65 carbon steel was used for each test to ensure reproducibility. These specimens were introduced into the glass cell using a three-electrode probe as shown on figure 2.3.

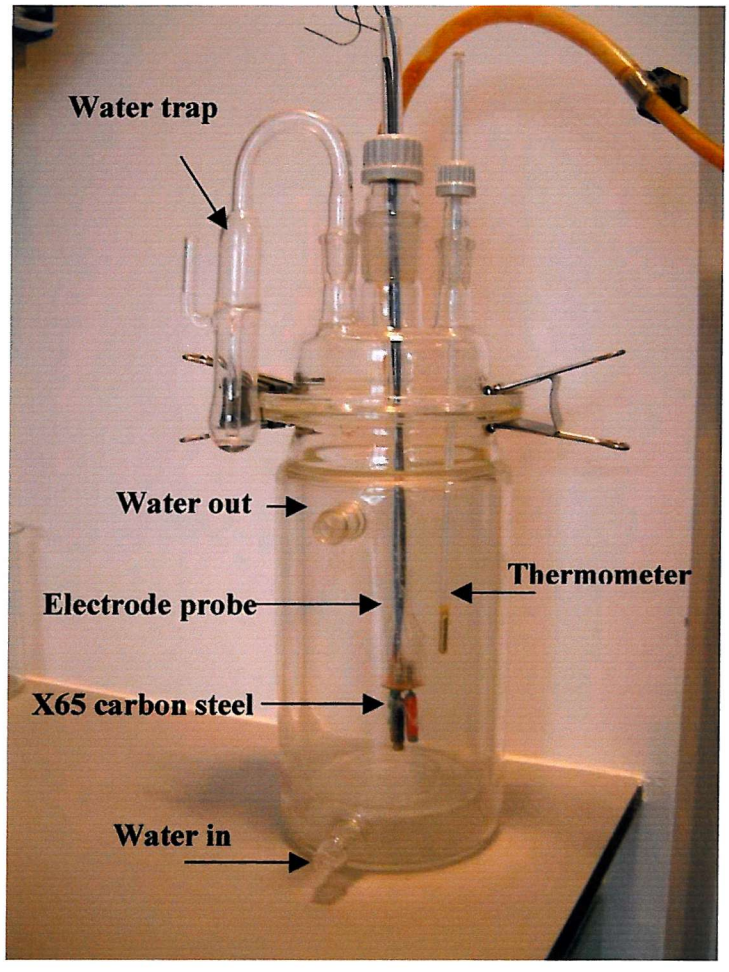

Figure 2. 3 *The glass cell used for Corrosion film studies.*

Latex gloves were worn to prevent contamination of the steel surface with grease from the skin. Three different immersion times were investigated 1 hour, 24 hours and 1 week. The experiment was only continued if the solution remained colourless; yellowing of the solution was taken as an indication of the formation of Fe (III) and hence that O_2 contamination had occurred. After being removed from the solution the corroded discs were rinsed with deionised water and let to dry into a dessicator. Typical SEM pictures were recorded within 1 hour of removal from the test cell.

2.7.4 Procedure for SEM

A specimen was placed inside the ESEM chamber and the image initially formed on the screen was set a low magnification, then the image was focused. When a satisfactory image was display on the computer screen, a photograph was taken. Afterwards, the magnification was increased and the photographs were taken for each one of them.

Chapter Three

3 Speciation within sodium acetate – carbon dioxide brine solutions

3.1 Introduction

The role of both the undissociated proton donors and the solution chemistry of the weak acid buffers has been much underestimated in the interpretation proposed for the acceleration of steel corrosion by acetate in the carbon dioxide saturated brines encountered during the recovery of oil [40-42]. The application of known electrochemistry of weak acids in aqueous solutions [123-134] to the practical corrosion environment requires an extension of the experiments on the reduction of acetic acid to the conditions where the steel corrosion occurs. A wide variety of brine compositions can be encountered in the oilfield environment, but in most experiments in this study, an aqueous 3 % sodium chloride solution containing different concentrations of sodium acetate was used as a simulant (following oil industry practice). Hence, this chapter attempts a quantitative discussion of the speciation in 3 % NaCl brines. During the later stages of this programme, it became clear that the discussion of oilfield brines was more complex. Firstly, they can contain a "high" level of bicarbonate such that the saturation by carbon dioxide does not cause the pH to drop to a value where there is significant conversion of acetate to acetic acid. Secondly, the ionic strengths of the oilfield brines can be high enough that the estimation of activity coefficients becomes imprecise. In the last section of this chapter, these solutions are discussed in a more qualitative fashion.

When saturated with carbon dioxide, the pH of the simulated brines was in the range of 4 – 6 and the predominant weak acid is acetic acid (pK_A = 4.75) [96] (it should be noted that acetic acid is a significantly stronger acid than carbonic acid;

pK_A = 6.35) [97]. Before data from such studies can be interpreted, however, it is essential to understand the speciation within the brines. In principle, the speciation can be calculated from thermodynamic data. Certainly, electrochemical data at Pt electrodes can be used to estimate the concentration of the key species and hence check the accuracy of the speciation calculations. In this thesis, the computer program, PHREEQC 2.2, available on the World Wide Web from the US Geological survey [141] has been used to calculate the concentrations of all species in the aqueous sodium chloride – sodium acetate – carbon dioxide system. In this chapter, the chemistry of the brine solutions is outlined. This discussion leads to the equations describing the speciation. In addition, the input data for the simulations is set out.

3.2 3 % NaCl Brines

3.2.1 Preliminary work

Preliminary calculations demonstrated that in order to obtain an acceptable agreement between experimental and calculated pH, it was essential to write the equilibria in terms of activities. This is to be expected since the mean ionic activity coefficient in the 3 % sodium chloride solution is ~ 0.66 [96]. Table 3.1 compares the measured pH for a series of deoxygenated acetate buffer solutions prepared by the addition of aliquots of 1 M acetic acid solution to a solution containing 3 % sodium chloride + 10 mM sodium acetate at 298 K.

Volume of 1 M HOAc added/ cm^3	**pH measured**	**pH (a = c)**	**pH (a = 0.66c)**
0.10	5.84	5.69	5.87
1.00	4.89	4.68	4.87
2.50	4.45	4.30	4.48
4.00	4.24	4.08	4.26
5.00	4.14	3.98	4.17

Table 3. 1 *Comparison of experimental and calculated pH at 298 K for an aqueous solution of 10 mM NaOAc + 3 % NaCl (200 cm^3) with various additions of 1 M acetic acid.*

The pH was calculated using the dissociation constant for acetic acid, $K_1 = 1.80 \times 10^{-5}$ and values of the mean ionic coefficient, $\gamma_{\pm} = 1.00$ (ideal behavior) and $\gamma_{\pm} = 0.66$. It can be seen that it is essential to take into account the deviation from ideality. When this was done, the agreement between theory and experiment is excellent. Similar agreement was found for buffers prepared with 1 and 100 mM sodium acetate as shown in table 3.2 and table 3.3.

Volume of 1 M HOAc added/ cm^3	pH measured	pH (a = c)	pH (a = 0.66c)
0.20	4.61	4.38	4.57
0.60	4.13	3.91	4.09
1.00	3.90	3.69	3.87
3.00	3.42	3.20	3.38
5.00	3.20	2.99	3.16

Table 3. 2 *Comparison of experimental and calculated pH at 298 K for an aqueous solution of 1 mM NaOAc + 3 % NaCl (200 cm^3) with various additions of 1 M acetic acid.*

Volume of 1 M HOAc added/ cm^3	pH measured	pH (a = c)	pH (a = 0.66c)
0.20	6.52	6.31	6.56
0.60	6.05	5.85	6.08
1.00	5.83	5.63	5.86
3.00	5.34	5.17	5.38
5.00	5.13	4.96	5.16

Table 3. 3 *Comparison of experimental and calculated pH at 298 K for an aqueous solution of 100 mM NaOAc + 3 % NaCl (200 cm^3) with various additions of 1 M acetic acid.*

3.3 Speciation in 3 % NaCl brines containing acetate and saturated with CO_2

3.3.1 Chemistry of the brine solutions

Oilfield brines have a wide range of electrolyte compositions. Potassium, calcium and magnesium cations and sulfate, bromide and bicorbonate anions are

commonly present in significant concentrations and there are also traces of many other species, including transition metal ions and carboxylates. In this work, and commonly in the literature as well as the oil industry, 3 % sodium chloride brine is used as a simulant. The solutions studied contain acetate and carbon dioxide and it is therefore necessary to consider the chemistry of carbon dioxide and acetate and the way in which their chemistries interact. It quickly becomes clear that it is necessary to consider the concentrations of Na^+, H^+, Cl^-, HCO_3^-, CO_3^-, OAc^-, HOAc, H_2O and CO_2.

When carbon dioxide is dissolved in water, the following equilibria [94,142] are considered:

$$CO_2\,(g) \xrightleftharpoons{K_1} CO_2^*\,(aq) \qquad (1)$$

where CO_2^* (aq) refers to the total dissolved carbon dioxide; that is the sum of both CO_2 (aq) and H_2CO_3, but does not include the ionized species, HCO_3^- and CO_3^{2-}. In aqueous solutions, the concentration of CO_2 is much higher than that of H_2CO_3. For example at 298 K ratio of $c_{H_2CO_3}/c_{CO_2}$ is 2.56×10^{-3}. Then,

$$CO_2^* + H_2O \xrightleftharpoons{K_2} H^+ + HCO_3^- \qquad (2)$$

$$HCO_3^- \xrightleftharpoons{K_3} H^+ + CO_3^{2-} \qquad (3)$$

where the equilibrium constants are defined by the equations:

$$K_1 = \frac{a_{CO_{2(aq)}}}{f_{CO_{2(g)}}} \qquad (3\text{-}1)$$

$$K_2 = \frac{a_{H^+} a_{HCO_3^-}}{a_{CO_{2(aq)}} a_{H_2O}} = \frac{\gamma_\pm^2 c_{H^+} c_{HCO_3^-}}{a_{CO_{2(aq)}} a_{H_2O}} \qquad (3\text{-}2)$$

$$K_3 = \frac{a_{H^+} a_{CO_3^{2-}}}{a_{HCO_3^-}} = \frac{\gamma_{\pm} c_{H^+} c_{CO_3^{2-}}}{c_{HCO_3^-}} \tag{3-3}$$

At 298 K, typical values of the equilibrium constants are $K_1 = 3.42 \times 10^{-2}$, $K_2 = 4.30 \times 10^{-7}$ and $K_3 = 5.61 \times 10^{-11}$ respectively [96]. If one wants to extend calculations to higher temperature, the variation of the equilibrium constants with temperature must be taken into account.

Plummer and Busenberg [143] have quoted the following polynomials for calculating the equilibrium constants as a function of temperature over the temperature range 273 – 373 K at 1 atm total pressure:

$$\log K_1 = 108.3865 + 0.01985076T - \frac{6919.53}{T} - 40.45154 \log T + \frac{669365}{T^2} \tag{3-4}$$

$$\log K_2 = -3560.3094 - 0.06091964T - \frac{21834.37}{T} + 126.8339 \log T + \frac{1684915}{T^2} \tag{3-5}$$

$$\log K_3 = -107.8871 - 0.03252849T - \frac{5151.79}{T} + 38.92561 \log T - \frac{563713.9}{T^2} \tag{3-6}$$

where T is the temperature (in K). Similar values for the equilibrium constants are also reported by Asada [97] and Keene [144].

When acetate is also present in the brine solution, the following equilibrium must also be considered:

$$HOAc \underset{}{\overset{K_4}{\rightleftharpoons}} H^+ + OAc^- \tag{4}$$

the equilibrium constant for which may be written

$$K_4 = \frac{a_{H^+} a_{OAc^-}}{a_{HOAc}} = \frac{\gamma_{\pm}^2 c_{H^+} c_{OAc^-}}{c_{HOAc}} \qquad (3\text{-}7)$$

K_4 has the value 1.8×10^{-5} at 298 K and it may be calculated as a function of temperature from the polynomial [145]:

$$\log K_4 = 18.67257 - 0.0076792T - 6.50923 \log T - \frac{1500.65}{T} \qquad (3\text{-}8)$$

In addition, the calculations use the mass balance equations for each species in the system, for example, for the acetate ion:

$$c_{HOAc} + c_{OAc^-} = c \qquad (3\text{-}9)$$

where c is the concentration of acetate initially added to the solution.

The activity coefficients for the ions in solution of low ionic strength can be estimated from the Debye-Hückel equation (3-10):

$$\log \gamma_{\pm} = -Az_i^2 \sqrt{I} \qquad (3\text{-}10)$$

where I is the ionic strength, z_i the charge on the ion and A is a temperature dependent constant (A $\approx$ 0.509 at 298 K). In this work, an extension of this equation (3-10) designed to handle more concentrated solutions was used:

$$\log \gamma_{\pm} = -Az_i^2 \left(\frac{I^{1/2}}{1 + I^{1/2}} - 0.31I \right) \qquad (3\text{-}11)$$

Because of the high concentration of sodium chloride in the brines, it is this specie that largely determines the value of the activity coefficient and the activity

coefficient is effectively insensitive to the acetate and the acetic acid concentrations. Equation (3-11) predicts a value of 0.66 for the activity coefficient for 3 % sodium chloride and this value agrees well with the experimental value [96].

3.3.2 Preliminary consideration of the speciation within acetate/carbon dioxide solutions

Assuming ideal behavior, i.e. mean ionic coefficient $\gamma_{\pm} = 1.00$, algebraic manipulation of equations (3-1), (3-2) and (3-7) along with the mass balance equation for acetate, equation (3-9), leads to

$$c_{H^+} = \frac{K_2 c_{CO_2}(1+K_1) \pm \left(\left(K_2 c_{CO_2}(1+K_1)\right)^2 + 4cc_{CO_2}K_2K_4(1+K_1)\right)^{1/2}}{2c} \qquad (3\text{-}12)$$

Table 3.4 lists the solubility of various gases in water at 298 K [146], illustrating that carbon dioxide is significantly more soluble than other common gases.

Gas	**Solubility of Gases in Water/ mM**
H_2	0.77
N_2	0.625
O_2	1.228
CO_2	31

Table 3. 4 *Solubility of some gases in water at 298 K.*

However, it should be noted that the solubility is not only dependent on partial pressure, but also on temperature [142]. At 333 K the solubility of carbon dioxide drops to 11 mM. The equilibrium proton concentration can be calculated for any initial acetate concentration using equation (3-12) and the equilibrium constants given K_1, K_2, K_3 and K_4.

Then using equation (3-7) in the form

$$K_4 = \frac{c_{H^+}(c - c_{HOAc})}{c_{HOAc}} \qquad (3\text{-}13)$$

it is possible to calculate the equilibrium concentration of acetate and acetic acid for that proton concentration.

c_{NaOAc}/ mM	pH	c_{H}^{+}/ mM	c_{HOAc}/ mM	c_{OAc}^{-}
1	4.63	0.0234	0.57	0.43
5	5.08	0.0083	1.60	3.40
10	5.25	0.0056	2.38	7.62
50	5.63	0.0023	5.74	44.3
100	5.79	0.0016	8.26	91.7

Table 3. 5 *Equilibrium concentrations of protons, acetic acid and acetate ion for aqueous solution of 3 % NaCl + NaOAc (concentrations shown in the table) saturated with carbon dioxide at 298 K estimated from equations (3-12) and (3-13). Concentration of carbon dioxide 31 mM at 298 K.*

In the absence of acetate in solution, the pH of the brine saturated with carbon dioxide is 3.90. It can therefore be seen that in any solution with significant acetate ion, the pH is higher than in the absence of acetate, but the concentration of acetic acid is far above that of the concentration of proton. Indeed, with increasing acetate concentration, the pH increases, as does the concentration of undissociated acetic acid. The calculated proton concentrations, however, do not agree well with those estimated from pH measurements of the solution.

The same calculation could in principle be carried out at any temperature. It was clear, however, that non–ideal behavior should be considered, and this significantly increases the complexity of the analytical approach to deriving equilibrium concentrations for all the species present. Hence, a computational

approach seemed more appropriate. The software package PHREEQC 2.2 was found to have all the capabilities required.

It is also helpful to understand the speciation of the system in a qualitative way. Figure 3.1 shows the variation of the various carbon dioxide and acetate derived species as a function of pH. Again the calculations assume ideality.

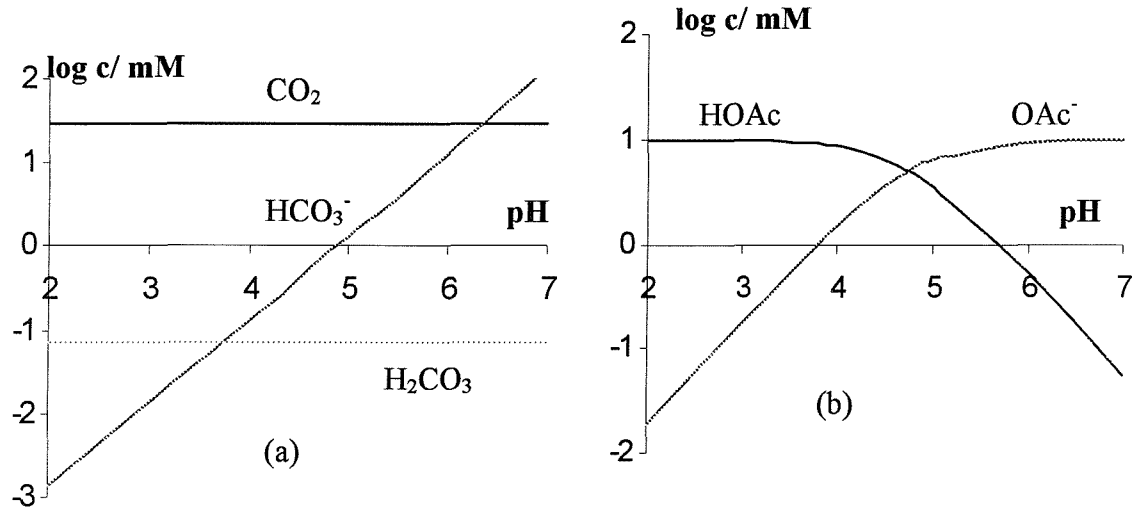

Figure 3. 1 *Equilibrium distribution of species as a function of pH in solutions of (a) water in contact with an atmosphere of CO_2 and (b) 10 mM NaOAc. Temperature 298 K.*

In understanding the chemistry of the system it is also helpful to recognize the presence of several potential weak acids (see table 3.7 page 3-16). This is important because the cathodic reaction in corrosion can have several contributions:

- The reduction of free protons present in solution (reflected by the measured pH).

- The reduction of carbonic acid. This contribution is always insignificant because of the very low concentration (0.074 mM) at all pH.

- A kinetic current due to the conversion of carbon dioxide to carbonic acid followed by the reduction of the acid. The limiting current is readily estimated using the equation given by Bard and Faulkamer [140], the equilibrium constant and the known rate constant for hydration. The value found is 0.12 mA cm^{-2}.

- The reduction of acetic acid.

- Water and bicarbonate are not strongly enough proton donors to contribute to hydrogen evolution at the corrosion potential.

3.3.3 Speciation using computer program PHREEQC 2.2

While PHREEQC 2.2 is designed to allow calculation of complex equilibria involving several phases and including transport processes in natural or polluted water [141], in this thesis, it was only employed to establish equilibrium concentrations in a single phase.

3.3.3.1 Program limitations

PHREEQC uses ion-association and Debye Hückel expressions to account for the non-ideality of aqueous solutions. This type of aqueous model is adequate at low ionic strength but may break down at higher ionic strengths (in the range of seawater and above). An attempt has been made to extend the range of applicability of the aqueous model through the use of an ionic-strength term in the Debye Hückel expressions. These terms have been fitted for the major ions using chloride mean-salt activity-coefficient data [147]. Thus, in sodium chloride dominated systems, the model may be reliable at higher ionic strengths. The activity of the water is estimated from an approximation based on Raoult's law [141].

The other limitation of any simulation is the quality of the thermodynamic data used in the calculations. Two databases are included in PHREEQC 2.2 [148-151]. In these compendia, the log K 's and enthalpies of reaction have been taken from various literature sources. No systematic attempt has been made to determine the aqueous model that was used to develop the individual log K 's or whether the aqueous models defined by the current database files are consistent with the original experimental data. The database files provided with the program should be considered to be preliminary. Careful selection of aqueous species and thermodynamic data is left to the users of the program [141]. The data used in our calculations was extracted from the literature (as set out above) and came from several sources. Its accuracy is a major factor in the accuracy of the output concentrations. In this work, PHREEQC 2.2 has been used to calculate the equilibrium concentrations of acetic acid and the pH of brine solutions saturated with carbon dioxide at 298 and 333 K respectively. The set equations outlined early on, were used as input thermodynamic data and the deviation from ideal ionic behavior was taken into account using the extended version of the Debye Hückel equation (3-11).

3.3.3.2 Results

In the aqueous sodium chloride brine solutions containing both acetate ions and carbon dioxide, it is necessary to consider nine species, Na^+, H^+, Cl^-, HCO_3^-, CO_3^-, OAc^-, HOAc, H_2O and CO_2. The concentrations of sodium and chloride ions mainly influence the relative amounts of acetate and carbon dioxide derived species through the ionic strength of the solution. Also, the concentration of carbonate is negligible below pH 8 [97]. Hence, these species are not tabulated below. The water does however influence the speciation of the solution in an important way. Especially as the temperature rises, the vapour pressure of water above these solutions is significant approaching 0.2 atm at 333 K. As a result, the fugacity of carbon dioxide is lowered and, consequently, its equilibrium concentration in the aqueous solutions is significantly decreased. This effect is taken into account in the

calculations. In principle, similar values are possible with other weak acid solutions but in reality the full input data are not available. Table 3.6 reports the equilibrium concentrations of the other five species (H^+, HOAc, OAc^-, HCO_3^- and CO_2) in 3 % sodium chloride brine solutions containing several initial acetate concentrations and saturated with carbon dioxide. Data for two temperatures are tabulated; the latter represents a typical temperature of the liquids in an oilfield pipeline.

Intial conc. OAc^-/ mM	**Calculated Equilibrium Concentration/ mM**					**pH**	
	H^+	**HOAc**	**OAc^-**	**CO_2**	**HCO_3^-**	**Calc.**	**Exptl.**
298 K							
0	0.176	-	-	29.2	0.17	3.87	3.90
0.1	0.140	0.008	0.02	29.2	0.20	3.97	
0.5	0.075	0.33	0.17	29.2	0.32	4.24	
1	0.050	0.56	0.44	29.2	0.55	4.42	4.43
5	0.019	1.6	3.4	29.2	1.5	4.85	
10	0.013	2.4	7.6	29.1	2.2	5.02	5.01
50	0.0053	6.0	44	28.8	5.2	5.39	
100	0.0038	8.6	91.4	28.5	7.4	5.54	5.50
333 K							
0	0.121	-	-	11.7	0.11	4.04	
0.1	0.090	0.07	0.03	11.7	0.15	4.17	
0.5	0.045	0.28	0.22	11.7	0.29	4.47	
1	0.030	0.46	0.54	11.7	0.44	4.65	4.62
5	0.012	1.2	3.8	11.7	1.12	5.05	
10	0.008	1.8	8.2	11.7	1.64	5.22	5.18
50	0.0035	4.1	45.9	11.6	3.79	5.58	
100	0.0025	6.2	93.8	11.4	5.33	5.73	5.70

Table 3. 6 *Equilibrium concentrations at 298 and 333 K of species derived from sodium acetate and carbon dioxide, calculated using PHREEQC 2.2. The solution initially contains 3 % NaCl + NaOAc (concentration shown on table) and is saturated with CO_2.*

It can be seen that once again there is good agreement between the experimentally observed and calculated pH. It also confirms that the saturation of the brine solutions with carbon dioxide leads to an increase in the pH and the conversion of acetate ion into acetic acid.

The computations also show that:

- While the brine saturated with carbon dioxide (without acetate present) has a pH of 3.90, the presence of acetate (initially added as sodium acetate) leads to an increase in pH.

- The pH of the solutions as estimated by PHREEQC 2.2 agree closely with the values measured experimentally.

- Although the concentration of free proton is decreased, a significant fraction of the initial acetate is converted to acetic acid.

- In most of the solutions considered, the concentration of the proton donor, acetic acid, is much higher than that of the free proton.

- With increasing initial acetate concentration, the pH increases but the concentration of undissociated acetic acid also increases and this change is more important.

- At a temperature of 333 K, the solubility of carbon dioxide in aqueous solutions is decreased compared with 298 K and this leads to lower equilibrium concentrations of both free proton and undissociated acetic acid at the higher temperature.

- The concentration of bicarbonate is similar to that of acetic acid in most of the solution.

- ❖ The concentration of carbonic acid is constant but low (0.074 mM) at all pH because the solution is in equilibrium with a carbon dioxide atmosphere. Its contribution to the corrosion current density is however very limited because of the low concentration.

These trends are readily understood. The presence of carbon dioxide causes the solution to become somewhat acidic but when acetate ion is present, it acts as a buffer thereby decreasing the pH swing. The buffering action is achieved, however, by the formation of undissociated acetic acid. While carbon dioxide, carbonic acid and bicarbonate are all present, carbon dioxide is the totally dominant species at the pH of interest; bicarbonate is a very weak acid, $pK_A = 10.32$ and the concentration of carbonic acid is very low (and may be estimated by multiplying the equilibrium carbon dioxide concentration by 2.56×10^{-3}) – only 0.074 mM at 298 K [96-97]. The conversion of carbon dioxide to carbonic acetic acid is slow and hence the rate of hydrogen evolution by a mechanism $CO_2 \rightarrow H_2CO_3 \rightarrow H_2$ is low.

In considering the influence of weak acids and their anions on the corrosion of steel, it is critical to recognize that the chemistry and the electrochemistry of their solutions can be determined by the chemistry and the concentrations of the proton donor as well as the free proton. Conversely, it is important to recognize that the chemistry of carbon dioxide saturated brine will be identical to the equivalent acetate buffer prepared from sodium acetate and acetic acid. Further, when comparing table 3.5 with table 3.6, it can be seen that the calculated concentrations of free proton using equation (3-12) never agreed exactly with the values found using the computer program PHREEQC 2.2. This is not surprising since speciation calculations made using equation (3-12) did not take into account the non-ideality of the brine solution. However, it should be noted that the calculated concentrations of acetic acid are much higher than that of the free proton concentrations and are not significantly influenced by the non-ideal behavior of the ionic species. Hence, the simple calculation gives a reasonable estimate of the acetic acid concentrations in the brine solutions.

3.4 Oilfield brines

When samples of real oilfield brines were analysed (see Chapter Six), it became clear that the speciation is dependent on additional factors:

- Most importantly, the brines can contain bicarbonate as an independent species. As result, the pH of the brines could be determined by the CO_2/bicarbonate ratio. In the above discussion, the bicarbonate arises from the saturation by CO_2 and the pH results from the acetate/acetic acid ratio and the solubility of CO_2.

- The ionic strength of the brines can be much higher than the 3 % NaCl. This leads to problems in estimating the mean ionic activity coefficient.

- While we were assured that oilfield brines ranged in acetate concentration between 0 – 100 mM and these could also contain low or high bicarbonate concentrations, the brines provided generally combined low acetate concentration and/or high bicarbonate. Neither of these are good matches to the model solutions used for much of the work.

This section discusses the consequences of the presence of bicarbonate. Our above modeling ignored the presence of bicarbonate as an independent component of the brine. The solution composition was based on the presence of 3 % NaCl, NaOAc, and CO_2 and the only bicarbonate was that resulting from the saturation of the brine with carbon dioxide. When bicarbonate is present as an independent constituent of the brine, its presence must be taken into account. In this discussion, it will be assumed that the brine is in contact with carbon dioxide at atmospheric pressure (not necessary the real situation in the oilfield) and hence the concentration of CO_2 in the solutions is 29 mM At 298 K and 12 mM at 333 K.

Table 3.7 summarises the pK_As for all the potential proton donors in the system.

Species	pK_A
H_2CO_3	3.75
HOAc	4.75
CO_2	6.35
H_2O	7.00
$H_2CO_3^-$	10.32

Table 3. 7 *pK_A values for potential acids in the brine.*

In considering the speciation, it is necessary to consider the following equilibria:

$$HOAc \rightleftharpoons H^+ + OAc^- \quad (4)$$

$$H_2CO_3 \rightleftharpoons H^+ + HCO_3^- \quad (5)$$

The equilibrium constant for (1) and (2) are generally written as [97, 144]:

$$K_4 = \frac{\gamma_\pm^2 c_{H^+} c_{OAc^-}}{c_{HOAc}} = 1.8\times10^{-5} \quad (3\text{-}7)$$

$$K_5 = \frac{\gamma_\pm^2 c_{H^+} c_{HCO_3^-}}{c_{H_2CO_3} + c_{CO_2}} = 4.3\times10^{-7} \quad (3.14)$$

where the equilibrium

$$CO_2 + H_2O \rightleftharpoons H_2CO_3 \quad (6)$$

lies well to the left with $K_6 = 2.56\times10^{-3}$. For any composition, the solution has a unique pH. Hence, for a solution containing HOAc, OAc^-, H_2CO_3 and CO_2, manipulations of equations (3) and (4) readily lead to:

$$K_3 \frac{c_{HOAc}}{c_{OAc^-}} \approx K_4 \frac{c_{CO_2}}{c_{HCO_3^-}} \quad (3\text{-}15)$$

At 298 K, this can be written:

$$\frac{c_{HOAc}}{c_{OAc^-}} \approx 0.024 \frac{29\ \text{mM}}{c_{HCO_3^-}} \quad (3\text{-}16)$$

The concentration of acetic acid (and hence its importance in influencing the rate of steel corrosion) is determined by both the total acetate concentration and the bicarbonate level in the brine (or more precisely the ratio of HCO_3^-/CO_2 concentrations). This may be illustrated by considering three solutions at 298 K containing acetate saturated with CO_2 and containing different bicarbonate concentrations:

a) 290 mM HCO_3^-

The solution pH is determined by equation (3-14) and will be close to 7.3. At any acetate concentration, the concentration of acetic acid concentration is negligible.

b) 29 mM HCO_3^-

The solution pH is approximately 6.3. Approximately 2.4 % of the total acetate is present as acetic acid. A significant acetic acid will only result when the acetate concentration is very high.

c) < 2.9 mM HCO_3^-

The solution pH can drop into the range 4.5 – 6.0 where there is substantial conversion of acetate to acetic acid (note that HCO_3^- comes in the range 0.1 – 8 mM resulting from the saturation of an acetate solution by CO_2, see table 3.6, page 3-12). Even with total acetate concentration of 1 mM and below, the resulting acetic acid can influence the rate of corrosion.

Table 3.8 illustrates these statements.

Brines	Initial pH	pH after CO_2 saturation	[HOAc] after CO_2 saturation/ mM
5 mM NaOAc + 1 mM $NaHCO_3$	7.28	5.09	3.5×10^{-1}
5 mM NaOAc + 5 mM $NaHCO_3$	7.99	5.48	7×10^{-2}
5 mM NaOAc + 10 mM $NaHCO_3$	8.12	5.90	3.5×10^{-2}
5 mM NaOAc + 50 mM $NaHCO_3$	8.20	6.64	7×10^{-3}
5 mM NaOAc + 100 mM $NaHCO_3$	8.25	6.91	3.5×10^{-3}

Table 3. 8 *pH measured for solutions containing 5 mM NaOAc + different concentrations of $NaHCO_3$ saturated with carbon dioxide and equilibrium acetic acid concentrations estimated using equation (3 - 16). Temperature 298 K*

Table 3.8 reports the measured pH for solutions containing 5 mM NaOAc + different concentrations of sodium bicarbonate saturated with carbon dioxide at 298 K. Further, the estimated equilibrium concentrations of acetic acid (using equation (3-16)) after CO_2 saturation are also presented. It can be seen that with increasing concentration of sodium bicarbonate, the pH of the solutions increases. It should also be stressed that the acetic acid concentrations in these solutions are very low when the medium contains bicarbonate. For example with 100 mM HCO_3^-, after CO_2 saturation, the concentration of acetic acid is estimated as 3.5×10^{-3} mM.

3.5 Conclusions

It has been confirmed that the composition of brines containing both acetate ion and carbon dioxide can be predicted with reasonable accuracy by modifying the software available on the World Wide Web and using equilibrium constant data from the literature. However, it has been shown that it is essential to take into account the deviation from ideal ionic behavior. The calculations confirm that when CO_2 is dissolved, the solution becomes acidic but the presence of acetate ion moderates the

acid and, as a result the brines have a much higher concentration of proton donor, acetic acid, than free proton. In considering the influence of weak acid and their anions on the corrosion of steel, it is critical to recognize that the chemistry and the electrochemistry of their solutions can be determined by the chemistry and the concentrations of proton donor as well as free proton. Since the equilibrium

$$HOAc \rightleftharpoons H^+ + OAc^-$$

is rapid, the acetic acid (HOAc) can readily replenish any H^+ removed by an electrochemical or chemical reaction. If a brine contains bicarbonate as an independent species, at concentration above 2.9 mM it has a marked influence on the solution pH and therefore the speciation of the brine. This can be understood in a semi-quantitative way using simple concepts. Again, for a precise treatment the reduction of carbonic acid (both equilibrium and that formed by conversion of carbon dioxide) should also be recognized but the contribution of this reaction is practically insignificant (see page 3-9).

pH swing. The buffering action is achieved by the conversion of acetate to acetic acid and, as a result the brines have a much higher concentration of proton donor, acetic acid, than free proton. In considering the influence of weak acid and their anions on the corrosion of steel, it is critical to recognize that the chemistry and the electrochemistry of their solutions can be determined by the chemistry and the concentrations of proton donor as well as free proton. Since the equilibrium

$$HOAc \rightleftharpoons H^+ + OAc^-$$

is rapid, the acetic acid (HOAc) can readily replenish any H^+ removed by an electrochemical or chemical reaction. If a brine contains bicarbonate as an independent species, at concentration above 2.9 mM it has a marked influence on the solution pH and therefore the speciation of the brine. This can be understood in a semi-quantitative way using simple concepts. Again, for a precise treatment the reduction of carbonic acid (both equilibrium and that formed by conversion of carbon dioxide) should also be recognized but the contribution of this reaction is practically insignificant (see page 3-9).

Chapter Four

4 Electrochemistry of 3 % NaCl Brine Containing Acetate Ion and Carbon dioxide on a Pt Rotating Disc Electrode

4.1 Introduction

In this chapter a study of the voltammetry at a Pt rotating disc electrode (RDE) of (a) sodium acetate (NaOAc) + acetic acid (HOAc) in 3 % sodium chloride brine (NaCl) and (b) sodium acetate (NaOAc) + carbon dioxide (CO_2) in 3 % sodium chloride brine (NaCl) is reported. The detailed interpretation calls upon the speciation calculations in the previous chapter. It was noted in the introduction chapter that the voltammetry of acetate buffers has been widely studied at Pt rotating disc electrode and at Pt microelectrodes; it must be emphasized that the presence of 3 % sodium chloride in the solution changes the speciation significantly (see Chapter Three).

4.2 Voltammetry of acetate buffers at Pt rotating disc electrode

4.2.1 Voltammetry of acetate buffers at 298 K

Prior to recording voltammograms in the solution under study, the Pt rotating disc electrode was cleaned by cycling its potential at 100 mV s^{-1} between – 250 mV and + 1250 mV vs. SCE in 1 M sulphuric acid until the voltammogram had the classical form with sharp hydrogen adsorption and desorption peaks [151] as shown in figure 4.1.

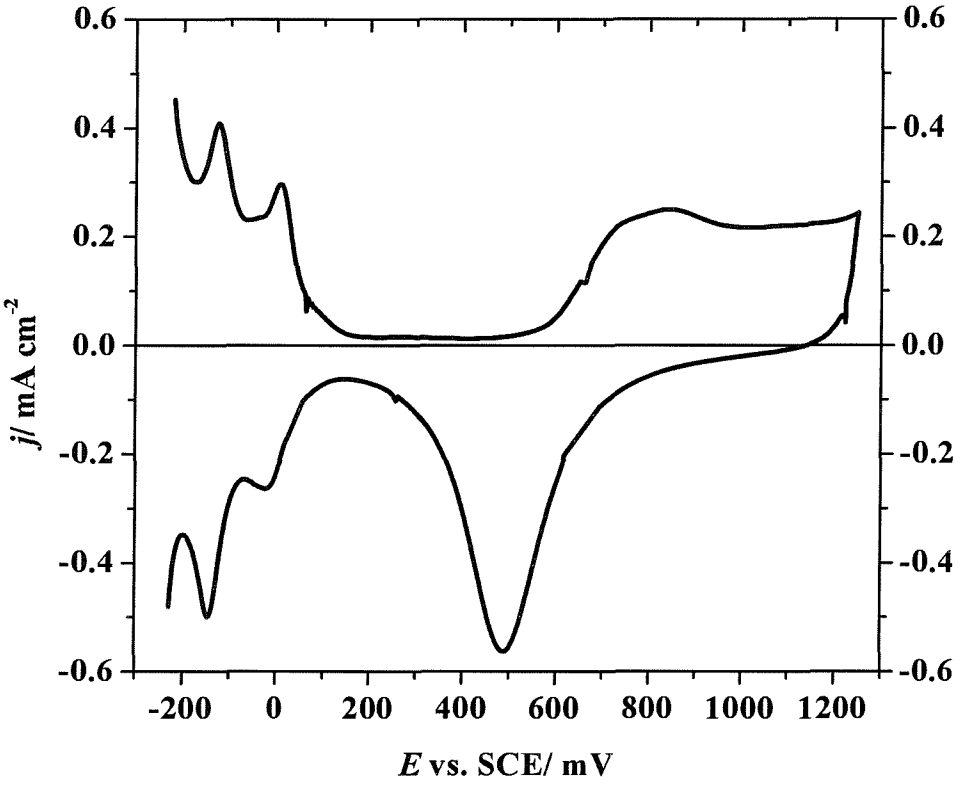

Figure 4. 1 *Cyclic voltammetry for a clean Pt rotating disc electrode in 1M H_2SO_4. Cleaning of the surface by successive potentiodynamic sweeps. Surface area of Pt RDE, 0.16 cm^2. Potential scan rate 100 mV s^{-1}.*

Figure 4.2 illustrates typical steady state voltammograms recorded at a precleaned Pt rotating disc electrode for a degassed aqueous solution of 3.34 mM HOAc + 10 mM NaOAc + 3 % NaCl (purged with N_2) over a range of rotation rates. A potential scan rate of 20 mV s^{-1} was used for this experiment. The potential limits were 0 mV vs. SCE and – 1000 mV vs. SCE. The experiment was performed at 298 K. It can be seen from the voltammograms that hardly any current is passed until – 475 mV versus SCE, then the currents increase smoothly until they reach a plateau around -650 mV versus SCE. Further, it can be noted that the general shapes of the voltammograms are similar to one another. A single, steep reduction wave with a well-developed limiting current plateau, j_{lim}, is observed at each rotation rate. The form of the responses is essentially identical to voltammograms recorded at Pt ultramicrodisc electrodes [128-134].

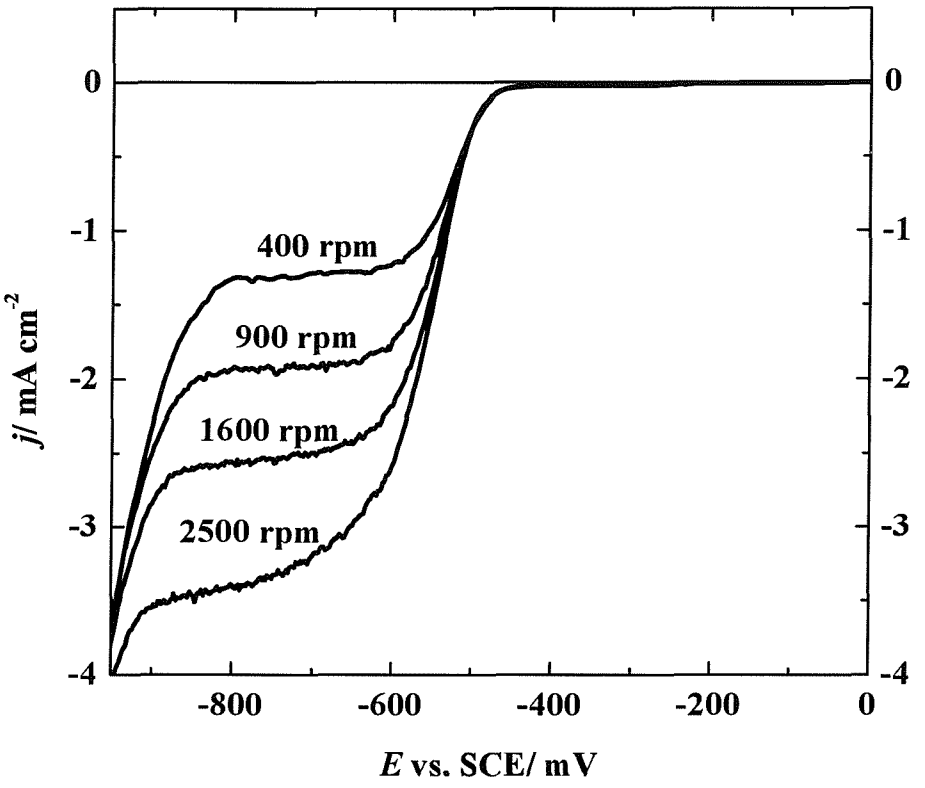

Figure 4. 2 *Voltammograms recorded at a precleaned rotating disc electrode (area, 0.16 cm^2) in a deoxygenated aqueous solution containing 3 % NaCl + 10 mM NaOAc + 3.34 mM HOAc. Rotation rates shown on the figure. Temperature 298 K.*

There were some noteworthy features in the current-potential curve presented in figure 4.2. First, at the foot of the reduction wave, it is clear that the current is independent of the rotation rate. Therefore, it can be inferred that the current is kinetically controlled during this part of the curve. Second, in the plateaux region of the curve, the limiting current densities depend strongly on the rotation rate of the Pt disc electrode. In fact, the limiting currents are proportional to the square root of the rotation rate of the disc electrode as predicted by the Levich equation [60]:

$$j_{\text{lim}} = 0.620nFD^{2/3}\nu^{-1/6}c\omega^{1/2} \qquad (4\text{-}1)$$

where j_{lim} is the limiting current density (in A m^{-2}); D is the diffusion coefficient in (m^{-2} s^{-1}); n is the number of electrons transferred, F is the Faraday constant in (C mol^{-1}), c is the concentration of the electroactive species in (mol m^{-3}), ω is of the

rotation rate in (rad s^{-1}) and ν is the kinematic viscosity in (m^2 s^{-1}). The kinematic viscosity is defined as the viscosity of the solution divided by its density. The kinematic viscosity of most aqueous solutions is approximately 1×10^{-6} m^2 s^{-1}. When the experiments were repeated for four different concentrations of acetic acid, plots of limiting current density versus the square root of the rotation rate are linear and pass through the origin as shown in figure 4.3.

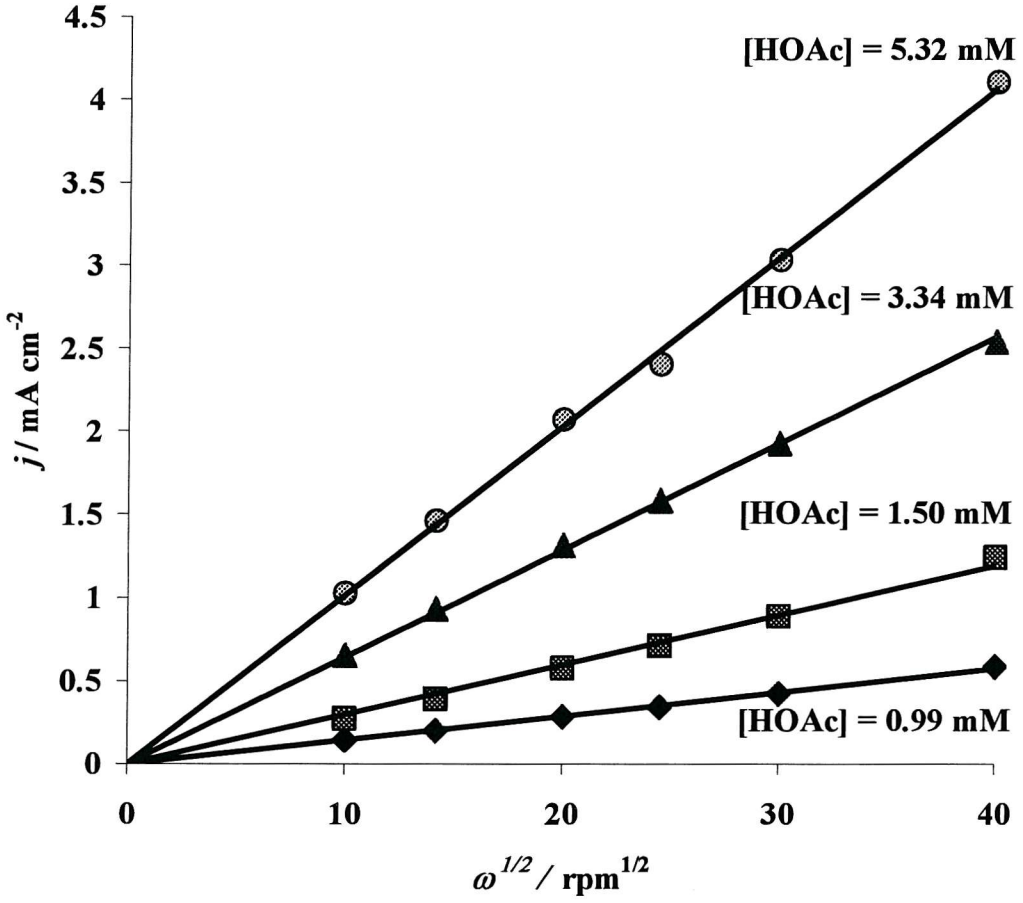

Figure 4. 3 *Plots of j versus $\omega^{1/2}$ at potentials in the plateau regions of the j-E curves in figure 4.2. Solution contains 10 mM NaOAc + 3 % NaCl over a range of pH (by addition of an aliquot of 1 M HOAc). Pt RDE (area 0.16 cm^2). Potential scan rate 20 mV s^{-1}. Temperature 298 K.*

In addition, when the rotation rate of the Pt rotating disc electrode was varied, the limiting currents are always proportional to the concentration of acetic acid as shown in figure 4.4. Similar behavior has been noted on Pt microelectrodes [126,127,134]. On the other hand, there is no relationship between the limiting

currents and the concentrations of free protons (as calculated in previous chapter, see table 3.6, Chapter Three, page 3-12). The limiting current can be larger than those predicted for mass transport of protons [152] by a factor > 100. The electrode reaction is therefore fully mass transport controlled in the plateau region and it is the transport of acetic acid that determines the current density.

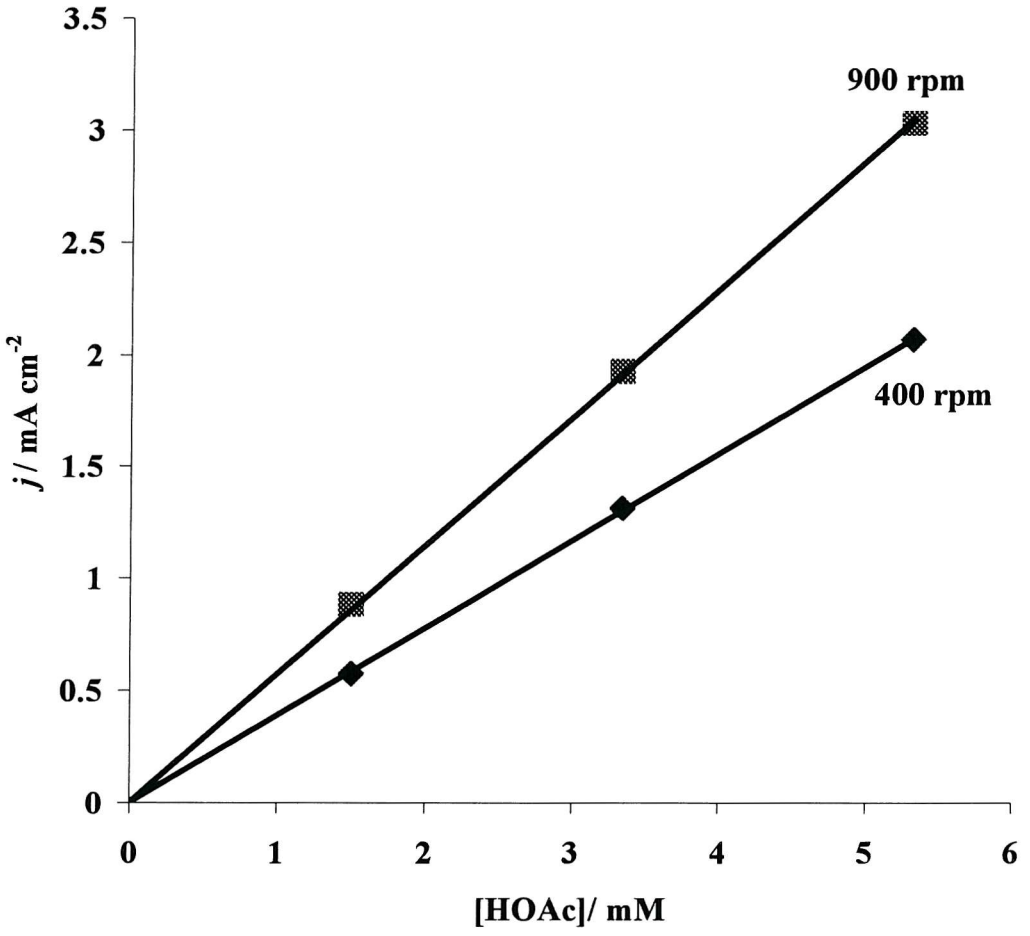

Figure 4. 4 *Variation of the current density at –750 mV vs. SCE at a Pt RDE (area, 0.16 cm^2) in 10 mM NaOAc + 3 % NaCl, with the concentration of acetic acid (rotation rate 400 and 900 rpm). Temperature 298 K.*

As an example of the application of the Levich equation, the diffusion coefficient of the acetic acid was evaluated. The measurement was carried out in a 10 mM sodium acetate solution + 3 % sodium chloride, with different concentrations

of acetic acid. The diffusion coefficients were calculated from the slopes of the Levich plots (see figure 4.3). The results obtained are summarized in table 4.1.

C_{HOAc}/ mM	pH	Slopes (Levich plots) A m^{-2} $rad^{-1/2}$ $s^{1/2}$	10^9 D_{HOAc}/ m^2 s^{-1}
1.50	5.43	0.92	1.05
3.34	5.00	2.01	1.00
5.32	4.80	3.19	1.00

Table 4. 1 *Experimental pH and estimated diffusion coefficient (D) for deoxygenated solutions of 10 mM NaOAc + 3 % NaCl with various additions of acetic acid. Diffusion coefficients calculated from the slopes of Levich plots (units, A m^{-2}/(radians $s^{-1})^{½}$). Area of Pt RDE, 0.16 cm^2.*

As expected the diffusion coefficient is independent of the acetic acid concentrations, for this concentration range. Further, the value obtained for the diffusion coefficient, *D*, for acetic acid is always ~ 1×10^{-9} m^2 s^{-1}, very close to that reported previously in the literature [124,135,130]. This confirms the conclusion in the literature that in the limiting current region all the acetic acid is reduced as it reaches the cathode surface. Further data taken from voltammograms recorded at three different pH are reported in table 4.2.

C_{HOAc}/ mM	pH	$E_{1/2}$ / mV	$E_{3/4} - E_{1/4}$ / mV
1.50	5.43	-552	39
3.34	5.00	-520	45
5.32	4.80	-545	55

Table 4. 2 *Data taken from voltammograms at a Pt RDE in deoxygenated solutions of 3 % NaCl + 10 mM NaOAc with various concentrations of acetic acid. Area of Pt RDE, 0.16 cm^2. Rotation rate 600 rpm. Temperature 298 K.*

The half wave potentials are only slightly negative of the equilibrium potential for the H^+/H_2 couple calculated using the Nernst equation [59,60]:

$$E_{eq} = E_e^o + \frac{2.3RT}{nF}\log\frac{a_{H^+}^2}{a_{H_2}} \quad (4\text{-}2)$$

leading to

$$E_{1/2} = -0.240 - 0.06pH \; vs.\; SCE \quad (4\text{-}3)$$

where E_{eq} is the equilibrium potential (in V), E_e is the formal potential for the couple in the solution under consideration (in V), R is the gas constant (in J K^{-1} mol^{-1}), T is the temperature (in K), n is the number of electrons transferred, F is the Faraday constant (in C mol^{-1}) and pH is the $-\log_{10} a_{H^+}$. For example, for the solution containing 10 mM NaOAc + 3 % NaCl + 5.32 mM HOAc, pH 4.80, the experimental half wave potential ($E_{1/2}$) is – 545 mV versus SCE and the value calculated assuming $a_{H^+} = c_{H^+}$ is – 529 mV versus SCE. Moreover, the Tomes slope values are very similar to the values reported at microelectrodes [125,130]. The Tomes slope is always < 60 mV consistent with a mechanism for hydrogen evolution that involves Pt-H intermediates as illustrated below:

$$H^+ + e^- + Pt \rightleftharpoons Pt\text{-}H \quad (1)$$

$$H^+ + e^- + Pt\text{-}H \rightleftharpoons Pt + H_2 \quad (2)$$

Both these features have been interpreted as being consistent with the mechanism described by the following equations [122,133,153]:

$$HOAc \overset{\text{solution}}{\rightleftharpoons} H^+ + OAc^- \quad (3)$$

$$H^+ + e^- \overset{\text{electrode}}{\rightleftharpoons} \tfrac{1}{2} H_2 \quad (4)$$

At the electrode surface, H^+ can be reduced but HOAc does not reduce directly. In the solution, the concentration of HOAc is much greater than H^+ since

HOAc is a weak acid. An equilibrium exists in the solution but close to the electrode surface because H^+ is continuously removed at the electrode and the equilibrium is pulled to the right. Because the concentration of HOAc greatly exceeds the concentration of H^+, it is HOAc, which supplies the protons for the electrode reaction, and the flux is related to its transport through the diffusion layer. Therefore, the limiting currents are those predicted for the mass transport controlled reduction of the HOAc in the solution.

4.2.2 Voltammetry of acetate buffers at 333 K

The voltammetry was also recorded at several temperatures over the range 298 – 333 K. Figure 4.5 illustrates a typical set of voltammograms recorded at a precleaned Pt rotating disc electrode for a solution in 3 % NaCl containing both acetate ion and acetic acid at a temperature of 333 K; in fact this voltammogram is for a solution containing 3.34 mM HOAc + 10 mM NaOAc + 3 % NaCl.

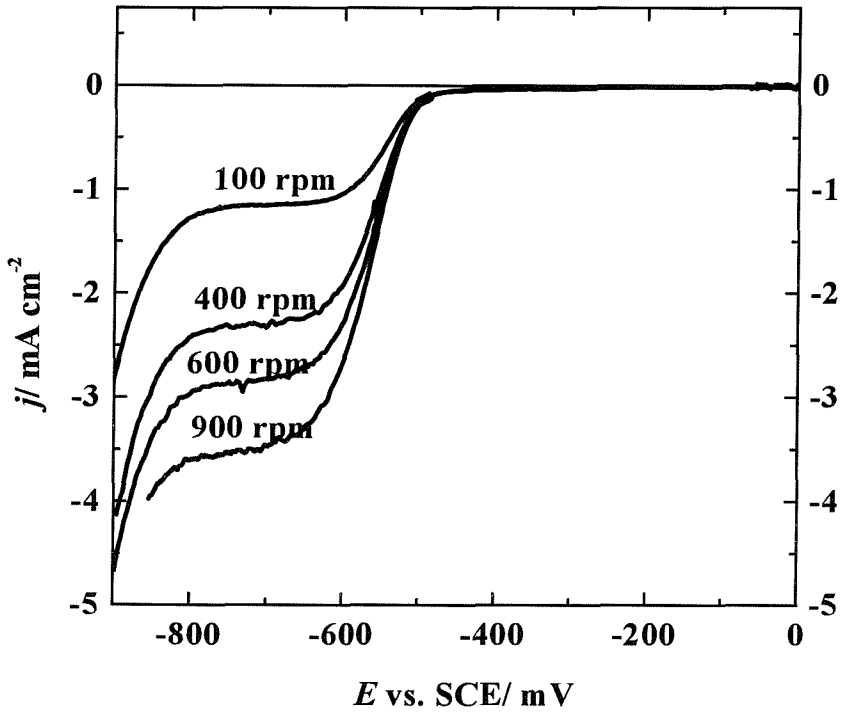

Figure 4. 5 *Steady state voltammograms recorded at a precleaned Pt rotating disc electrode (area, 0.16 cm^2) in a deoxygenated aqueous solution containing 3 % NaCl + 10 mM NaOAc + 3.34 mM HOAc at 333 K. Rotation rates shown on the figure.*

It can be noted that the voltammograms remain very similar to those at 298 K (see figure 4.2). A single, steep reduction wave, with a well-developed limiting current plateau was observed at each rotation rate. However, the most obvious change in the voltammograms with increasing the temperature is the increase in the limiting current densities. Perhaps, more surprisingly, the waves at 333 K are less steep; the higher value of RT/F is one contributing factor. It can be seen that the quality of all the responses is very high, and the quality is comparable with the best at Pt microelectrode [128,129,134]. Further, the limiting currents can be seen to be proportional to the square root of the rotation rates of the disc. Indeed, for several concentrations of acetic acid in 10 mM NaOAc + 3 % NaCl, plots of the limiting currents versus the square root of the rotation rate are linear and pass through the origin as shown in figure 4.6; the electrode reaction is therefore fully mass transport controlled in the plateau region.

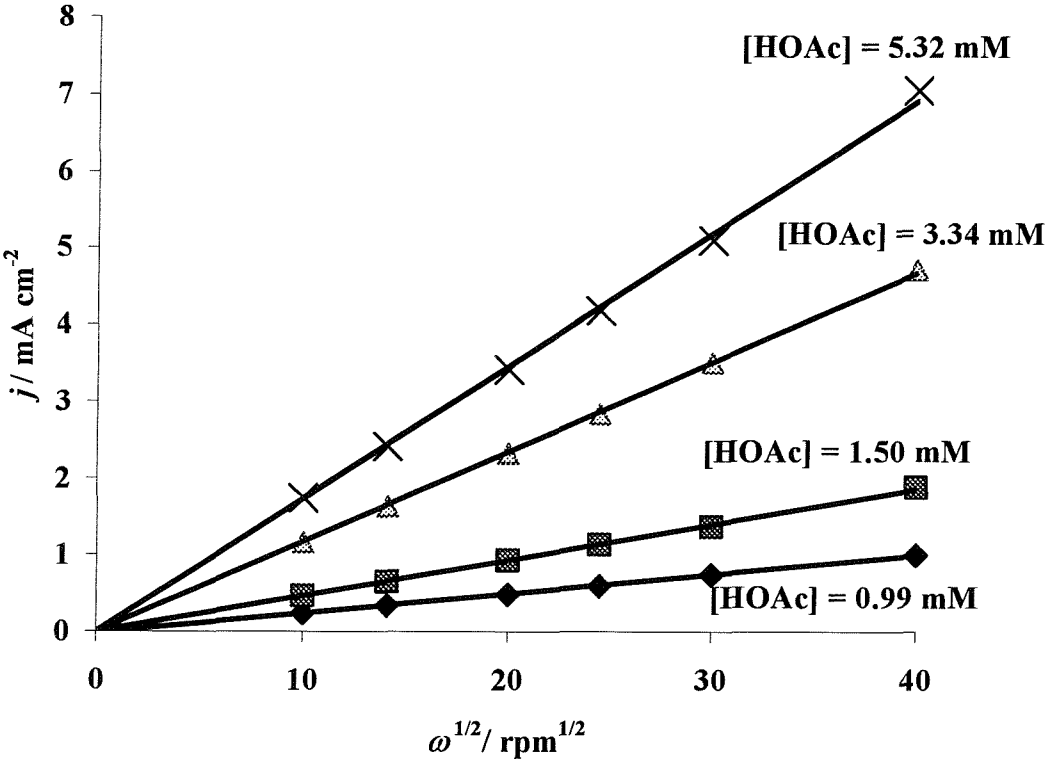

Figure 4. 6 *Plots of j_L versus $\omega^{1/2}$ at potentials in the plateau regions of the j-E curves in figure 4.5. Solution contains 10 mM NaOAc + 3 % NaCl over a range of pH (by addition of an aliquot of 1 M HOAc). Pt RDE (area 0.16 cm^2). Potential scan rate 20 mV s^{-1}. Temperature 333 K.*

The Levich equation (4-1) was used to estimate values for the diffusion coefficients of the acetic acid at 333 K. The measurements were carried out in a 10 mM NaOAc + 3 % NaCl solutions, with different concentrations of acetic acid. The diffusion coefficients were calculated from the slopes of the Levich plots (see figure 4.6) and the results obtained are summarized in table 4.3. From data shown in table 4.3, it appears that the average value for the diffusion coefficient of acetic acid is 2.24×10^{-9} m^2 s^{-1}. Further, it is evident that the diffusion coefficient is independent of the acetic acid concentrations. Also, by increasing the temperature from 298 K to 333 K, the diffusion coefficient increases as expected.

C_{HOAc}/ mM	pH	Slopes (Levich plots)	10^9 D_{HOAc}/ m^2 s^{-1}
1.50	5.43	1.43	2.04
3.34	5.00	3.61	2.43
5.32	4.80	5.42	2.25

Table 4. 3 *Experimental pH and estimated diffusion coefficient (D) for deoxygenated aqueous solutions of 10 mM NaOAc + 3 % NaCl with various addition of aliquots of 1 M acetic acid. Area of Pt RDE, 0.16 cm^2. Diffusion coefficients calculated from the slopes of Levich plots (units, A m^{-2}/(radians s^{-1}) $^{1/2}$). Temperature 333 K.*

Moreover, a plot of log D versus 1/T from voltammograms run at 900 rpm for the series of temperatures was linear as shown in figure 4.7, and leads to an energy of activation for the diffusion of acetic acid of ~ 25 kJ $mole^{-1}$.

It should be noted that the activation energy, E_A, was estimated using equation (4-4):

$$\ln D = \ln D^0 - \frac{1}{T}[\frac{E_A}{R}] \qquad (4\text{-}4)$$

where D is the diffusion coefficient of the acetic acid (in m^2 s^{-1}), T is the temperature (in K), E_A is the activation energy (in kJ $mole^{-1}$), and R is the gas constant (in J K^{-1} mol^{-1}).

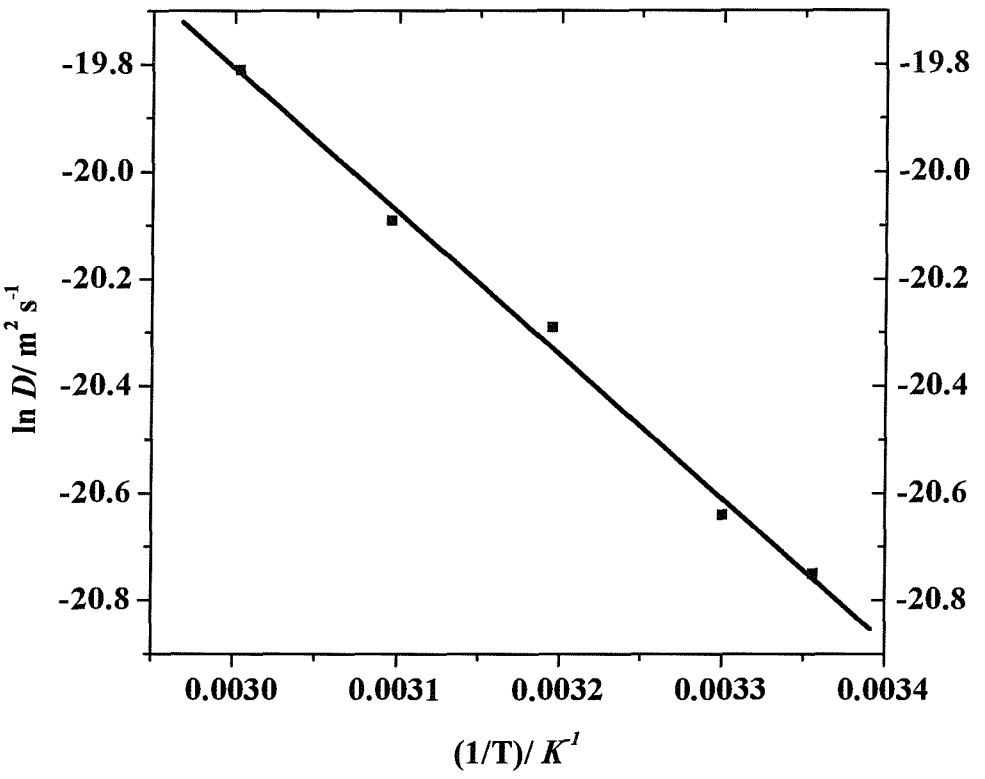

Figure 4. 7 *Arrhenius plot for the Diffusion coefficient of acetic acid.*

Further data taken from the responses at 333 K for solutions of 10 mM NaOAc + 3 % NaCl, with different concentrations of acetic acid are reported in table 4.4.

C_{HOAc}/ mM	pH	$E_{1/2}$/ mV	$E_{3/4} - E_{1/4}$/ mV
1.50	5.43	-557	59
3.34	5.00	-566	57
5.32	4.80	-555	55

Table 4. 4 *Data taken from voltammograms at a Pt RDE in deoxygenated solution of 3 % NaCl + 10 mM NaOAc with various concentrations of acetic acid. Area of Pt RDE, 0.16 cm^2. Rotation rate 600 rpm. Temperature 333 K.*

According to table 4.4, several observations can be made:

It can be seen that the data obtained at 333 K remain very similar to those at 298 K. The half wave potentials are only slightly negative to the equlibrium for the

H^+/H_2 couple at these pH, while the Tomes slopes [$E_{3/4} - E_{1/4}$] are not constant as a function of acetic acid concentration and are consistent with the values reported at Pt microelectrodes [125,130]. However, a small cathodic shift is observed for the reduction currents on going from 298 K to 333 K. It should be noted immediately that the corrosion potentials for the steel in the brine solutions are in the range – 650 mV to – 900 mV (see later). Such potentials are well negative of the equilibrium potentials for the reduction of acetic acid to hydrogen. Indeed, at Pt, admittedly a good catalyst for the reaction, the reduction of acetic acid is fully mass transport controlled at the corrosion potentials of the steel in the media.

4.3 Voltammetry of other carboxylic acids at Pt rotating disc electrode

The voltammetry of other weak acids (formic acid, propionic acid and lactic acid) at a precleaned Pt rotating disc electrode in 3 % NaCl brine was investigated at 298 K. Experiments were carried out on solutions with known ratios of anion/acid. Figure 4.8 illustrates typical voltammograms recorded at a Pt rotating disc electrode for deoxygenated aqueous solutions of (a) 2.5 mM propionic acid + 10 mM sodium propionate + 3 % NaCl and (b) 2.5 mM lactic acid + 10 mM sodium lactate + 3 % NaCl (purged with N_2) over a range of rotation rates. A potential scan rate of 20 mV s^{-1} was used for these experiments. All voltammograms were recorded at 298 K. The form of the responses is identical to voltammograms obtained for sodium acetate/acetic acid buffers (see figure 4.2). A single, well-defined sigmoidal reduction wave with a well-developed limiting current plateau is observed at each rotation rate for both propionic and lactic acid. Moreover, it should be noted that limiting current densities are essentially identical and depend strongly on the rotation rates of the Pt rotating disc electrode. In addition, at all concentrations of weak acids used, plots of limiting current versus the square root of the rotation rate are linear and pass through the origin. The electrode reaction is therefore fully mass transport controlled in the plateau region and it is the transport of the weak acids to the electrode surface that determines the current density.

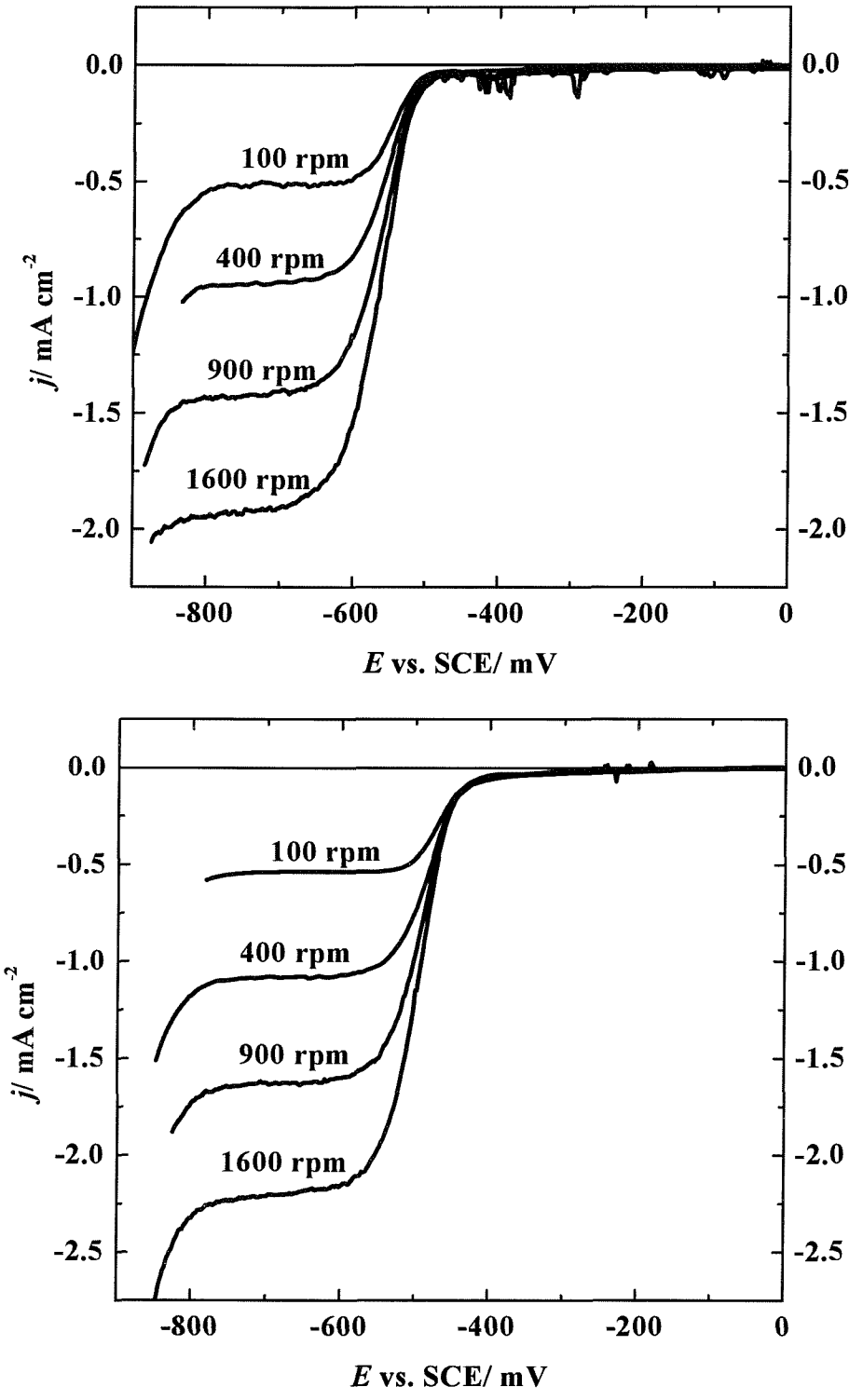

Figure 4. 8 *Voltammograms recorded at a precleaned Pt rotating disc electrode (area, 0.16 cm^2) in degassed aqueous solutions containing (a) 2.5 mM propionic acid + 10 mM sodium propionate + 3% NaCl and (b) 2.5 mM lactic acid + 10 mM sodium lactate + 3 % NaCl. Rotation rates shown on the figure. Temperature 298 K.*

Further data taken from the voltammograms for brines with known weak acids concentrations (~ 2.5 mM) are reported in table 4.5. The responses obtained for formic acid were similar to those in figure 4.8.

Acid	Dissociation constants	pH	$E_{1/2}$/ mV	$E_{3/4} - E_{1/4}$/ mV	$10^9 D_{acid}$/ $m^2 s^{-1}$
Formic acid	1.77×10^{-4}	4.10	-485	55	1.45
Acetic acid	1.75×10^{-5}	5.22	-550	41	1.08
Propionic acid	1.34×10^{-5}	5.29	-558	45	1.07
Lactic acid	1.38×10^{-4}	4.22	-490	45	1.28

Table 4. 5 *Data taken from voltammograms recorded at a Pt RDE, rotation rate 900 rpm, for deoxygenated aqueous solutions of 3 % sodium chloride + 10 mM sodium salt of weak acid + 2.5 mM of weak acid. Temperature 298 K.*

It should be noted that the diffusion coefficients for the acids in the brines, were calculated from plots of limiting current densities versus the square root of rotation rates of the rotating disc electrode. From table 4.5, it is evident that, at fixed concentration of weak acids, the half wave potentials show a small shift towards more negative potentials, with decreasing value for the dissociation constants of the acids. Similar behavior has been reported in the literature for experiments carried out on Pt microelectrodes [134]. Further, the pH for each solution is reported in table 4.5, and as expected the pH decreases with increasing value for the dissociation constants of the acids.

A further set of experiments was carried out with three different weak acids at a fixed pH of 4.80. Voltammograms were recorded at the Pt rotating disc electrode and the expected well-shaped reduction wave was recorded. Table 4.6 reports the half wave potential ($E_{1/2}$) and the limiting current densities (j_{lim}) for responses at 400 rpm.

Acid	Dissociation constants	pH	$E_{1/2}$ / mV	[Acid]/ mM	j_{lim}/ mA cm^{-2}	
					Expt.	Calc.
Formic acid	1.77×10^{-4}	4.80	-510	0.60	0.26	0.28
Acetic acid	1.75×10^{-5}	4.80	-539	5.82	2.23	2.38
Propionic acid	1.34×10^{-5}	4.80	-550	7.05	2.65	2.87

Table 4. 6 *Data taken from voltammograms recorded at a Pt RDE, rotation rate 400 rpm, for aqueous solutions of 3 % sodium chloride + 10 mM sodium salt of weak acid, pH 4.80 (by addition of aliquots of 1 M weak acid). Temperature 298 K.*

According to table 4.6, it can be seen that with increasing the dissociation constant of the acid, there is a small shift in the half wave potential towards more positive potentials but the limiting current decreases. This observation is consistent with work done by Stojek and co-workers [128]. This decrease reflects the lower concentration of proton donor with increase in the dissociation constant. In fact, during the preparation of the solutions, aliquots of 1 M acid were added to adjust to pH 4.80. The calculated concentration of acid from these additions is reported in table 4.6. Since the concentrations of the acid in the three solutions are known, it is possible to calculate the expected limiting current (using the diffusion coefficients from table 4.5). The experimental and the calculated values of the limiting current, j_{lim}, are compared in table 4.6 and it can be seen that the agreement is excellent.

4.4 Voltammetry of acetate solutions saturated with CO_2 at Pt RDE

4.4.1 Voltammetry of acetate solutions saturated with CO_2 at 298 K

Typical steady state voltammograms recorded at 20 mV s^{-1} for a solution containing 10 mM NaOAc + 3 % NaCl, saturated with carbon dioxide, pH 5.01 (after carbon dioxide saturation), but without addition of acetic acid, using a Pt rotating

disc electrode over a range of rotation rates are reported in figure 4.9. The experiment was carried out at 298 K.

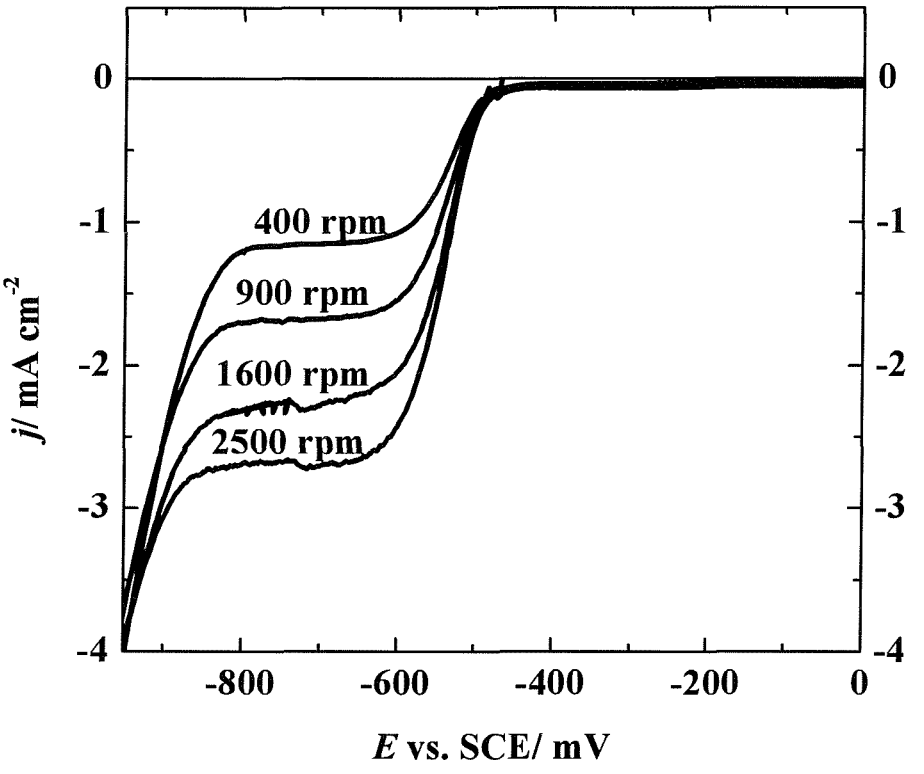

Figure 4. 9 *Steady state voltammograms recorded at a Pt RDE (area, 0.16 cm^2), for an aqueous solution of 10 mM NaOAc + 3 % NaCl, saturated with carbon dioxide. Rotation rates shown on the figure. Temperature 298 K.*

The potential was swept from 0.0 mV to – 1000 mV versus SCE. The similarity of the voltammograms to those in figure 4.2 is again striking. Single well-formed reduction waves, close to – 550 mV versus SCE with well-developed limiting current plateaux, are again observed. Further, negative to – 600 mV versus SCE, the height of the current plateaux increases with the rotation rate of the Pt RDE. In addition, plot of j_{lim} versus the square root of the rotation rates according to the Levich equation (4-1) was found to be linear and pass through the origin, confirming that the reduction current is entirely mass transport controlled as shown in figure 4.10. Moreover, the half wave potentials are close to those calculated for the reversible reduction of protons at the pH of the solution using the Nernst

equation (4-2). It is to be expected that saturation of the brine containing acetate with the acid gas, CO_2, will lead to the formation of acetic acid (see previous chapter) and in view of the similarity between figure 4.9 and figure 4.2, there can be no doubt that the observed reduction waves result from the reduction of acetic acid in the solution (the limiting currents are again far too large to result from the reduction of free proton alone).

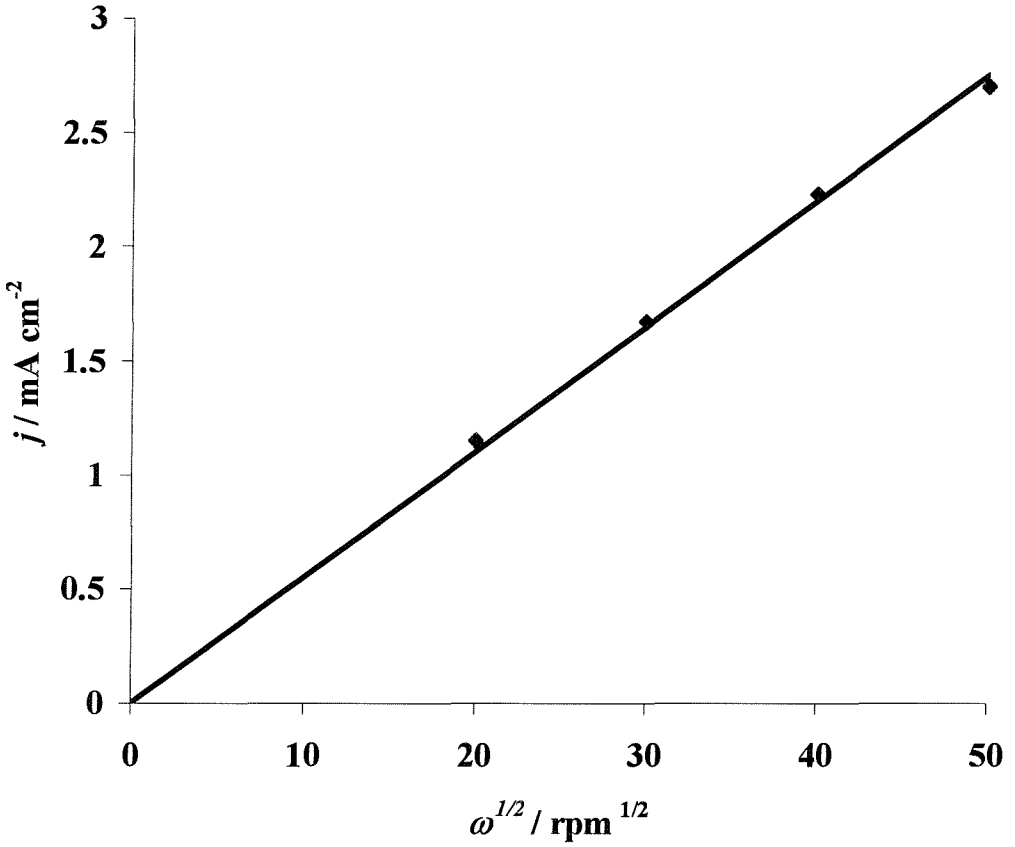

Figure 4. 10 *Plot of j_L versus $\omega^{1/2}$ at potentials in the plateau regions of the j-E curves in figure 4.9. Solution contains 3 % NaCl + 10 mM NaOAc saturated with carbon dioxide. Temperature 298 K.*

The same experiments were repeated using 3 % NaCl brines but containing 1 mM and 100 mM NaOAc. Figure 4.11 shows voltammograms recorded at the Pt RDE for aqueous solutions of 1 mM and 100 mM NaOAc + 3 % NaCl, saturated with carbon dioxide, pH 4.43 and 5.50 respectively (after carbon dioxide saturation),

at 298 K and a rotation rate of 400 rpm. Also, the 10 mM NaOAc data for saturated carbon dioxide brine (pH 5.01) has been included for comparison.

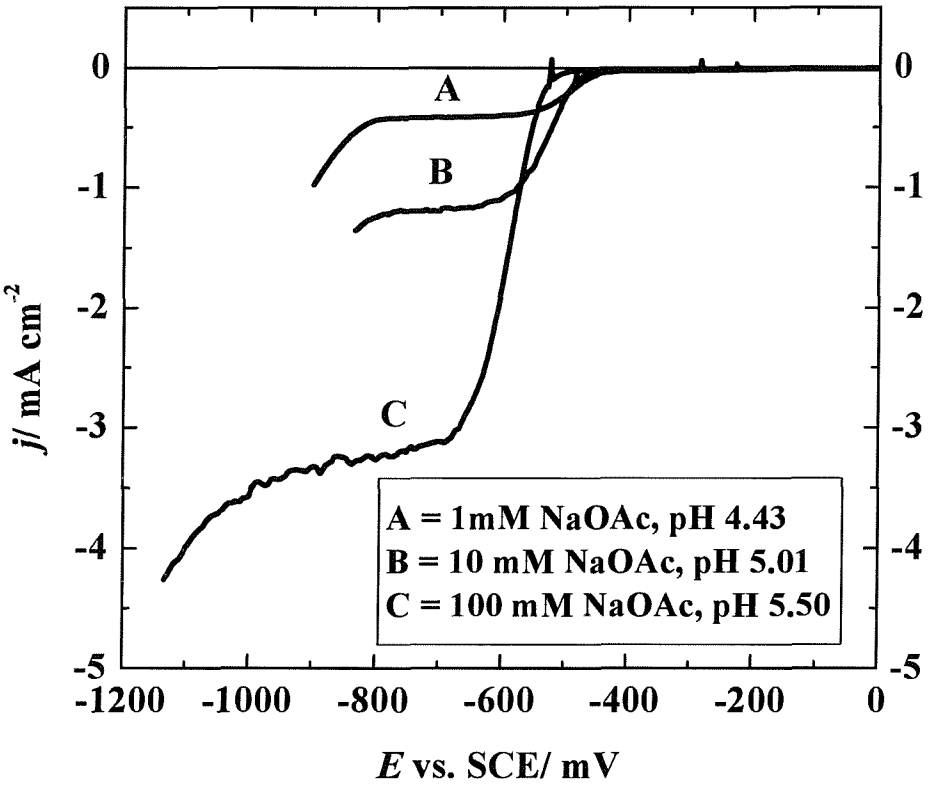

Figure 4. 11 *Voltammograms recorded at a Pt rotating disc electrode (area, 0.16 cm ^{2}, rotation rate 400 rpm) in solutions containing 3 % NaCl + NaOAc (concentration shown on the figure), saturated with CO_2. Temperature 298 K.*

In all cases, the voltammetry has the key features described above. Steep reduction waves, and with well-developed limiting current plateaux, are again observed for all brines. Further, figure 4.11 again provides compelling evidence that with increasing acetate concentration, the concentration of undissociated acetic acid increases despite the rise in pH. Overall, it is largely the dissolved carbon dioxide that fixes the pH. In the pH range resulting from the carbon dioxide, the concentration of acetic acid always seems to be above that of the free proton when significant acetate is present. For both solutions, 1 and 100 mM NaOAc, voltammograms were recorded over a range of rotation rates. The voltammograms obtained show similar characteristics to those obtained for 10 mM NaOAc solution

(see figure 4.9), the height of current plateaux increases with the rotation rate of the Pt rotating disc electrode. This clearly indicates that the reaction occurring at the Pt RDE electrode is mass transport controlled. This observation was confirmed when analyzing the variation of the cathodic current density with the square root of the rotation rate according to the Levich equation (4-1). Plots of the limiting current densities (j_{lim}) versus the square root of the rotation rate of the rate ($\omega^{1/2}$), for both solutions, 1 mM and 100 mM NaOAc, were found to be linear and to pass through the origin as shown in figure 4.12, confirming a fully mass transport controlled reaction. Again, the 10 mM NaOAc data for saturated carbon dioxide brine has been included for comparison.

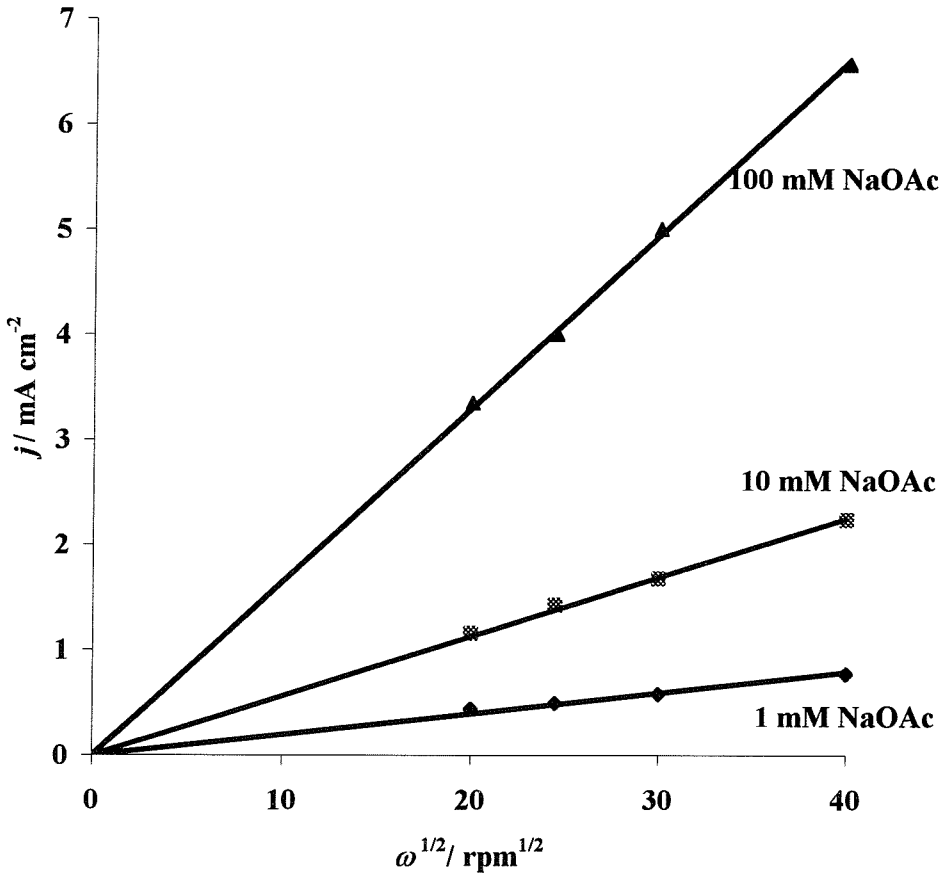

Figure 4. 12 *Plots of j_{lim} vs $\omega^{1/2}$ at potentials in the plateau regions of the j-E curves in figure 4.10. Solutions contains 3 % NaCl + different concentrations of sodium acetate (concentrations are shown on figure), saturated with CO_2. Pt RDE (area, 0.16 cm^2). Potential scan rate 20 mV s^{-1}.*

We were interested in examining the quantitative fit of the speciation simulation to the observed voltammetry. Theoretical slopes of the Levich plots were estimated from equation (4-5) that recognizes that transport of both free proton and undissociated acetic acid can occur in the acetate buffer solutions (in fact, the proton transport is only significant for the lowest concentration of sodium acetate):

$$\frac{dj_{\lim}}{d\omega^{1/2}} = 0.62F\nu^{-1/6}(D_{HOAc}{}^{2/3}c_{HOAc} + D_{H^+}{}^{2/3}c_{H^+}) \qquad (4\text{-}5)$$

ν is the kinematic viscosity of the solution (estimated as 10^{-6} m^2 s^{-1}). The concentrations of protons and acetic acid used were those estimated by PHREEQC 2.2, (see table 3.6 in Chapter Three page 3-11), and the values used for the diffusion coefficient for acetic acid was 1.02×10^{-9} m^2 s^{-1} at 298 K. The diffusion coefficient of the free proton was taken as 9.3×10^{-9} m^2 s^{-1} at 298 K [154]. The comparison of the experimental and theoretical values of $j_{\lim}/\omega^{1/2}$ is shown in table 4.7.

NaOAc	$j_{\lim}/\omega^{1/2}$ at 298 K	
	Calc.	**Exptl.**
1	0.49	0.61
10	1.49	1.56
100	5.23	5.11

Table 4. 7 *Comparison of the experimental values for $j_L/\omega^{1/2}$ (units A m^{-2}/(radians $s^{-1})^{1/2}$) with values estimated using equation (4-5) and the concentrations of free protons and dissociated acetic acid calculated by PHREEQC 2.2. Solutions contained 3 % NaCl + NaOAc (concentration in the table), saturated with CO_2. Pt RDE (area, 0.16 cm^2). Temperature 298 K.*

It can be seen that the trends are reproduced well. Further some data taken from the responses in figure 4.11 are also reported in table 4.8. The discrepancy at the lowest acetate concentration may arise because we have not taken into account a small

contribution from the kinetically controlled reaction of carbon dioxide via carbonic acid [109].

[NaOAc] mM	pH after CO_2 saturation	$E_{1/2}$ mV	$E_{3/4} - E_{1/4}$ mV	j_{lim} mA cm^{-2}
1	4.43	-490	51	0.44
10	5.01	-550	50	1.06
100	5.50	-600	52	3.30

Table 4. 8 *Data taken from voltammograms recorded at a Pt RDE, rotation rate 400 rpm, for solutions of 3 % NaCl with various concentrations of NaOAc. Area of Pt RDE, 0.16 cm^2. Temperature 298 K.*

According to table 4.8, it can be seen that a shift of the half wave potential towards more negative values is observed as the concentration of sodium acetate increases. Further, the values of the Tomes slope separation [$E_{3/4} - E_{1/4}$] are essentially identical to those reported in table 4.2. The limiting current densities again reflect the concentrations of acetic acid in the solution.

4.4.2 Voltammetry of acetate solutions saturated with CO_2 at 333 K

The voltammetry was also recorded at 333 K. Figure 4.13 shows sets of voltammograms with the Pt RDE for a solution containing 3 % NaCl + 10 mM NaOAc and saturated with carbon dioxide. The voltammograms have the expected features. Well defined reduction waves and with well-developed limiting current plateaux are again observed. Once again, the most obvious change in the voltammograms with increasing the temperature from 298 K to 333 K is the increase in the limiting current densities at all potentials. Moreover, negative to – 600 mV versus SCE the limiting currents are also proportional to the square root of the rotation rate of the Pt disc. Plots of the limiting current densities versus the square root of the rotation rate of the Pt disc electrode was found to be linear and pass

through the origin confirming that the electrode reaction is fully mass transport controlled.

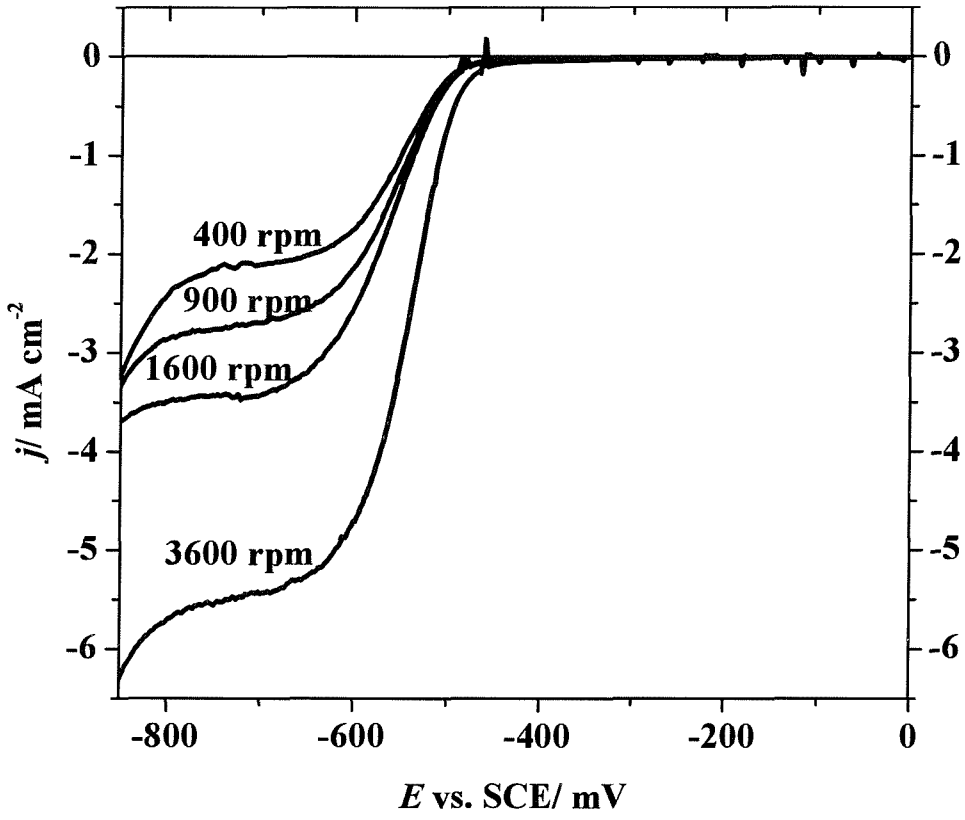

Figure 4. 13 *Voltammograms recorded at a Pt rotating disc electrode (area, 0.16 cm^2), in a solution containing 10 mM NaOAc + 3 % NaCl, saturated with CO_2. Rotation rates shown on figure. Temperature 333 K.*

We were again interested in examining the quantitative fit of the speciation simulation to the observed voltammetry. Figure 4.14, shows voltammograms at the Pt RDE for three concentrations of sodium acetate (also containing 3 % NaCl) saturated with CO_2 at 333 K. In all cases, the voltammetry has the same key features as described above. Steep reduction waves with a well developed limiting current plateaux, are again observed. The limiting currents were plotted versus the square root of the rotation rate (Levich plots); good linear plots passing through the origin were obtained and the slopes are reported in table 4.9. Once again, figure 4.14 provides compelling evidence that with increasing acetate concentration, the concentration of acetic acid increases although the pH rise is observed.

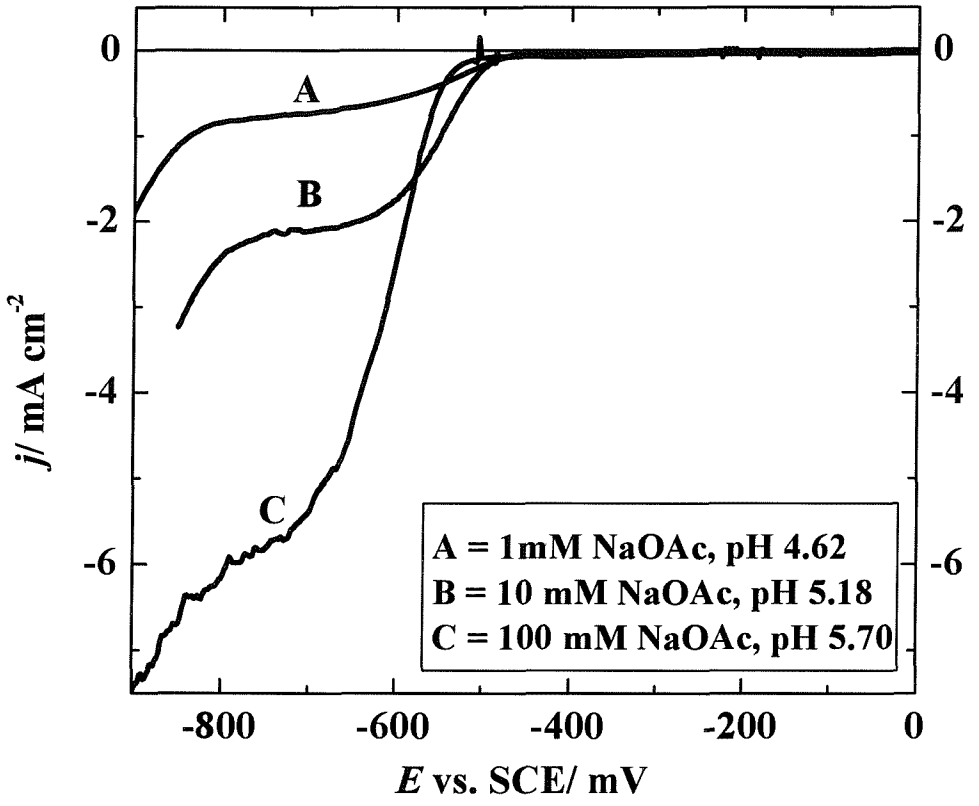

Figure 4. 14 *Voltammograms recorded at a Pt rotating disc electrode (area, 0.16 cm^2, rotation rate 400 rpm) in a solution containing 3 % NaCl + NaOAc (concentration shown on figure), saturated with CO_2. Temperature 333 K.*

The concentration of protons and acetic acid were those estimated by the computer program PHREEQC 2.2 (see table 3.6 in Chapter Three page 3-11) and the value for the diffusion coefficient for acetic acid was 2.24×10^{-9} m^2 s^{-1}. The diffusion coefficient for the free proton was taken as 9.3×10^{-9} m^2 s^{-1} [154] and it was assumed that the energies of activation for proton and acetic acid diffusion were the same. The comparison of the experimental and theoretical values of the Levich plots is shown in table 4.9.

According to table 4.9, it can be seen that the trends are reproduced well although the agreement is not perfect. There are systematic differences at all acetate concentrations. Again the calculation does not take into account a contribution from the kinetically controlled reduction of carbonic acid and this will become more significant with increasing temperature. In addition, it may be that incorrect values

for thermodynamic constants are being used at this temperature; this is not surprising, since input data taken from several sources and some assumptions are being made in extending the calculations from 298 K to 333 K.

NaOAc	$j_{lim}/\omega^{1/2}$ at 333 K	
	Calc.	**Exptl.**
1	0.62	0.97
10	1.91	2.67
100	6.49	8.17

Table 4. 9 *Comparison of the experimental values for $j_{lim}/\omega^{1/2}$ (units A m^{-2}/(radians s^{-1}) $^{1/2}$) with values estimated using equation (4-5) and the concentrations of free protons and dissociated acetic acid calculated by PHREEQC 2.2. Solutions contained 3 % NaCl + NaOAc (concentration shown in table), saturated with CO_2. Pt RDE (area, 0.16 cm^2). Temperature 333 K.*

4.5 Voltammetry of other carboxylate solutions saturated with CO_2 at Pt RDE at 298 K

In another set of experiments, 10 mM solutions of the sodium salts of other weak acids (formic acid, propionic acid and lactic acid) in 3 % NaCl brine were saturated with carbon dioxide and voltammograms were recorded.

Figure 4.14 shows typical voltammograms recorded at a Pt rotating disc electrode for (a) 10 mM sodium formate and (b) 10 mM sodium lactate in 3 % NaCl, saturated with carbon dioxide over a range of rotation rates. The same experiment with sodium propionate gave curves identical to those for sodium acetate. A potential scan rate of 20 mV s^{-1} was used for these experiments. All voltammograms were recorded at 298 K.

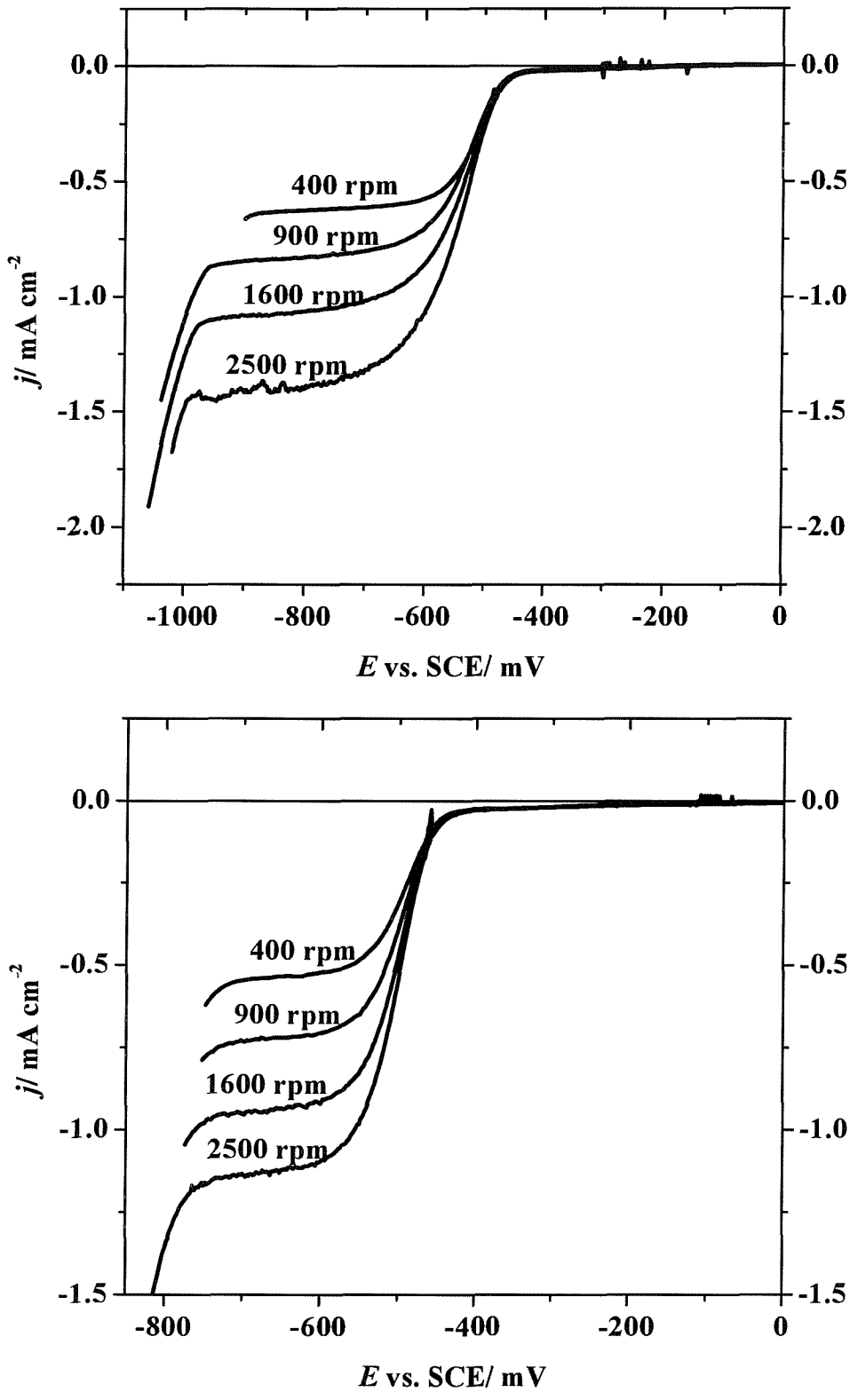

Figure 4. 15 *Voltammograms recorded at a precleanedPt rotating disc electrode (area, 0.16 cm^2) in aqueous solutions containing (a) 10 mM sodium formate and (b) 10 mM sodium lactate + 3 % NaCl, saturated with CO_2. Rotation rates shown on figure. Temperature 298 K.*

Again very high quality waves are obtained. Steep reduction waves with well-developed limiting current plateaux are observed. Furthermore, negative to – 700 mV versus SCE, the limiting currents can be seen to be dependent on the rotation rate of the disc electrode. In addition, plots of the limiting current versus the square root of the rotation rate of the disc electrode are linear and pass through the origin; the electrode reactions are therefore fully mass transport controlled in the plateau region. The voltammetry is entirely consistent with the addition of CO_2 leading to the formation of carboxylic acids that reduce by the same mechanism as acetic acid. Further data taken from these experiments are summarized in table 4.10. The responses for sodium propionate were similar.

Acid	Dissociation constant	pH	$E_{1/2}$ / mV	$E_{3/4} - E_{1/4}$ / mV	j_{lim}/ mA cm^{-2}
Formic acid	1.77×10^{-4}	4.51	-500	52	0.63
Acetic acid	1.75×10^{-5}	5.00	-537	50	1.17
Propionic acid	1.34×10^{-5}	4.94	-536	45	1.33
Lactic acid	1.38×10^{-4}	4.59	-490	48	0.54

Table 4. 10 *Data from voltammograms recorded at a Pt rotating disc electrode (area, 0.16 cm^2), rotation rate 400 rpm, for solutions containing 3 % NaCl + 10 mM sodium salt of weak acid, saturated with CO_2 at 298 K.*

According to table 4.10, it can be seen that the half wave potential, $E_{1/2}$, shows a small shift towards a more positive value with decreasing pK_A. Further after saturating the solutions with carbon dioxide, with the stronger acids, the pH is lower but the fraction of anion converted to weak acid is decreased leading to lower limiting current densities.

Since it has been widely proposed [109] that the reduction of carbonic acid could have an important role in determining the corrosion rate in the oilfield pipelines, some experiments have been carried out on solutions containing 3 % NaCl containing bicarbonate and saturated with CO_2 (but without acetate). Figure 4.15

reports a voltammogram for a precleaned Pt rotating disc electrode in a solution containing 2.9 mM bicarbonate + 3 % NaCl and having a pH of 5.01 after CO_2 saturation. The voltammogram shows two major reduction waves at $E_{1/2}$ = - 830 mV and – 1230 mV versus SCE and neither of these waves are observed in the absence of bicarbonate [155]. In addition, there is a reduction wave at $E_{1/2}$ = -530 mV versus SCE but it is only just discernable with the current scale shown.

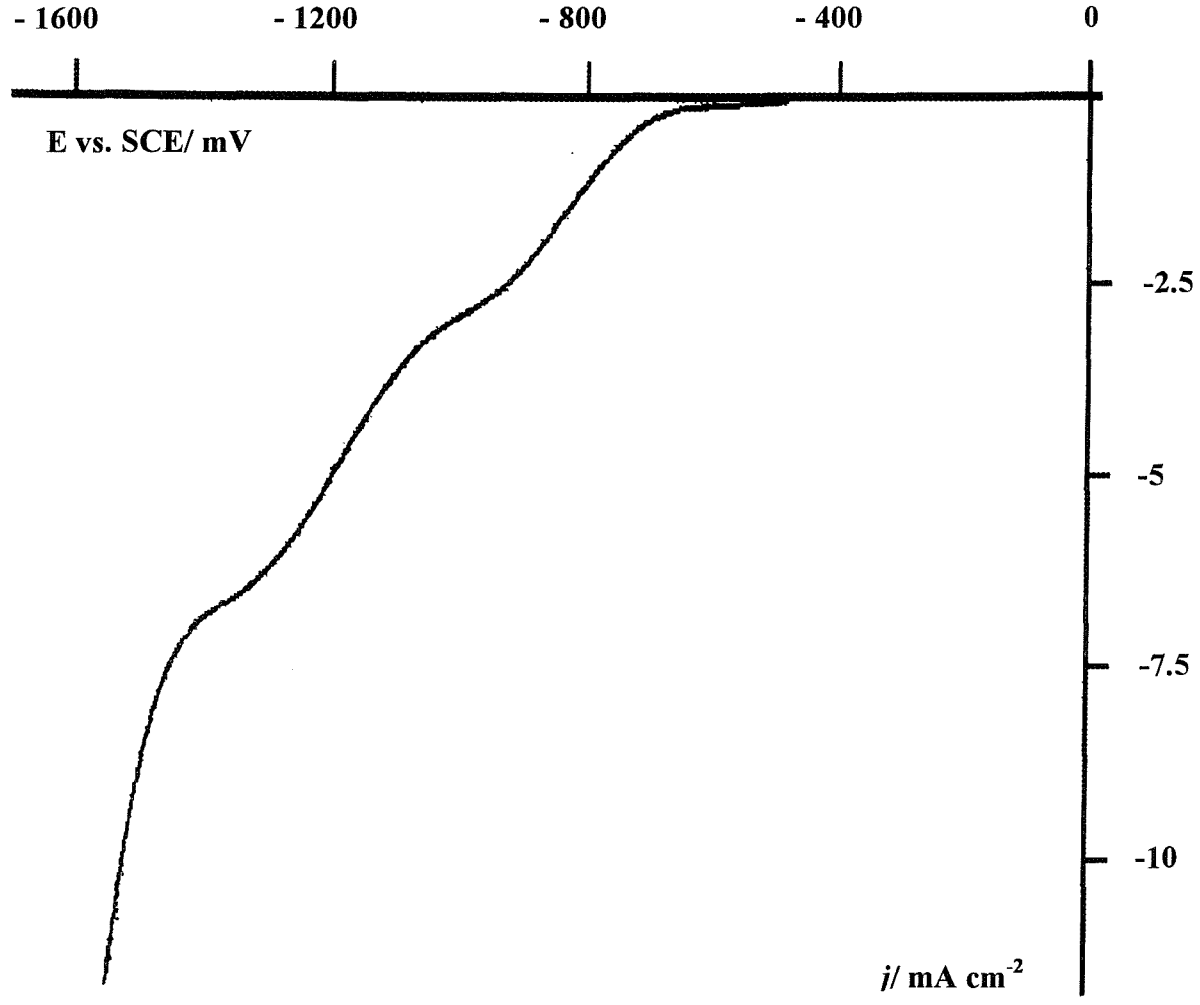

Figure 4. 16 *Voltammogram recorded at a precleaned Pt rotating disc electrode (area, 0.16 cm^2) in a solution containing 3 % NaCl + 2.9 mM Bicarbonate (no acetate present) saturated with CO_2 (pH 5.01). Rotation rate 900 rpm. Temperature 298 K.*

This small wave results from the reduction of free proton with a minor contribution from the mechanism:

$$CO_2 + H_2O \longrightarrow H_2CO_3 \quad (5)$$

$$H_2CO_3 \longrightarrow HCO_3^- + H^+ \quad (6)$$

$$H^+ + e^- \longrightarrow \tfrac{1}{2} H_2 \quad (7)$$

In fact the rate of hydrogen evolution by this mechanism is very low [97] because of the low equilibrium concentration of carbonic acid and the slow rate of reaction (5) (rate constant 3.75×10^{-2} s^{-1}). In contrast, the dissociation of acetic acid is a rapid reaction (rate constant 10^6 s^{-1} [124]); likewise, reaction (4) and most protonation and deprotonation reactions in water are also rapid. Hence, the mechanism involving reaction (3) and (4) is the major contributor in acetate buffers. It also follows that the reduction of carbonic acid is likely to play a very minor role in the corrosion of carbon steel in brines containing acetic acid.

The reduction of free proton and the slow reduction of carbonic acid may well lead to an enhancement in the corrosion current density for steel [109] in the absence of acetic acid but to a minor extent compared with the effect of acetic acid in acetate containing brines. The limiting current for the major reduction waves on the voltammogram of figure 4.16 at $E_{1/2}$ = - 830 mV and – 1230 mV versus SCE are independent of the rotation rate of the Pt rotating disc electrode so these reactions are fully kinetically controlled.

The nature of the cathode reaction leading to these waves is not immediately clear but they are likely to be associated with the reduction of carbon dioxide [144] rather than hydrogen evolution. More importantly to the discussion of corrosion, it should be noted that at steel, a much less catalytic surface than Pt, these reactions are unlikely to occur at a significant rate at potentials close to the corrosion potential.

Hence, not unexpectedly, voltammograms recorded at a X65 carbon steel rotating disc electrode in solutions containing 3 % NaCl brine containing various concentration of bicarbonate and carbon dioxide as well as temperatures of 298 K and 333 K, never showed these reduction waves. Indeed, there was never a significant cathodic current positive of – 850 mV versus SCE. Overall, we conclude that the reduction of carbon dioxide and bicarbonate plays no role in the corrosion of steel in solutions containing acetate and acetic acid.

A further set of experiments was carried out on solutions containing 3 % NaCl but also containing 29 mM and 290 mM sodium bicarbonate respectively. Figure 4.17 reports voltammograms recorded at the precleaned Pt rotating disc electrode for aqueous solutions of 29 mM and 290 mM bicarbonate saturated with CO_2, pH 5.90 and 6.92 (after CO_2 saturation) at 298 K and rotation rates of 100 rpm and 900 rpm respectively (it can be seen that the current density scale is different for each voltammogram). It should immediately be noted that with increasing the initial sodium bicarbonate concentration, the pH of the solution of interest increases after carbon dioxide saturation. According to figure 4.17, for the 29 mM sodium bicarbonate solution the voltammogram shows again two major reduction waves at $E_{1/2}$ = - 850 mV and – 1250 mV versus SCE. However, the response obtained is a little more drawn out (compared to figure 4.16) and the limiting current plateau for the second reduction wave is less discernable. The experiment was repeated over a range of rotation rate, and the limiting currents for the two major reduction waves were found to be independent of the rotation rate of the Pt rotating disc electrode, so these electrode reactions are fully kinetically controlled. However, the response obtained for the 290 mM sodium bicarbonate solution is slightly different. The voltammogram appears to show only one major reduction wave, $E_{1/2}$ = - 1000 mV versus SCE, with a well developed limiting current plateau, but it is very drawn out and maybe the result of overlapping waves. Once again, the limiting current was found to be independent of the rotation rate of the Pt rotating disc electrode. The electrode reaction is again kinetically controlled.

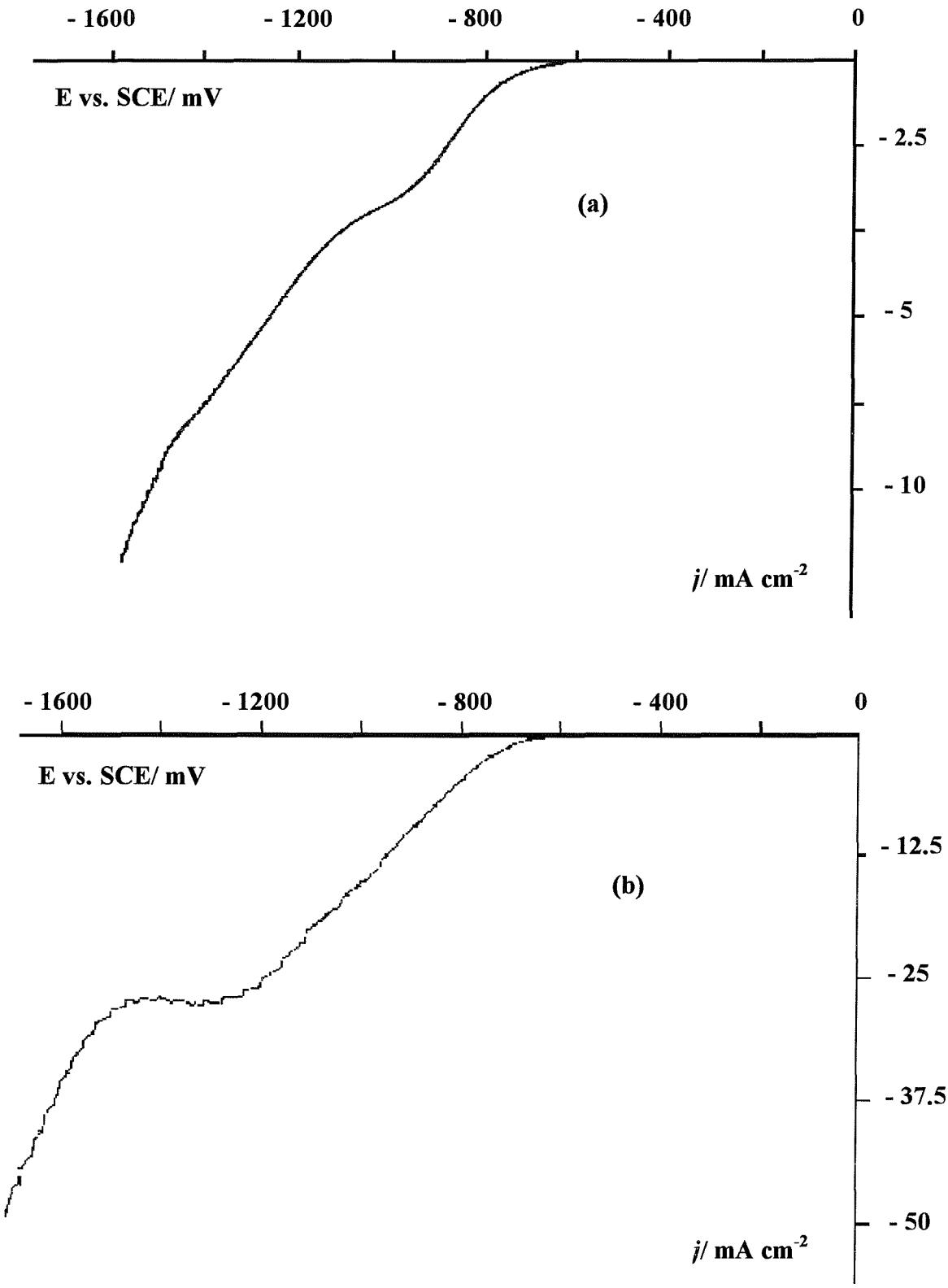

Figure 4. 17 *Voltammograms recorded at a precleaned Pt rotating disc electrode (area, 0.16 cm^2) in 3 % NaCl solution containing (a) 29 mM sodium bicarbonate and (b) 290 mM sodium bicarbonate, saturated with CO_2, pH 5.90 and 6.92 respectively (after CO_2 saturation). Rotation rates (a) 100 rpm and (b) (900 rpm). Temperature 298 K.*

4.6 Conclusion

In this chapter, an experimental investigation concerning the reduction of weak carboxylic acids on a Pt rotating disc electrode has been described. It has been shown that the electrochemistry of the weak acid solutions at Pt reflects the total concentration of the proton donor in the solution because the dissociation of the carboxylic acids is a rapid reaction. The current potential curves are essentially identical to voltammograms recorded at Pt microelectrodes [128-134]. Hence, the cathodic current equivalent to the mass transport controlled reduction reaction of the carboxylic acid in the medium can be observed. Futher, the reduction of the carboxylic acid to hydrogen is a simple and rapid reaction occurring close to the equlibrium potential, while the Tomes separations are very similar to those reported at Pt microelectrodes [125,130]. Our results confirm that the electrochemistry of acetate buffers on Pt is occurring by a preceding chemical reaction (CE), a sequence:

$$HOAc \xrightleftharpoons{\text{solution}} H^+ + OAc^- \qquad (3)$$

$$H^+ + e^- \xrightleftharpoons{\text{electrode}} \tfrac{1}{2} H_2 \qquad (4)$$

It has been demonstrated conclusively that it makes no difference whether the organic carboxylic acids present in solution result from the addition of an aliquot of 1 M of the acid or from the carbon dioxide saturation of the solution containing acetate. The electrochemistry of these solutions saturated with carbon dioxide can be understood in a semi-quantitative way in terms of the equilibrium concentration of the carboxylic acid in solution and not the concentration of free protons. At sufficient negative potential, all the acetic acid is reduced via the mechanism, reaction (3) followed by reaction (4). In the brine saturated with carbon dioxide, the weak acid concentration depends on the pH of the solution and the sodium acetate concentration. Indeed, with increasing the acetate concentration, the pH increases but this is tied with an increase in undissociated acetic acid concentration. Temperature influences the response obtained, increasing the temperature displaces the cathodic

current towards more positive potential values. Further, the limiting current density and the diffusion coefficient of acetic acid increase with increasing the temperature. A similar role for carbonic acid in brines without carboxylates has been proposed [109]. The effect is however, much smaller and in the presence of carboxylate, the influence of carboxylic acid will dominate. The reasons are (i) although carbonic acid is a stronger acid (see table 3.7, page 3-16) it is only present at very low concentration, (ii) the conversion of carbon dioxide to carbonic acid is slow, (iii) in the systems under study, the acetic acid concentration is significant and the dissociation is rapid. Indeed, when both acetic acid and carbonic acid are both present, the reduction of the latter will not influence the corrosion rate significantly. Hydrogen evolution from bicarbonate is never significant because bicarbonate is a very weak acid, $pK_A = 10.32$.

Chapter Five

5 *Electrochemical Studies of the Corrosion of X65 carbon Steel in 3 % NaCl Brine Containing Acetate*

5.1 Introduction

In this chapter, the influence of acetate ion on the corrosion rate of carbon steel (X65) in 3 % NaCl brine containing (a) sodium acetate (NaOAc) + acetic acid (HOAc) and (b) sodium acetate (NaOAc) + carbon dioxide (CO_2) has been investigated using voltammetry at a rotating disc electrode. It is shown that the rate of corrosion can only be understood if it is recognized that the cathodic process in steel does not distinguish between the reduction of free protons and the reduction of undissociated proton donor, acetic acid. Hence, for any brine composition it is important to consider the concentration of acetic acid as well as the pH of the brine in explaining the rates of corrosion of the carbon steel. This requires the ability to predict the speciation of these complex solutions (see Chapter Three).

5.2 Preliminary Studies

5.2.1 Neutral solutions

It should be emphasized that unless otherwise stated all voltammograms at the carbon steel rotating disc electrode, used discs polished immediately before each experiment. Also the potential was scanned (usually 5 mV s^{-1}) in a positive direction from the negative limit. These steps were taken in order to minimize the influence of corrosion films on the voltammetric response and to ensure reproducibility. Figure 5.1 shows voltammograms recorded at a rotating X65 carbon steel electrode

(area, 0.17 cm^2, rotation rate 400 rpm) in a deoxygenated (using N_2) solution containing 3 % NaCl + 100 mM NaOAc, pH 7.6, at two temperatures, 298 K and 333 K.

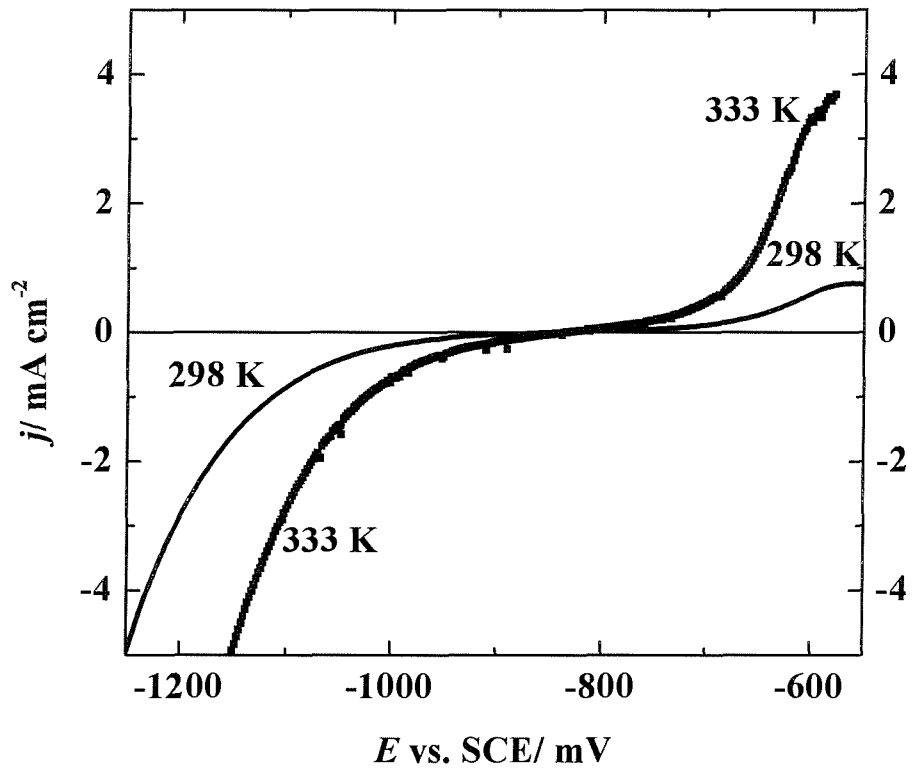

Figure 5. 1 *Voltammograms recorded at a X65 carbon steel rotating disc electrode (area, 0.17 cm^2, rotation rate 400 rpm) in a deoxygenated aqueous solution containing 3 % NaCl + 100 mM NaOAc, pH 7.6. Temperature 298 K and 333 K.*

The potential was swept from – 1300 mV to – 500 mV versus SCE. The corrosion potential, E_{corr}, at both temperatures is close to – 860 mV versus SCE. No reduction waves are observed on the voltammograms. Rather, the cathodic currents increase smoothly at potentials away from the corrosion potential (as E – E_{corr} becomes more negative). In contrast, the anodic currents at potentials positive to the corrosion potential do have a tendency to reach a limiting value, especially at 298 K. As expected both the anodic and cathodic currents increase much more markedly with (E - E_{corr}) at the higher temperature. In these oxygen free solutions, the corrosion potential occurs where the rate of dissolution of iron:

$$Fe - 2e^- \longrightarrow Fe\ (II) \qquad (1)$$

and the rate of hydrogen evolution by the reactions

$$2H^+ + 2e^- \longrightarrow H_2 \qquad (2)$$

$$2H_2O + 2e^- \longrightarrow H_2 + 2OH^- \qquad (3)$$

are equal. A 3 % sodium chloride solution, without the sodium acetate gave essentially identical responses to those of figure 5.1 at both 298 K and 333 K. Hence, in neutral solutions, acetate has no significant influence on the rate of corrosion of steel in brine.

5.2.2 Acetate Buffers

In order to understand the role of acetic acid in the corrosion of steel in these acetate media, the voltammetry was investigated over a wide potential range. Figure 5.2 reports voltammograms recorded at 298 K for a carbon steel disc in a degassed aqueous solution containing 3 % NaCl + 100 mM NaOAc + 24.4 mM HOAc. The pH of the solution was 5.15.

The responses obtained are now quite different compared to figure 5.1. Firstly, the corrosion potential has shifted to a significantly more positive value, - 672 mV versus SCE. Secondly, positive to the corrosion potential, the anodic current density rises much more steeply than in the neutral solution. Thirdly and most importantly to the present study, negative to the corrosion potential, a reduction wave is observed with $E_{1/2} \approx -1050$ mV versus SCE. Moreover, the plateaux currents are reasonably defined and appear to be proportional to the square root of the rotation rate of the disc electrode as expected for a mass transfer controlled reduction.

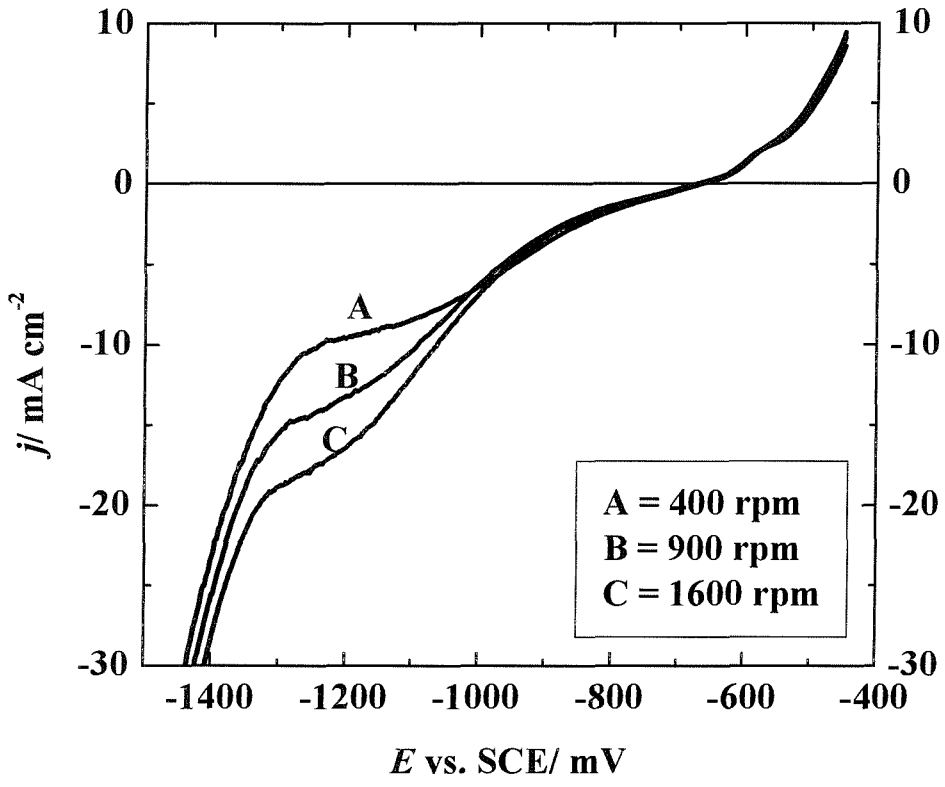

Figure 5. 2 *Voltammograms recorded at 298 K for a X65 carbon steel electrode (area, 0.17 cm^2) in a deoxygenated aqueous solution containing 3 % NaCl + 100 mM NaOAc + 24.4 mM HOAc, pH 5.15 as a function of rotation rates.*

Figure 5.3 compares the responses obtained at Pt and X65 carbon steel rotating disc electrodes for a deoxygenated solution containing 3 % NaCl + 100 mM NaOAc + 24.4 mM HOAc at 298 K. Both voltammograms were recorded at a rotation rate of 900 rpm. Platinum is, of course, stable to corrosion and an excellent catalyst for hydrogen evolution. As a result, no anodic current is seen in the potential range studied and a steep reduction wave is observed at $E_{½}$ = -535 mV versus SCE, a value close to the equilibrium potential for the H^+/H_2 couple at the solution pH. The reduction wave has also a well-developed limiting current plateau and the current in this region is proportional both to the square root of the rotation rate of the Pt disc electrode and the acetic acid concentration. There is no doubt that the limiting current density is determined by the mass transport of both proton and undissociated acetic acid to the electrode surface and that the transport of the acetic acid is the dominant process in the pH range considered (see Chapter Four). In comparison, the

voltammogram at the X65 carbon steel shows anodic current for iron dissolution (reaction 5-1), and the reduction wave for hydrogen evolution is both drawn out and shifted to a much more negative potential. On the other hand, the limiting current density at steel is very similar to that at Pt and it shows the same dependence on rotation rate (see figure 5.2) and acetic acid concentration. Hence it must be concluded that at a potential of – 1150 mV versus SCE, the reduction of acetic acid is occurring at a mass transfer controlled rate.

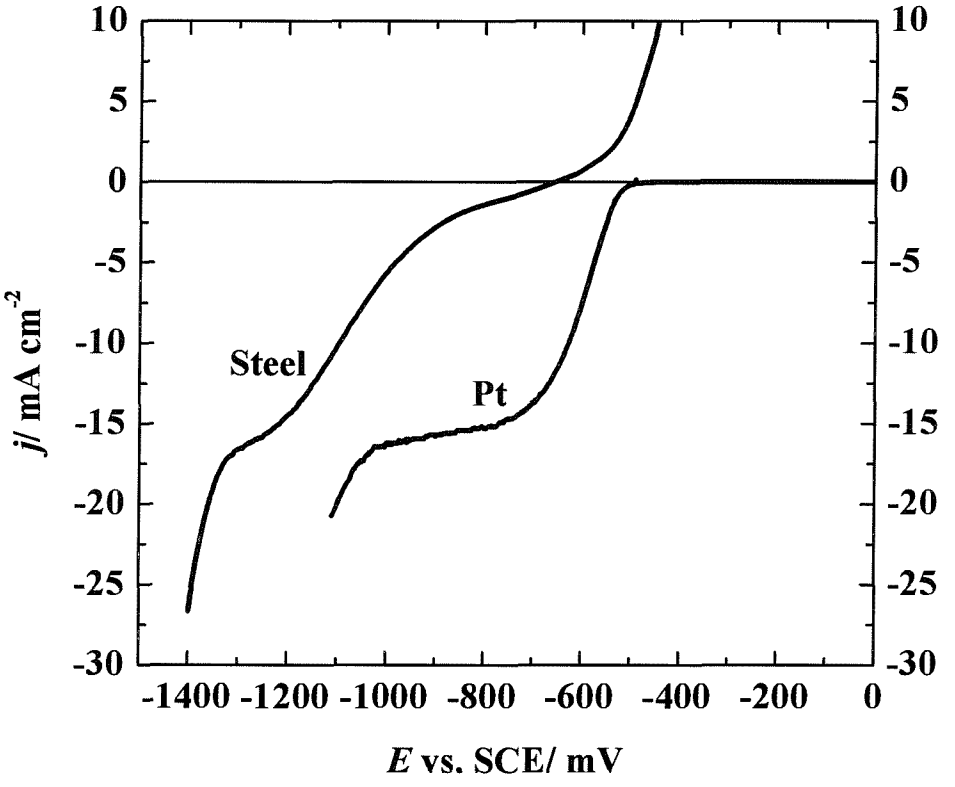

Figure 5. 3 *Voltammograms recorded at Pt and X65 carbon steel rotating disc electrode in a deoxygenated aqueous solution containing 3 % NaCl + 100 mM NaOAc + 24.4 mM HOAc. Temperature 298 K. Rotation rate 900 rpm.*

It should be immediately noted that the corrosion potentials for the steel in these acetate/acetic acid + sodium chloride brines are in the range of – 650 mV to – 850 mV versus SCE. At such potentials the reduction of acetic acid is thermodynamically favorable (as shown by the voltammetry at Pt) and, indeed, on a

good catalytic surface such as Pt, the reductions of both acetic acid and protons are mass transfer controlled.

The Levich equation, together with the diffusion coefficients for acetic acid found from the experiments with the Pt RDE (1.02×10^{-5} cm^2 s^{-1}) were used to estimate the mass transport controlled current density for the reduction of acetic acid at the X65 carbon steel disc electrode. The calculated and experimental current densities agree satisfactorily. For example, at a rotation rate of 900 rpm in the experiments reported in figure 5.3, the value is 15 mA cm^{-2} for the steel electrode, 15 mA cm^{-2} for the Pt electrode compared to a value of 14 mA cm^{-2} from the Levich equation. This is further confirmation that the cathode reaction at carbon steel is acetic acid reduction and that this reaction becomes mass transport controlled at sufficiently negative potentials. As at the Pt RDE, the reaction:

$$HOAc + e^- \longrightarrow \tfrac{1}{2} H_2 + OAc^- \qquad (4)$$

is predominant in determining the voltammetry negative to the corrosion potential of the X65 carbon steel surface.

The question to be resolved is then the extent to which a reduction process with $E_{1/2}$ = - 1050 mV vs. SCE can influence the corrosion process occurring at significantly more positive potential, - 670 mV vs. SCE. We believe that this cathode reaction does, indeed, have a role and we would offer two key pieces of evidence. Firstly, by comparing figures 5.1 and 5.2, it can be seen that at - 860 mV versus SCE, the corrosion potential in the neutral solution, there is a very significant cathodic current density resulting from the reduction of acetic acid when it is also present in the solution. Secondly, in the medium containing acetic acid, some slow reduction of the proton donor is probably occurring even at the corrosion potential, - 670 mV versus SCE; it must be stressed that the experimental current/potential curve is the net response from the summation of the anodic and cathodic components. Close to the corrosion potential, the actual contributions from the

reduction of acetic acid could both be substantial so the current for the reduction of acetic acid close to this potential may be larger than it appears. Certainly, it appears that the positive shift in the corrosion potential arises because the main cathodic reaction in the corrosion of steel in the medium containing acetic acid has become reaction (4) rather than reaction (2) and (3).

5.3 More detailed studies

5.3.1 Influence of Temperature

The voltammetry was also recorded at several temperatures over the range 298 – 333 K. Figure 5.4 compares the voltammograms for the X65 carbon steel electrode in 3 % NaCl + 100 mM NaOAc + 24.4 mM HOAc at temperatures 298 K and 333 K.

When the temperature is increased to 333 K, the response at the steel electrode becomes more complex as can be seen in figure 5.4. The voltammogram obtained at 333 K clearly shows two reduction processes labeled wave 1 and wave 2 on the figure. Further, at the higher temperature, the current densities are higher at all potentials and the reduction wave at $E_{1/2} \approx$ - 1050 mV (Wave 2) remains well defined. There is, however clearly a prewave (Wave 1) at approximately - 700 mV versus SCE. At 298 K, this first reduction wave/prewave may still be present but it is relatively small compared to the reduction step, Wave 2. The magnitude of the prewave will clearly have the major influence on the corrosion behaviour at the corrosion potential in the oilfield environment.

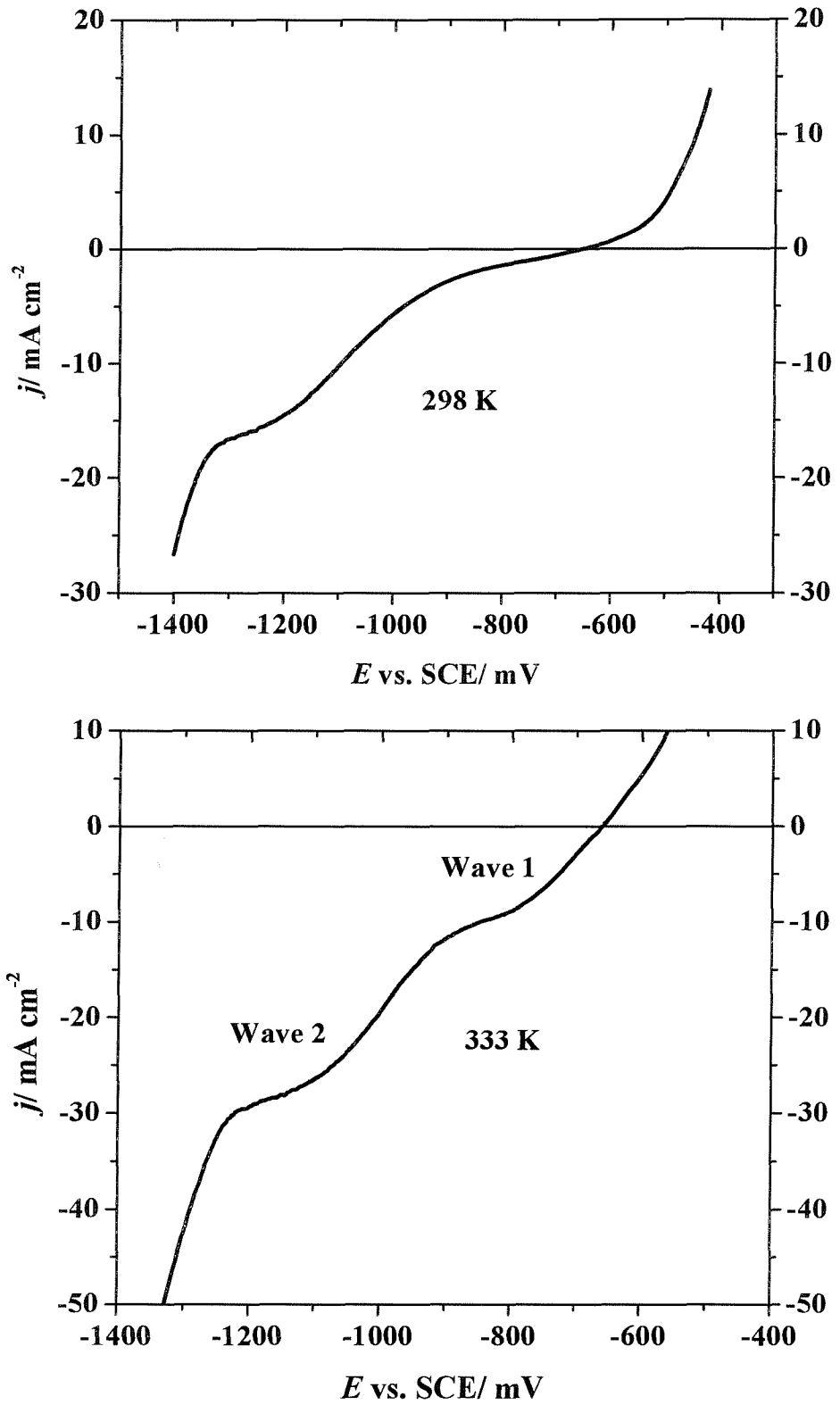

Figure 5. 4 *Voltammograms recorded at a X65 carbon steel rotating disc electrode (area, 0.17 cm^2) in a deoxygenated aqueous solution containing 3 % NaCl + 100 mM NaOAc + 24.4 mM HOAc, pH 5.15. Rotation rate 900 rpm. Temperatures shown on figure.*

Tables 5.1 summarises the influence of temperature and the rotation rate of the X65 carbon steel disc on the corrosion potential and the limiting current for the reduction of acetic acid (measured at – 1000 mV vs. SCE as sum of Wave 1 + Wave 2) for a solution containing 3 % NaCl + 100 mM NaOAc + 24.4 mM HOAc, pH 5.15.

Temperature/ K	Rotation rate/ rpm	E_{corr}/ mV vs. SCE	J_{lim}/ mA cm^{-2}
298	900	-672	14
303	900	-664	15
323	900	-660	22
333	400	-672	19
333	900	-696	28
333	1600	-706	37
333	2500	-714	48

Table 5. 1 *The influence of temperature and rotation rate on the corrosion potential and the limiting current for the reduction of acetic acid. Solution contains 3 % NaCl + 100 mM NaOAc + 24.4 mM HOAc, pH 5.15. X65 carbon steel RDE (area, 0.17 cm^2).*

It can be seen that the corrosion potential shows a small but complex shift with temperature but this is not surprising in view of the change in voltammetry with temperature. With increasing rotation rate at 333 K, the shift is towards more negative potentials. The limiting current density is again confirmed as proportional to the square root of the rotation rate and the slope of this plot leads to a value for the diffusion coefficient for acetic acid of ~ 2.7 x 10^{-9} m^2 s^{-1}, comparable to that found from the data at Pt and 333 K. The limiting current almost doubles with the 35 K rise in temperature. This corresponds to an energy of activation of 25 kJ mol^{-1} for the diffusion of acetic acid. This value of the energy of activation is essentially identical to the values extracted from the data at Pt. We believe that the overall level to which the data for the two metals fits, is conclusive proof that the same cathode reaction predominates.

Figure 5.5 illustrates typical voltammograms recorded at Pt and X65 carbon steel rotating disc electrode for a degassed (using N_2) aqueous solution containing both acetate ion and acetic acid at a temperature of 333 K; in fact this voltammogram is for a solution containing 3 % NaCl + 100 mM NaOAc + 24.4 mM HOAc. It can be seen that the total limiting current for the two reduction processes (Wave 1 + Wave 2) remains similar to the limiting current density at Pt. Hence, at rather negative potentials, all the acetic acid is reduced at a mass transport controlled rate.

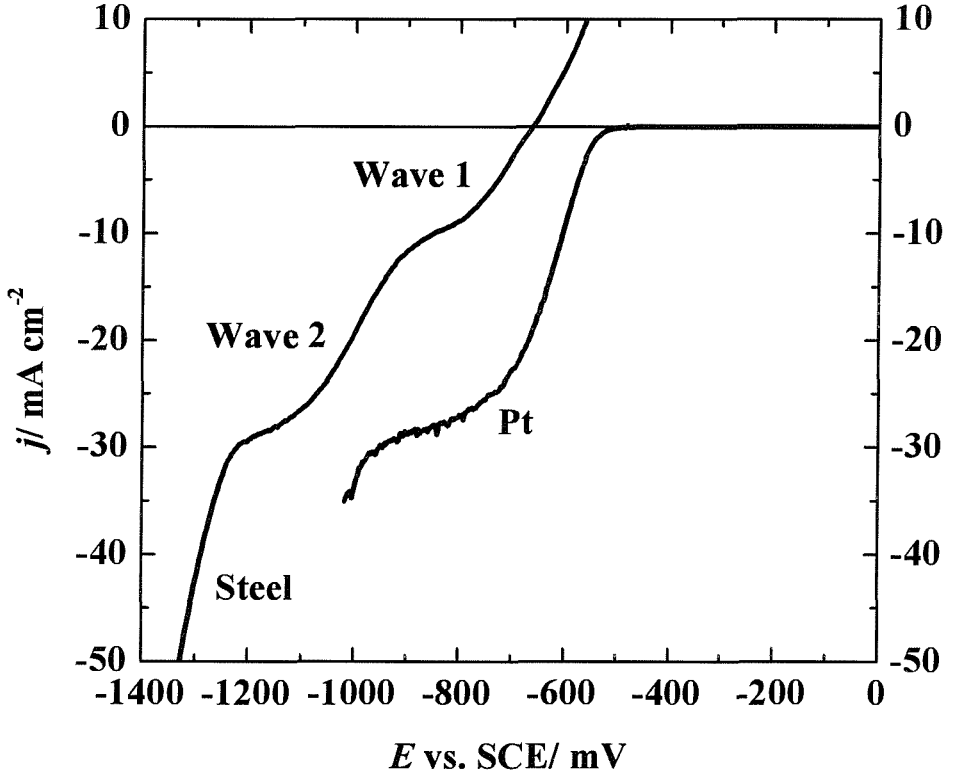

Figure 5. 5 *Voltammograms recorded at a Pt and a X65 carbon steel rotating disc electrode in a deoxygenated aqueous solution containing 3 % NaCl + 100 mM NaOAc + 24.4 mM HOAc. Temperature 333 K. Rotation rate 900 rpm.*

5.3.2 Influence of the rotation rates

The origin of the two reduction processes on the steel was therefore examined further. In a large number of preliminary experiments, it was demonstrated that Wave 1 was clearly observed at low rotation rates and at low acetic acid concentrations and at the higher temperature.

Figure 5.6 illustrates the effect of rotation rate for a X65 carbon steel rotating disc electrode in a deoxygenated aqueous solution containing 3 % NaCl + 10 mM NaOAc + 5 mM HOAc, pH 4.80, at 298 K. It can be seen that at the low rotation rate (100 rpm), only Wave 1 is observed just negative to the corrosion potential, but with the higher rotation rate (900 rpm), Wave 2 certainly appears to be the dominant feature. This should not be interpreted as suggesting that the process leading to Wave 1 does not occur at the higher rotation rates. Rather, the observations imply that under these conditions the rate of the reduction process leading to Wave 1 reaches a limiting value that is small compared to that of Wave 2 and therefore less evident on the voltammogram at high rotation rate.

Further with the solution containing 3 % NaCl + 100 mM NaOAc + 24.4 mM HOAc (for the steel electrode), it was found that the current at – 870 mV versus SCE was insensitive to the rotation rate of the disc electrode but the limiting current at – 1150 mV versus SCE is proportional to the square root of the rotation rate of the disc, hence, Wave 1 is most evident at low rotation rates.

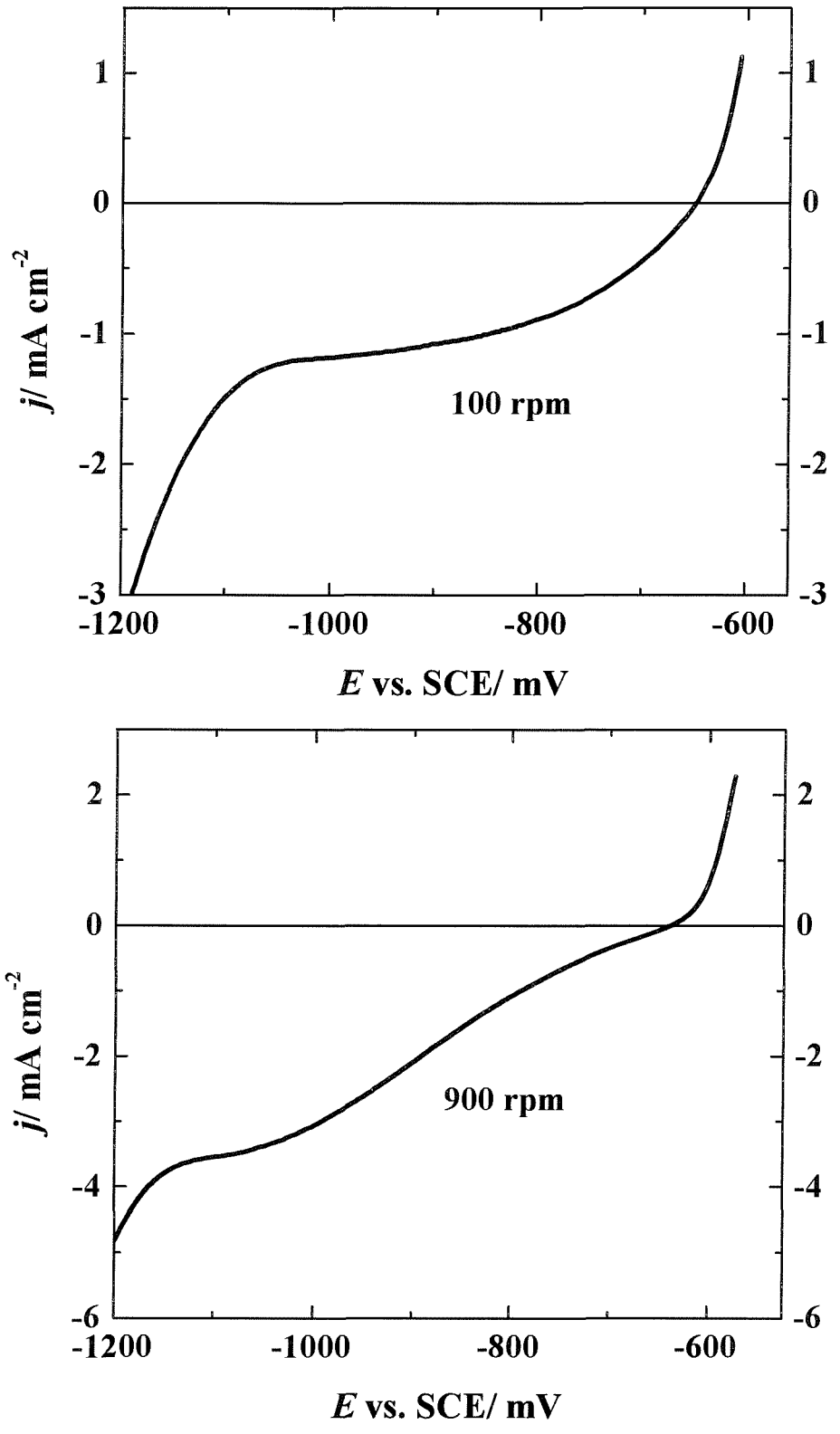

Figure 5. 6 *Voltammograms recorded at a X65 carbon steel rotating disc electrode in a deoxygenated solution containing 3 % NaCl + 10 mM NaOAc + 5 mM HOAc, pH 4.80. Temperature 298 K. Rotation rates shown on figure.*

Therefore the influence of the rotation rate of the X65 carbon steel rotating disc electrode at – 860 mV versus SCE on the current density for a solution containing a low acetic acid concentration was investigated, in fact containing 3 % NaCl + 1 mM NaOAc + 0.65 mM HOAc, pH 4.80. The experiment was carried out at 298 K. The result obtained is reported in figure 5.7. The inset shows the plot of the limiting current densities as function of the square root of the rotation of the disc electrode. Clearly, the reduction of acetic acid is partially mass transport controlled. It should be stressed that for this condition, essentially only the reduction process positive to – 860 mV versus SCE is seen (Wave 1).

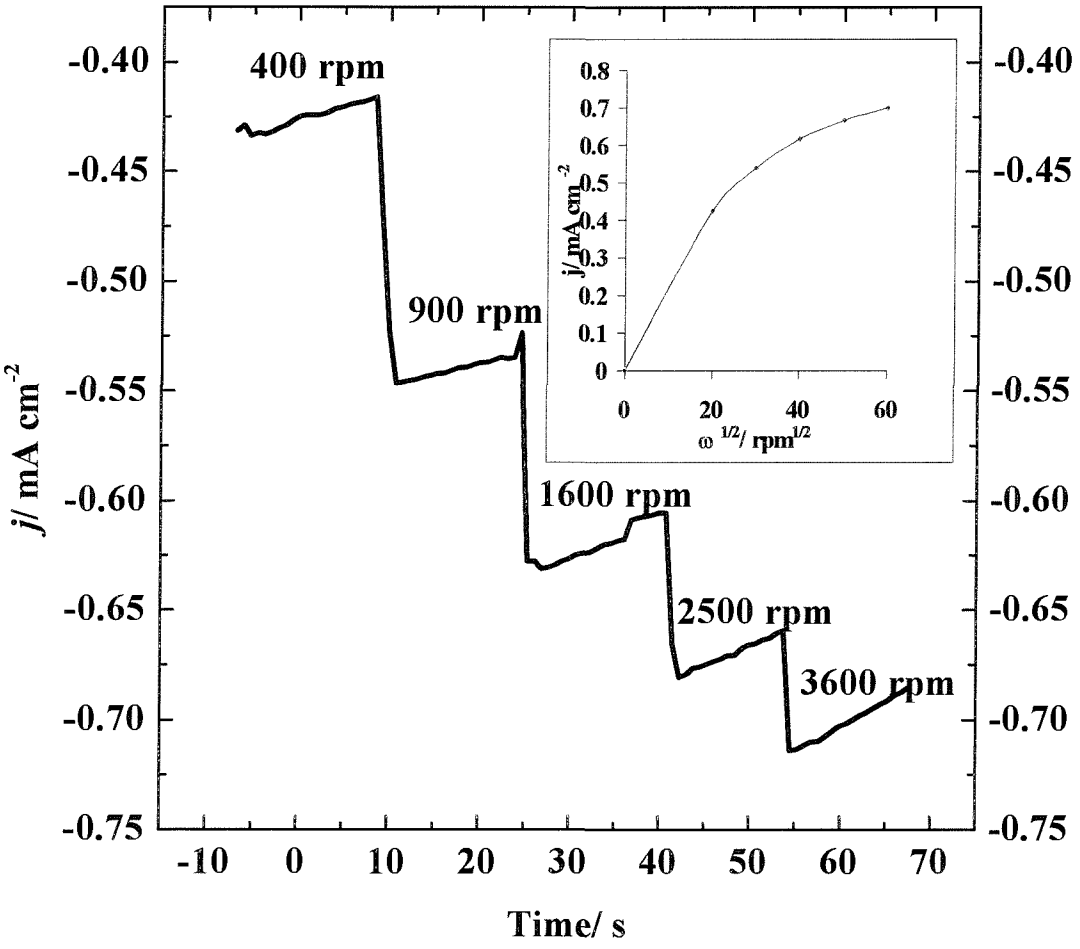

Figure 5. 7 *Variation in the current density at – 860 mV with the rotation rate of the steel disc electrode for a deoxygenated aqueous solution containing 3 % NaCl + 1 mM NaOAc + 0.65 mM HOAc, pH 4.80. Temperature 298 K. Rotation rates shown on the figure. The inset shows the plot of the limiting current density as a function of the square root of the rotation rate of the disc electrode.*

Then, the influence of the rotation rate of the X65 carbon steel rotating disc electrode on the current density for a deoxygenated solution containing 3 % NaCl + 10 mM NaOAc + 5 mM HOAc, pH 4.80, at 298 K was also investigated. It should be noted that this solution has the same pH as the 1 mM sodium acetate, however the concentration of acetic acid is approximately 8 times higher. The limiting current densities measured at –850 mV and – 1150 mV versus SCE were plotted versus the square root of the rotation rate of the disc electrode. At – 1150 mV versus SCE, a good linear plot passing through the origin was obtained as shown in figure 5.8. The electrode reaction is therefore fully mass transfer controlled at this potential. However, at – 850 mV versus SCE, the current density was found to increase only slightly with the rotation rate of the disc electrode as shown in figure 5.8.

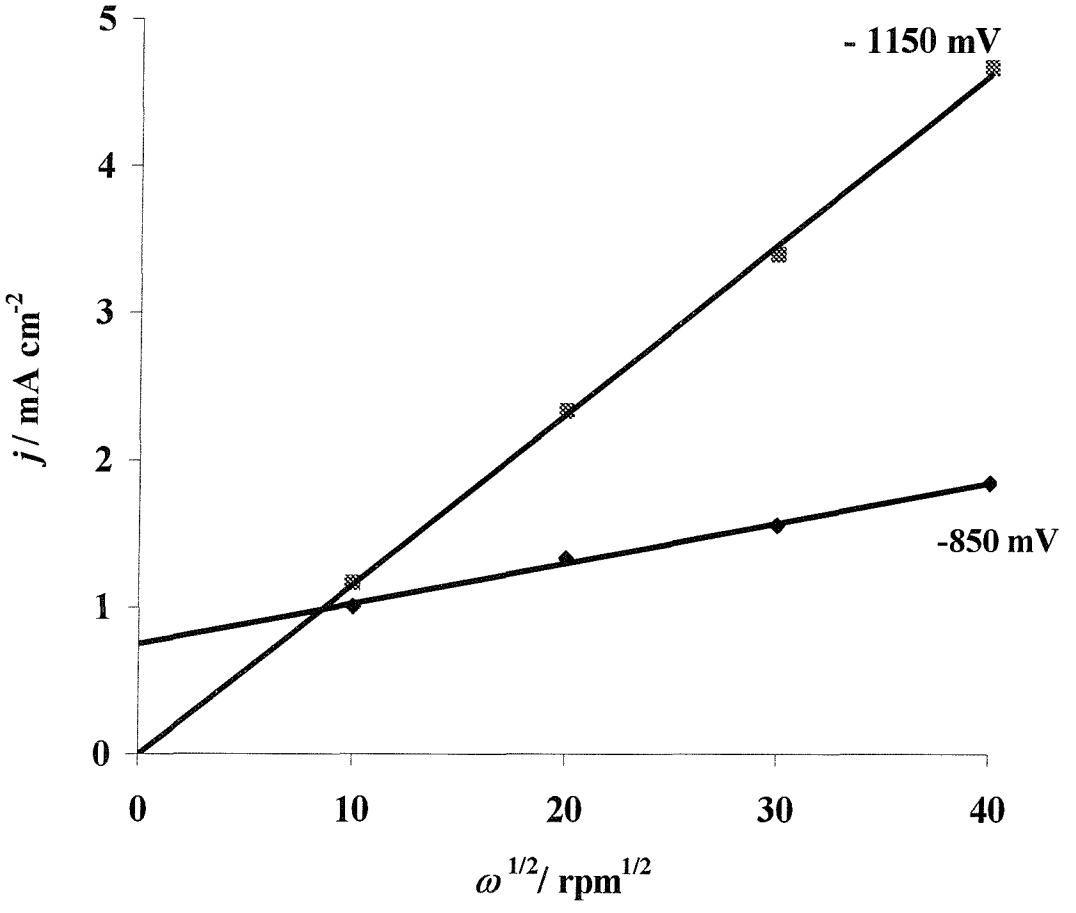

Figure 5. 8 *Variation of the limiting current density at – 1000 mV vs SCE at a X65 carbon steel disc (area, 0.17 cm^{-2}) in 3 % NaCl + 10 mM NaOAc + 5 mM HOAc with the square root of the rotation rate of the disc. Temperature 298 K.*

The current-potential curve obtained for the brine containing 3 % NaCl + 100 mM NaOAc + 24.4 mM HOAc, pH 5.15, at 333 K was examined further. The variation of the limiting current densities at – 850 mV versus SCE (in the plateau for Wave 1), and – 1150 mV versus SCE (in the plateau for Wave 2) as a function of the rotation rate of the disc electrode was investigated. The results obtained are reported in figure 5.9.

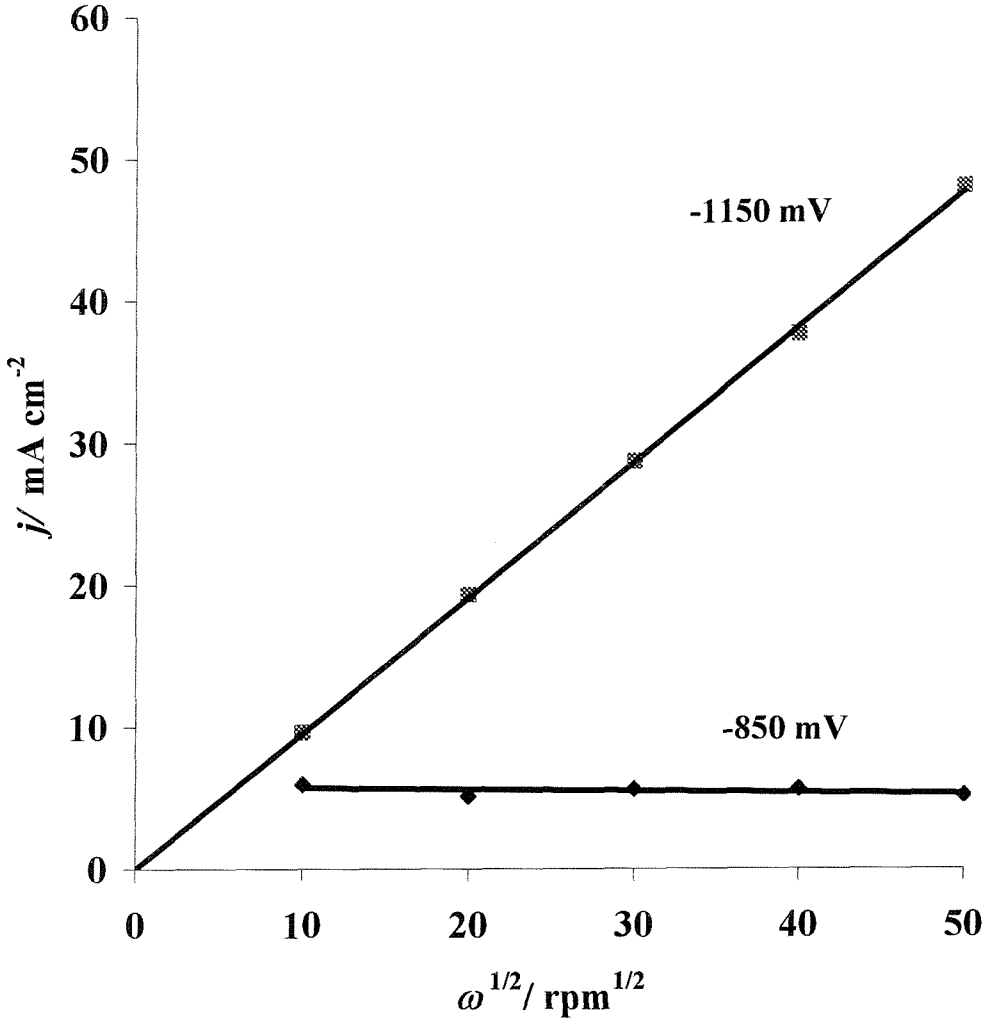

Figure 5. 9 *Variation of the limiting current density at – 850 mV and – 1150 mV vs SCE at a X65 carbon steel disc (area, 0.17 cm^2) in 3 % NaCl + 10 mM NaOAc + 24.4 mM HOAc with the square root of the rotation rate of the disc. Temperature 333 K.*

5.3.3 Influence of Acetic acid concentration

Figure 5.10 reports the variation of the limiting current densities at – 850 mV and – 1250 mV versus SCE as a function of acetic concentration (rotation rate, 400 rpm) at 333 K.

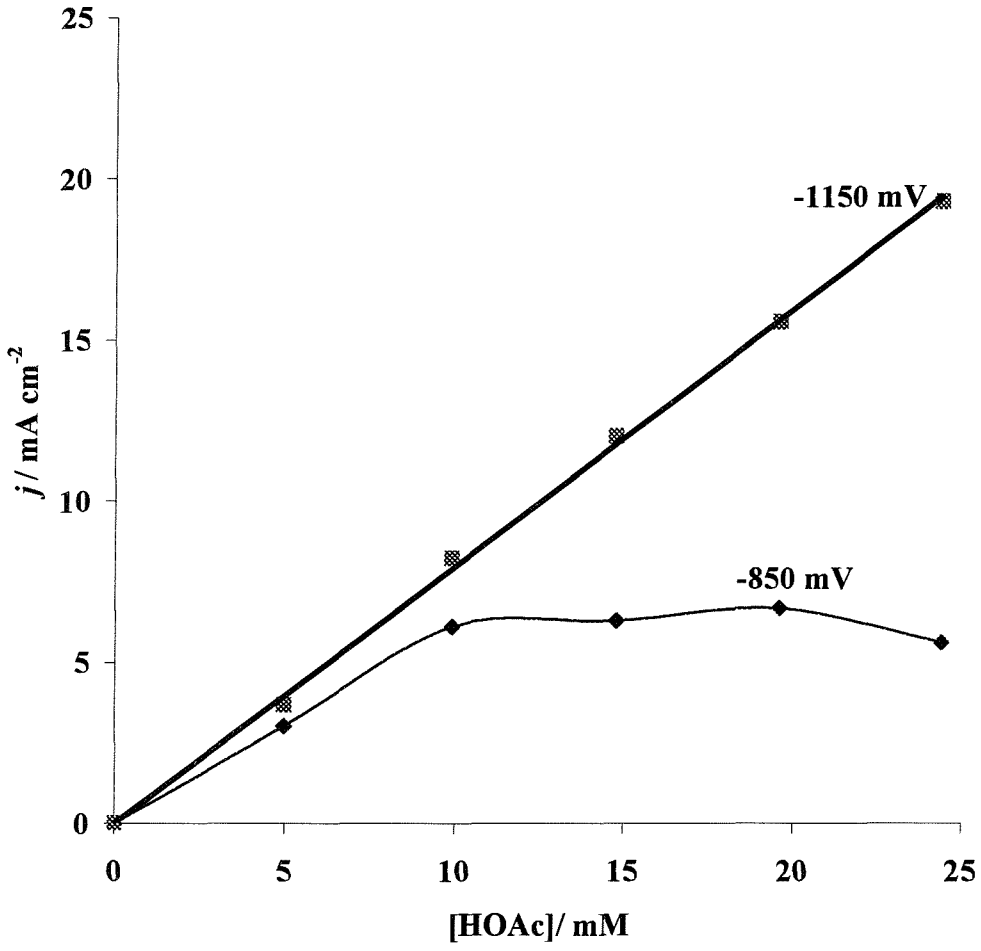

Figure 5. 10 *Variation of the limiting current density at – 850 mV and – 1150 mV versus SCE at a X65 carbon steel disc (area, 0.17 cm^2) in 3 % NaCl + 10 mM NaOAc with concentrations of acetic acid (rotation rate, 400 rpm). Temperature 333 K.*

According to figure 5.10, it can be seen that at – 1150 mV versus SCE, the limiting current densities increase linearly as acetic acid is added to the solution (as expected for a mass transport controlled reaction). However, at – 850 mV versus SCE, the current quickly reaches a limiting value.

Figure 5.11 shows two voltammograms to illustrate the effect of acetic acid concentration, in fact for the X65 carbon steel in two acetate buffers with the same pH, pH 4.80, where acetic acid was added to different concentration of sodium acetate, 1 and10 mM respectively to get the desired pH (the 1 mM sodium acetate solution will, of course, contain a much lower acetic acid concentration).

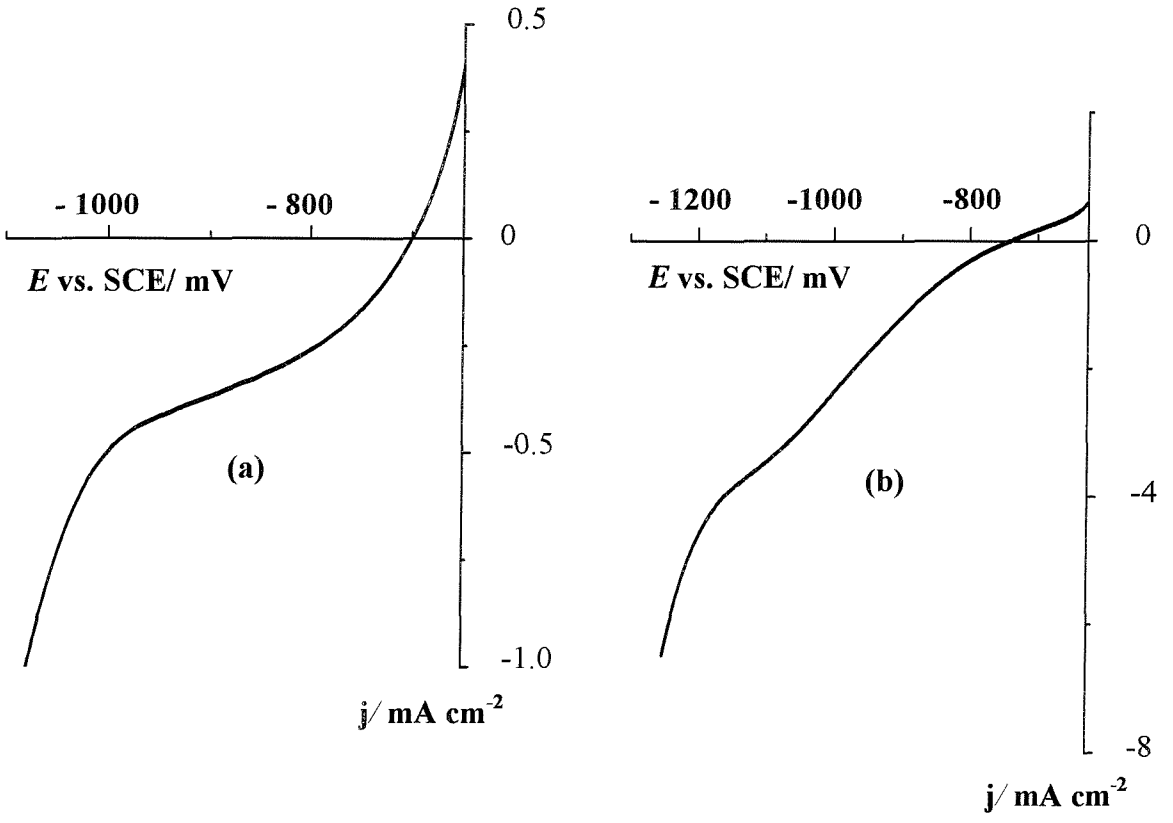

Figure 5. 11 *Voltammograms recorded at a X65 carbon steel rotating disc electrode in two acetate buffers with the same pH, 4.80, (a) 1 mM NaOAc and (b) 10 mM NaOAc. Temperature 298 K. Rotation rate 900 rpm.*

It should be immediately noted that these curves are recorded on different current density scales. With the low acetic concentration (voltammogram (a)), essentially only the first reduction process (Wave 1) is observed and it is seen immediately negative to the corrosion potential. With the solution with the higher concentration of acetic acid (voltammogram b), cathodic current is still observed immediately negative to the corrosion potential, but the second reduction process (Wave 2) at $E_{1/2} \approx$ - 1050 mV versus SCE becomes relatively more important and

certainly appears to be the dominant feature. This is not to suggest that the currents positive to – 850 mV versus SCE are diminished but they become a smaller fraction of the limiting current density at – 1150 mV versus SCE. It can also be seen that the limiting current densities vary by almost a factor of ten as expected for these two solutions.

5.3.4 Voltammetry of X65 carbon steel RDE in other carboxylic acid solutions

The voltammetry of other weak organic acids (formic acid and propionic acid) at a X65 carbon steel rotating disc electrode in 3 % NaCl brines was investigated at 298 K. Experiments were carried out on solutions with known ratios of anion/acid.

Figure 5.12 shows typical voltammograms recorded at a X65 carbon steel rotating disc electrode in N_2 saturated solutions containing (a) 24.4 mM propionic acid + 10 mM sodium propionate + 3 % NaCl and (b) 24.4 mM formic acid + 10 mM sodium formate + 3 % NaCl at 900 rpm. A potential scan rate of 5 mV s^{-1} was used for these experiments. All voltammograms were recorded at 298 K.

The form of the responses is identical to voltommograms obtained for sodium acetate/acetic acid buffers (see figure 5.2). The corrosion potential has shifted to significantly more positive values (compare to solutions were no acid is added), -666 mV versus SCE and – 657 mV versus SCE for propionic and formic acids respectively. It is also evident that the voltammograms have the same general features as described for solutions with acetic acid. Positive to the corrosion potential, an oxidation is clearly visible due to the anodic dissolution of steel as expressed in reaction (1). Further, there is a cathodic current at all potential negative to the corrosion potential. A reduction wave is observed with $E_{1/2} \sim$ –980 mV versus SCE for propionic acid and – 1000 mV versus SCE for formic acid.

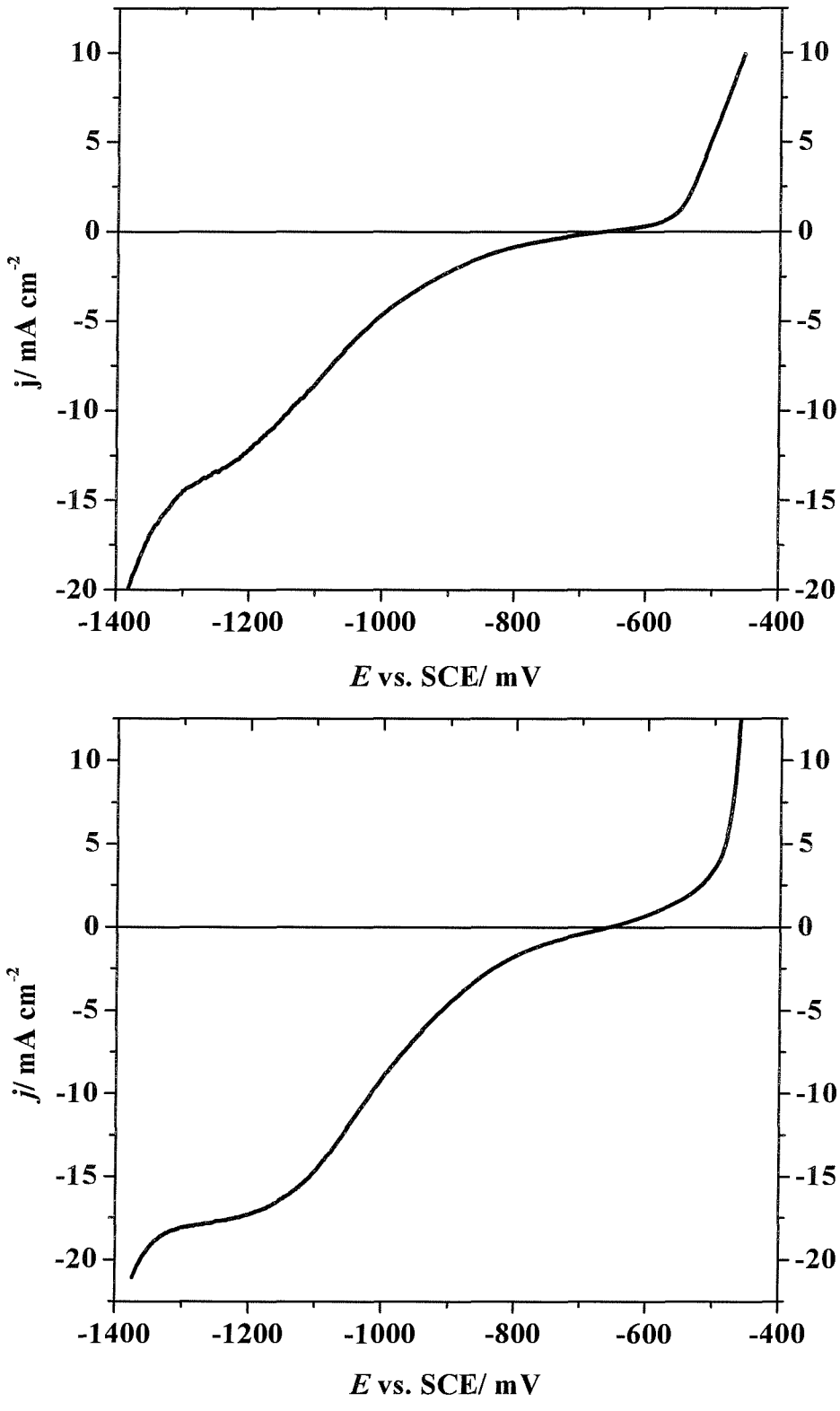

Figure 5. 12 *Voltammograms recorded at a X65 carbon steel rotating disc electrode (area, 0.17 cm^2) in deoxygenated aqueous solutions containing (a) 24. 4 mM propionic acid + 100 mM sodium propionate + 3 % NaCl and (b) 24.4 mM formic acid + 100 mM sodium formate + 3 % NaCl. Rotation rate 900 rpm. Temperature 298 K.*

Moreover the plateaux current are reasonably defined. In addition, this reduction wave increases in importance as the rotation rate of the X65carbon steel electrode is increased, and in the plateau region negative to – 1100 mV versus SCE, the limiting current density is proportional to the square root of the rotation rate of the disc electrode as shown in figure 5.13.

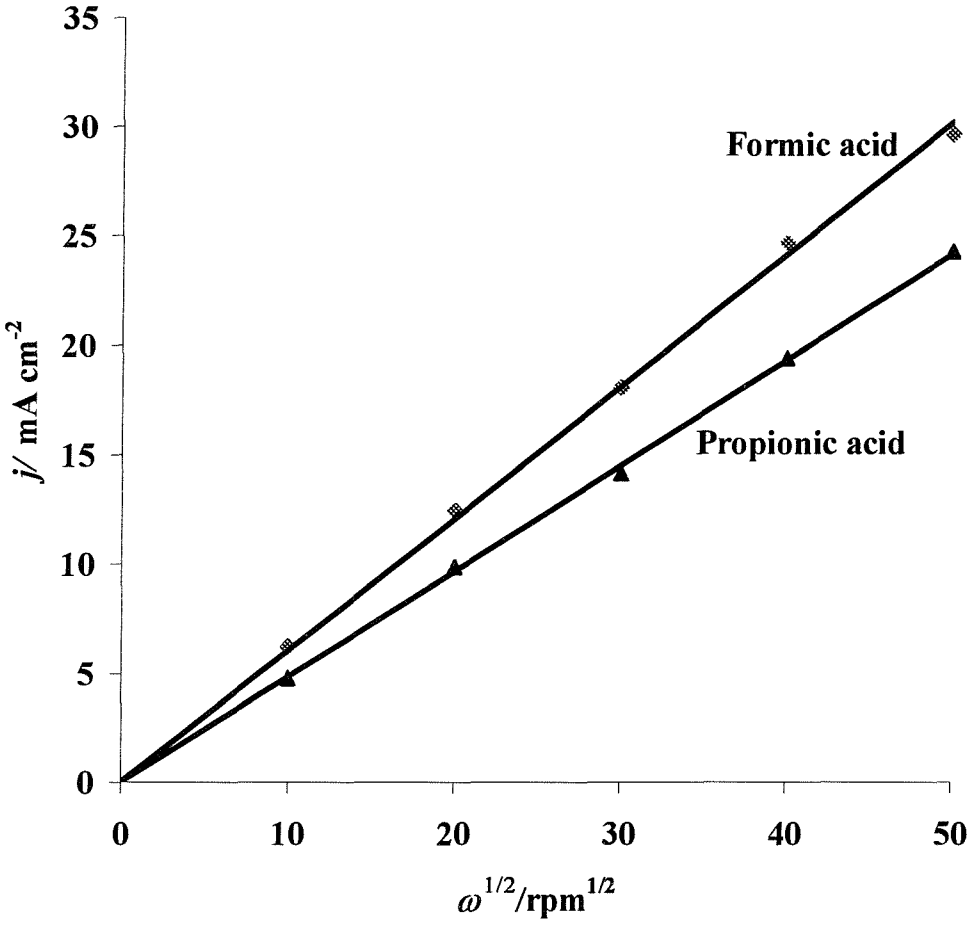

Figure 5. 13 *Plots of j_L versus $\omega^{1/2}$ at potentials in the plateau region of the j-E curves in figure 5.12. Solutions contains 3 % NaCl and (a) 10 mM sodium propionate + 24.4 mM propionic acid and (b) 10 mM sodium formate + 24.4 mM formic acid. X65 carbon steel RDE (area, 0.17 cm^2). Temperature 298 K.*

The electrode reactions are therefore mass transport controlled in the plateau regions and it is the transport of the weak organic acids at the electrode surface that determines the current density.

Further data taken from the voltammograms shown in figure 5.12 are reported in table 5.2. Also, the data obtained for a deoxygenated solution containing 3 % NaCl + 10 mM NaOAc + 24.4 mM acetic acid has been included for comparison.

Acid	Dissociation constants	[Acid]/ mM	pH	E_{corr}/ mV	10^9 D_{Acid}/ m^2 s^{-1}
Formic acid	1.77×10^{-4}	24.4	3.04	-657	1.42
Acetic acid	1.75×10^{-5}	24.4	4.19	-624	1.10
Propionic acid	1.34×10^{-5}	24.4	4.14	-666	1.04

Table 5. 2 *Data taken from voltammograms recorded at a X65 carbon steel RDE, rotation rate 900 rpm, for solutions containing 3 % sodium chloride + 10 mM sodium salt of weak acid + 24.4 mM of weak acid. Temperature 298 K.*

It should be noted that the diffusion coefficient for the acids in the brines, were calculated from the slopes of plots of the limiting current densities versus the square root of the rotation rates of the disc electrode (see figure 4.13). From table 4.5, it is evident that at fixed concentration of weak acids, the pH decreases with increasing value for the dissociation constant of the acids. Further, the values of the diffusion coefficient for the different acids remain very similar to those calculated at the Pt RDE (see table 4.5). The value in the formate medium is high because of a contribution to the limiting current of the diffusion of free protons.

5.3.5 Conclusion to studies with acetate/acetic buffers

It has been shown that the electrochemistry of weak acids solutions at the X65 carbon steel, as well as Pt, reflect the total concentration of proton donor (acetic acid) in the solution because the dissociation of carboxylic acid is a rapid reaction. Hence, a cathodic current equivalent to the mass transport controlled reduction of the carboxylic acid in the medium can be observed. However, the reduction of acetic acid at steel is more complex than at Pt, and it only occurs with a significant overpotential. Even so, the reduction of acetic acid to hydrogen is a significant

significant reaction at the corrosion potential. As well as having slower kinetics, the reaction occurs by two mechanisms leading to two distinct waves.

Wave 1 clearly has the stronger influence on the cathodic current density at the corrosion potential. With a low acetic acid concentration wave 1 is at least partially mass transport controlled and then Wave 2 is absent. The rate of the electrode reaction leading to Wave 1 apparently cannot exceed a certain value, and if this limitation is exceeded, the mass transport controlled reduction of the remaining acetic acid reaching the surface is seen as Wave 2. Wave 2 is most clearly seen in conditions of rapid mass transport, due to either high rotation rate or high acetic acid concentration and when the rate of reaction leading to Wave 1 is low (298 K). All the experimental data imply that both reduction waves, Wave 1 and Wave 2, are associated with the reduction of acetic acid but the rate of the processes are determined by different factors. There is no doubt that with high acetic concentrations, Wave 1 is kinetically limited but this is not the case with low acetic concentrations. Indeed, the influence of rotation rate on the limiting current density shows that Wave 1 can be at least partially mass transport controlled with low acetic acid concentrations. Hence, we envisage a mechanism for the reaction leading to Wave 1 where the reduction of acetic acid to hydrogen is occurring at a limited number of active sites on the steel surface.

These sites can become saturated at either high acetic acid concentrations, efficient mass transport or lower temperatures, when the rate of desorption at these sites becomes too slow. For example, one can envisage a mechanism

$$HOAc + \text{active site} \longrightarrow H_{ads} + OAc^- \qquad (5)$$

$$2\,H_{ads} \longrightarrow H_2 + 2 \text{ active sites} \qquad (6)$$

where either step could be the rate determining step. At the potentials of Wave 2, the reduction must occur by a different mechanism and in all conditions the reaction

becomes mass transport controlled at sufficiently negative potential. The two reduction mechanisms for acetic acid arise only from the higher driving force for the reduction at more negative potentials, i.e. other sites on the surface become active. Alternatively, the two mechanisms may be occurring on different surfaces, for example, at the more negative potentials, the current resulting from reduction of acetic acid on a relatively clean steel surface and this reaction is mass transport controlled. But as the potential is scanned towards positive potentials, a corrosion film forms on the steel surface and inhibits the reduction of acetic acid. The current then drops to a lower value that is kinetically controlled and therefore very dependent on temperature. The voltammograms would suggest that the corrosion film would be forming positive to - 1000 mV versus SCE and this is not unreasonable in view of the corrosion potential in the absence of acetic acid, - 860 mV versus SCE.

5.4 Voltammetry of X65 carbon steel RDE in sodium acetate solutions saturated with carbon dioxide

5.4.1 Preliminary studies

Figure 5.14 shows voltammograms recorded at two rotation rates for a X65 carbon rotating disc electrode in a brine containing 3 % NaCl + 100 mM NaOAc saturated with carbon dioxide at 298 K (PHREEQC 2.2 calculates the acetic acid concentration as 8.6 mM); the pH was measured as 5.50. The potential was swept from – 1200 mV to – 600 mV versus SCE. The corrosion potential shifts from – 860 mV versus SCE in the 3 % NaCl brine + 100 mM sodium acetate without carbon dioxide to – 668 mV versus SCE (after carbon dioxide saturation). It is also evident that the voltammogramms have the same general features as described for the solutions with added acetic acid. Positive to –668 mV, an oxidation current is clearly visible due to the anodic dissolution of steel as expressed in reaction (1). Further, there is a cathodic current at all potentials negative to the corrosion

potentials and the response could be deconvoluted into two waves at – 750 mV and – 950 mV versus SCE.

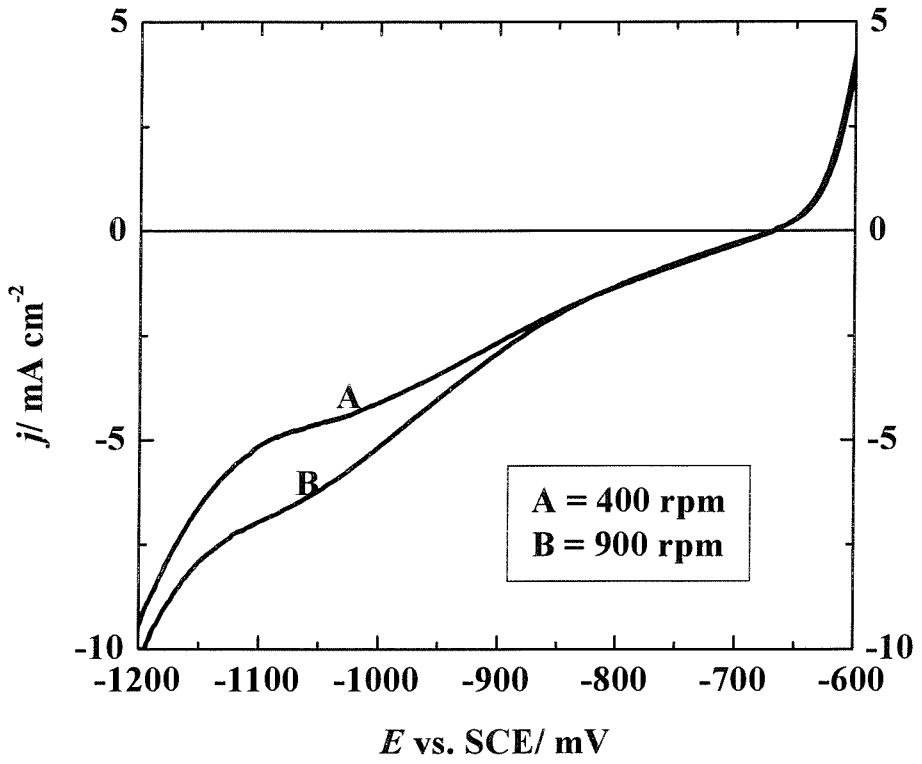

Figure 5. 14 *Voltammograms recorded for a X65 carbon steel rotating disc electrode (area, 0.17 cm^2) in a solution containing 3 % NaCl + 100 mM NaOAc saturated with carbon dioxide, pH 5.50. Temperature 298 K.*

The second reduction wave increases in importance as the rotation rate of the carbon steel rotating disc electrode is increased and, in the plateau regions negative to – 1100 mV versus SCE, the limiting current is proportional to the square root of the rotation rate of the disc electrode as shown in figure 5.15. A good linear plot passing through the origin was obtained as shown in figure 5.15. The electrode reaction is therefore fully mass transport controlled at this potential. Overall, the responses are very similar to those obtained for the solutions containing acetic acid and sodium acetate. At the corrosion potential the cathodic reactions to be considered are now reactions (2), (3) and (4) as well as:

$$2H_2CO_3 + 2e^- \longrightarrow H_2 + 2HCO_3^- \qquad (6)$$

The reduction of bicarbonate will not contribute because the pK_A of bicarbonate is 10.35, significantly higher than water.

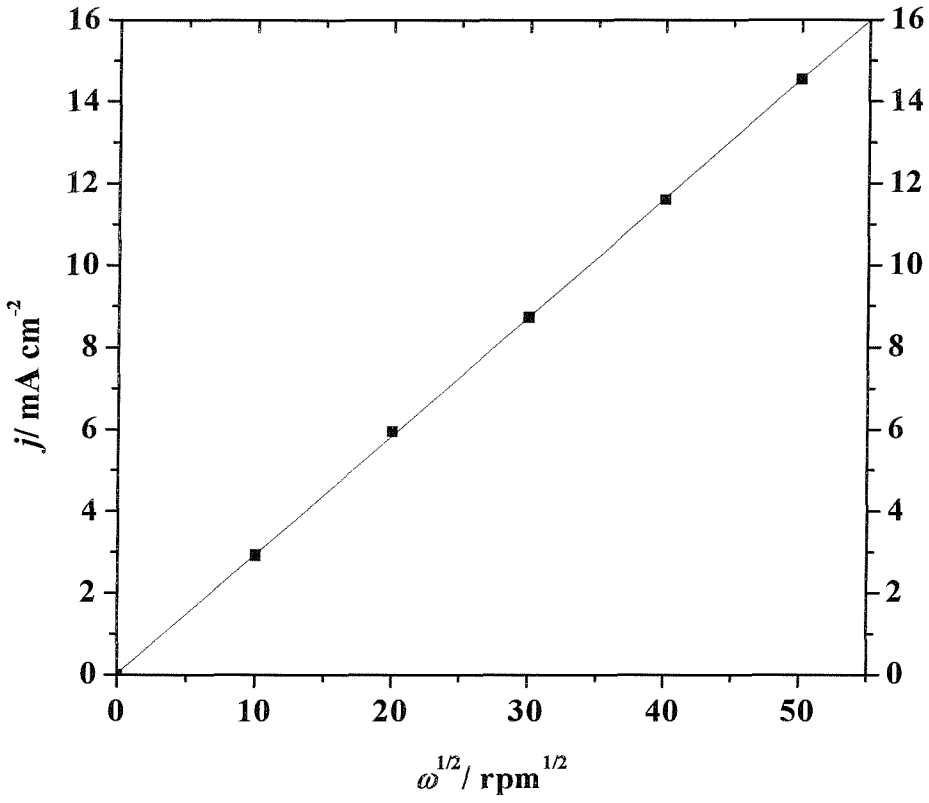

Figure 5. 15 *Variation of the limiting current density at – 1100 mV versus SCE at a X65 carbon steel rotating disc electrode (area, 0.17 cm^2) in an aqueous solution containing 3 % NaCl + 100 mM NaOAc saturated with carbon dioxide, pH 5.50, with the square root of the rotation rate of the disc electrode. Temperature 298 K.*

5.4.2 Influence of sodium acetate concentrations

Figure 5.16 reports the voltammograms for 3 % NaCl brine solutions saturated with carbon dioxide with three different concentrations of sodium acetate (it should be noted that the current density scale is different in each voltammogram). All the voltammograms show the positive shift in the corrosion potential (cf. figure 5.1). Positive to the corrosion potential, oxidation currents are clearly visible due to the anodic dissolution of steel as expressed in reaction (1). Further, cathodic currents are visible immediately negative to the corrosion potential.

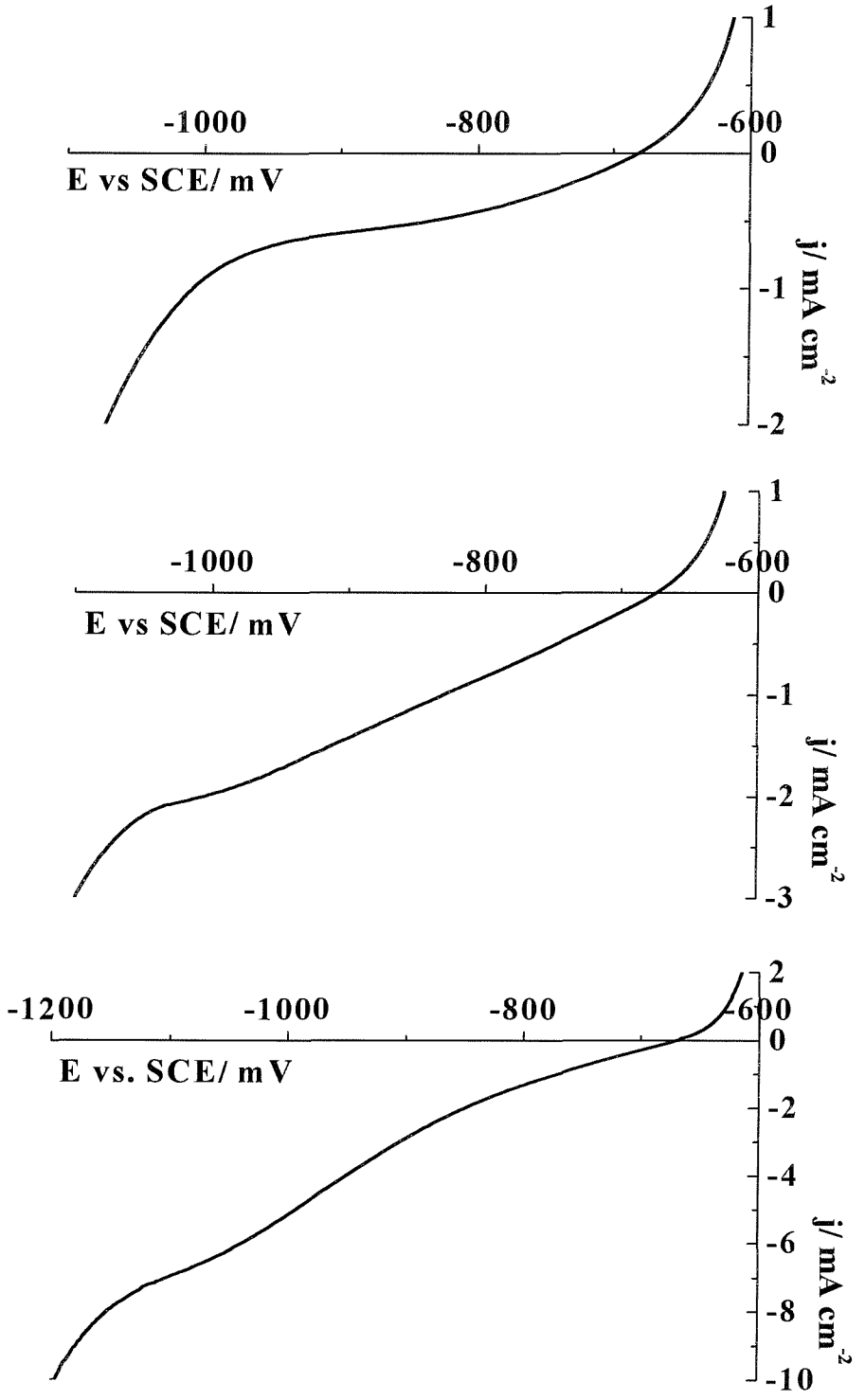

Figure 5. 16 *Voltammograms recorded for a X65 carbon steel rotating disc electrode (area, 0.17 cm^2) in 3 % NaCl brine containing (a) 1 mM, (b) 10 mM and (c) 100 mM NaOAc saturated with carbon dioxide. Rotation rate 900 rpm. Temperature 298 K. PHREEQC 2.2 estimates the concentration of acetic acid as (a) 0.56 mM, (b) 2.4 mM and (c) 8.6 mM.*

The form of the voltammogram negative to the corrosion potential again reflects the concentration of acetic acid in the solution (in fact 0.56 mM, 2.4 mM and 8.6 mM as estimated by PHREEQC 2.2). At the low acetic concentration, all the reduction current is observed just negative to the corrosion potential but with the most concentrated solution, the dominant feature is a reduction wave with $E_{1/2} \approx -990$ mV versus SCE. The limiting current densities for the three voltammograms are 0.53 mA cm^{-2}, 2.05 mA cm^{-2} and 6.8 mA cm^{-2} directly reflecting the concentrations of acetic acid in the solutions. As with the Pt rotating disc electrode, it can be seen that the electrochemistry at a steel cathode of these solutions saturated with carbon dioxide can be understood in a semi-quantitative way in terms of acetic acid in solution. At both X65 carbon steel and Pt, at sufficiently negative potential all the acetic acid is reduced via the mechanism, reaction (7)

$$HOAc \rightleftharpoons H^+ + OAc^- \qquad (7)$$

followed by the reduction of the free proton, reaction (3):

$$2H^+ + 2e^- \rightleftharpoons 2H_2 \qquad (3)$$

Moreover, even close to the corrosion potential for the steel, the reduction of acetic acid contributes significantly to the cathodic component of the current. With increasing acetate concentration, the pH may increase but this is tied to an increase in undissociated acetic acid concentration. Hence, with acetate ions present in the carbon dioxide saturated medium, the reduction of acetic acid, reaction (4):

$$HOAc + e^- \longrightarrow \tfrac{1}{2} H_2 + OAc^- \qquad (4)$$

takes over from the reduction of proton, reaction (3) as the cathodic process for corrosion.

5.4.3 Influence of rotation rates

Figure 5.15 compares the effect of the rotation rate for a X65 carbon steel rotating disc electrode in an aqueous solution containing 3 % NaCl + 10 mM NaOAc saturated with carbon dioxide, pH 5.01 (after CO_2 saturation) at 298 K (PHREEQC 2.2 calculates the concentration of acetic acid as 2.4 mM). It should be immediately noted that figure 5.15 is very similar to figure 5.6. Again with the low rotation rate (100 rpm), all the reduction current (Wave 1) is observed just negative to the corrosion potential. However at the higher rotation rate (900 rpm), Wave 2 appears to be the dominant feature.

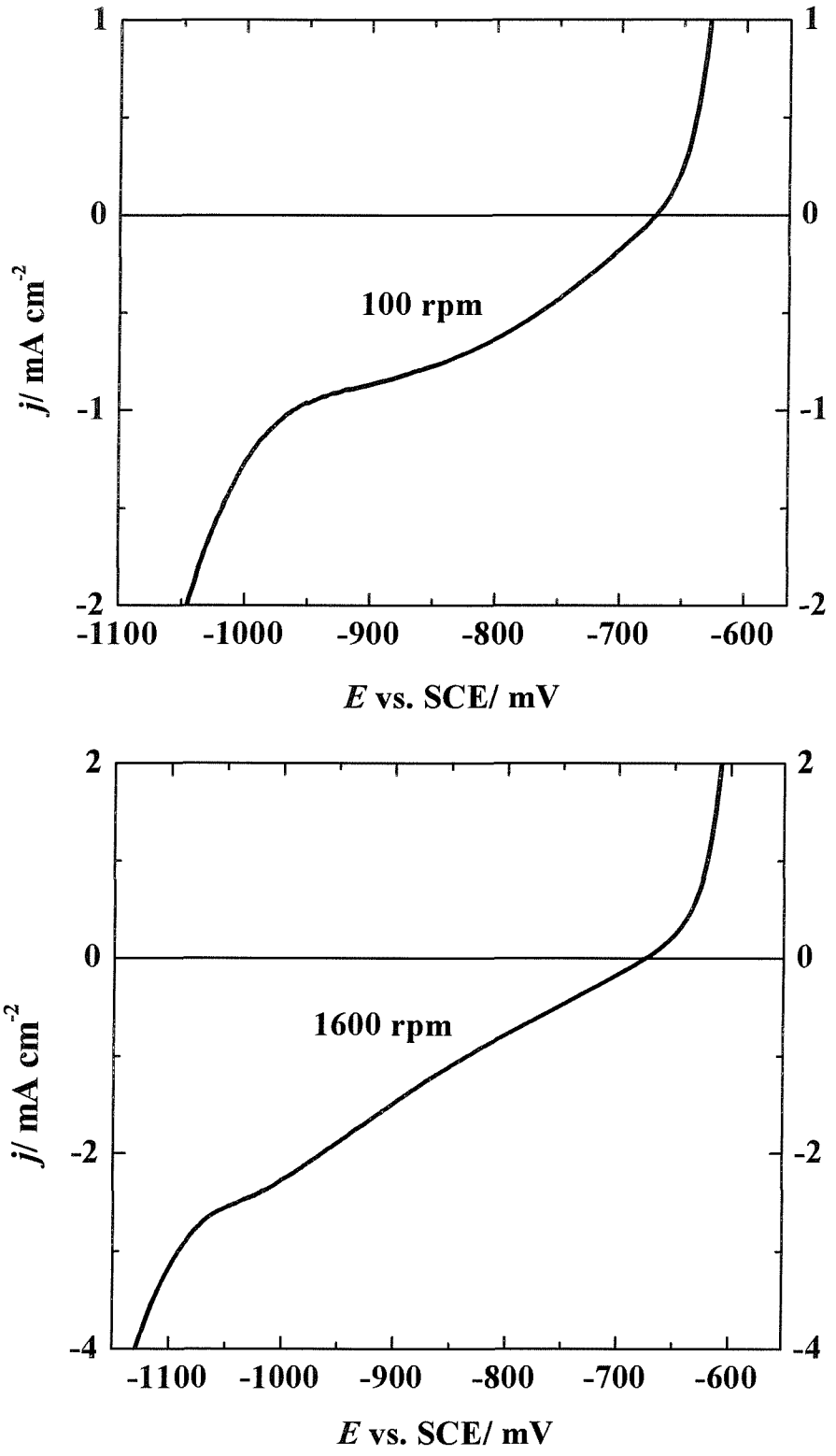

Figure 5. 17 *Voltammograms recorded for a X65 carbon steel rotating disc electrode in a solution containing 3 % NaCl + 10 mM NaOAc saturated with carbon dioxide, pH 5.01 (after CO_2 saturation). Temperature 298 K. Rotation rates shown on figure.*

The influence of the rotation rate of the X65 carbon steel rotating disc electrode on the current density at – 860 mV vsersus SCE (in the plateau for Wave 1) was investigated, for 3 % brine solutions saturated with carbon dioxide with three different concentrations of sodium acetate. The experiments were carried out at 298 K. The results obtained are presented in figure 5.18.

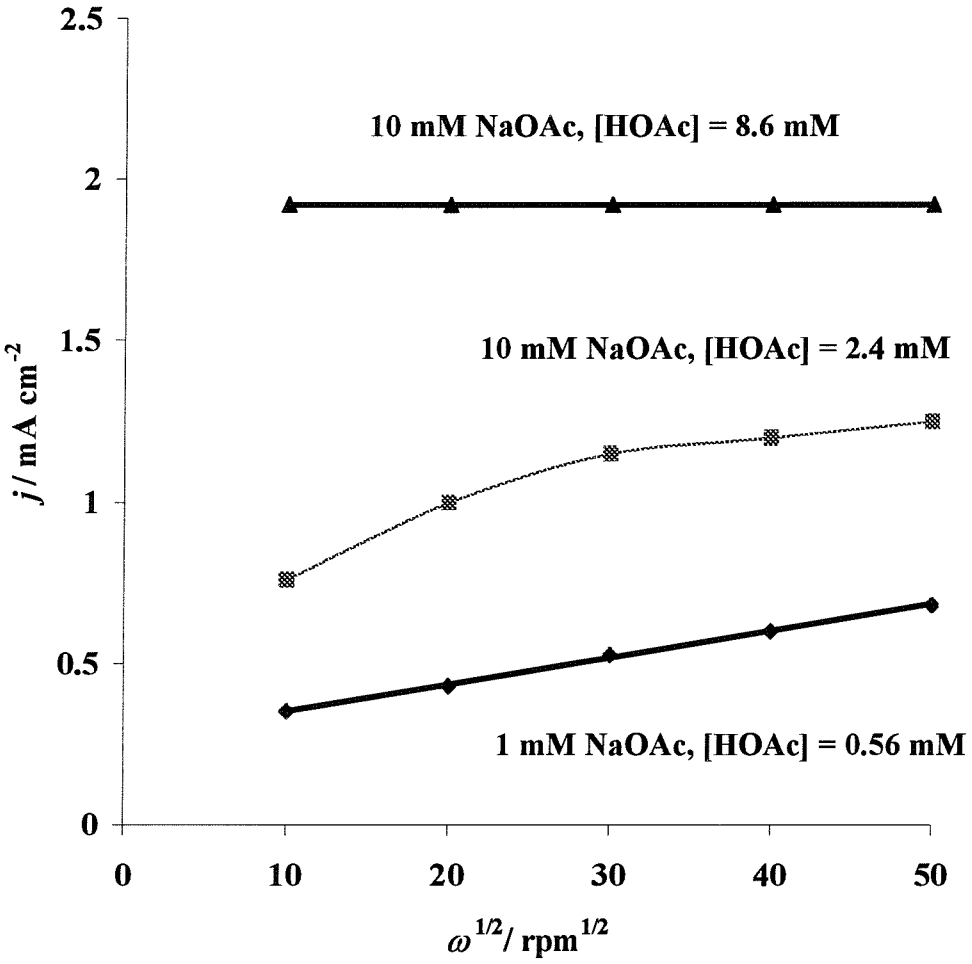

Figure 5. 18 *Variation of the limiting current density at – 860 mV versus SCE at a X65 carbon steel disc (area, 0.17 cm^2) in 3 % NaCl + NaOAc saturated with carbon dioxide, with the square root of the rotation rate of the disc electrode. Temperature 298 K.*

According to figure 5.18, it can be seen that the influence of the rotation rate on the current densities beyond Wave 1 for these sodium acetate brines saturated with carbon dioxide depends strongly on the concentration of acetic acid within the brines. With the 1 mM sodium acetate solution (low acetic acid concentration i.e.

PHREEQC 2.2 calculates the acetic acid concentration as 0.56 mM, only Wave 1 is clearly seen on voltammograms) the reduction of acetic acid appears to be partially mass transport controlled. With the 10 mM sodium acetate solution (PHREEQC 2.2 calculates the acetic acid concentration as 2.4 mM, Wave 1 is seen at low rotation rate, but at high rotation rates Wave 2 appears to be the dominant feature), the current density quickly reaches a limiting value. And finally, with the 100 mM sodium acetate solution (higher acetic acid concentration, i.e. PHREEQC 2.2 calculates the acetic acid concentration as 8.6 mM, Wave 1 is lost in the foot of Wave 2), the current density at –860 mV versus SCE is independent of the rotation rate of the disc electrode. However, it should be noted that for the 10 and 100 mM sodium acetate solutions, when plotting the total limiting current density (Wave 1 + Wave 2) at – 1150 mV versus SCE versus the square root of the rotation are of the disc electrode, good linear plots passing through the origin were obtained. The electrode reaction is therefore mass transport controlled at this potential.

5.4.4 Influence of temperature

The experiments were repeated at 333 K. Figure 5.18 compares typical voltammograms recorded at a X65 carbon steel rotating disc electrode for an aqueous solution containing 3 % NaCl + 100 mM NaOAc saturated with carbon dioxide at 298 K and 333 K. The pHs of the solution were 5.50 and 5.70 respectively after carbon dioxide saturation. Both voltammograms were recorded at a rotation rate of 900 rpm. The potential was swept from – 1200 mV to – 600 mV versus SCE at a potential scan rate of 5 mV s^{-1}. For both sets of temperature, an oxidation current is clearly visible just positive to the corrosion potential due to the anodic dissolution of iron as expressed in reaction (1). Further, it should be noted that the reduction wave commences at a potential positive to the corrosion potential for the same brine at 298 K. There is a substantial positive shift in the corrosion potential on increasing the temperature of the brine from 298 K to 333 K and the current density close to the corrosion potential is significantly higher. Moreover, at the higher temperature the response obtained at the steel electrode becomes more complex.

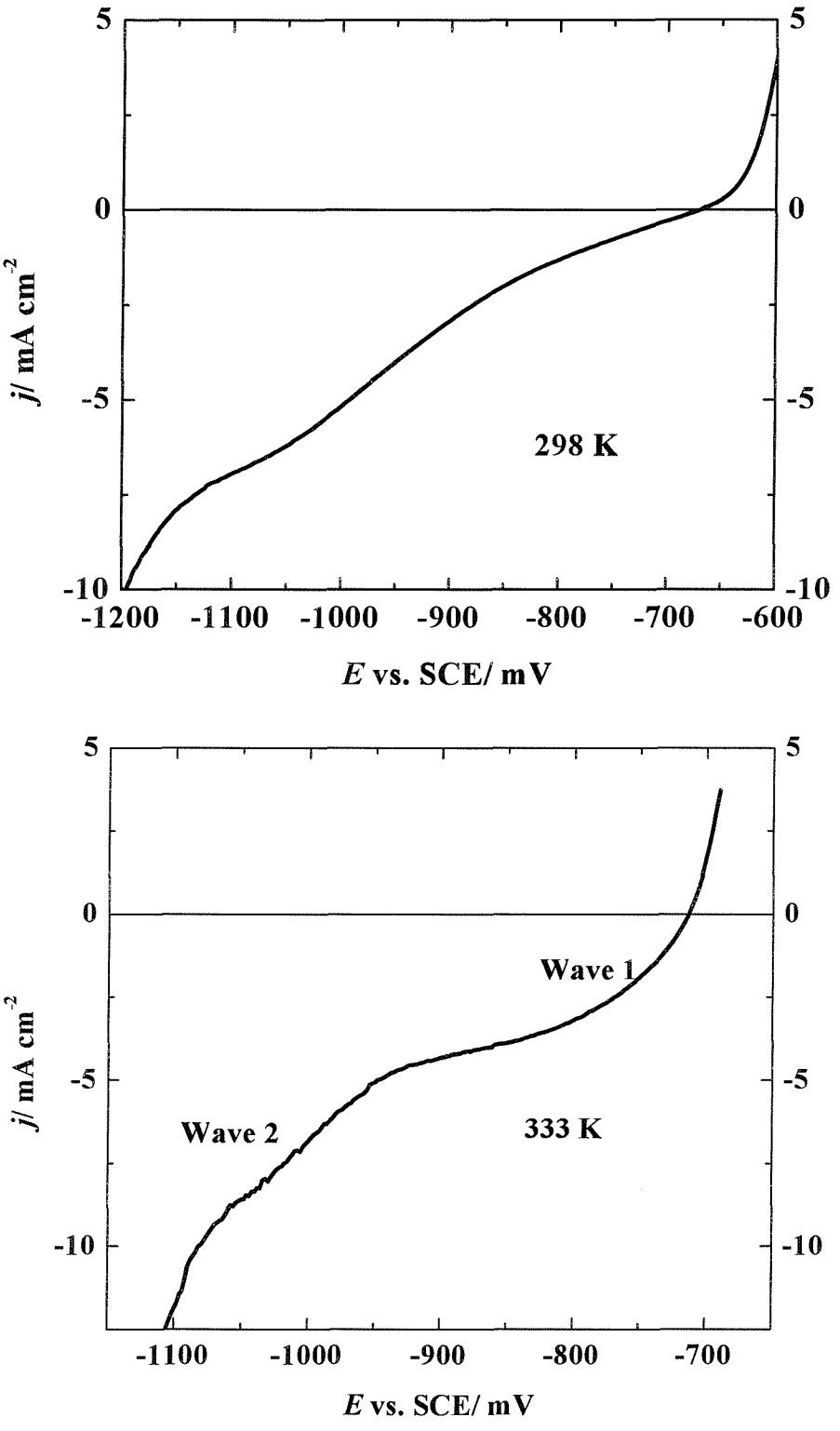

Figure 5. 19 *Voltammograms recorded at a X65 carbon steel RDE in a solution containing 3 % NaCl + 100 mM NaOAc saturated with carbon dioxide, pH 5.50 and 5.70 respectively after carbon dioxide saturation. Rotation rate 900 rpm. Temperatures shown on figure. PHREEQC 2.2 estimates the concentration of acetic acid as 8.6 mM, and 6.2 mM at 298 K and 333 K respectively.*

The voltammogram can clearly be deconvoluted into two reduction waves at – 850 mV and – 1000 mV versus SCE respectively, with the second wave becoming the dominant feature as the rotation rate of the steel disc is increased. Also, figure 5.19 provides again compelling evidence that the magnitude of the first reduction process (Wave 1) will clearly have a major influence on the corrosion behavior at the open circuit potential in the oilfield environment. However, it can be seen that Wave 2 is more drawn out and a slightly less defined than seen previously.

Then, current – potential curves were recorded for the 100 mM NaOAc + 3 % NaCl, saturated with carbon dioxide at 333 K as a function of rotation rates. The voltammograms obtained remain very similar to those described in figure 5.17. At the low rotation rate (100 rpm), only Wave 1 is visible just negative to the corrosion potential. At the higher rotation rate (900 rpm to 2500 rpm) Wave 1 is still visible just negative to the corrosion potential, but the reduction current increases continuously until it reaches a plateau around – 1000 mV versus SCE (Wave 2). Further, at this potential the height of the current plateau increases with the rotation rate of the disc electrode indicating a mass transport controlled reaction.

This observation was confirmed when analyzing the variation of the cathodic current density with the square root of the electrode according to the Levich equation [60]. A plot of the limiting current densities versus the square root of the rotation rate of the disc electrode was found to be linear and pass through the origin (Wave 1 + Wave 2). However, at – 850 mV versus SCE, the current density was found to be almost independent of the rotation rate of the disc electrode as shown in figure 5.20. The results obtained using these sodium acetate brines saturated with carbon dioxide remain very similar to those described earlier for sodium acetate brines with known concentration of acetic acid. The electrochemistry of these solutions saturated with carbon dioxide can be understood in a semi-quantitative way in terms of the equilibrium concentration of carboxylic acid in solution and not simply the concentration of free proton. In these solutions, the strongest proton donor

is acetic acid and at the usual pH of the brines, the concentration of acetic acid is substantially higher than that of free proton. As a result, the concentration of the proton donor, the undissociated weak acid rather than the pH is the critical factor determining the rate of corrosion of the carbon steel. Further, a quantitative interpretation of the voltammetry and the corrosion behaviour requires a knowledge of the speciation within these complex aqueous solutions.

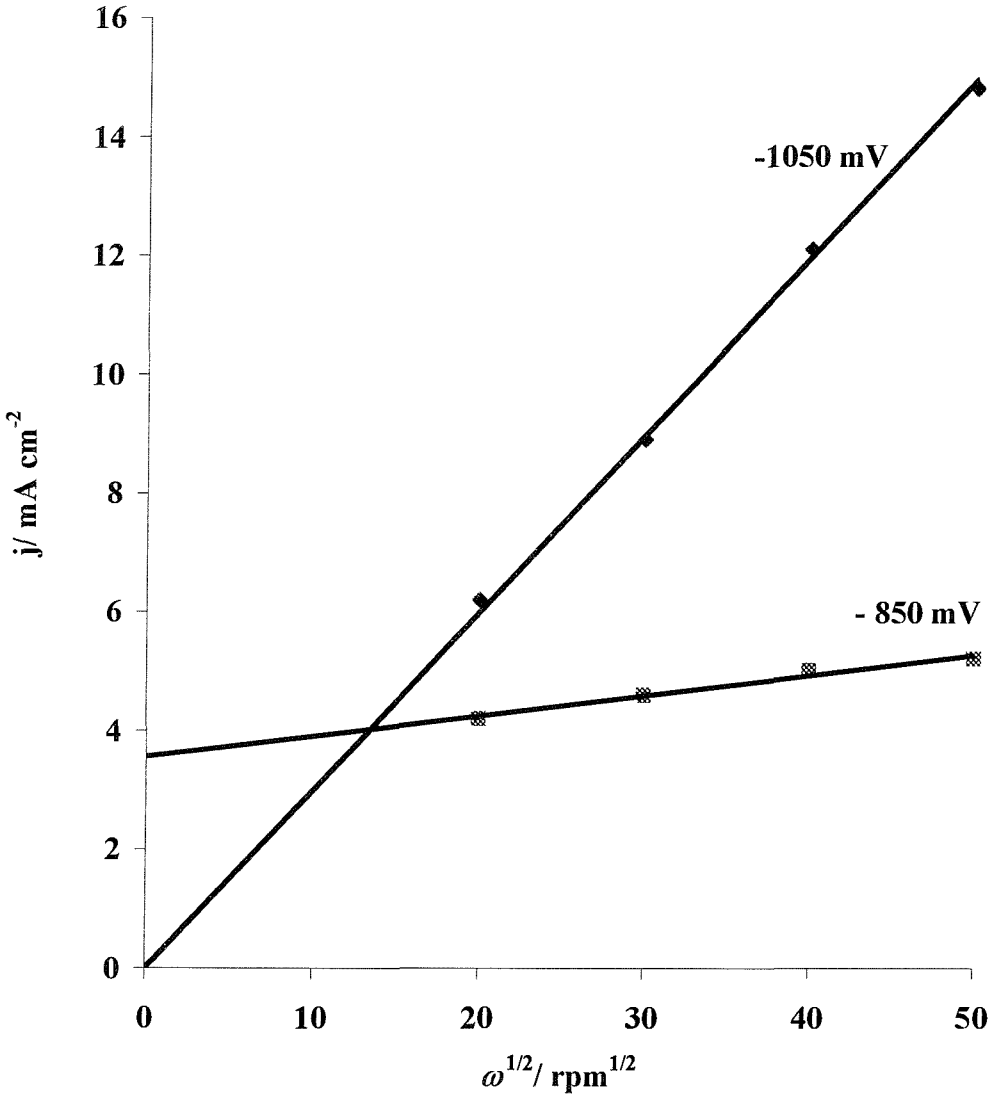

Figure 5. 20 *Variation of the limiting current density at – 850 mV and – 1050 mV versus SCE at a X65 carbon steel rotating disc electrode (area, 0.17 cm^2) in 3 % NaCl + 100 mM NaOAc saturated with carbon dioxide, pH 5.70, with the square root of the rotation rate of the disc electrode. Temperature 333 K.*

5.5 Application of electrochemical techniques to measure the corrosion rate of X65 carbon steel in different brines

The purpose of this section is to define the rate of corrosion of the X65 carbon steel in the simulated brines and the role of acetate ions and carbon dioxide in increasing the corrosion rate. Several parameters such as environmental conditions (i.e. acetic acid concentration, sodium acetate concentration presence of CO_2 and temperature) are examined. An extensive series of electrochemical experiments, (including Tafel polarization and Linear Resistance Polarisation) were used to determine the rate of corrosion of theX65 carbon steel. Voltammograms recorded at a scan rate of 5 mV s^{-1}, for a deoxygenated aqueous solution containing 3 % NaCl +10 mM NaOAc using a X65 carbon steel rotating disc electrode (area, 0.17 cm^2) at a rotation rate of 0 and 1600 rpm and temperature of 298 K and 333 K are reported in figure 5.21.

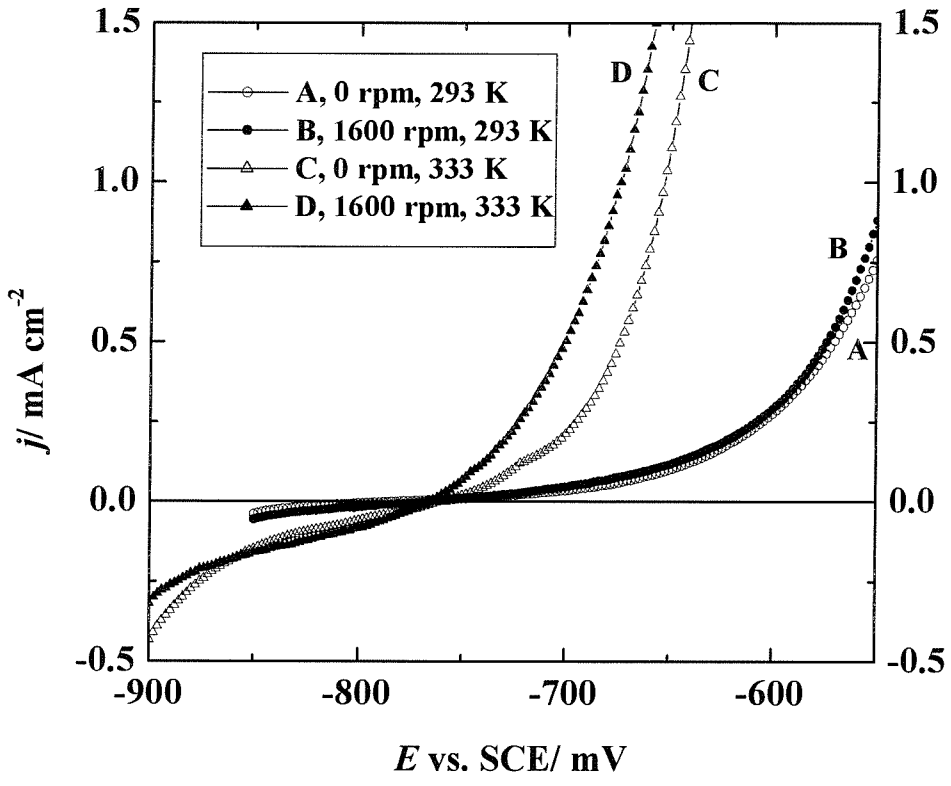

Figure 5. 21 *Voltammogramms recorded for a deoxygenated solution containing 3 % NaCl + 10 mM NaOAc, using a X65 carbon steel rotating disc electrode (area, 0.17 cm^2). Rotation rates 0 and 1600 rpm. Temperature 298 K and 333 K. Potential scan rate 5 mV s^{-1}.*

According to figure 5.21, a strong dependence of the current close to the corrosion potential on the temperature of the solution was observed. It is clear that as the temperature of the solution is increased from 298 K to 333 K, current recorded close to the corrosion potential, E_{corr}, similarly increased. Further this increase is most marked for the oxidation part of the curve. However, it can be seen that there is no strong variation on the current – potential curves when increasing the rotation rate of the carbon steel rotating disc electrode. The corrosion potentials were also not particularly sensitive to the temperature.

5.5.1 Polarisation measurements

Cathodic and anodic polarization measurements (Tafel plots) were recorded to gain an understanding of the different corrosion behaviour exhibited by the carbon steel with the various additions of acetate and carbon dioxide. Typical polarization curves for carbon steel specimens immersed in a deoxygenated 3 % NaCl brine containing 10 mM NaOAc at 298 K and 333 K are shown in figure 5.22. These polarization curves were recorded at rotation rates of 0 and 1600 rpm using a scan rate of 5 mV s^{-1}. Although the experiments were repeated several times with fairly good reproducibility, only a selected number of these experiments are presented.

In the data shown in figure 5.22, a quite good Tafel line can be drawn through the data positive to the corrosion potential, E_{corr}. The Tafel slope for the Fe/Fe^{2+} couple is in the range 62 – 75 mV. Negative to corrosion potential, E_{corr}, the increase in current density from the corrosion current density is small and it is not possible to define a meaningful Tafel slope. This is to be expected since the limiting current for wave 1 is low. In the calculations for the corrosion current density, j_{corr}, from the linear resistance polarization curves the Tafel slopes for hydrogen evolution and iron dissolution were taken as β_c = 120 mV and β_a = 60 mV. The data is, however, typical to that reported in the literature [42] and standard in the oil industry.

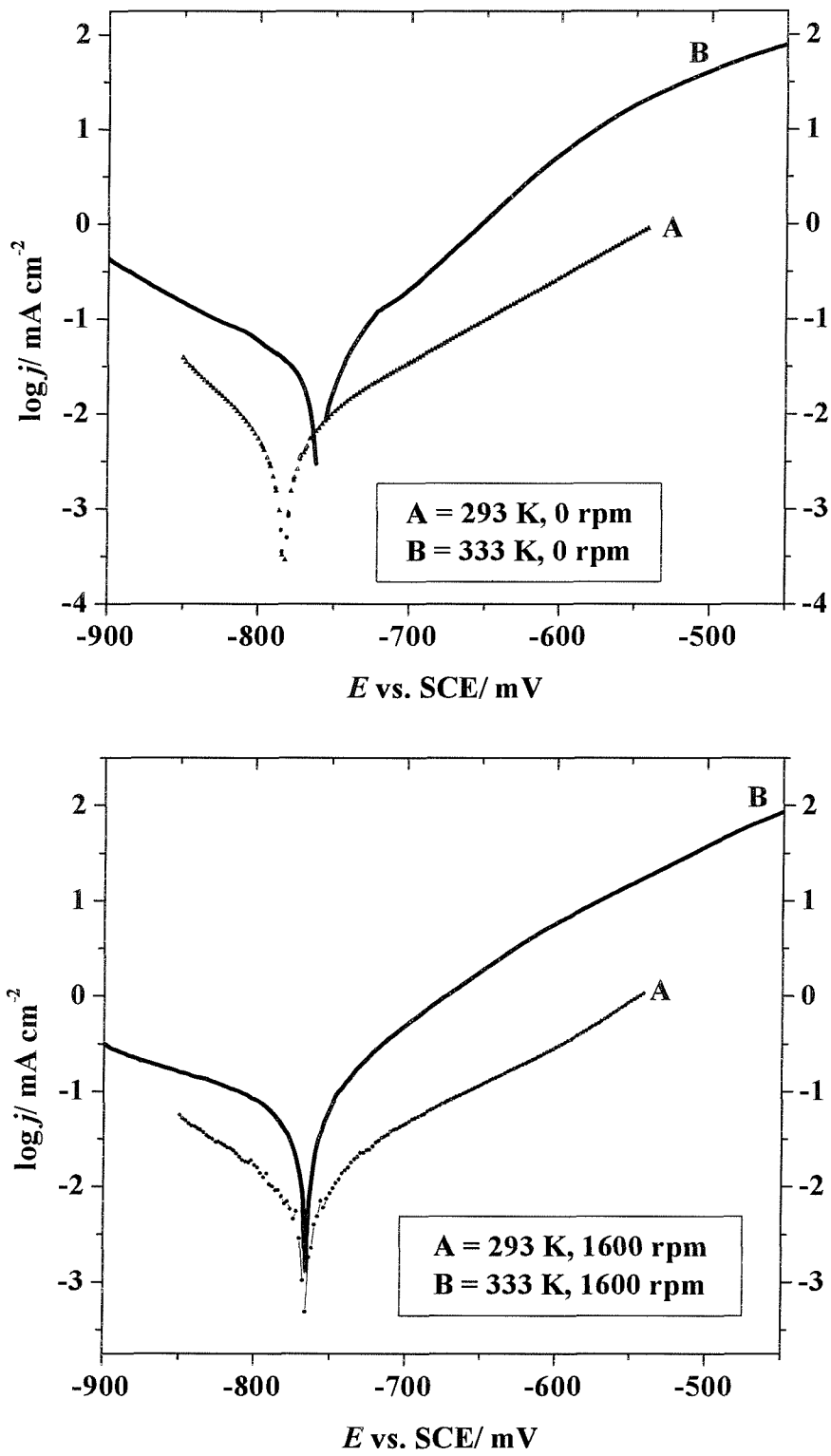

Figure 5. 22 *Tafel polarization curves for a X65 carbon steel rotating disc electrode (area, 0.17 cm^2) immersed in a deoxygenated aqueous solution containing 3 % NaCl + 10 mM NaOAc. Rotation rates 0 and 1600 rpm. Potential scan rate 5 mV s^{-1}. Temperature 298 K and 333 K.*

In order to estimate the influence of acetic acid and carbon dioxide on the X65 carbon steel specimen, the same experiments were repeated with a deoxygenated aqueous solution containing 3 % NaCl and 10 mM NaOAc + HOAc (by addition of an aliquot of 1 M acetic acid), and a solution containing 3 % NaCl and 10 mM NaOAc saturated with carbon dioxide. Figure 5.23 shows polarization curves recorded at the X65 carbon steel electrode for a deoxygenated aqueous solution containing 3% NaCl + 10 mM NaOAc + 2.2 mM HOAc, pH 5.18, at 298 K and 333 K using rotation rates of 0 and 1600 rpm.

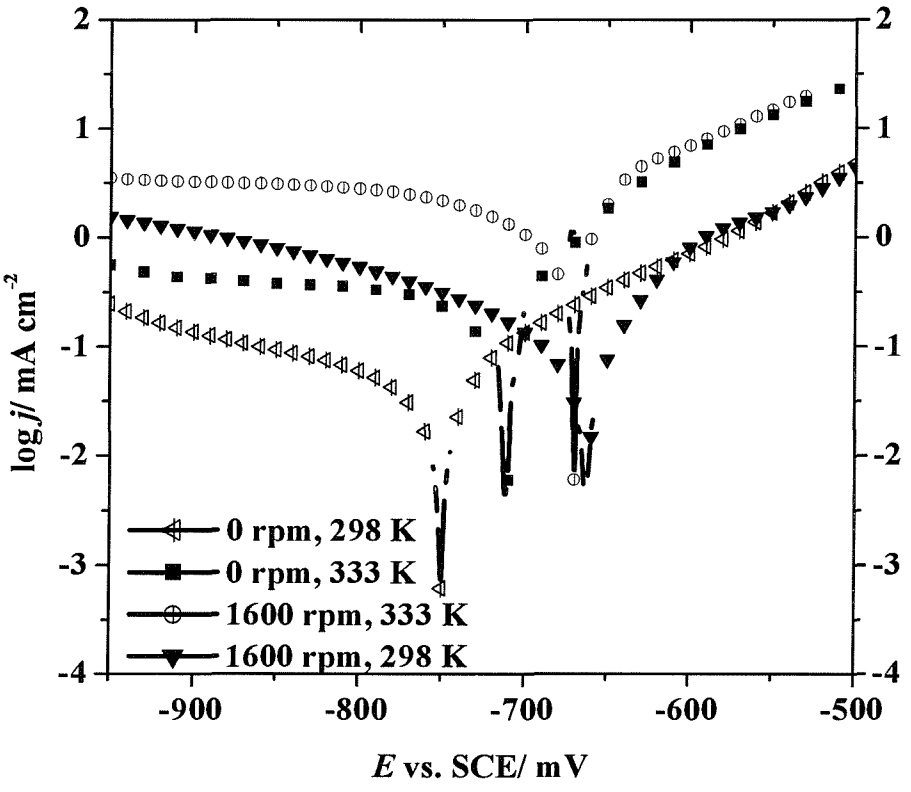

Figure 5. 23 *Tafel polarization curves recorded for a X65 carbon steel immersed in a deoxygenated aqueous solution containing 3 % NaCl + 10 mM NaOAc + 2.2 mM HOAc, pH 5.18. Temperature 298 K and 333 K. Rotation rates 0 and 1600 rpm.*

The polarization behavior of the X65 carbon steel specimen is shown at the lowest curve in figure 5.23, for the lowest temperature (298 K) and rotation rate (0 rpm) indicative of the smallest j_{corr}. As shown in figure 5.23, the effect of temperature and rotation rate on the steel corrosion is very pronounced. The overall

shapes of the polarization curves are consistent with those measured by Gray et al. [109]. Increasing the rotation rate of the disc electrode also had a considerable effect on the cathodic branch of the curve, by displacing it to the highest current density. The most pronounced effect of the temperature increase is the displacement of both the anodic and cathodic lines towards higher current density. However, it can be seen for all curves that at high cathodic potentials, the cathodic branch of the curve does not exhibit a clear Tafel line, the current densities clearly appear to be significantly limited.

Figure 5.24 reports typical polarization plots for a X65 carbon steel specimen immersed in a solution containing 3 % NaCl + 10 mM NaOAc saturated with carbon dioxide at 298 K and 333 K, using rotation rates of 0 and 1600 rpm.

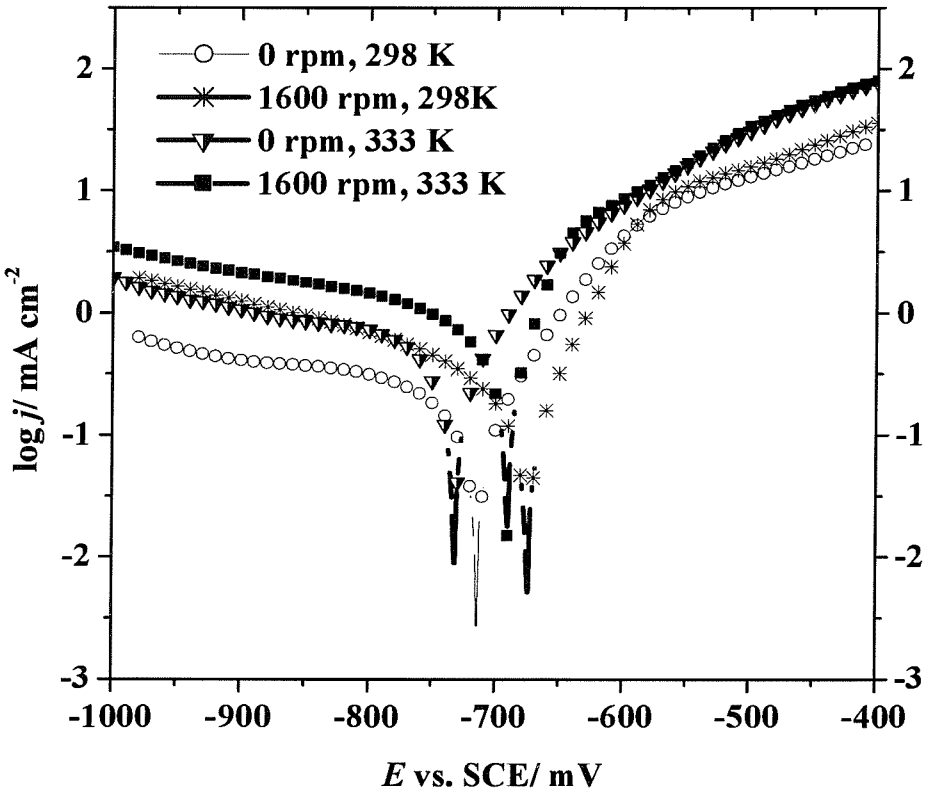

Figure 5. 24 *Tafel polarization curves for a X65 carbon steel electrode immersed in an aqueous solution containing 3 % NaCl + 10 mM NaOAc, saturated with CO_2, pH 5.03 and 5.26 respectively (after CO_2 saturation) recorded at rotation rates of 0 and 1600 rpm. Temperature 298 K and 333 K.*

In all cases, the polarization curves shown in figure 5.24 have the same key features as described above. Figure 5.24, again provides compelling evidence that with increasing the rotation rate of disc electrode and the temperature of the brine, the cathodic branch of the polarization curves is displaced towards higher current densities. The same experiments were repeated using 3 % NaCl brines but containing 1 mM and 100 mM NaOAc. Figure 5.25 shows polarization curves recorded at the X65 carbon steel electrode for solutions of 1 mM and 100 mM NaOAc + 3 % NaCl, saturated with carbon dioxide at 298 K and using rotation rates of 0 and 1600 rpm.

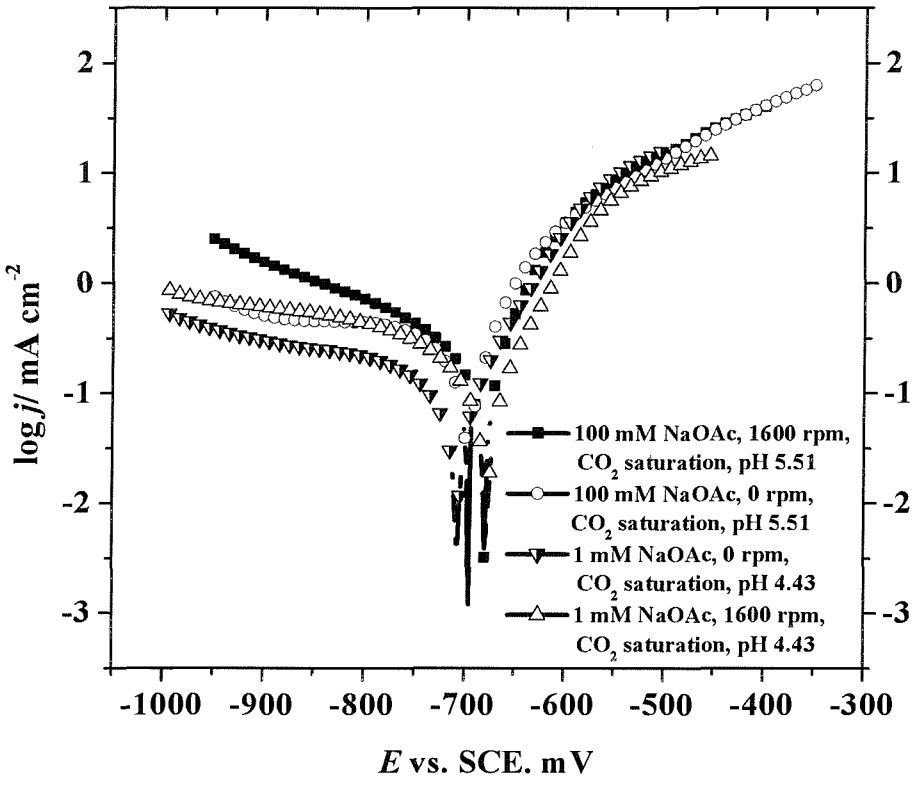

Figure 5. 25 *Tafel polarization curves recorded for a X65 carbon steel electrode in solutions containing 3% NaCl + NaOAc (concentrations and pHs shown on figure) saturated with carbon dioxide at 298 K. Rotation rate 0 and 1600 rpm.*

Once again, the polarization curves shown in figure 5.25 remains very similar to those described earlier in figure 5.23 and 5.24. As shown in chapter three, it is to be expected that saturation of the brine containing NaOAc with CO_2 will lead to the formation of acetic acid, and in the view of the similarity between figure 5.24 and

figure 5.25 with figure 5.23, there can be no doubt that the presence of acetic acid (either by direct addition or by saturating the acetate brine with CO_2) influences the cathodic branch of the polarization curves. Further, it can be seen for all the polarization curves, that the current densities are sensitive to the rotation rate of the disc electrode. Figure 5.26 compares the Tafel polarization curves for the X65 carbon steel rotating disc electrode (rotation rate 100 rpm) in a deoxygenated 3% NaCl brine containing different acetate and acetic concentrations but both with a pH of 4.90. Both polarization curves were recorded at a temperature of 333 K.

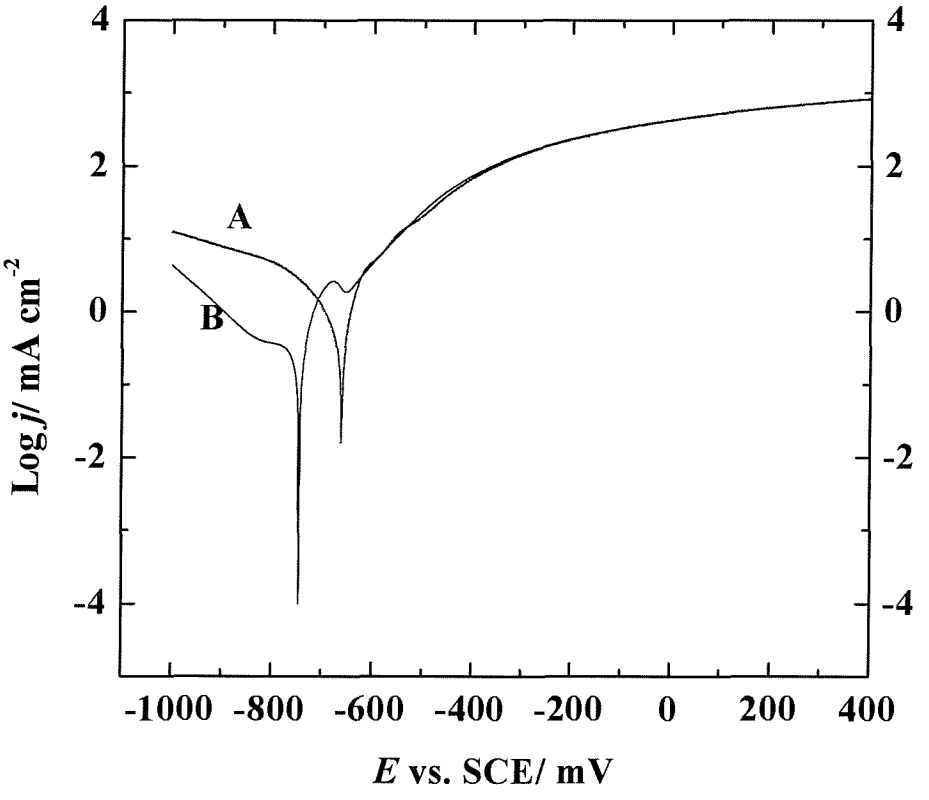

Figure 5. 26 *Tafel polarization plots for X65 carbon steel in 3 % NaCl + (A) 100 mM NaOAc and (B) 10 mM NaOAc adjusted to pH 4.90 with acetic acid. Temperature 333 K. Rotation rate 100 rpm.*

Despite the two solutions having the same concentration of free proton (same pH), the responses are clearly different with the most prominent features occurring at potential negative to the corrosion potential. It is clear that the partial cathodic current density increases substantially with the higher undissociated acetic

acid concentration present in solution for curve (A) in figure 5.26. It must therefore be concluded that the cathodic reaction has a major role on the corrosion rate of the X65 carbon steel specimen.

5.5.2 Linear polarization resistance measurements

Corrosion potentials and corrosion current densities were determined using the Linear Polarization Resistance (LPR) technique for a large number of solutions as both, a function of temperature and rotation rate of the X65 carbon steel rotating disc electrode. Corrosion potentials were also checked by direct measurement with a Digital Voltmeter (DVM). Current vs. potential data were collected using a linear potential scan from 300 mV negative to 300 mV positive to the corrosion potential The data between ± 10 mV was used for the linear analysis. The corrosion current density was estimated using the Stern – Geary equation:

$$j_{corr} = \left[\frac{\beta_a \beta_c}{2.3(\beta_a + \beta_c)}\right]\frac{\Delta j}{\Delta E} \qquad (5\text{-}1)$$

where $\frac{\Delta j}{\Delta E}$ is the slope of the graph (see figure 5.27), β_a and β_c are the anodic and cathodic Tafel slopes. As in the paper by Hedges et al. [42] and in line with general practice in corrosion laboratories in the oil and gas industry, the Tafel slopes for hydrogen evolution and iron dissolution were taken as 120 mV and 60 mV respectively. Typical sets of data are shown in figure 5.27.

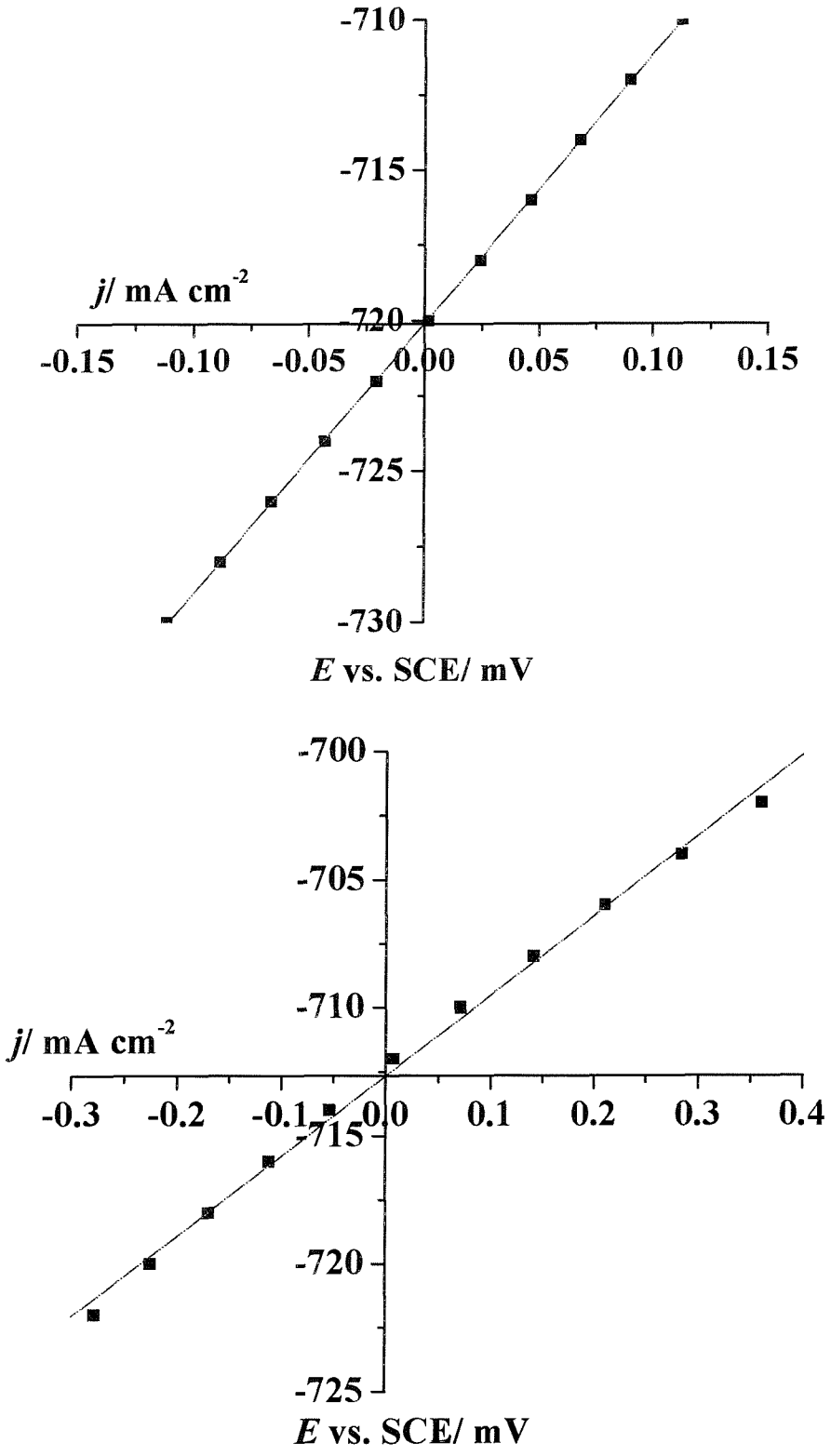

Figure 5. 27 *Linear polarization plots for X65 carbon steel in 3 % NaCl brine + (A) 100 mM NaOAc + 5 mM HOAc and (B) 10 mM NaOAc saturated with CO_2. Temperature 333 K.*

Table 5.4 reports the corrosion potentials for the steel in 3 % NaCl brines with various additions of acetate and CO_2.

Initial Solution	Purge Gas	pH (at 298 K)	Corrosion Potential vs. SCE/ mV	
			298 K	333 K
3 % NaCl +100 mM NaOAc	N_2	7.60	-790	-785
3 % NaCl +100 mM NaOAc	CO_2	5.50	-680	-695
3 % NaCl +10 mM NaOAc	N_2	7.60	-765	-765
3 % NaCl +10 mM NaOAc	CO_2	5.01	-680	-685
3 % NaCl +100 mM NaOAc + 1.5 mM HOAc	N_2	4.70	-680	-690
3 % NaCl +100 mM NaOAc	CO_2	4.43	-680	-685

Table 5. 3 *Corrosion potentials for the X65 carbon steel in 3 % NaCl brines with various additions of acetate and CO_2.*

It can be seen that the addition of acetic acid to the solutions, either by direct addition or by passing CO_2 through an acetate solution, led to a positive shift in the corrosion potential by approximately 100 mV. The presence of CO_2 in the absence of acetate does not lead to a marked change in the value of the corrosion potential for the steel in 3 % NaCl. The corrosion potentials were also not particularly sensitive to the temperature or the concentration of acetic acid (at least, over the range 1 – 10 mM). When acetic acid is present in the solution, however, the corrosion potential does shift positive with increasing rotation rate. This is compatible with an increase in the cathodic partial current with enhanced mass transport at the corrosion potential.

To quantify further the influence of acetic acid on the rate of corrosion of the X65 carbon steel at 333 K, corrosion current densities were determined for a solution containing 3 % NaCl + 10 mM NaOAc with various additions of acetic acid.

Two sets of results obtained with a stationary disc (0 rpm) and a disc rotating at 1600 rpm are reported in figure 5.28.

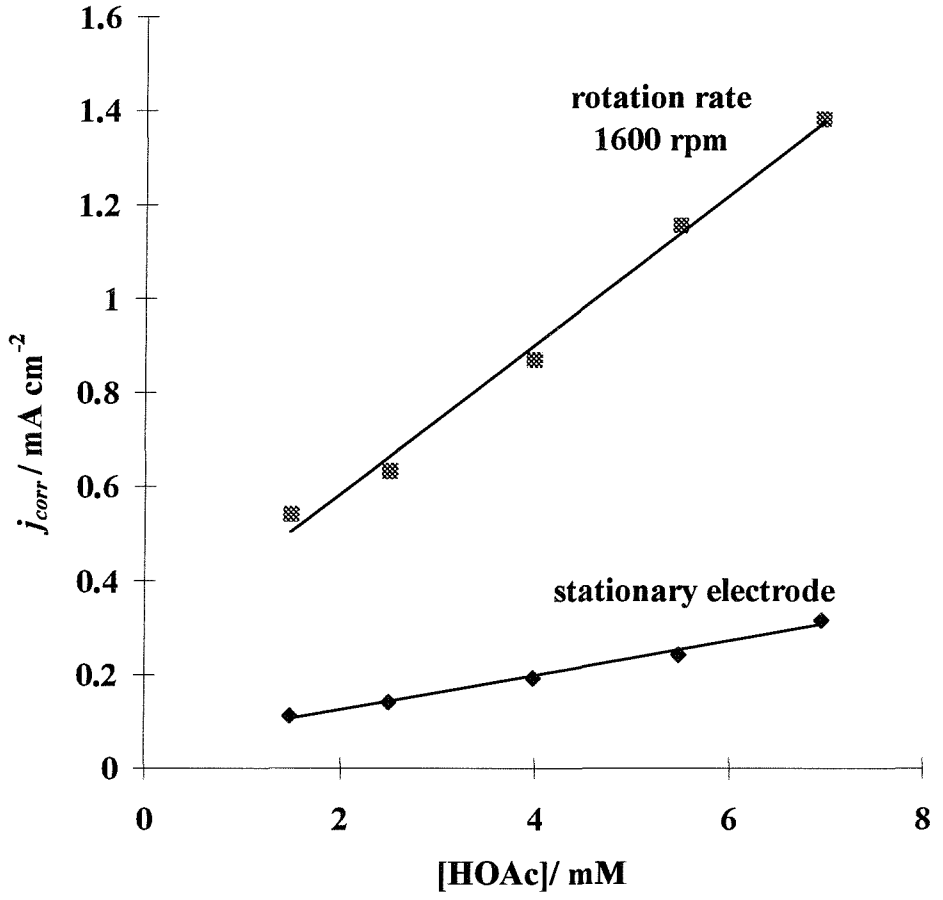

Figure 5. 28 *Corrosion current densities for X65 carbon steels as a function of acetic acid in 3 % NaCl + 10 mM NaOAc. Temperature 333 K. Rotation rates shown on figure.*

It can clearly be seen that the corrosion current densities increase with increasing acetic acid concentration, and, indeed, the dependence is linear. Of course, the positive intercept on the y-axis confirms that some corrosion will still occur in the absence of acetic acid. The figure again demonstrates conclusively that the mass transport regime is a further parameter influencing the corrosion rate of the carbon steel. Additional experiments confirmed that the corrosion current densities are a strong function of temperature (for example, with 2.5 mM acetic acid and a rotation rate of 1600 rpm, the corrosion current densities are 0.09 mA cm^{-2} and

0.63 mA cm^{-2} at 298 K and 333 K. It is helpful to note that a corrosion current density of 1 mA cm^{-2} is equivalent to a metal loss rate of 11.6 mm/year. It should be also noted that the corrosion current densities reported here must be regarded as "initial corrosion rates" since, in their determination, every effort has been made to minimize the formation of a corrosion film prior to the measurement.

The corrosion current densities were also determined in brine containing different concentrations of sodium acetate and saturated with carbon dioxide. The results, together with the corrosion potentials and the speciation calculation within the brine (as calculated by the computer software PHREEQC 2.2) are reported in table 5.4.

Initial [NaOAc]/ mM	**Equilibrium speciation**		E_{corr}/ **mV vs. SCE**	j_{corr}/ **mA cm^{-2}**
	$[H^+]$/ μM	**[HOAc]/ mM**		
1	30	0.46	-692	0.40
10	8	1.9	-689	0.44
40	4	4.0	-686	0.77
70	3	5.4	-697	1.03
100	2.5	6.5	-701	1.33

Table 5. 4 *Corrosion potentials and current densities for X65 carbon steel as a function of sodium acetate concentration. Brines contain 3 % NaCl + saturated with CO_2. Temperature 333 K. Rotation rate 1600 rpm.*

In all cases, the concentration of proton donor, the undissociated acetic acid, is much greater than that of free proton. The corrosion potential does not change markedly but with increasing acetate concentration, the corrosion current density increases substantially despite the steady decrease in the proton concentration (increase in pH). This can be readily understood when the corrosion current density is plotted versus the equilibrium concentration of acetic acid as has been done in figure 5.29. A linear dependence is obtained and, indeed, figure 5.29 looks remarkably similar to figure 5.28. There can be no doubt that the corrosion rate is

largely determined by the concentration of the proton donor, the undissociated acetic acid.

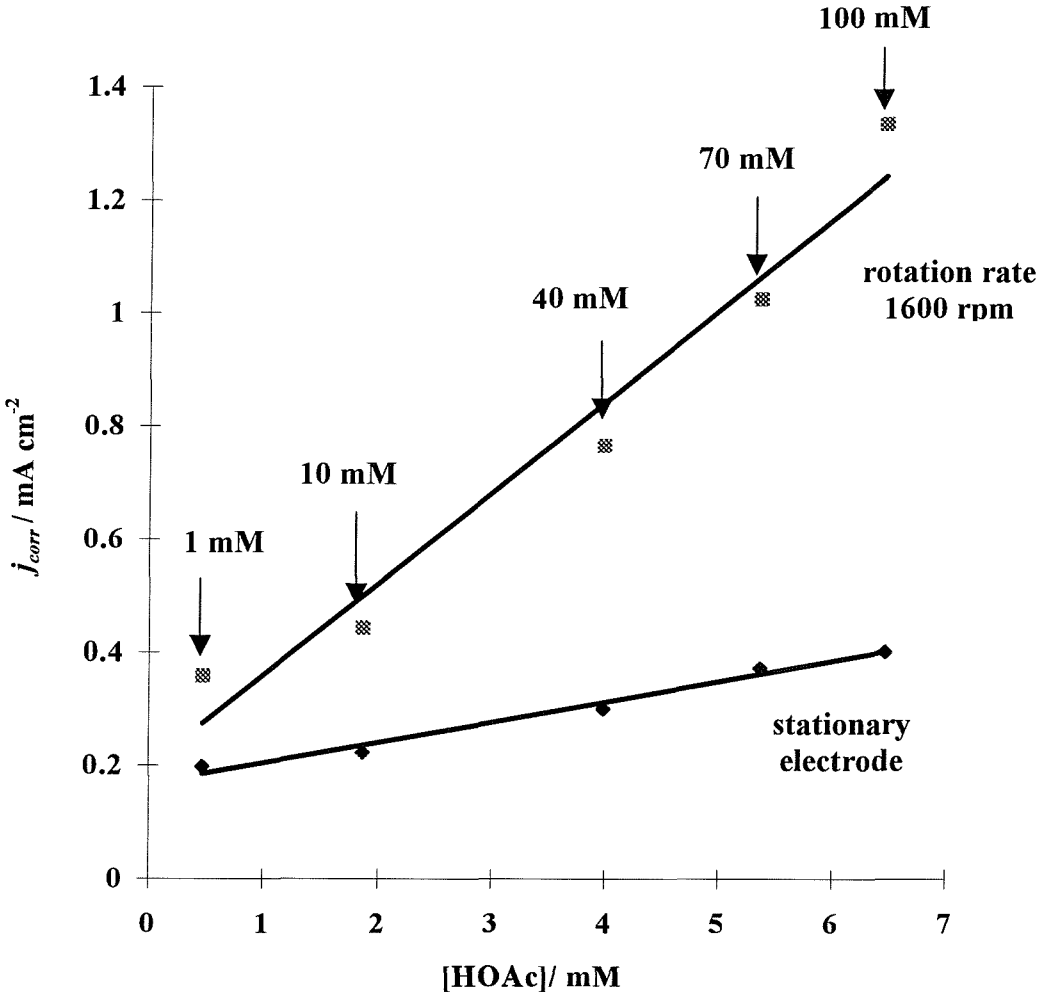

Figure 5. 29 *Corrosion current densities for X65 carbon steels as a function of acetic acid concentration in 3 % NaCl brine + NaOAc, saturated with CO_2. The total acetate concentrations are shown on the figure. Temperature 333 K.*

Table 5.5 compares the corrosion rates recorded by Hedges et al. [42] for a X65 carbon steel specimen in a 3 % NaCl brine solution, saturated with CO_2 at 333 K where an aliquot of sodium acetate has been added and the corrosion rates recorded during this work for a X65 carbon steel electrode in 3 % NaCl brine solutions containing 10 and 100 mM NaOAc, saturated with CO_2 at 333K.

Hedges et al.		This work		
[NaOAc]/ ppm	**Corrosion rate/ mm year^{-1}**	**[NaOAc]/ ppm**	**Corrosion rate/ mm year^{-1}**	
			0 rpm	1600 rpm
500	7.94	600	2.58	5.12
5000	6.60	6000	4.65	15.45

Table 5. 5 *Corrosion rates recorded for X65 carbon steel electrode in 3 % NaCl brines containing different concentrations of sodium acetate (shown in table) saturated with CO_2 by Hedges et al. and during this work.*

In all data during this programme, as the concentration of sodium acetate increases so does the corrosion rate. Further, the corrosion rates obtained during this work are of the same order of magnitude to those reported by Hedges et al [42]. However, they are not identical. This difference may arise because the experimental conditions for both works are different. For the experiments done by Hedges et al. [42] a stirred "becker cell" and a stationary electrode were used. The corrosion rate was determined by linear resistance polarization (LPR), after the electrode has been allowed to corrode for about one hour. In our case, the solution was stirred more efficiently using the steel rotating disc electrode. Also the electrode was not allowed to corrode prior to recording the voltammogram. Further, the electrode surface was removed from solution immediately after the voltammogram was recorded. The surface was then polished between each scan.

5.6 SEM Results

The purpose of this section is to investigate how the surface morphology of the X65 carbon steel is affected by the presence of acetate ions in the simulated brine saturated with CO_2. After surface pretreatment (see Chapter Two, page 2-6), the X65 carbon steel specimens were immediately immersed into the glass cell. In order to obtain a representative set of analyses a minimum of three corroded surfaces were analysed in each condition. Three different immersion times were investigated

1 hour, 24 hours and 1 week in different environmental conditions. Figure 5.30 reports the picture of a freshly polished X65 carbon steel surface.

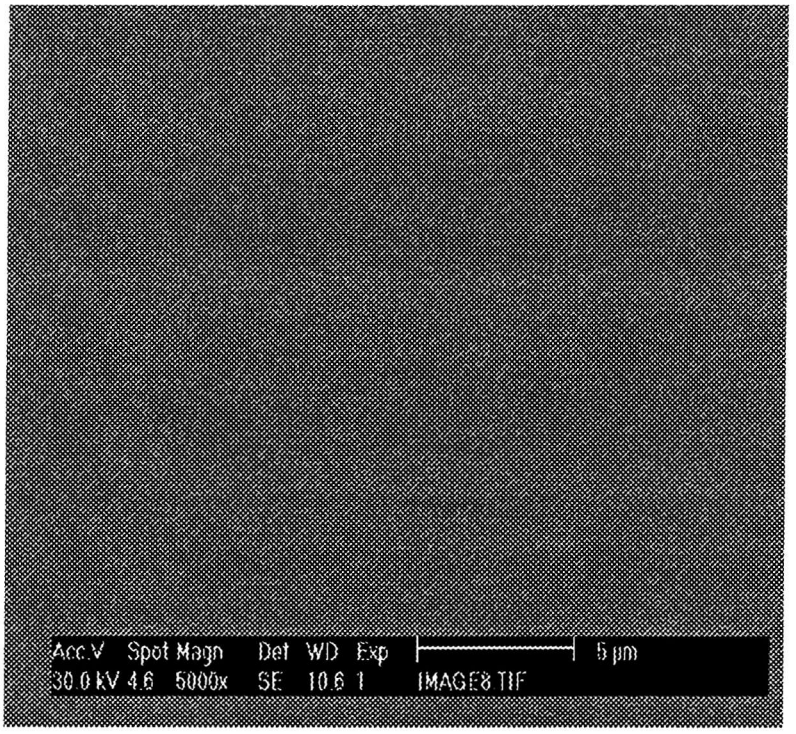

Figure 5. 30 *An SEM picture of a freshly polished X65 carbon steel surface, x5000.*

With a magnification of 5000, the surface appears totally flat and smooth; no traces of scratches are clearly visible. It should be noted that all SEM experiments were carried out at 333 K (as oilfield). As outlined in the experimental section, extensive precautions were taken to ensure that O_2 did not interfere. The presence of O_2 in solution can be recognized because Fe (II), the product of corrosion is oxidised homogenously to Fe (III) and this is yellow. The period between the termination of the corrosion procedure and obtaining the SEM was typically 1 hour.

5.6.1 X65 carbon steel immersed in 3 % NaCl

Figure 5.31 reports a typical view of a corroded steel surface obtained after 1 hour of exposure in a 3% NaCl brine saturated with CO_2 at 333 K.

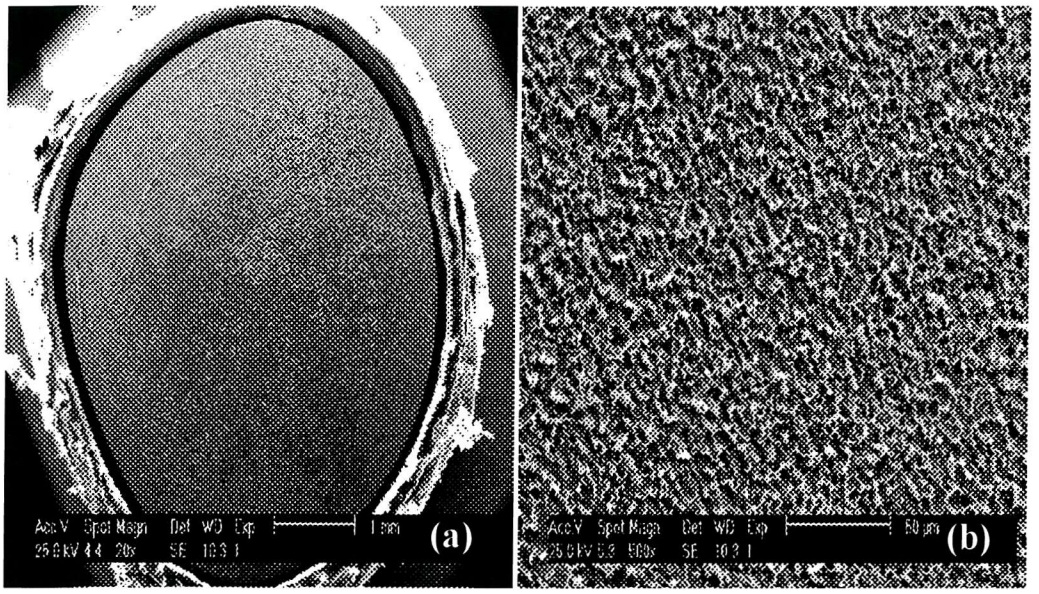

Figure 5. 31 *SEM pictures of a steel surface exposed to 3 % NaCl and saturated with CO_2 at 333 K. Exposure time 1hour, (a) x20 and (b) x500.*

After 1 hour exposure, the original surface is clearly different. A uniform corrosion film can be seen on the steel surface even at magnification 20. The smooth surface seen in figure 5.30 has completely disappeared. Rather, the electrode surface appears to be porous as shown in figure 5.31 (b) at higher magnification. Figure 5.32 illustrates a SEM picture taken for the same sample but a higher magnification.

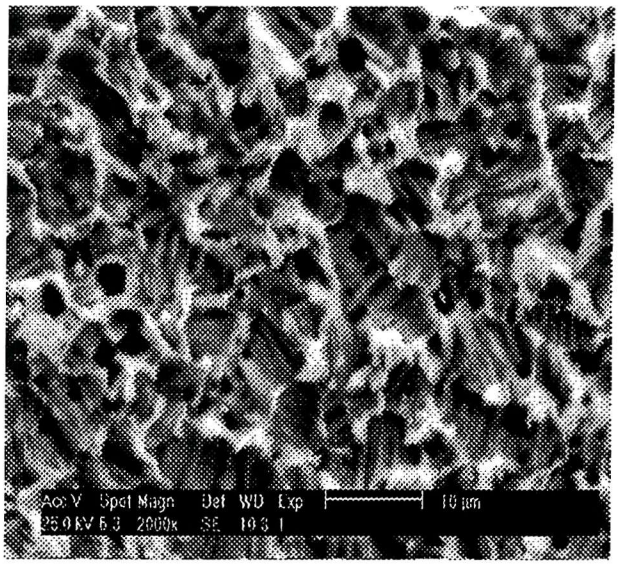

Figure 5. 32 *SEM pictures of a carbon steel surface exposed to 3 % NaCl and saturated with CO_2 at 333 K. Time exposure 1hour, x2000.*

There is no evidence of grain boundary features or pitting corrosion. Indeed, the film is porous and rather structureless. The same experiment was repeated but the steel specimens were left in the solution for 24 hours. The SEM pictures obtained were very similar to those shown above. A uniform corrosion film was clearly visible on the steel surface but no structure, or corrosion pitting was observed. Figure 5.33 reports, typical SEM pictures recorded for corroded steel surface after 24 hours exposure in the 3 % NaCl brine saturated with CO_2 at 333 K.

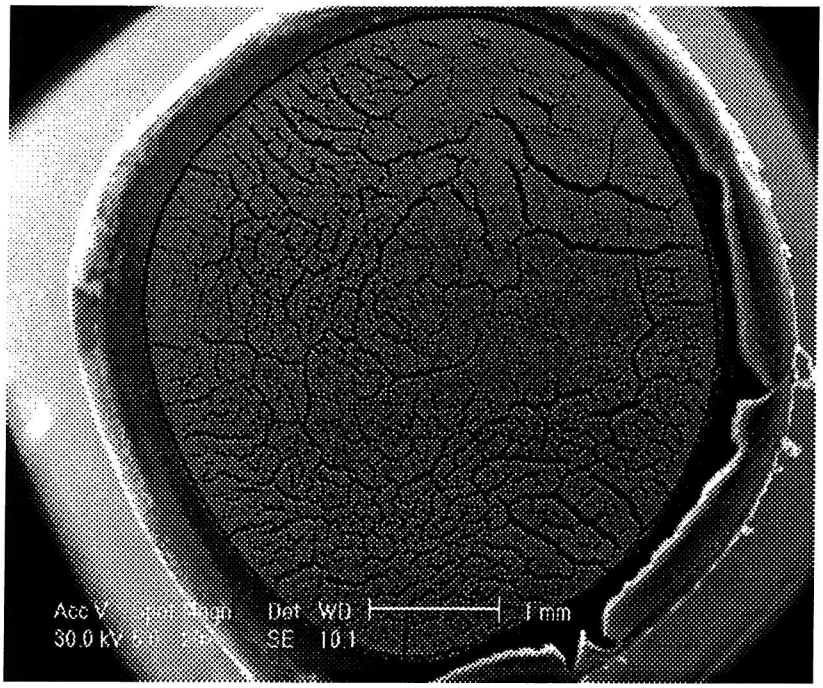

Figure 5. 33 *SEM pictures of a steel surface exposed to 3 % NaCl and saturated with CO_2 1 at 333 K. Exposure time 24 hours, x20.*

After 24 hours of exposure in the brine solution, once again a uniform film can be seen on the surface of the steel electrode. It is thicker and cracks are also visible and these are thought to result from the drying of the steel surface within the SEM. More detailed pictures of the steel surface were taken, and some of these pictures are illustrated in figure 5.34.

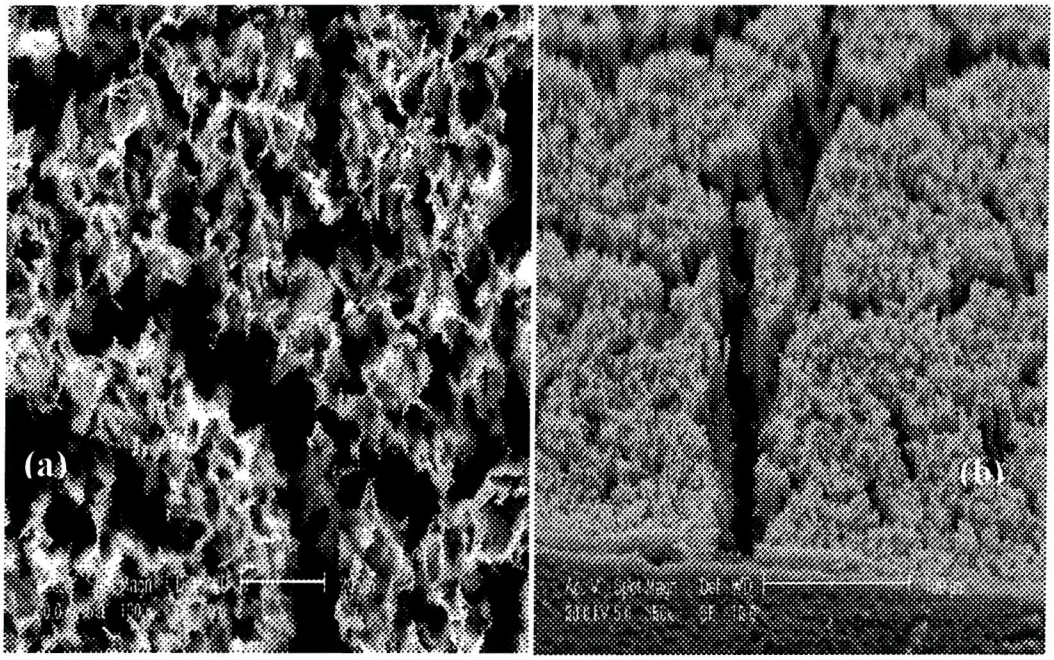

Figure 5. 34 *SEM pictures of a steel surface exposed to 3 % NaCl and saturated with CO_2 at 333 K. Exposure time 1 week, (a) x1000 and (b) x350, 70°.*

Once again the picture shown in figure 5.34 (a) remains very similar to the one in figure 5.32. The corrosion film appears to be relatively thick and very porous. It is also rather structureless and lacks special features. The results obtained were compared with work carried out by Maguire [156]. In her thesis, SEM pictures obtained for mild steel in 3 % NaCl saturated with CO_2 at 328 K were presented. The steel specimens were exposed in the brine solution for 24 hours and 1 week.

Despite the surface preparation being exactly the same for both sets of work, the SEM pictures presented by Maguire were clearly different. After 24 hours of exposure, the steel surface texture was dominated by well-shaped cubic structures set in a finer grained matrix. After 1 week, the corrosion layer was composed of two layers, a fibrous layer and cubic structures, and the density of the cubes increase. The reasons for such differences in the response obtained during this work are not defined. However, we believe that the steel microstructure and composition play an important role on the formation of corrosion film and indeed the composition of the

steel used by Maguire may be different to the one used during this work. Maguire was also using SEM located away from the laboratory and there were extended periods between the test and the SEM examination.

5.6.2 X65 carbon steel immersed in 3 % NaCl + 10 mM NaOAc

In order to investigate the influence of acetate ion and carbon dioxide on the corrosion film, experiments were carried out using the X65 carbon steel in 3 % NaCl + 10 mM NaOAc, saturated with CO_2 at 333 K. The electrolyte was saturated with CO_2 for 1 hour prior to immersion of the carbon steel into the vessel. A CO_2 gas stream was kept into the vessel during all the time. Figure 5.35 reports typical SEM pictures for X65 carbon steel specimens in such medium after 1hour exposure.

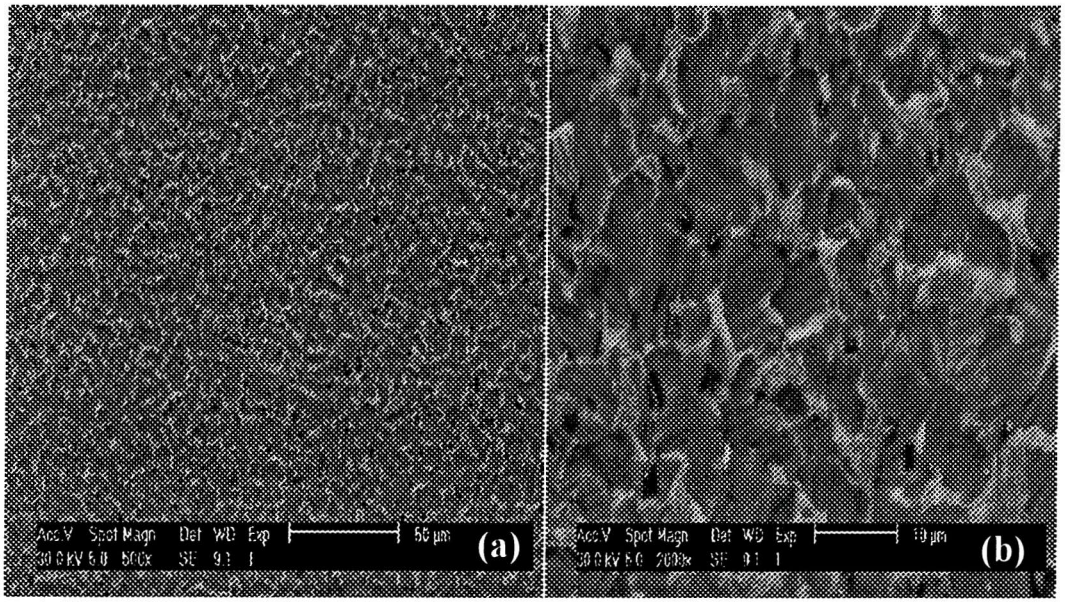

Figure 5. 35 *SEM pictures of a steel surface exposed to 3 % NaCl and saturated with CO_2 at 333 K. Exposure time 1 hour, (a) x500 and (b) x2000.*

Once again, a uniform corrosion film can be observed on the steel surface, and the similarity of figure 5.35 (b) with figure 5.32 is striking. No cubic structure or corrosion pitting is seen on the picture. The presence of acetate does not seem to change the corrosion film markedly. The experiment was repeated for longer period of exposure, 24 hours and 1 week .The responses obtained remain very similar to the

one described above, and figure 5.36 resumes some of the pictures obtained for these specific conditions.

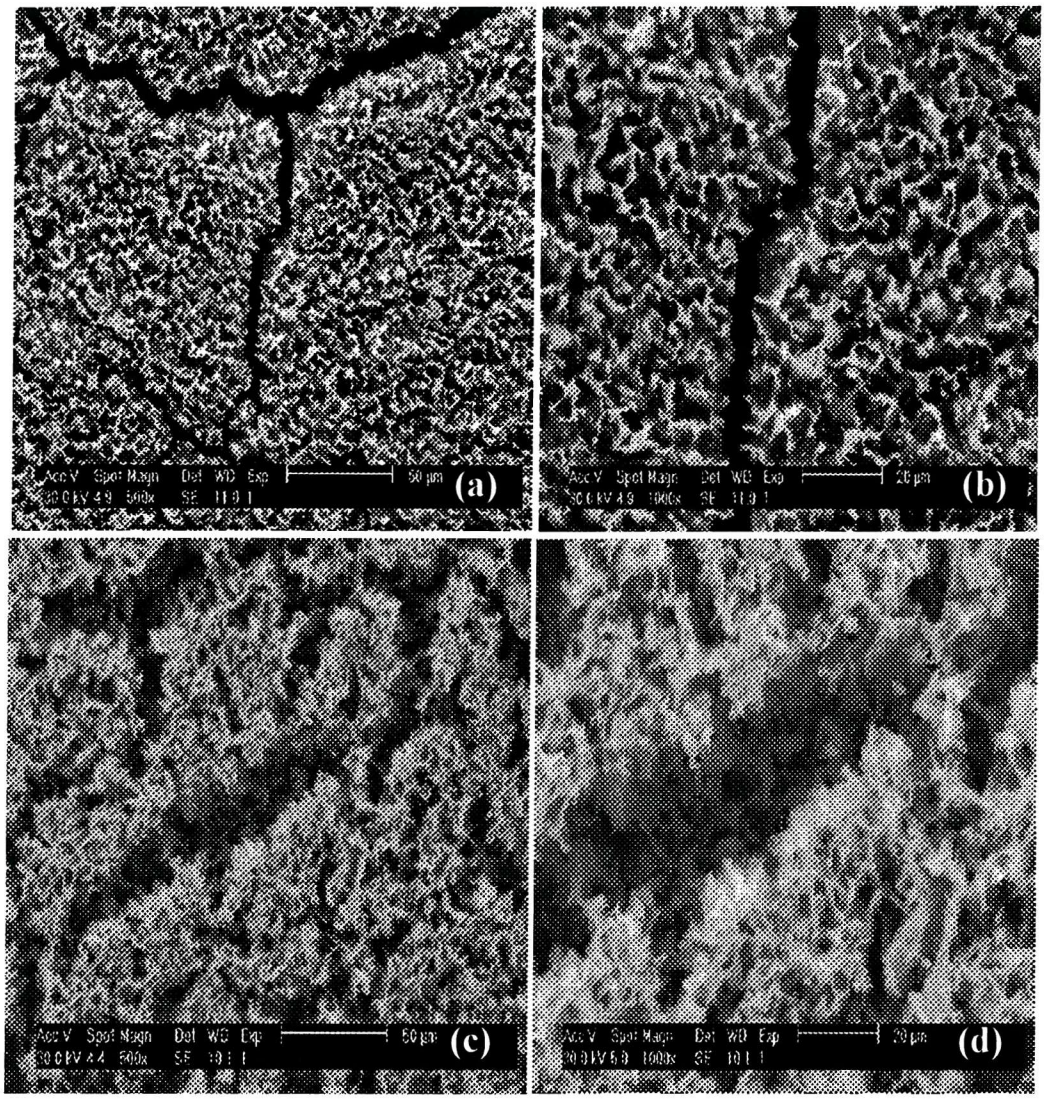

Figure 5. 36 *SEM pictures for a steel surface exposed in 3 % NaCl + 10 mM NaOAc saturated with CO_2 at 333 K for (a) & (b) 24 hours and (c) & (d) 1 week exposure. (a) & (c), x500, (b) & (d), x1000.*

5.6.3 X65 carbon steel immersed in 3 % NaCl + 10 mM NaOAc + 24.4 mM HOAc

The influence of acetic acid on the carbon steel surface was also investigated. Figure 5.37 reports SEM pictures recorded for a X65 carbon steel in a deoxygenated simulated brine (with N_2) solution containing 3 % NaCl + 10 mM NaOAc +

24.4 mM HOAc at 333 K after a week exposure. From figure 5.37, it can be seen that the flat surface (see figure 5.30) has completely disappeared. Rather, a thick uniform corrosion film can be observed on the entire surface on the X65 carbon steel surface. Further, deep cracks are also clearly visible, and those are thought to result from the drying process. Once again, no cubic structures or pitting corrosion or crystal structure is observed.

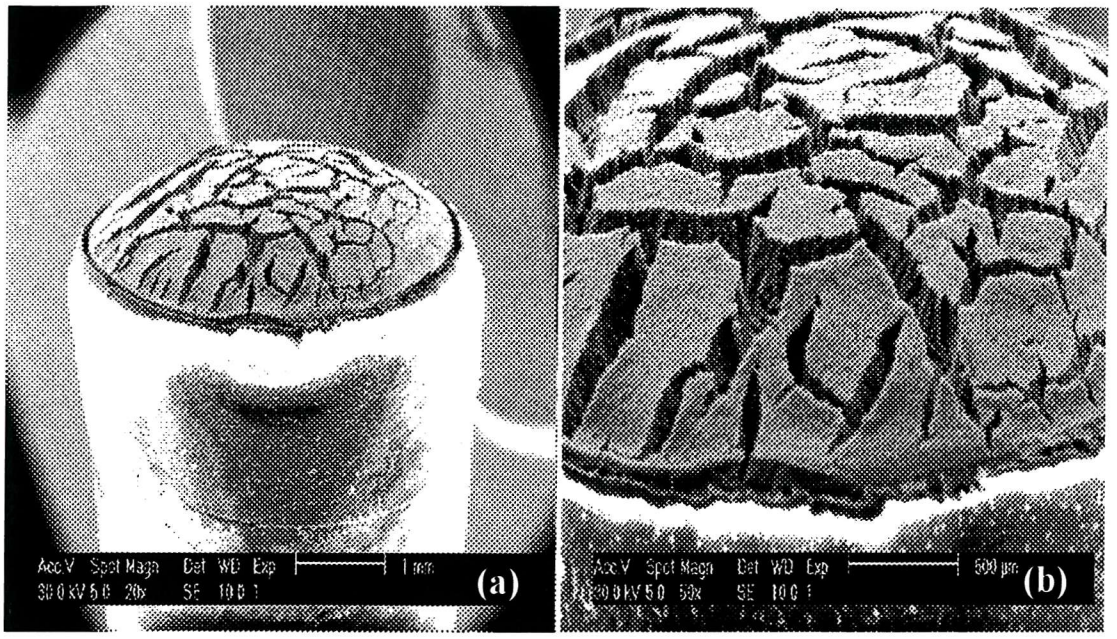

Figure 5. 37 *SEM pictures for X65 steel surface exposed in a simulated brine solution containing 3 % NaCl + 10 mM NaOAc + 24.4 mM HOAc (solution deoxygenated using N_2) at 333 K after 1 week exposure. (a) x20 and (b) x50.*

More detailed pictures of the sample in this simulated brine are presented in figure 5.38.

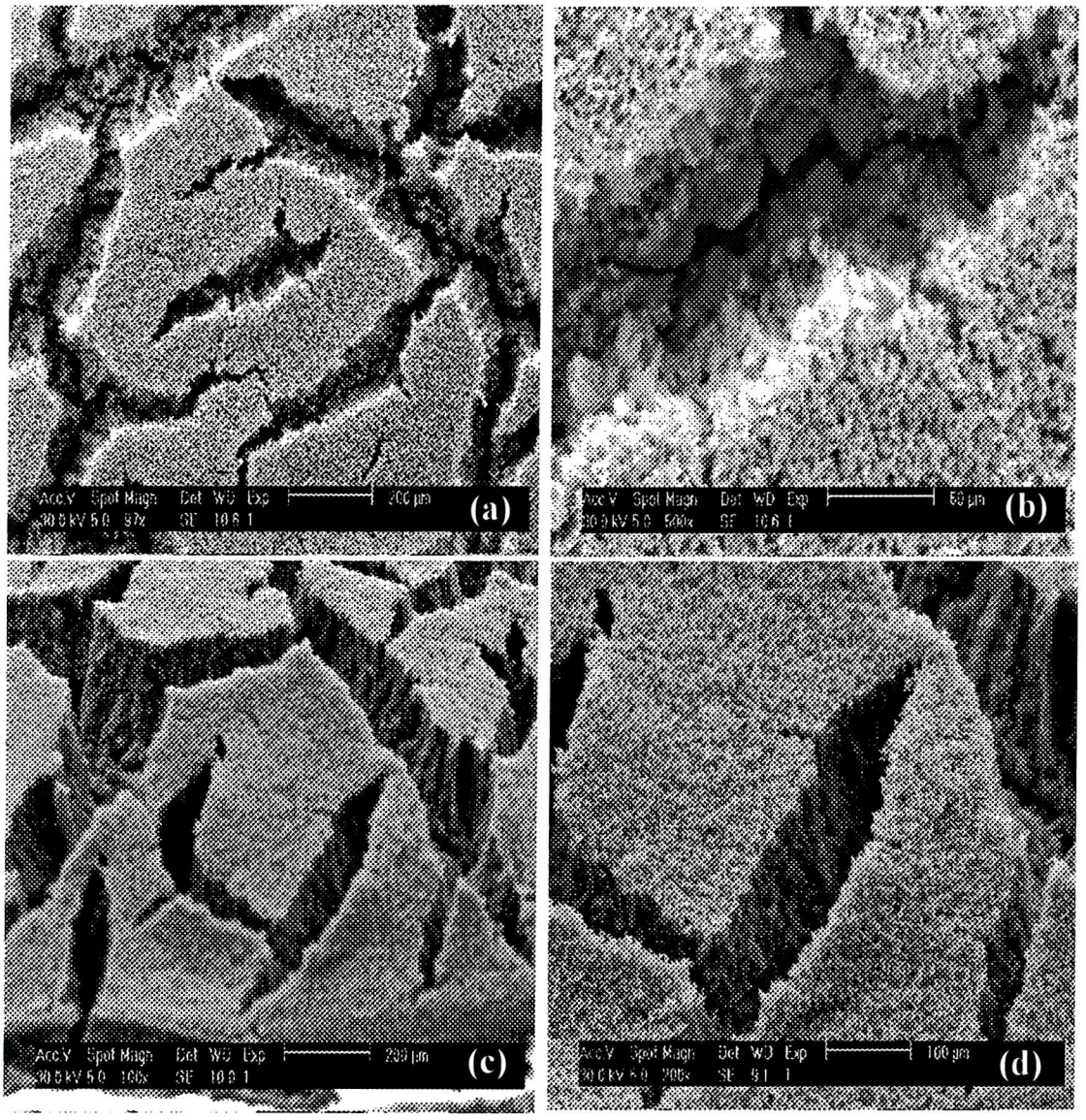

Figure 5. 38 *SEM pictures for a steel surface exposed in simulated brine containing 3 % NaCl + 10 mM NaOAc + 24.4 mM HOAc (deoxygenated with N_2) at 333 K for 1week exposure. (a) & (b) flat pictures and (c) & (d) 70°. (a) x100, (b) x500, (c) x100 and (d) x200.*

5.7 Conclusions

Before summarizing our conclusions, we would reiterate that the experiments have, as far as possible, been carried out with steel surfaces that are free from corrosion films. In consequence, while we believe that the results provide a valuable background to assist the interpretation of oilfield pipeline corrosion, it is important to

stress that we would not expect to obtain identical data at surfaces with extensive corrosion films and this is clearly the steady state situation within the working pipelines.

A steel specimen in a neutral environment corrodes with water reduction as the cathodic reaction. The increase in corrosion rate for the steels in CO_2 saturated brine or brine with acetic acid additions indicates that the cathodic reaction is not solely due to the reduction of water or free protons. There must be another source of reducible species present to account for the increased cathodic current density. The most readily reduced species in the solution other than the free protons and water molecules is acetic acid. The mechanism of acetic acid reduction at steel is essentially similar to that at platinum. The voltammetry therefore allows a thorough understanding of the way in which acetate influences the rate of steel corrosion in 3 % NaCl/saturated CO_2 solutions.

We believe that when steel is in a medium containing acetate and carbon dioxide, the dominant cathodic reaction in the corrosion process is

$$HOAc + e^- \rightleftharpoons \tfrac{1}{2} H_2 + OAc^- \qquad (4)$$

Certainly, at the corrosion film free surface, it has been demonstrated conclusively that the electrode cannot distinguish between proton and undissociated acetic acid because of the rapid dissociation of acetic acid at the surface. Moreover, in the media of interest, the concentration of acetic acid is much higher than that of free protons. The rate of corrosion is essentially determined by the concentration of acetic acid (eg. see figures 5.28 and 5.29). The shift in corrosion potential resulting from the presence of acetic acid (see table 5.3) and the form of the Tafel plots (see figure 5.23 to 5.26) provide further evidence to support this conclusion. We also believe that the major role of CO_2 in this chemistry is only to change the speciation by changing the pH. As noted in Chapter Three, acetic acid is the dominant weak acid because the equilibrium concentration of carbonic acid is low, and the interconversion of carbon

dioxide to carbonic acid is slow. The contribution of carbonic acid reduction to the partial cathodic current density at the corrosion potential will be much less than the contribution from the reduction of acetic acid.

In order to understand the system, we stress the importance in knowing accurately the speciation of the critical species in the brine and this requires software to deal with the several interacting equilibria and the non-ideality of the ions in the brine media. An important caveat must be that the corrosion film resulting from more extended contact of the steel with the solution may well be different in the presence of bicarbonate/carbonic acid. On the other hand, this does not negate the fact that the CO_2 will continue to have a determining role in the speciation within the solution and the solution chemistry will be critical to the corrosion rate of the steel. We have also sought to highlight the importance of mass transport regime to the rate of corrosion and this effect will extend to the oilfield pipeline. The corrosion current densities and the corrosion potentials are also sensitive to the rotation rate of the disc electrode. All data is consistent with the rate of the cathodic reaction in the corrosion increasing with the rotation rate of the disc electrode. It should be stressed that the purpose of this work was to investigate the influence of solution composition on the mechanism of steel corrosion in brines containing weak acids and saturated with carbon dioxide. This does not rule out the probability that carboxylate ions influence the corrosion process in other ways. Thus, for example, it is to be expected that the acetate ion may also influence the iron dissolution rate by acting as a complexing agent for Fe (II); certainly the addition of acetate can be seen to influence anodic current for the dissolution of iron.

In this discussion we have stressed the role of direct reduction of acetic acid as explaining the corrosion behavior of the relatively film free surfaces. Also, the acetic acid in solution may influence the composition, structure and/or thickness of the corrosion film. In the different situation of a fully filmed surface, the concentration of acetic acid in the medium will still have a critical role in determining the rate of corrosion. Then, in addition to electron transfer one could

consider chemical reaction between the acetic acid and the corrosion film on the steel surface leading to film thinning. But again, in understanding such processes, it is critical to recognize that because of its rapid dissociation, the acetic acid in solution acts as a pool for either protons or acetate ions as they react at the corroding surface. No mechanism for steel corrosion in these brines can be correct unless it fully takes into account the solution speciation and also recognize that the surface chemistry will not distinguish free proton and acetic acid because the dissociation of acetic acid is rapid.

Low acetic acid concentration arising from simulated brine and CO_2 do not seem to change the film significantly. In all conditions, a uniform corrosion film is observed at the steel surface, and this film is porous and rather structureless. Further, there is no evidence of grain boundary features or pitting corrosion. However, the very high concentration of acetic acid (24.4 mM) certainly led to a thicker film but of similar appearance.

Chapter Six

6 Studies related to Oilfield conditions

6.1 Introduction

In some oilfields, including Wytch Farm on the South East of England and Trinidad in Central America, enhanced rates of corrosion are thought to result from the presence in the brine of the anion of weak acids particularly acetate ions. In Chapter Four, we reported the rates of corrosion of carbon steel (X65) in simulated brines containing 3 % NaCl and various concentration of sodium acetate (NaOAc), each saturated with carbon dioxide. It was demonstrated that the rate of corrosion could be understood in terms of the concentration of undissociated acetic acid formed when acetate containing brines were acidified by contact with carbon dioxide. Further, the speciation of the solutions was calculated and it was confirmed that the chemistry and electrochemistry (at both Pt and carbon steel) of the acetate/CO_2 solutions is identical to an acetate buffer of the same pH prepared by simple addition of acetic acid to aqueous sodium acetate. In laboratory simulated brines containing only NaCl and NaOAc saturated with CO_2, the pH and the concentration of acetic acid is a function only of the acetate concentration and hence there is a direct relationship between the corrosion rate and the acetate content of the simulated brine.

This chapter reports the extension of these studies to oilfield brines. Inevitably, such brines have a much more complex composition. They have different ionic strengths and contain an assortment of additional inorganic ions as well as organic contaminants. The former, particularly bicarbonate, may be expected to influence the pH of the solutions and hence the concentration of acetic acid while the latter could adsorb on the steel surface and thereby also influence the rate of corrosion. The

studies have employed brines from oilfields Wytch Farm (Oilfied A) and Trinidad (Oilfield B) oilfields.

In general, the speciation of the medium can influence the corrosion of the metal through either the composition of the film formed on the surface of the corroding metal or through the thermodynamics and kinetics of the anodic and/or cathodic reactions leading to corrosion. In the case of carbon steel, a dominant factor resulting from the presence of acetate and carbon dioxide is the formation of acetic acid. This leads to a change in the main cathodic reaction leading to corrosion from:

$$H^+ + e^- \longrightarrow \tfrac{1}{2}H_2 \qquad (1)$$

or

$$H_2O + e^- \longrightarrow \tfrac{1}{2}H_2 + OH^- \qquad (2)$$

or

$$H_2CO_3 + e^- \longrightarrow \tfrac{1}{2}H_2 + HCO_3^- \qquad (3)$$

to

$$HOAc + e^- \longrightarrow \tfrac{1}{2}H_2 + OAc^- \qquad (4)$$

Reaction (4) occurs by the mechanism where reaction (4) is followed by reaction (1):

$$HOAc \rightleftharpoons H^+ + OAc^- \qquad (5)$$

Reaction (5) is a rapid reaction and hence the hydrogen evolution reaction on a metal surface does not distinguish between free protons and undissociated acetic acid as reactants [123,124,126,130,134]. Moreover, in many of the brines containing acetate and carbon dioxide, the concentration of acetic acid is far higher than that of free proton and it is this that leads to an enhancement of the rate of corrosion by acetate.

6.2 The Oilfield Brines

Table 6.1 reports the analysis of 4 samples of brines taken at two oilfields in England and Trinidad. It can be immediately seen that the compositions are complex and using 3 % NaCl as a simulant is an oversimplification.

Oilfield	Acetate[#] /mM	Bicarbonate /mM	pH[‡]	Other Species/mM
A1	0.66	0.97	4.46	Na^+, 2750; Ca^{2+}, 101; K^+, 54; Mg^{2+}, 34; Sr^{2+} 1.3; Zn^{2+}, Cu^{2+}, Fe^{3+}, all < 0.1; Cl^-, 2997; SO_4^{2-}, 11; Br^-, 0.7.
A2[†]	0.78	1.50	4.60	Na^+, 2620; Ca^{2+}, 99; K^+, 53; Mg^{2+}, 36; Sr^{2+} 1.3; Zn^{2+}, Cu^{2+}, Fe^{3+}, all < 0.1; Cl^-, 2854; SO_4^{2-}, 13; Br^-, 0.7.
B1	11.0	13.5	5.70	Na^+, 366; Ca^{2+}, 4.2; K^+, 1.5; Mg^{2+}, 1; Zn^{2+}, Cu^{2+}, Fe^{3+}, all < 0.1; Cl^-, 342; SO_4^{2-}, 0.1; Br^-, 0.8.
B2	4.4	16.7	6.12	Na^+, 302; Ca^{2+}, 3; K^+, 1; Mg^{2+}, 2; Zn^{2+}, Cu^{2+}, Fe^{3+}, all < 0.1; Cl^-, 294; SO_4^{2-}, 0.3; Br^-, 0.8.

includes traces of other carboxylates.
‡ after resaturation with CO_2.
† contains corrosion inhibitor.

Table 6. 1 *Composition of four samples of brines at two oilfields sited at two different parts of the world.*

Firstly, it can be seen that the ionic strength of the brines differs appreciably. The brines from oilfield A (Wytch Farm Facility, Britain) contain ~ 16 % NaCl while those from oilfield B (Trinidad) ~ 2 %. Such differences have a significant influence on the speciation through the deviations of the solutions from ideality. Indeed, in very concentrated electrolytes, it is difficult to estimate the mean ionic activity coefficients and thereby calculate the concentrations of ionic species in the brine with a high degree of precision.

In this section, however, we wish to stress the influence of bicarbonate on the rate of corrosion of the steel. It can be seen that the brines in table 6.1 do contain bicarbonate. In our early modeling (see Chapter Three) the presence of bicarbonate

as an independent component in the brine was ignored. The solution composition was based on the presence only of 3 % NaCl, NaOAc and CO_2 and the only bicarbonate present was that resulting from the saturation of the brine with carbon dioxide. When bicarbonate is an independent constituent of the brine, its presence must be taken into account. This was attempted in a more qualitative way in section 3.4, see Chapter Three. It can be seen in table 6.1 with respect to the bicarbonate content, the two oilfields are quite different. Oilfield A has a low bicarbonate level (case (c) on page 3-17) and significant conversion of acetate to acetic acid will occur on contact with 1 atm CO_2. Oilfield B has a relatively high level of bicarbonate (case (b) on page 3-17) and the fractional conversion of acetate to acetic acid will be low. It should again be stressed that the bicarbonate level determines the pH of the CO_2 saturated solutions, see table 6.1.

6.3 Oilfield A

6.3.1 Voltammetry of Oilfield A at Pt rotating disc electrode

Two brines from different sampling points were investigated. As reported in table 6.1, both brines are relatively low in bicarbonate and, as expected, their pH dropped to ~ 4.5 when resaturated with CO_2. In addition, it should be noted that the total acetate concentrations are also relatively low compared to those employed in our earlier studies (see Chapter Four and Five). Figure 6.1 shows voltammograms recorded at 298 K for a Pt rotating disc electrode (area, 0.16 cm^2) in a sample of brine from the Wytch Farm oilfield A1 (a) when residual CO_2 and O_2 accumulated during handling and transportation had been removed with a stream of N_2 and (b) when the sample was resaturated with CO_2.

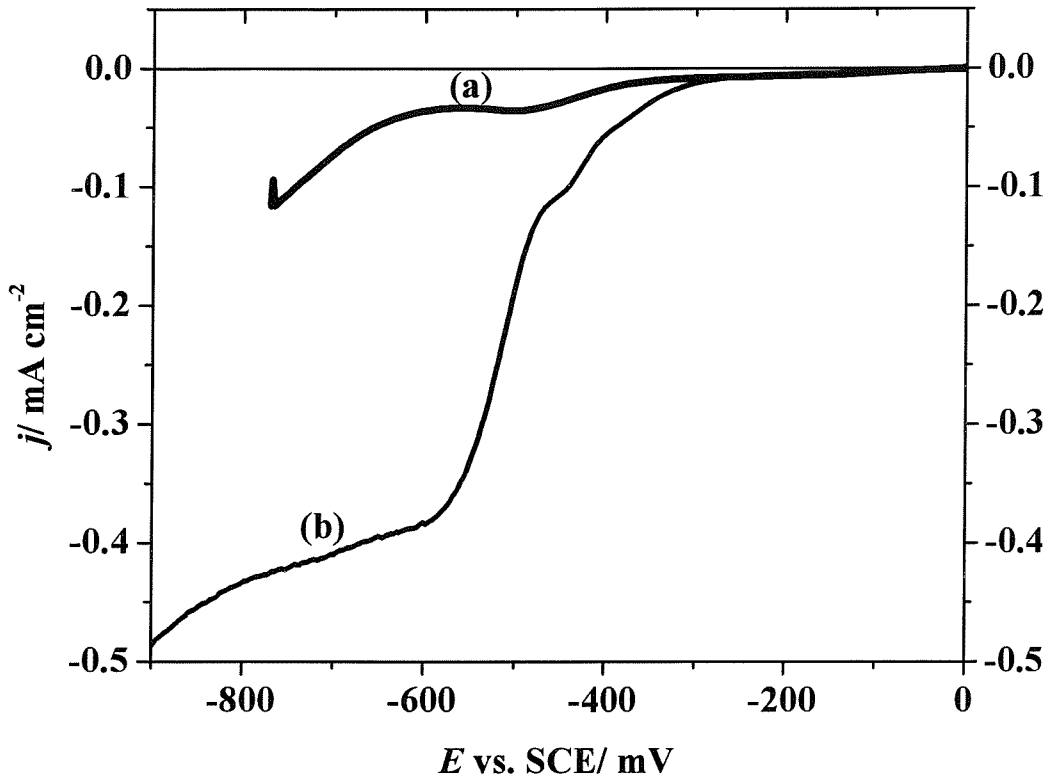

Figure 6. 1 *Voltammograms recorded at a precleaned Pt rotating disc electrode (area, 0.16 cm^2) for the brine sample A1 (a) N_2 saturated, pH 6.01, and (b) resaturated with CO_2, pH 4.46 at 298 K. Rotation rate 400 rpm.*

When fully degassed, the solution has a pH of 6.01 (there can be almost no carboxylic acids present) and the voltammogram shows only a small reduction wave at $E_{1/2}$ = - 470 mV versus SCE with a limiting current density of 0.036 mA cm^{-2}. The height of this wave is independent of the rotation rate of the Pt disc electrode. The origin of the wave is not known, but the oilfield brine inevitably contains a number of organic and inorganic impurities. When resaturated with CO_2, the pH drops to 4.46 and a well-formed reduction wave is seen at $E_{1/2}$ = -520 mV versus SCE. This is the potential where acetic acid reduction (and other organic acids with the same pK_A) is expected to occur.

In addition, this reduction wave increases in importance as the rotation rate of the Pt rotating disc electrode is increased, and in the plateau region negative to - 600 mV versus SCE, the limiting current density is proportional to the square root

of the rotation rate of the electrode as illustrated in figure 6.2. The electrode reaction is therefore mass transport controlled in the plateau region. The acetic acid concentration in the brine saturated with CO_2 can be estimated using a modified version of the Levich equation that recognizes that the transport of both free proton and undissociated acetic acid can occur in the oilfield brine (equation 4-5, Chapter Four, page 4-20) The values used for the diffusion coefficient for acetic acid was taken as 1.02×10^{-9} m^2 s^{-1} at temperature of 298 K (see page 4-6, Chapter Four). The diffusion coefficient for the free proton was taken as 9.3×10^{-9} m^2 s^{-1} at 298 K [154], and the concentration of free proton was estimated from the pH of the oilfield brine after CO_2 resaturation (pH 4.46).

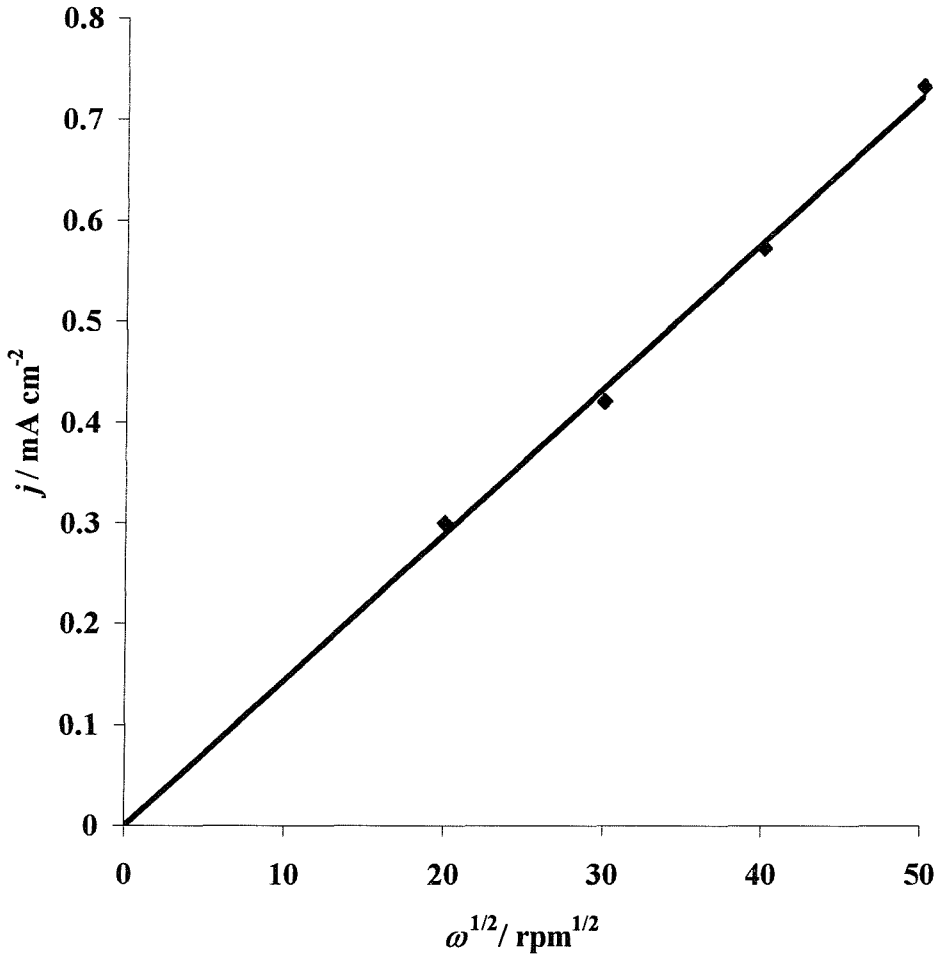

Figure 6. 2 *Plot of j_L versus $w^{1/2}$ at potentials in the plateau region of the j-E curves in figure 6.1 for Wytch Farm oilfield brine A1 resaturated with CO_2, pH 4.46 at 298K.*

The value calculated is 0.59 mM. Making no correction for non-ideality, this is equivalent to a total acetate concentration of 0.90 mM (cf. analytical value of 0.66 mM) a reasonable agreement in view of the uncertainties in the calculations. There can be no doubt that lowering the pH by saturation with CO_2 has led to the conversion of a fraction of the acetate in the brine to acetic acid.

The same experiment was repeated for the brine sample A2 in the same conditions. Figure 6.3 reports a typical voltammogram recorded for sample A2. When the sample has been resaturated with CO_2, the pH of the brine drops to 4.60.

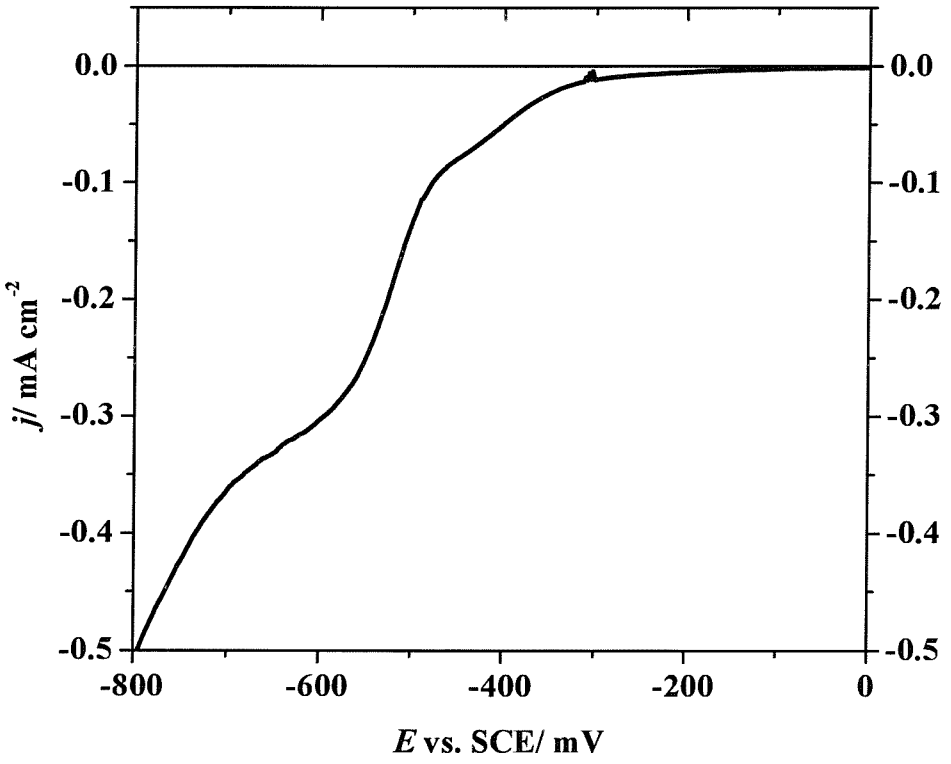

Figure 6. 3 *Voltammogram recorded at a precleaned Pt rotating disc electrode (area, 016 cm^2) for the brine sample A2 resaturated with CO_2, pH 4.60. Temperature 298 K. Rotation rate 400 rpm.*

The voltammogram for sample A2 in the same conditions is very similar to that for sample A1. Once again, a well-formed reduction wave is seen at $E_{1/2}$ = -520 mV versus SCE confirming the formation of acetic acid. The limiting current densities for the CO_2 saturated brine at each rotation rate are slightly higher with

brine A2. As previously, the limiting current is proportional to the square root of the rotation rate of the Pt disc electrode. Using the same procedure as above, the concentration of acetic acid in the CO_2 saturated brine is estimated as 0.71 mM. Again, making no allowances for non-ideality, this is equivalent to a total acetate concentration of 1.22 mM (cf. the analytical value of 0.78 mM). It should be noted that it is more difficult to obtain reproducible results from the oilfield samples than with the simulated brines prepared with purified water and high purity chemicals. The above voltammograms had to be recorded with freshly cleaned surfaces and immediately after immersion in the sample (whether with brine A1 or A2). Without these precautions, the voltammograms showed changes and, in general lower current densities and waves were more drawn out along the potential scale as illustrated in figure 6.4. Indeed, if a constant potential was applied, the current density decayed rather rapidly, even after a few seconds. This behaviour can be attributed to other constituents in the oil brines, most likely organics adsorbing on the metal.

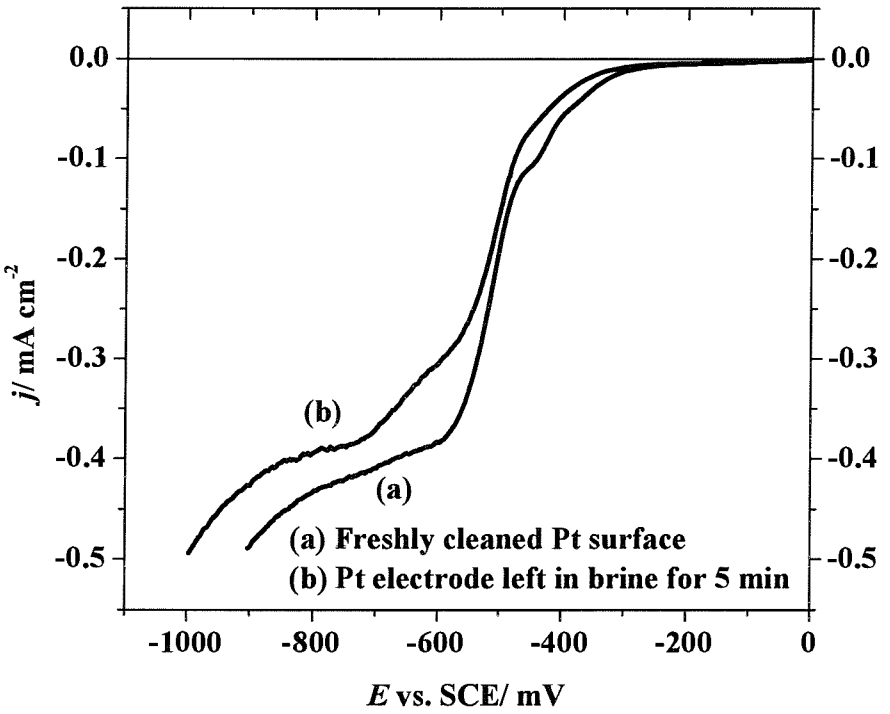

Figure 6. 4 *Votammograms recorded at a Pt rotating disc electrode for the brine sample A1 resaturated with CO_2 (a) wish freshly cleaned Pt surface, (b) with a Pt electrode left in the brine for 5 minutes. Temperature 298 K. Rotation rate 900 rpm.*

It should also be recognized that the acetate concentration in these brines is low compared with the model solutions and background currents will therefore be more significant. The voltammetry was also recorded at 333 K. Figure 6.5 illustrates a typical voltammogram recorded at a precleaned Pt rotating disc electrode for the sample A1 when resaturated with CO_2 and at 333 K. It should be noted that after resaturation with CO_2 the pH of the brine to drops 4.56. Also, the voltammogram obtained for the same brine sample at 298 K has been included for comparison.

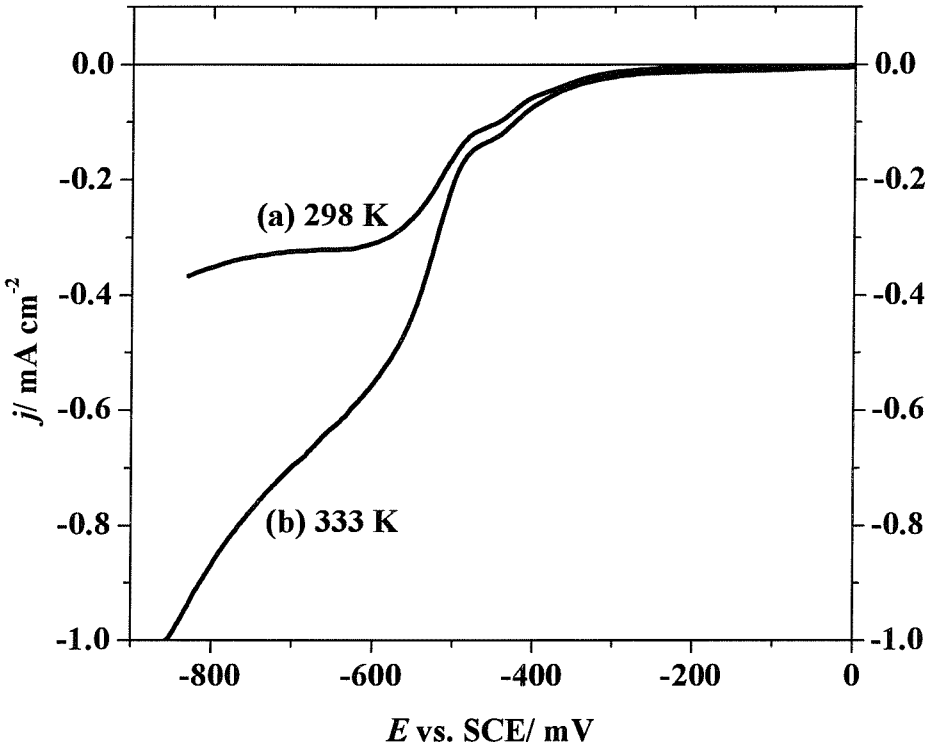

Figure 6. 5 *Voltammograms recorded at a precleaned Pt rotating disc electrode (area, 0.16 cm^2), for the brine sample A1 (a) at 298 K and (b) at 333 K. Brine A1 resaturated with CO_2 pH 4.46 and 4.56 respectively. Rotation rate 400 rpm.*

According to figure 6.5, it can be noted that the voltammogram at 333 K remains very similar to the one at 298 K. A well-formed reduction wave is observed at $E_{1/2}$ = -500 mV versus SCE. However, the most obvious change in the voltammogram with increasing the temperature is the increase in the limiting current densities. Further, the limiting current plateau is less defined and more drawn out on the potential axis. The experiment was repeated over a range of rotation rates, and

the voltammograms obtained show similar characteristics to the one presented in figure 6.5. This clearly indicates that the reaction occurring at the Pt RDE electrode is mass transport controlled. A plot of limiting current versus the square root of rotation rate of the Pt disc electrode was found to be linear and pass through the origin, confirming a fully mass transport controlled reaction.

6.3.2 Voltammetry of Oilfield A at X65 carbon steel rotating disc electrode

It should be emphasized that for all voltammograms at the carbon steel rotating disc electrode, the potential was scanned (usually 5 mV s^{-1}) in a positive direction from the negative limit. This step was taken in order to minimize the influence of corrosion films on the voltammetric response and to ensure reproducibility. Figure 6.6 shows voltammograms recorded at 298 K at both X65 carbon steel and Pt rotating disc electrodes for the Wytch Farm oilfield brine A1.

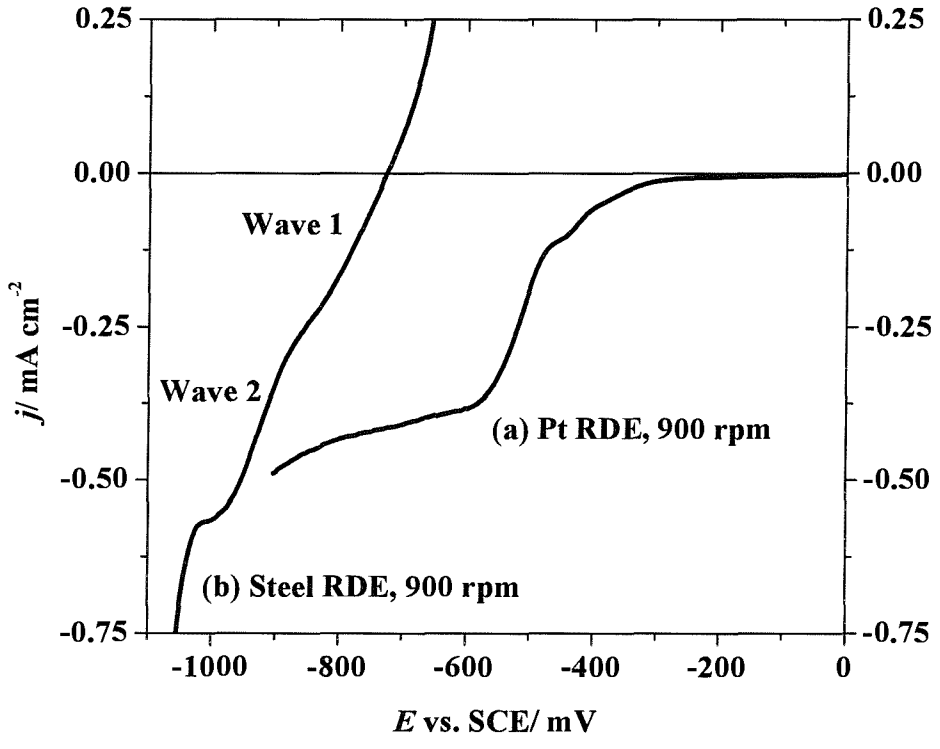

Figure 6. 6 *Voltammograms recorded at (a) Pt and (b) X65 carbon steel rotating disc electrode for the brine sample A1 after CO_2 resaturation. Temperature 298 K. Rotation rate 900 rpm.*

At the steel electrode, the corrosion potential, E_{corr}, is –720 mV versus SCE and the dissolution of iron is observed at potentials immediately positive to this value. Negative to the corrosion potential, the current also increases steeply and two reduction steps are observed. These two reduction steps seem to correspond closely to Wave 1 and Wave 2 reported for the reduction of acetic acid at steel (see Chapter Five cf. 5.3.2, page 5-11). Wave 1 was attributed to a kinetically controlled reduction of acetic acid, while beyond Wave 2 acetic acid reduction becomes mass transport controlled. It should further be noted that the limiting current at the carbon steel is very similar to that at Pt again confirming that both reduction waves at the X65 carbon steel rotating disc electrode are for the reduction of acetic acid. The response for the brine sample A2 at steel is similar to that for the brine sample A1. Figure 6.6 shows the voltammogram at the X65 carbon steel rotating disc electrode for sample A1 when the temperature is raised to 333 K.

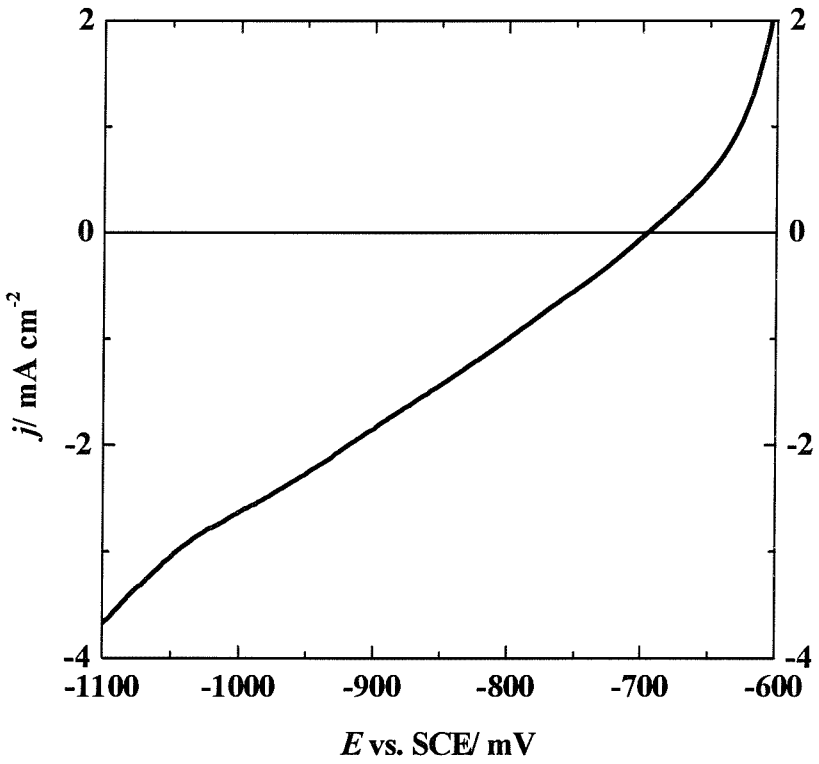

Figure 6. 7 *Voltammogram recorded at a X65 carbon steel rotating disc electrode (area, 0.17 cm^{-2}) for brine sample A1 resaturated with CO_2 at 333 K. Rotation rate 1600 rpm.*

At all potentials, the current densities are higher than that at 298 K but the voltammogram is now rather featureless. Certainly, Wave 2 cannot be observed. This is, however, to be expected from our earlier studies (see Chapter five). With decreasing acetate concentration and increasing temperature, it was found that the process leading to Wave 1 became dominant and with a concentration of acetate < 1 mM at 333 K only Wave 1 is to be expected. Furthermore, as for Pt, it should be reported that it is more difficult to obtain reproducible results with the oilfield samples. All voltammograms had to be recorded with freshly cleaned surfaces and immediately after immersion of the carbon steel disc in the sample (whether A1 or A2). Figure 6.8 illustrates a typical log j versus E plot for the X65 carbon steel in the brine A1 resaturated with CO_2. A reasonable Tafel slope is observed positive to the corrosion potential (slope = 1/67 mV)$^{-1}$ but the limiting current for acetic acid reduction is too low to obtain meaningful Tafel slope from the data negative to the corrosion potential.

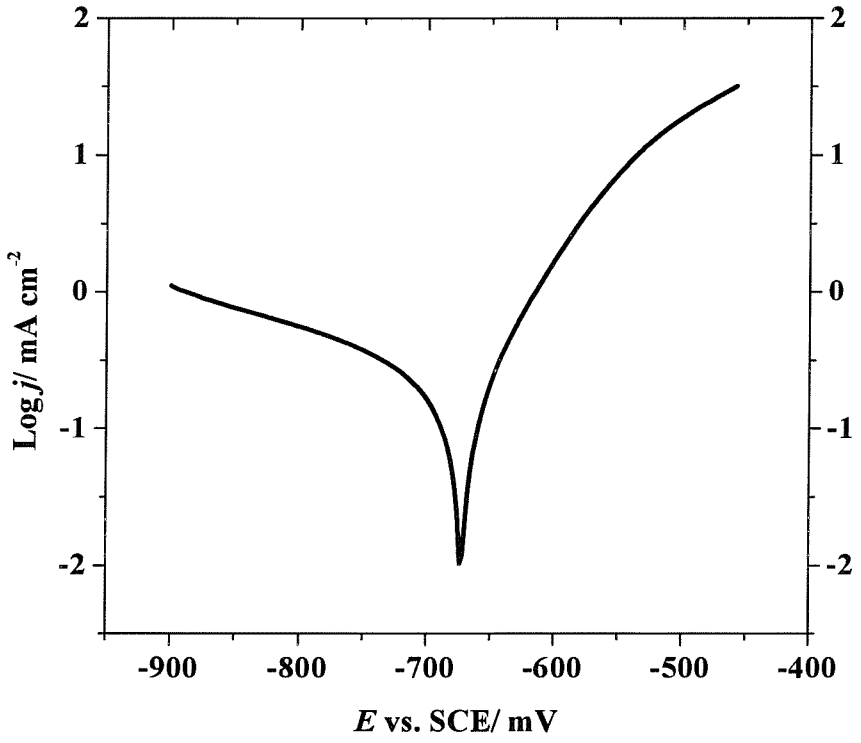

Figure 6. 8 *Log j versus E plot for brine sample A1 resaturated with carbon dioxide at a X65 carbon steel electrode at 298 K.*

For comparative purposes, it was desired to estimate a corrosion current. This is normally done from the linear polarization plots and using the Stern and Geary equation (6-1):

$$j_{corr} = \left[\frac{\beta_a \beta_c}{2.3(\beta_a + \beta_c)}\right]\frac{\Delta j}{\Delta E} \qquad (6\text{-}1)$$

where $\frac{\Delta j}{\Delta E}$ is the slope of the polarization plot (see figure 6.9), β_a and β_c are the anodic and cathodic Tafel slopes. Figure 6.9 reports the linear polarization responses for the X65 carbon steel in the brine A1 resaturated with carbon dioxide, pH 4.46 after CO_2 saturation at 298 K.

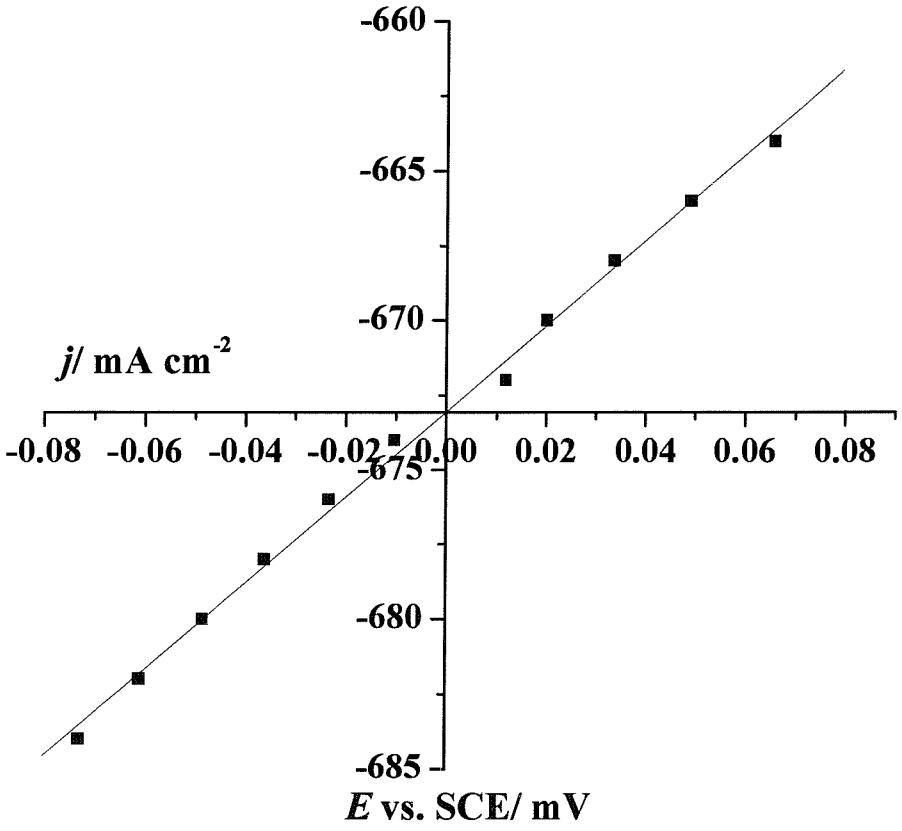

Figure 6. 9 *Linear polarization plot for the X65 carbon steel electrode in the brine A1 resaturated with CO_2 at 298 K. pH 4.46 after CO_2 saturation.*

The corrosion current densities were calculated from the slopes of such linear polarization plots, making standard assumptions that the Tafel slopes for iron dissolution and hydrogen evolution are 60 and 120 mV respectively. Table 6.2 reports the corrosion potential, E_{corr}, the corrosion current densities calculated for the two brines A1 and A2 at two temperatures and also reiterates our conclusions about the acetic acid concentrations in the brines.

Brine	T/ K	C_{HOAc}/ mM	E_{corr}/ mV vs. SCE	j_{corr}/ mA cm^{-2}
A1	298	0.59	-702	0.12
	333		-716	0.29
A2	298	0.71	-700	0.07
	333		-713	0.18

Table 6. 2 *Corrosion current densities for X65 carbon steel in oilfield brines A measured at a stationary disc electrode at two temperatures, 298 and 333 K respectively.*

In general terms, the rate of corrosion increases with temperature. The lower solubility of CO_2 at the higher temperature will lead to a higher pH and a lower conversion of acetate to acetic acid but the increased rates of reaction at 333 K more than overcome this effect. The values for the corrosion current densities at 333K are also in line with those reported in Chapter five although the level of acetate in the oilfield brines fall outside the range chosen for study with the simulated brines (see Chapter Five, page 5-46). It is not possible to consider the influence of acetic acid concentration on the corrosion current density because the brine A2 (but not brine A1) contains a corrosion inhibitor.

6.4 Oilfield B

6.4.1 Voltammetry of Oilfield B at a Pt rotating disc electrode

6.4.1.1 Voltammetry of oilfield B1

Voltammograms were recorded at a Pt rotating disc electrode for the oilfield brine B1. Figure 6.10 reports voltammogram at Pt rotating disc electrode for the sample B1 when residual CO_2 and O_2 accumulated during handling and transportation had been removed with a stream of N_2 bubbles. After N_2 saturation, the solution pH increased above 7, and no reduction wave is visible positive to – 800 mV versus SCE.

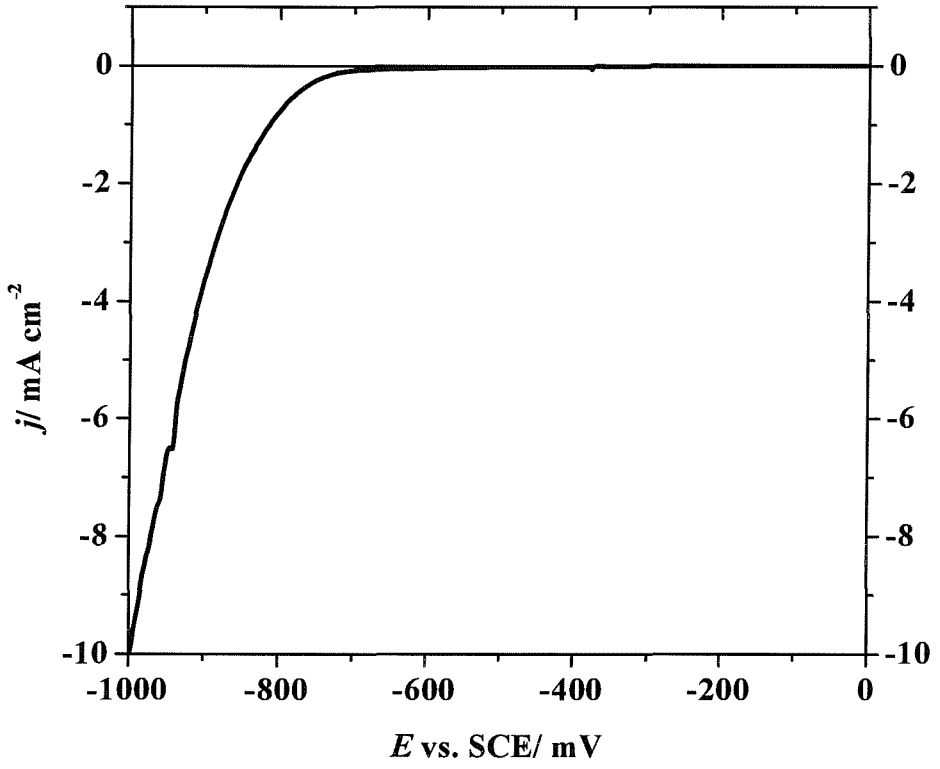

Figure 6. 10 *Voltammograms recorded at a precleaned Pt rotating disc electrode (area, 0.16 cm^2) for the brine sample B1 after N_2 saturation at 298 K. Rotation rate 900 rpm.*

When the brine B1 was resaturated with carbon dioxide, the voltammetry was quite different. Figure 6.11 reports the voltammogram recorded at a precleaned Pt rotating disc electrode in the oilfield brine B1 resaturated with carbon dioxide, the pH drops to 5.70. The voltammogram was recorded at 298 K and with a disc rotating at 1600 rpm

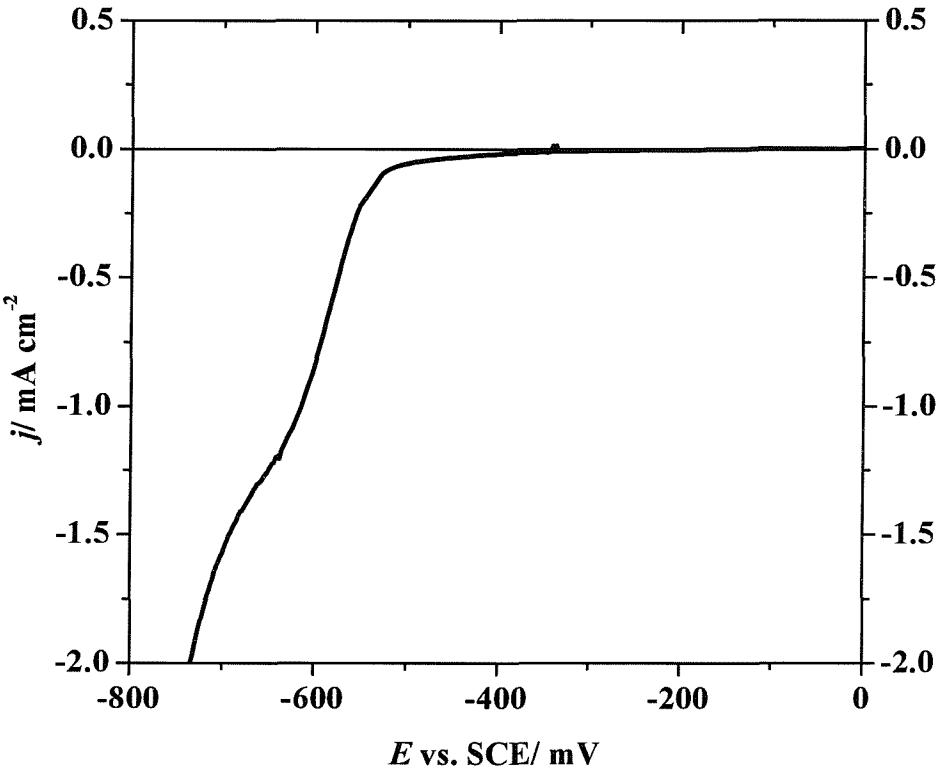

Figure 6. 11 *Voltammogram recorded at a precleaned Pt rotating disc electrode (area, 0.16cm^2) for the oilfield brine sample B1 resaturated with CO_2 at 298 K. pH drops to 5.70 after CO_2 saturation. Rotation rate 1600 rpm.*

The brine B1 showed a well-formed reduction wave at $E_{1/2}$ = -580 mV versus SCE, the potential predicted for the reduction of acetic acid in an acetate buffer, pH 5.70 (cf. –520 mV versus SCE at pH 4.70). Just negative to – 600 mV versus SCE, the height of this reduction wave was found to be dependent of the rotation rate of the Pt disc electrode. The limiting current is proportional to the square root of the rotation rate of the Pt disc electrode as shown in figure 6.12; the electrode reaction is therefore fully mass transport controlled. It can also be seen that the limiting current

plateau is very short and another electrode reaction occurs at potentials just negative to the wave.

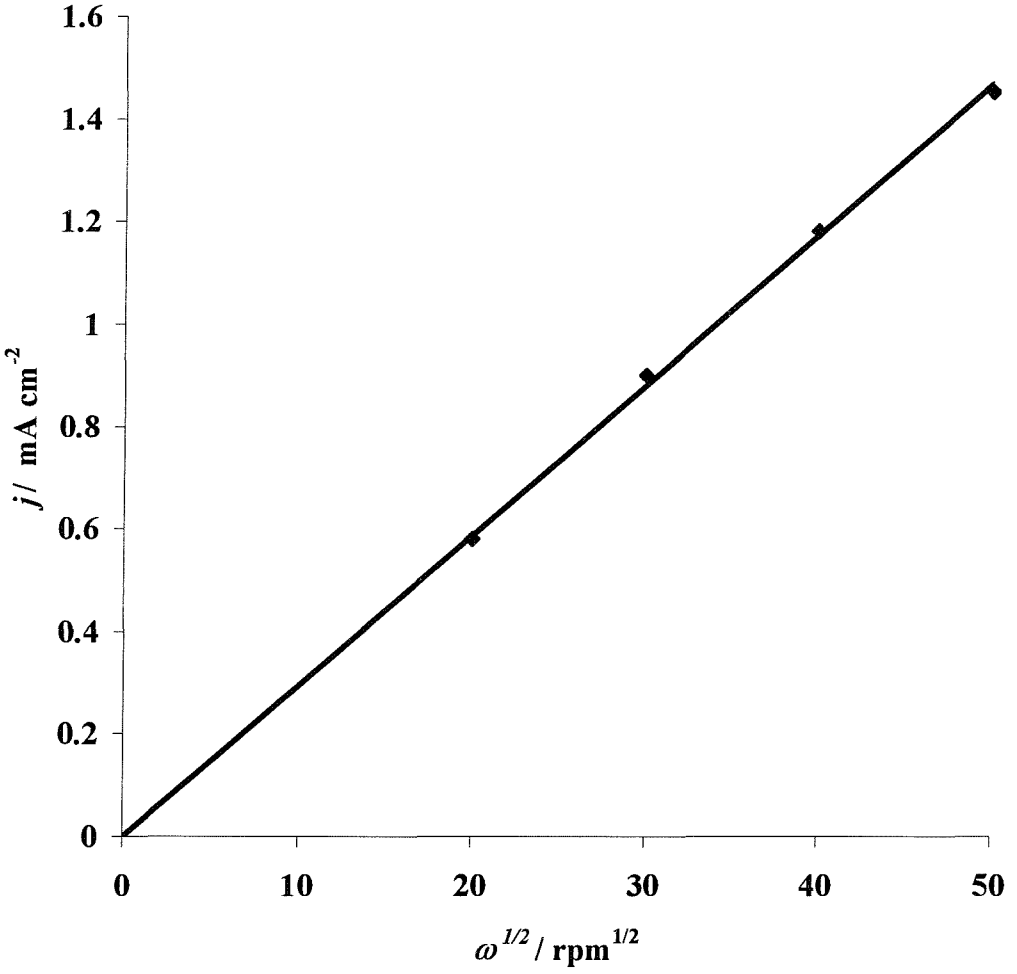

Figure 6. 12 *Plot of j_L versus $\omega^{1/2}$ at potentials in the plateau region of the j-E curves in figure 6.11 for oilfield brine B1 resaturated with CO_2, pH 5.70 at 298K.*

As previously, the acetic acid concentration in oilfield B1 was estimated using equation (6-3). The value calculated is 1.55 mM. Using the pH of the brine after CO_2 saturation, 5.70, this allows an estimate of 13.8 mM for the total acetate in the brine and this compares well with the analysts value of 11.0 mM (see table 6.1). In addition, it should be noted that at more negative potential, the CO_2 saturated brine shows large reduction waves associated with electrochemistry of bicarbonate [155] as illustrated in figure 6.13 (compare with figure 4-16, see page 4-27).

However, it is not thought that such reactions influence the corrosion of steel. Further, it should be noted that when the brines from oilfield B were resaturated with CO_2, their pHs were measured as close to 6. This is consistent with the higher level of bicarbonate, see table 6.1.

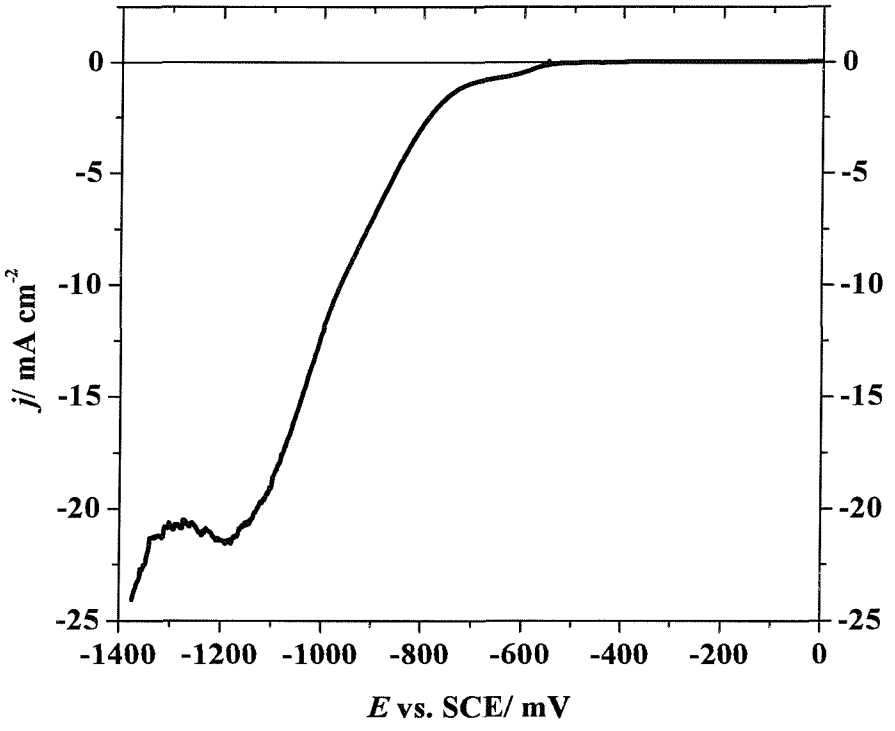

Figure 6. 13 *Voltammogram recorded at a precleaned Pt rotating disc electrode (area, 0.16 cm^2) for the oilfield brine sample B1 resaturated with CO_2 at 298 K. pH drops to 5.70 after CO_2 saturation. Rotation rate 400 rpm.*

6.4.1.2 Voltammetry of Oilfield B2

Figure 6.14 reports the voltammogram recorded for brine B2 at 298 K at a precleaned Pt rotating disc electrode when it is (a) a deoxygenated using a stream of N_2 and (b) resaturated with CO_2. After N_2 saturation, the pH of the solution is 7.22, and this drops to 6.12 on CO_2 saturation. Neither voltammogram shows a reduction wave positive to – 800 mV versus SCE. Saturation by carbon dioxide is not leading to the formation of acetic acid.

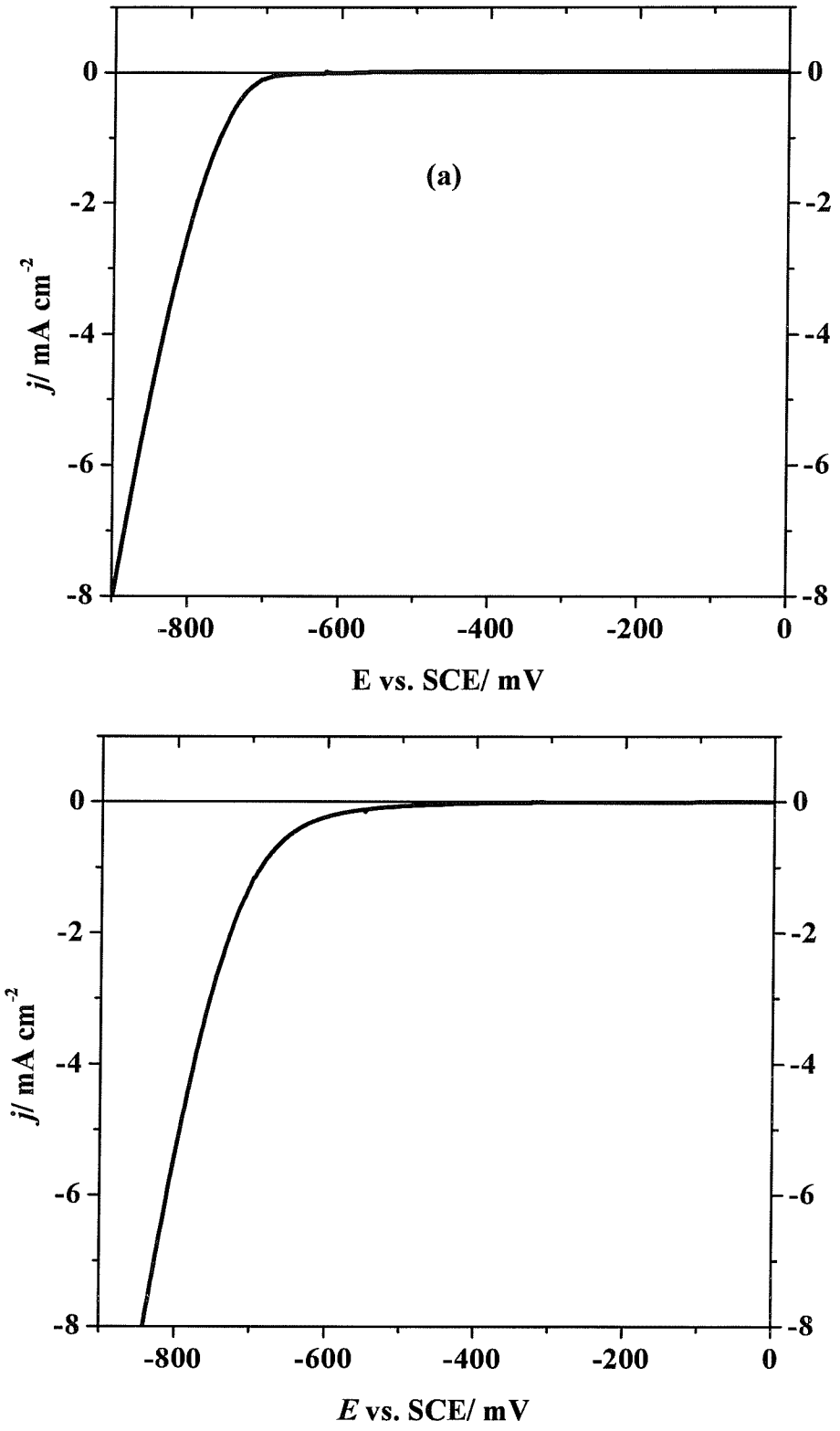

Figure 6. 14 *Voltammogram recorded at a precleaned Pt rotating disc electrode (area, 0.16 cm^2) for the oilfield brine sample B2 (a) N_2 saturated and (b) resaturated with CO_2 at 298 K. pH drops to 6.12 after CO_2 saturation. Rotation rate 900 rpm.*

This is consistent with the analysis of the brine; it contains a lower level of acetate, 4.4 mM and at the higher pH of 6.12, the estimated concentration of acetic acid is < 0.2 mM (not taking into account deviations from ideal solution behaviour). We would therefore expect to see only a very small acetic acid reduction wave and certainly the contribution of acetic acid to corrosion in brine B2 will be low.

6.4.2 Voltammetry of oilfield B at X65 carbon steel rotating disc electrode

6.4.2.1 Voltammetry of oilfield B1 at X65 carbon steel rotating disc electrode

Figure 6.15 illustrates the voltammetry of the carbon steel in the brine B1 resaturated with CO_2. This curve was recorded at 298 K but it has the same essential features as discussed with figure 6.7.

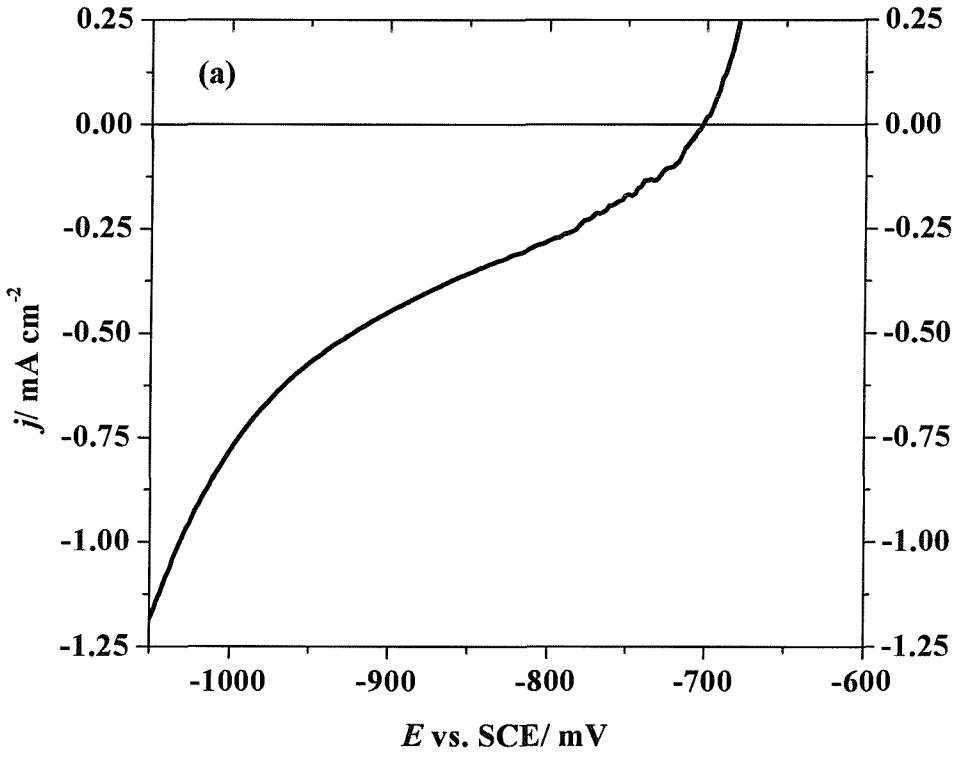

Figure 6. 15 *Voltammogram recorded at X65 carbon steel rotating disc electrode (area, 0.17 cm^2) for the oilfield brine sample B1 resaturated with CO_2 at 298 K. pH drops to 5.70 after CO_2 saturation. Rotation rate 900 rpm.*

Dissolution of iron is observed immediately positive of the corrosion potential. Most importantly, the corrosion potential is – 705 mV versus SCE and the current for the reduction of acetic acid is clearly visible immediately negative to the corrosion potential As for the Pt rotating disc electrode, the voltammograms were recorded for a larger potential scale window, and once again a large reduction wave was observed, as shown in figure 6.16. The height of this wave is dependent of the rotation rate of the X65 carbon steel disc but its origin was not investigated. However, we do not believe that such reactions influence the corrosion of the carbon steel specimen.

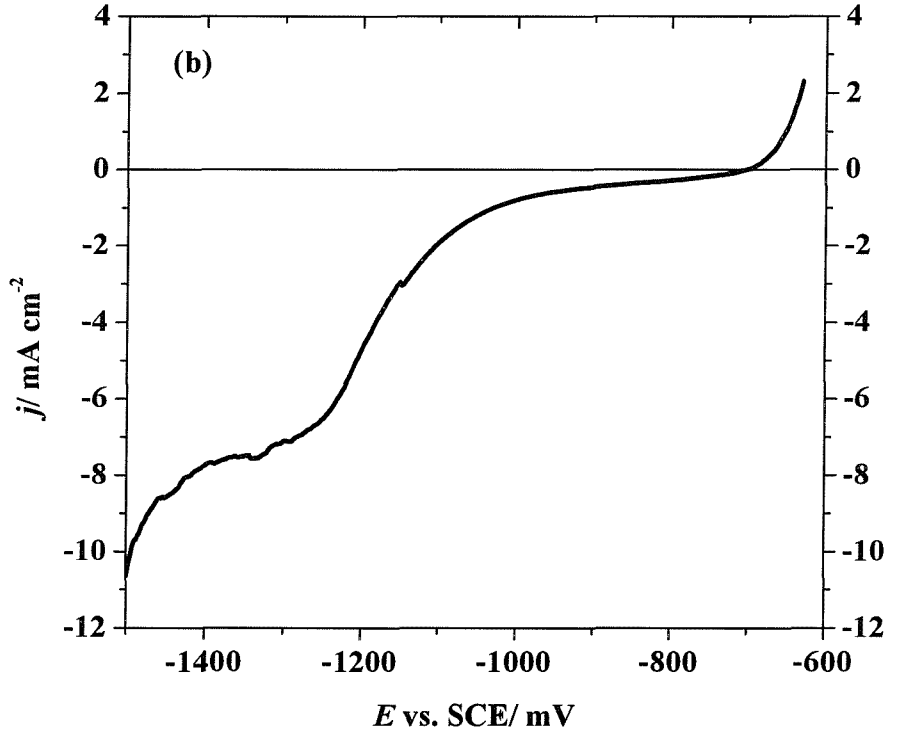

Figure 6. 16 *Voltammogram recorded at X65 carbon steel rotating disc electrode (area, 0.17 cm^2) for the oilfield brine sample B1 resaturated with CO_2 at 298 K. pH drops to 5.70 after CO_2 saturation. Rotation rate 900 rpm.*

6.4.2.2 Voltammetry of oilfield B2 at X65 carbon steel rotating disc electrode

Voltammetry was also recorded at X65 carbon steel rotating disc electrode for the oilfield brine B2. Figure 6.17 reports a typical voltammogram recorded at

298 K for the X65 carbon steel electrode in the brine B2 resaturated with CO_2. The voltammogram for the brine B2 leads to a corrosion potential of – 820 mV versus SCE and a very much slower increase in current negative to this potential. Again there is no evidence for the presence of significant acetic acid reduction or enhancement of corrosion in the oilfield brine B2.

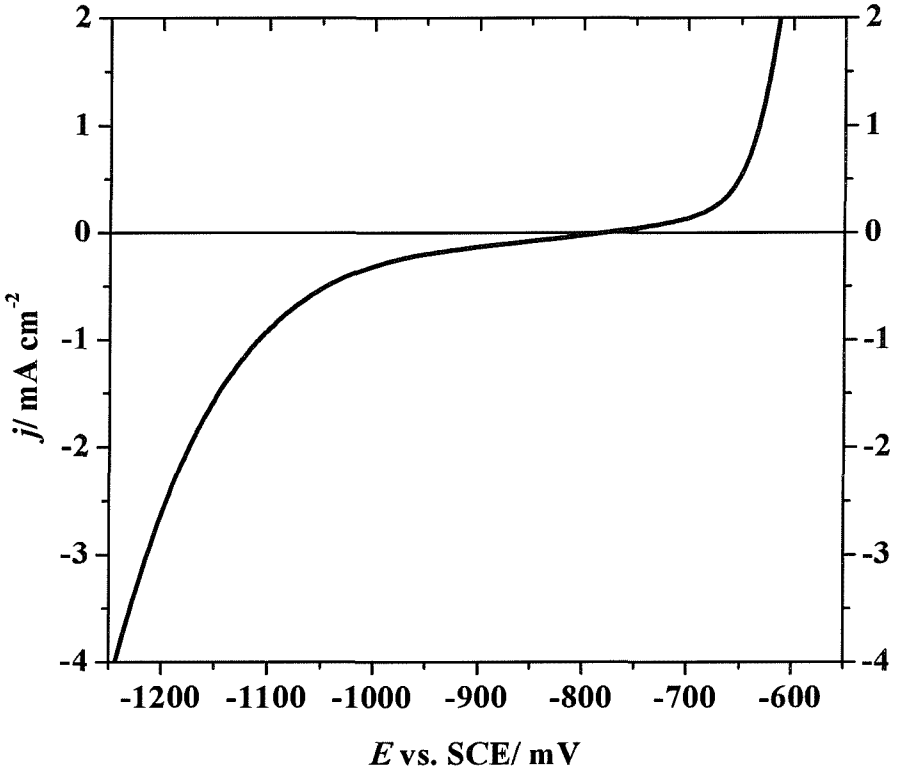

Figure 6. 17 *Voltammogram recorded at X65 carbon steel rotating disc electrode (area, 0.17 cm^2) for the oilfield brine sample B2 resaturated with CO_2 at 298 K. pH drops to 6.12 after CO_2 saturation. Rotation rate 900 rpm.*

Moreover, it can be seen that the voltammogram shown in figure 6.17 remains very similar to the one presented in figure 5.1 (see Chapter five, page 5-2) for neutral simulated solution. Table 6.3 reports the corrosion current densities calculated for oilfield brine B1 at two temperatures, and also reiterates our conclusions about acetic acid concentration in the brine. Further, corrosion potentials estimated from linear polarization measurement are also presented.

Brine	T/ K	C_{HOAc}/ mM	E_{corr}/ mV vs. SCE	j_{corr}/ mA cm^{-2}
B1	298	1.55	-705	0.15
	333		-745	0.29
B2	298	<0.2	-820	-

Table 6. 3 *Corrosion current densities for X65 carbon steel in oilfield brines B measured at a stationary disc electrode at two temperatures, 298 and 333 K respectively.*

According to table 6.3, it can be seen that once again the rate of corrosion increases with temperature. The values of the corrosion current densities can also be seen to reflect the concentration of the acetic concentrations in the oilfield brine.

6.5 Conclusion

This study of some oilfield brines has demonstrated, that the key factor determining the enhancement of corrosion by acetate is the concentration of acetic acid in the brine. In term, this depends on the level of any constituent of the brine that can influence its pH. Here, the focus has been on the bicarbonate level in the brine and it has been shown that a "high" bicarbonate concentration can lead to a brine pH that is high enough that the conversion of acetate to acetic acid is low. Then, the impact of any acetate in the brines on the rate steel corrosion is very low. It has also been noted that the definition of a "high" bicarbonate concentration depends on the CO_2 concentration and hence both temperature and pressure. Acetate enhanced corrosion is characterised by a positive shift in the corrosion potential and an increase in the corrosion current density. The importance of acetate enhanced corrosion depends on the concentrations of both acetate and bicarbonate while the presence of bicarbonate in sufficient concentration to negate the enhancement in corrosion rate by acetate is clearly indicated by a measurement of pH.

Then, one should pose the question as to whether carbonic acid has other roles in addition to being component of a buffer? It has been suggested that carbonic acid acts as the reactant for the cathode reaction by mechanism equivalent to reactions (5)

and (1). It should be recognized, however, that the concentration of carbonic acid is very low and its contribution for the cathode reaction in steel corrosion when acetic acid is present is small. This has already been discussed in Chapter Three (page 3-9).

The corrosion data for the four brines studied is summarised in table 6.2 and 6.3. While the changes in the voltammetry at Pt and the X65 carbon steel are very convincing, the trend in corrosion current densities is less so. We believe that this arises because of the particular brines so far available for study; because of unfortunate combinations of acetate and bicarbonate levels, all are low in acetic acid concentration after saturation with CO_2. Certainly, the acetic acid concentrations in the brine are low compared with those used in our earlier correlation plots (see figures 5.28 and 2.59 in Chapter Five). As in Chapter Four and Five, we would stress the critical role of the concentration of acetic acid in the brine in determining the extent of enhanced corrosion of steel by acetate. The acetic acid is a good proton donor and electron transfer at the steel (or, indeed, any metal surface) does not distinguish free proton and undissociated acetic acid.

Chapter Seven

7 *Conclusions*

Although the presence of acetate could influence the composition of the corrosion film, we believe that when steel is in a brine containing acetate and CO_2, the rate of corrosion is increased because the main cathodic reaction in the corrosion process becomes:

$$HOAc + e^- \rightleftharpoons \tfrac{1}{2} H_2 + OAc^-$$

All SEM experiments have shown that when the steel is in contact with a medium containing acetate and carbon dioxide, a uniform film is observed at the steel surface. This film is porous, allowing continuing supply of acetic acid to the surface. Further, the film thickens with time and acetic acid concentration but its structure does not seem to change. It is important to know accurately the speciation of the critical species in the brine solutions, and in this work, this has been achieved using a software package, PHREEQC 2.2, available on the World Wide Web, to deal with several interacting equilibria and the deviation from ideal solution behavior. Speciation calculations show that when CO_2 is dissolved, the solution becomes somewhat acidic, but the presence of acetate moderates the pH swing. The buffering action is achieved by the conversion of acetate to acetic acid, and has a result the brines have much higher concentration of proton donor, than free proton. It has been demonstrated conclusively that it makes no difference whether organic acids present in brines containing NaCl/NaOAc result from the addition of an aliquot of 1 M acetic acid or from carbon dioxide saturation of the solution. These solutions behave identically.

The electrochemistry of the weak acid solutions, at steel and Pt, reflects the concentrations of both free proton (pH) and the total concentration of proton donor in

the solution because the dissociation of the carboxylic acid (in this study, mainly acetic acid) is a rapid reaction. The dominant proton donor in the brines of interest is acetic acid, and at the usual pH of the brines (4.40 –5.80), the concentration of acetic acid is substantially higher than that of free proton as well as carbonic acid. Hence, a cathodic current equivalent to the mass transport controlled reduction of the acetic acid in the medium is observed. As a result the concentration of acetic acid rather than of free proton is a critical factor in determining the rate of corrosion. Depending on the experimental conditions, the reduction of acetic acid at steel leads to one or two reduction waves. Wave 1 clearly has the stronger influence on the cathodic current density at the corrosion potential. Wave 2 is most clearly seen in conditions of rapid mass transport and when the rate of reaction leading to Wave 1 is low. Wave 1 and Wave 2 are both associated with the reduction of acetic acid but the rate is determined by different factors. The most likely explanation for the two waves would be that they arise from the reduction of acetic acid on two different surfaces or by different mechanisms.

Measurements of the corrosion rate and corrosion current densities using Linear Polarisation, show that the rate of corrosion of the X65 carbon steel is directly dependent to the concentration of acetic acid. Indeed, this dependence is linear. It has been found that a minimum of ~ 1 mM HOAc in the brine is essential in order to enhance the corrosion of steel (compared to $NaCl/CO_2$). This can be understood because of the difference in diffusion coefficients for free proton (H^+) and acetic acid (HOAc), $D_{H^+} \approx 9\ D_{HOAc}$ and hence the mass transfer controlled current for H^+ reaction at pH 4.0 is equivalent to that for HOAc, when the concentration HOAc is equal to 0.5 mM. The reduction of carbonic acid (via kinetically controlled conversion of carbon dioxide) is again somewhat smaller at pH 4.0 although at high pH it replaces free proton reduction as major competing process. Works carried out with the Oilfield brines demonstrated that the influence of other species, particularly bicarbonate has to be considered. Sufficient concentration of bicarbonate can lead to brine with a high pH, therefore the conversion of acetate to acetic acid is low. Hence, the impact of any acetate on the rate of steel corrosion is very low. The major role of

CO_2 in this chemistry is only to change the speciation by changing the pH. Carbonic acid is a much weaker acid than acetic and the interconvertion of carbon dioxide to carbonic acid is slow so the contribution of carbonic acid reduction to the partial current density at the corrosion potential will be much less than the contribution from acetic acid. In the oil industry, there is a general need for models to predict corrosion rates in the oilfield environment. The model should take into account the ionic strength and the pH of the brines. In addition, the CO_2 pressure, the temperature and the acetate concentration are also important parameters to take into consideration. Then, the model will lead to the calculation of the organic acid concentration, therefore to the rate of corrosion of the steel specimens.

Literature

References

1. *World oil*, **216**, p. 17, (1995).
2. Hatfield, C. B., *Nature*, **387**, p. 121, (1997).
3. Palacios, C. A., and Shadley, J.R., *Corrosion*, **47**, p. 123, (1991).
4. Bryant, J.R. and Chitwood G.B, *NACE Corrosion 84*, Houston, **Paper 163**, (1984).
5. Uhlig, H., *Chemical and Engineering News*, **97**, p. 2764, (1949).
6. Trethewey, K. R., and Chamberlain, J., *"Corrosion for Students of Sciences and Engineering"*. Longman Group Limited, UK, (1988).
7. **BP**, *"BP Exploration costs of corrosion 1990 to 1992"*, BP: Marine Offshore management Ltd., Aberdeen (1993).
8. Shreir, L. L. and LaQue, F. L., *Corrosion*, Vol. 2, in Corrosion Control. L. L. Shreir, (Ed.), Newness-Butterworths, Boston, p. 20:35, (1976).
9. Lewis, R. E. and Bardin, D.K., *Mat. Perf*, p. 15, (1994).
10. Grast, W. F., *Mat. Perf*, p. 23, (1986).
11. Dougherty, J. A., *NACE Corrosion 98,* **Paper 15**, (1998).
12. Riggs, O. L., *"Corrosion Inhibitors"*, ed. Nathan, C. C., NACE, Houston, p.7, (1973).
13. Hedges, W. M., *Per. Comm. "Correxit Corrosion Inhibitors"*.
14. Ho-Chung-Qui, D.F., and Williamson, A. I., *NACE Corrosion 87*, **Paper 46**, (1987).
15. Bonis, M. R., and Crolet, J-L., *NACE Corrosion 98*, **Paper 103**, (1998).
16. Kowata, K., and Takahashi, K., *NACE Corrosion 96*, **Paper 219**, (1996).
17. Malik, H., *Corrosion*, **51**: p. 321, (1995)
18. Kapusta, S. D., Rhodes, P. R., and Silverman, S. A., *NACE Corrosion 91*, **Paper 471**, (1991).

19. Dougherty, J. A., and Stegmann, D. W., *NACE Corrosion 95*, **Paper 113**, (1995).
20. Crolet, J-L., 10th European Corrosion. Congr., Barcelona, p. 473, (1993).
21. Bacon, T. S., and Brown, E. A., *Oil and Gas J*, **41**: p. 91-92, (1943).
22. Debery, D. W., and Clark, W. S., U.S Dept. of Energy Report (DOE/MC/08442-1), (1979).
23. Newton, L. E., and Hausler, R. H., *"CO_2 corrosion in Oil and Gas production"*, NACE, Houston, (1984).
24. Dugale, P.J. and Bartman. G. R., in *Process Conference, Advances in Petroleum Recovery and Upgrading,* AOSTRA, Calgary, Alberta, (1981).
25. Gray, L. G. S., and. McCormack. M. E., *Proc. 4th UNITAR Int. Conf. Heavy Crude and Tar Sands*, Edmonton, Alberta, (1988).
26. Crolet, J-L., Institute of Materials, London, p. 1, (1994).
27. Todt, F., *Korros. Korrosionschutz*, **18,** (1962), as cited in DeWaard, C. and Milliams, D. E., *Corrosion*, **31**, p. 177, (1975).
28. Rozenfeld, I. L., "*Corrosion Inhibitors*", McGraw-Hill, New York, p. 272, (1981).
29. Burke, P. A., *Advances in CO_2 Corrosion*, Vol. 1, NACE, p. 3, (1984).
30. Ikeda, A., Ueda, M., and Mukai, S., *Advances in CO_2 Corrosion*, Vol. 1, NACE, p. 39, (1984).
31. Ikeda, A., Mukai, S., and Ueda, M., *NACE Corrosion 84*, (1984).
32. De Waard, C., Lotz, U., and Milliams, D. E., *NACE Corrosion 91*, p. 976 (1991).
33. Videm, K., Kvarekvaal, J., Perez, T., and Fitzsimons, G., NACE *Corrosion 96*, **Paper 1**, (1996).
34. Manuel, R.W.,*Corrosion*, **3,** (1947).
35. Mishra, B., Al-Hassan, S., and Olson. D. L., *NACE Corrosion 93*, CAN 121:6240, (1993).
36. Chitwood, G. B., Coyle, W. R., and Hilts, R.L., *NACE Corrosion 94*, (1994).
37. Schmidt, G., and Ladus, B. N., *NACE Corrosion 94*, **Paper 37**, (1994).
38. Ueda, M., and Ikeda, A., *NACE Corrosion 96*, **Paper 13**, (1996).

39. Legezin, N. E., and Zarembo, K. S., *Mater. Nanch. Tech*, (1964), as cited in Ueda, M., and Takade, H., *NACE Corrosion 98*, **Paper 35**, (1998).
40. Crolet, J-L. and. Bonis. M. R., *NACE Corrosion 83*, **Paper 160**, (1983).
41. Crolet, J-L., Thevenot, N., and Dugstad, A., *NACE Corrosion 99*, **Paper 24**, (1999).
42. Hedges, W. M., and McVeigh, L., *NACE Corrosion 99*, **Paper 21**, (1999).
43. Singh, M. M., and. Gupta, A., *Corrosion*, **56**, (4), p. 371, (2000).
44. Tebbal, S., and Hackerman, N., **34,** (11), p.1787, (1993).
45. Kabasakaloglu, M., Guner, A. F., and. Aksu, M. L., *Chimica Acta Turcica*, **26**, p. 45, (1998).
46. Beleevskii, V.S., Kudelin, Yu. I., Lisov, S. F., and Timonin, V. A., Translated from: *Zashchita Metallov*, **26,** (5), p. 723, (1990).
47. Beleevskii, V.S., Kudelin, Yu. I., Lisov, S. F., and Timonin, V. A., Translated from: *Fiziko-Khimicheskaya Mekhanika Materialov*, **26,** (6), p. 16, (1990).
48. Menaul, P. L., *Oil & Gas J.,* **43,** (27), p.80, (1944).
49. Waldrip, H. E., *Corrosion*, **4,** (12), p. 611, (1948).
50. Hillenbrand, L. J., Condens. Well Corr. Committee, Tulsa, Oklahoma (1953).
51. Shock, D.A., and Sudbury, J. D., *World oil*, **133,** (5), p.180, (1951).
52. *"Corrosion in Oil and Gass-Well Equipment"*, API, Dallas, TX, (1958) as cited in Crolet, J-L., Thevenot, N., and Dugstad, A., *NACE Corrosion 99*, **Paper 24**, (1999).
53. Crolet, J-L., and Bonis, M. R., *Corrosion*, **39,** (2) p. 39, (1983).
54. Bonis, M. R. and Crolet, J-L., *NACE Corrosion 89*, **Paper 446**, (1989).
55. Hedges, W. M., *Pers. Comm.*, Esso Facts-Offshore, (1992).
56. Crolet, J-L., and Bonis, M. R., *Mat. Perf,* **25,** (3), p.41, (1986).
57. Faroulis, Z.A., 5th European Symposium On Corrosion Inhibitors, (1980).
58. Wagner, C., and Traud, W., *Z. Elektrochem.*, **44**, p. 391, (1938).
59. Greef, R., Peat, R., Peter, L. M., Pletcher, D., and Robinson, J., *"Instrumental Methods in Electrochemistry"*, Ellis Horwood Ltd., (1993).

60. Pletcher, D., *"A first Course in Electrode Processes"*, The Electrochemistry Consultancy, England, (1991).

61. Tafel, J., *Zeitschrift fuer Physikalische Chemie*, **50**, p. 641 (1904).

62. Smyrl, W. H., *"Electrochemistry and Corrosion on Homogeneous and Heterogeneous Metal Surface"*, in Comprehensive treatise of Electrochemistry, Vol. 4, Bockris, J. O'M., Conway, B.E., Yeager, E., and White, E., (Eds.), Plenum Press, New York, p. 97, (1981).

63. Fontana, M .G., *"Corrosion Engineering"*, McGraw-Hill, New York, p. 345, (1987)

64. Oldman, K. B. and Mansfeld, F., *Corr. Sci.*, **13**, p. 813 (1973).

65. Mansfeld, F., *Advances in Corrosion Science and Corrosion Engineering*, Eds. Mansfeld, M., Staehle, R., Vol. 6, Plenum Press, New York, (1976).

66. Stern, M. and Geary, A. L,. *J. Electrochem Soc.*, **104**, p. 56, (1957).

67. Stern, M., and Weisert, E. D., *Proc. Am. Soc. Testing Materials*, **59**, p.1280, (1959).

68. Clerbois, L., Rapports Techniques CEBELCOR 108, RT. 155, (1969).

69. Bonhoeffer, K. F., and Jena, W., *Z. Elektrochem.*, **55**, p.787, (1951).

70. Simmons, E., *Corrosion*, **13**, p.250, (1950).

71. Skold, R.V. and T. E., Larson, *Corrosion*, **13**, p. 139, (1957).

72. Stern, M., *Corrosion*, **14**, p. 440, (1958).

73. Evans, S., and Koelher, E. L., *J. Electrochem Soc.*, **107**, p. 576, (1961).

74. Kilpatrick, J. M., *Oil & Gas J*, **62**, p. 245, (1964).

75. Wilde, B. E., *Corrosion*, **23**, p. 379, (1967).

76. Leroy, R. L., *Corrosion*, **29**, p 272, (1973).

77. Macdonald, J.R., *"Impedance Spectroscopy: Emphasing Solid Materials and Systems"*, Ed. Wiley, New York, (1987).

78. Kending, M.W., F. Mansfeld, and T. S, *Corr. Sci.*, **23**, p. 317, (1983).

79. Mansfeld, F., *"Recording and analysis of ac impedance data for corrosion studies"*, *Corrosion*, **37**, p. 301-307, (1981).

80. Macdonald, D. D., *NACE Corrosion 87*, San Francisco, **Paper 479**, (1987).

81. Gabrielli, C., Keddam, M., and Takenouti, H., *Corros. Sci.*, **31**, p129, (1990).

82. Epelboin, I., Keddam, M., and Takenouti, H., *J. Appl. Electrochem.*, **2**, p.71, (1972).

83. Lorenz, W. J., and Mansfeld, F., *Corros. Sci.*, **21**, p. 647, (1981).

84. Hladky, K., Callow, K. M., and Dawson, J. L., *Br. Corros. J.*, **15**, p. 20, (1980).

85. Macdonald, D.D., and McKubre, M. C. H., *"Electrochemical impedance techniques in corrosion science"*, Electrochemical Corrosion Testing. STP 727, (Ed.), Mansfeld, F., and Bertocci, U., STP 27, ASTM, Philadelphia.

86. Blanc, G., Epelboin, I., Gabrielli, C., and Keddam, M., *J. Electroanal. Chem.*, **75**, p. 97, (1977).

87. Hladky, K. and Dawson, J. L., *Corros. Sci.*, **22**, p. 231 (1982).

88. Bertocci, U., *J. Electrochem Soc.*, **127**, p. 520, (1980).

89. Searson, P. C., and Dawson, J. L., *J. Electrochem Soc.*, **135**, p. 1909, (1988).

90. Gabrielli, C., Huet, F., Keddam, M., and Raillon, L., *Corrosion*, **46**, p. 266, (1988).

91. Harden, R. G., Lambert, P., and Page, C. L., *Br. Corros. J.*, **23**, p. 225, (1988).

92. Roberge, P. R., Beaudoin, R., and Shastri, V. S., *Corros. Sci.*, **29**, p. 1231, (1989).

93. De Waard, C., and Lotz, U., *NACE Corrosion 93*, **Paper 69**, (1993).

94. Palmer, D. A., and Eldik, R. V., *Chem. Rev.*, **83**, p. 651, (1983).

95. De Waard, C., and Milliams, D. E., *Corrosion*, **31**, p. 177, (1975).

96. Weast, R. C., *"Handbook of Chemistry and Physics", 53rd ed.*, CRC press, Cleveland, (1972).

97. Asada, K., in: Inoue, S., and Yamazaki, N. (Eds.), *"Organic and Biorganic Chemistry of Carbon dioxide"*, Halsted Press, Tokyo, p. 188, (1982).

98. Schmitt, G., *NACE Corrosion 83*, **Paper 43**, (1983).

99. Schmitt, G., Advances in CO_2 corrosion, p. 10, NACE, Houston, Texas, (1984).

100. Schmitt, G., in: Hausler, R., and Giddard, H. P. (Eds.), Advances in CO_2 corrosion, Vol. 1, p. 1, NACE, Houston, Texas, (1984).
101. Ikeda, A., Ueda, M., and Mukai, S., in Hausler, R., and Giddard, H. P. (Eds.), Advances in CO_2 corrosion, Vol. 1, p. 39, NACE, Houston, Texas, (1984).
102. Schmitt, G., and Rothmann, B., *Werkst. Korros.*, **28**, p. 816, (1977).
103. Schmitt, G., and Rothmann, B., *Werkst. Korros.*, **29**, p. 98, (1978).
104. Wieckowski, A., Ghali, E., Szklarczyk, M., and Sobkowski, J., *Electrochim. Acta.*, **28**, p. 1619, (1983).
105. Hurlen, T., Gunvaldsen, S., Tunold, R., Blaker, F., and Lunde, P.G., *J. Electroanal. Chem.*, **180**, p. 511, (1984).
106. Nesic, S., Solvi, G. T., and Enerhaug, J., *Corrosion*, **51**, p. 773, (1995).
107. Nesic, S., Postlethwaite, J. and Olsen, S., *Corrosion*, **52**, p. 280, (1996).
108. De Waard, C. and Milliams, D. E., **31**, p.131, (1975).
109. Gray, L. G. S., Anderson, B. G., Danysh, M. J., and Tremaine, P. R., *NACE Corrosion 89*, New Orleans, **Paper 464**, (1989).
110. Gray, L. G. S., Anderson, B. G., Danysh, M. J., and Tremaine, P. R., *NACE Corrosion 90*, Las Vegas, Nevada, **Paper 40**, (1990).
111. Hurlen, T., Gunvaldsen, S., and Blaker, F., *Electrochim. Acta.*, **29**, p. 1163, (1984).
112. Rogers, W. F., and Rowe, J. A., in: Proc. Fourth World Petroleum Congress, Section II/G, Paper 3, Houston, Texas, (1955).
113. Ogundele, G. I. and White, W. E., *Corrosion*, **42**, p. 71, (1986).
114. Castro, E. B., Vilche, J. R., and Arvia, A. J., *Corr. Sci.*, **32**, p. 37, (1991).
115. Castro, E. B. and Vilche, J. R ., *J. Electroanal. Chem.*, **323**, p. 231, (1992).
116. Ikeda, A. and Ueda, M., Working Party Report, Institute of Materials, London, p. 59, (1994).
117. Davies, D. H., and Burstein, G. T., *Corrosion*, **36,** (8), p. 416, (1980).
118. Bockris, J. O. M., Drazic, D., and Despic, A. R., *Electrochim. Acta.*, **4**, p. 325, (1961).
119. Videm, K., and Dugstad, A., *NACE Corrosion 87*, **Paper 42**, Houston, Texas, (1987).

120. Videm, K., and Dugstad, A., *NACE Corrosion 88*, **Paper 186**, Houston, Texas, (1988).

121. Vetter, K. J., "*Electrochemical Kinetics - Theoretical and Experimental Aspects*", Academic Press, New York, p. 506, (1967).

122. Albery, W. J., "*Electrode Kinetics*", Clarendon Press, Oxford, p. 125, (1975).

123. Vielstich, W., and Jahn, D., *Z. Elektrochem.*, **64**, p. 43, (1960).

124. Albery, W. J., and. Bell., R. P., *Proc. Chem. Soc.*, p. 169, (1963).

125. Fleischmann, M., Lassare, F., Robinson, J., and Swan, D., *J. Electroanal. Chem.*, **177**, p. 97, (1984).

126. Ciszkowska, M., Stojeck, Z., Morris, S. E., and Osteryoung, J. G., *Anal. Chem.*, **64**, p. 2372, (1992).

127. Troise, F. M .H. and Denault, G., *J. Electroanal. Chem.*, **354**, p. 3311, (1993).

128. Stojek, Z., Ciszkowska, M., and Osteryoung, J. G., *Anal. Chem.*, **66**, p. 1507, (1994).

129. Ciszkowska, M., Stojek, Z., and. Osteryoung, J. G., *J. Electroanal. Chem.*, **398**, p. 49 (1995).

130. Daniele, S., Lavagnini, I., and Baldo, M. A., *J. Electroanal. Chem.*, **404**, p. 105, (1996).

131. Ciszkowska, M., Jaworski, A., and Osteryoung, J. G., *J. Electroanal. Chem.*, **423**, p. 95, (1997).

132. Daniele, S., Lavagnini, I., and Baldo, M. A., *Anal. Chem.*, **70**, p. 285, (1998).

133. Daniele, S., Baldo, M. A., and Simonetto, F., *Analytica. Chimica. Acta.*, **331,** (1-2), p. 117, (1996).

134. Daniele, S., Baldo, M. A., Bragato, C., and Lavagnini, I., **361**, p. 141, (1998).

135. Wightman, R. M., and Wipf, D.O., in: Bard A. J., (Ed.), "*Electroanalytical Chemistry*", Vol. 15, Marcel Dekker, New York, 1989.

136. Pletcher, D., in: Montenegro, I., Querios, M. A, and Daschbach, J. L., (Eds.), *"Microelectrodes: Theory and Applications"*, Kluwer Academic Publishers Dordrech, (1991).

137. Denault, G., *Chem Ind-London,* **18**, p. 678, (1996).

138. Oblonsky, L. J., and Divine, T. M., *J. Electrochem Soc.*, **144**, p. 1252, (1997).

139. Oldhman, K. B., *Anal. Chem.*, **68**, p. 4173, (1996).

140. Bard, A. J., and Faulkaner, L., in:Wiley, (Ed.)," *Electrochemical Methods"*, New York, (1980).

141. Parkhurst, D.L. and Appelo, C. A. J., *Water-Resources Report 99-4259*, U.S Geological Survey, U.S Department of Interior.

142. Warburton, P. R. G., *Ph. D Thesis*, 1988, University of Southampton, UK, (1988).

143. Plummer, L. N., and Busenberg, E., *Geochim. Cosmochim.*, **46**, p. 1011, 1982.

144. Kenne, F.R., in: Sullivan, B. P., Krist, K., and Guard, H. E., (Eds.), *"Electrochemical and Electrocatalytic Reactions of Carbon Dioxide"*, Elsevier, Amsterdam, (1993).

145. Harned, H. S., and Ehlers, R. W., *J. Am. Soc.*, **55**, p. 652, (1933).

146. Stark, J.G. and Wallace, H. G., in Murray, J., (Ed.), *"Chemistry Data Book"*, London, (1978).

147. Truesdell, A. H. and Jones, B. F., Journal of Research, U.S. Geological Survey, **2**, p.233, (1974).

148. Ball, J. W. and Nordston, D. K., U.S. Geological Survey, (1991).

149. Nordston, D. K., Plummer, L. N., and. Parkhurst, D. L., in Basset, R. L., and Melchior, D., (Eds.), Americain Chemical Society Symposium Series 416, Chapt 31, p. 398, Washington D.C, (1990).

150. Allison, J. D., Brown, D. S., and Novo-Gradac, K. J., Environmental Research Laboratory, Office of Research and Development U.S, Environmental Protection Agency, Athens, Georgia, (1990).

151. Angerstein-Kozlowska, H., in: Yeager, E., Bockris, J. O'. M., Conway, B. E., and Sarangapani (Eds.), *"Cmprehensive Treatise of Electrochemistry"*, Vol. 9., Plenum Press, p.28, New York, (1984).

152. Gleitenberg, D., Kustcher, A., and Stackelberg, M.V., *Ber. Bunsenges.*, **72**, p. 152, (1968).

153. Appleby, A. J., Kita, H., Chemla, M., and G. Bronoel., in: Bard, A. J., and Dekker, M., (Eds.), *"Encyclopedia of the Elements, Volume IX,* p.384, (1982).

154. Atkins, P. W., *"Physical Chemistry"*, 2nd ed., Oxford University Press, Oxford, UK, p. 905, (1983).

155. Garsany, Y., Pletcher, D., Hedges, W. M., *J. Electroanal. Chem.*, **00**, p. 1, (2002).

156. Maguire, S., *Ph. D Thesis 1998*, University of Southampton, UK, (1998).